

# Arsenic Speciation in a Minerotrophic Peatland: Natural Organic Matter and Mineral Controls





DISS. ETH NO. 21617

**ARSENIC SPECIATION IN A MINEROTROPHIC PEATLAND:  
NATURAL ORGANIC MATTER AND MINERAL CONTROLS**

A dissertation submitted to  
ETH ZURICH  
for the degree of  
Doctor of Sciences

presented by  
**PEGGY HOFMANN**  
Dipl.-Geol., TU Bergakademie Freiberg

born September 04, 1984  
citizen of Germany

accepted on the recommendation of

Prof. Dr. Ruben Kretzschmar, examiner  
Dr. Christian Mikutta, co-examiner  
Dr. James J. Rothwell, co-examiner

2013



*to my husband Richard, and our children Yannek and Maja*



# Table of contents

<b>Summary</b> .....	V
<b>Zusammenfassung</b> .....	IX
<b>1. Introduction</b> .....	1
1.1. Research motivation .....	1
1.2. Biogeochemistry of arsenic .....	4
1.2.1. Speciation of dissolved arsenic .....	4
1.2.2. Mineral controls .....	6
1.2.3. NOM controls .....	10
1.3. Research objective and approach .....	15
References .....	18
<b>2. Arsenic sequestration by organic sulfur in peat</b> .....	29
2.1. Introduction .....	30
2.2. Materials and methods .....	32
2.2.1. Field site and sampling .....	32
2.2.2. General sample characterization .....	32
2.2.3. Synchrotron measurements .....	33
2.3. Results and discussion .....	34
2.3.1. The field system and its characteristics .....	34
2.3.2. Solid-phase speciation of arsenic .....	37
2.3.3. Local coordination of arsenic in As(III)-NOM complexes .....	39
2.3.4. Solid-phase speciation of iron .....	42
2.4. Environmental implications .....	44
References .....	48
<b>3. Spatial distribution and speciation of arsenic in peat studied with microfocused X-ray fluorescence spectrometry and X-ray absorption spectroscopy</b> .....	53
3.1. Introduction .....	54
3.2. Materials and methods .....	56
3.2.1. Field site and sampling .....	56
3.2.2. Sample preparation and synchrotron measurements .....	56
3.3. Results .....	59
3.3.1. Peat characterization .....	59

3.3.2. Bulk XAS analyses .....	60
3.3.3. $\mu$ -XRF and $\mu$ -XAS analyses .....	63
3.4. Discussion .....	67
References .....	72
<b>4. Oxidation of organosulfur-coordinated arsenic and realgar in peat:</b>	
<b>Implications for the fate of arsenic</b> .....	77
4.1. Introduction .....	78
4.2. Materials and methods .....	80
4.2.1. Experimental setup .....	80
4.2.2. Adenosine triphosphate measurements .....	83
4.2.3. Selective extractions .....	83
4.2.4. Bulk X-ray absorption spectroscopy .....	84
4.3. Results .....	84
4.3.1. Changes in geochemical parameters .....	84
4.3.2. Arsenic speciation changes .....	85
4.3.3. Iron speciation changes .....	88
4.3.4. Sulfur speciation changes .....	90
4.4. Discussion .....	92
4.4.1. Changes in geochemical parameters .....	92
4.4.2. Oxidation of realgar and organosulfur-coordinated arsenic .....	93
4.4.3. Fate of arsenic released .....	95
4.5. Environmental implications .....	96
References .....	98
<b>5. Conclusions and outlook</b> .....	103
References .....	108
<b>A. Supporting Information to Chapter 2</b> .....	113
A.1. Location of the field site .....	114
A.2. Vegetation at the sampling sites .....	115
A.3. Element distribution and geochemical conditions .....	117
A.4. Analytical methods .....	118
A.4.1. X-ray fluorescence spectrometry - method validation .....	118
A.4.2. X-ray diffraction .....	118
A.5. X-ray absorption spectroscopy references .....	119
A.5.1. Arsenic reference compounds .....	119
A.5.2. Iron reference compounds .....	121
A.5.3. Principal component analysis .....	123
A.5.4. Target-transform testing and linear combination fitting .....	124



A.6. Scanning electron microscopy – energy-dispersive X-ray spectroscopy analyses of realgar ( $\text{As}_4\text{S}_4$ ) and pyrite ( $\text{FeS}_2$ )	125
A.7. Wavelet-transform analysis	127
References	132
<b>B. Supporting Information to Chapter 3</b>	<b>135</b>
B.1. Synchrotron measurements and data analyses	136
B.1.1. Bulk X-ray absorption spectroscopy – arsenic and iron	136
B.1.2. Bulk X-ray absorption spectroscopy – sulfur	136
B.1.3. Microfocused X-ray fluorescence spectrometry and X-ray absorption spectroscopy	137
B.1.4. Synchrotron X-ray diffractometry	138
B.2. Concentrations of major elements in peat cores B3II, B5II, B1II	139
B.3. Bulk arsenic, iron, and sulfur speciation results	140
B.4. Synchrotron XRD analysis	142
B.5. Light microscopy analysis	143
B.6. Elemental correlation plots	145
B.7. Tricolor elemental maps	148
B.8. Thermodynamic data	149
B.9. $E_h$ -pH diagrams	150
B.10. Arsenic concentrations in plants	152
References	154
<b>C. Supporting Information to Chapter 4</b>	<b>157</b>
C.1. Synchrotron measurements and data analysis	158
C.1.1. Sample preparation	158
C.1.2. Bulk X-ray absorption spectroscopy – arsenic and iron	158
C.1.3. Bulk X-ray absorption spectroscopy – sulfur	159
C.2. Bulk arsenic <i>K</i> -edge and iron <i>K</i> -edge XANES spectra	160
C.3. Phosphate extraction results	161
C.4. Bulk sulfur <i>K</i> -edge XANES spectra and Gaussian curve fitting parameters	162
C.5. Bulk arsenic, iron, and sulfur speciation results	164
C.6. Oxidation kinetics of reduced sulfur	166
C.7. Dissolved organic carbon in water and phosphate extracts	167
References	168
<b>Acknowledgements</b>	<b>171</b>
<b>Curriculum vitae</b>	<b>173</b>



## Summary

Wetlands cover more than 6% of the global ice-free land area and have been recognized as important sinks for the trace element As. Wetland soils and sediments are subject to frequent changes in redox conditions, driven by water-table fluctuations and shifts in biological activity. In aerated soils and sediments, As has a strong affinity toward mineral surfaces, rendering it comparatively immobile. Under oxygen-depleted conditions, the microbe-mediated decomposition of natural organic matter (NOM) can drive the reductive dissolution of metal-(hydr)oxides and the concomitant release of associated As. The released As may subsequently be sequestered by Fe sulfides or mixed valence Fe-(hydr)oxides, or precipitate as As sulfide. Furthermore, the binding of As to particulate NOM is thought to additionally suppress the mobility of As under reducing conditions, but no conclusive spectroscopic evidence for the governing binding mechanisms and their environmental relevance has been presented so far. The major goal of this thesis was thus to provide fundamental data on (i) the relevance of NOM for As binding at an As-enriched field site characterized by a high abundance of NOM and low mineral matter content, (ii) the dominating mechanism of As binding to NOM, and (iii) the effect of changing redox conditions on the fate of As in NOM-rich environments. Therefore, the speciation and distribution of As was investigated at the naturally As-enriched minerotrophic peatland *Gola di Lago* (canton Ticino, Switzerland) using primarily synchrotron X-ray absorption spectroscopy (XAS) and X-ray fluorescence (XRF) spectrometry. Based on these results, potential formation processes of As species identified in the peat were inferred.

The investigations in the *Gola di Lago* peatland revealed two distinct As enrichment patterns characterized by a different As speciation and microscale distribution: The near-surface peat layers (<41 cm), which are subject to annual changes in redox conditions due to fluctuations of the water table, showed primarily micrometer-sized (10-50  $\mu\text{m}$ ) intense hotspots of As consisting of the As sulfide mineral realgar ( $\alpha\text{-As}_4\text{S}_4$ ). To a minor extent, As was associated with Fe(III)-(hydr)oxides mainly located on highly altered gneiss fragments or present as  $\sim 10\text{-}\mu\text{m}$  sized arsenopyrite (FeAsS) particles partially

strung along plant fibers. In the permanently anoxic deep peat layers (150-250 cm), As was more diffusely distributed and mostly associated with particulate NOM of varying decomposition stages. X-ray absorption spectroscopy analyses revealed that the NOM-associated As was coordinated as trivalent As to 2-3 sulfhydryl groups ( $R_{\text{As-S}} = 2.26 \text{ \AA}$ ).

The assessment of the spatial distribution, elemental correlations, and chemical speciation of As in the *Gola di Lago* peat samples by microfocused XRF and XAS analyses additionally provided new insights into geochemical conditions favoring particular As sequestration pathways. These findings suggested an authigenic formation of realgar and arsenopyrite in strongly reducing microenvironments of the near-surface peat layers, while the organosulfur-coordinated As in the deep peat layers may be formed by the passive sorption of As(III) to NOM. Despite the presence of high amounts of pyrite ( $\text{FeS}_2$ ) and Fe(III)-NOM complexes in the anoxic deep peat layers as revealed by Fe XAS, As was primarily associated with reduced organic S, suggesting that the complexation of As by sulfhydryl groups was highly favorable and effectively inhibited other As sequestration reactions like the substitution of As for S in pyrite. Because of the lack of evidence for ternary As(III)-Fe(III)-NOM complex formation and As(III) reaction schemes involving hydroxylic/phenolic groups of NOM in the *Gola di Lago* peat, the covalent binding of trivalent As to reduced organic S species was proposed as major As-NOM interaction mechanism for S- and NOM-rich anoxic environments.

Because changes in redox potential due to water-table fluctuations, shifts in biological activity, or land-use changes frequently occur in peatlands and affect the dynamics of redox-sensitive elements like As, the oxidation kinetics of organosulfur-coordinated As and realgar were investigated under prolonged oxidizing conditions. Results showed that the oxidation kinetics of organosulfur-coordinated As and realgar in the peat were comparatively slow with calculated half-life times of 312-379 and 215-312 days, respectively, and mainly controlled by abiotic processes. Arsenic released during the oxidation of these As species was almost entirely sequestered by pre-existing and newly formed Fe(III)-(hydr)oxides (>97%). However, their efficiency to sorb As was limited, presumably due to a reduced accessibility of mineral sorption sites for As, causing As solution concentrations to rise beyond common drinking water limits. The considerably faster oxidation kinetics observed for reduced S species (e.g., mercaptans and pyrite)

in comparison to those of organosulfur-coordinated As and realgar suggests a rapid loss of reactive As-sequestering S species following a drop in the water table. Overall, the oxidation experiment revealed that oxidizing conditions render the *Gola di Lago* peatland a long-term source for As. Consequently, the maintenance of anoxic conditions is regarded the prime strategy for the management of this and geochemically related As-rich wetlands.

In summary, this thesis markedly improved our understanding of the geochemical conditions favoring different As sequestration pathways in NOM-rich environments, and demonstrated that NOM can be a quantitatively important sorbent for As in S-rich reducing environments. This finding highlights the need to properly account for NOM when assessing the speciation, mobility, and toxicity of As in NOM-rich environments.



## Zusammenfassung

Feuchtgebiete bedecken mehr als 6% der eisfreien Erdoberfläche und stellen eine wichtige Senke für das Spurenelement As dar. Böden und Sedimente von Feuchtgebieten unterliegen häufigen Schwankungen im Redoxpotential, primär ausgelöst durch saisonale Änderungen des Wasserspiegels und der mikrobiellen Aktivität. In gut durchlüfteten Böden und Sedimenten ist As zumeist an die mineralische Festphase gebunden und daher vergleichsweise immobil. Unter reduzierenden Bedingungen hingegen kann die mikrobielle Zersetzung der natürlichen organischen Substanz (Engl., *natural organic matter*, NOM) zur reduktiven Auflösung von Metall(hydr)oxiden und damit der Freisetzung von mineralisch gebundenem As führen. Potentiell kann das dabei freigesetzte As wieder an Eisensulfid- oder Eisen(II/III)(hydr)oxid-Mineralen gebunden werden oder als Arsensulfid präzipitieren. Darüber hinaus wird diskutiert, ob unter reduzierten Bedingungen auch die Bindung von As an NOM zu dessen Immobilisierung beitragen könnte. Jedoch fehlte es bisher an spektroskopischen Belegen für entsprechende Bindungsmechanismen sowie deren Umweltrelevanz. Das Ziel der vorliegenden Doktorarbeit war es daher (i) die Bedeutung der NOM für die Arsenbindung in einem mit As angereicherten Feldsystem, welches sich durch einen hohen Anteil an NOM und einen geringen Mineralbestand auszeichnet, abzuschätzen, (ii) den dominierenden Bindungsmechanismus aufzuklären und (iii) den Effekt von Redoxpotentialschwankungen auf die Arsenmobilität in NOM-reichen Systemen zu evaluieren. Zu diesem Zweck wurde die Spezierung und Verteilung von As im geogen mit As angereicherten Niedermoor *Gola di Lago* (Kanton Tessin, Schweiz) primär mittels Röntgenabsorptionsspektroskopie (Engl., X-ray absorption spectroscopy, XAS) und Röntgenfluoreszenzanalyse (Engl., X-ray fluorescence spectrometry, XRF) untersucht. Auf der Basis dieser Befunde wurden potentielle Bildungsprozesse der im Torf identifizierten As Spezies abgeleitet.

Die Untersuchungen im *Gola di Lago* Niedermoor offenbarten zwei Anreicherungsmuster von As, welche sich durch eine unterschiedliche Arsenspezierung

und -verteilung auszeichneten: In den oberen Torfschichten (<41 cm), die jährlichen Schwankungen des Redoxpotentials durch Veränderungen des Wasserspiegels unterliegen, waren hauptsächlich scharf abgegrenzte, mikrometergroße (10-50 µm) As-Anreicherungen in Form von Realgar ( $\alpha\text{-As}_4\text{S}_4$ ) zu beobachten. Zu einem geringeren Anteil konnten an Eisen(hydr)oxiden gebundenes As auf stark zersetzten Gneispartikeln und ca. 10 µm große, hauptsächlich mit Pflanzenfasern assoziierte Arsenopyrite ( $\text{FeAsS}$ ) als weitere Arsenspezies identifiziert werden. Die tieferen, permanent anoxischen Torfschichten (150-200 cm) zeichneten sich vornehmlich durch eine diffuse Verteilung von As aus, welches zumeist mit partikulärer NOM unterschiedlichen Zersetzungsgrades assoziiert war. Mittels XAS konnte gezeigt werden, dass NOM-assoziiertes As im dreiwertigen Oxidationszustand mit 2-3 Sulfhydrylgruppen koordiniert ist ( $R_{\text{As-S}} = 2.26 \text{ \AA}$ ).

Die Untersuchungen zur räumlichen Verteilung, zu Elementkorrelationen und der chemischen Spezifizierung von As in den *Gola di Lago* Torfproben mittels Mikro-XRF und Mikro-XAS Analysen ergaben wertvolle Hinweise auf die Bildungsbedingungen der im Torf identifizierten Arsenspezies. Für die oberen Torfschichten ist demnach die authigene Bildung von Realgar und Arsenopyrit in stark reduzierten Mikrohabitaten naheliegend, wohin gehend das durch Sulfhydrylgruppen komplexierte As in den unteren Torfschichten am wahrscheinlichsten durch die passive Sorption von Arsenit an die NOM zu erklären ist. Obwohl die Analyse der Fe XAS Spektren einen hohen Anteil an Pyrit ( $\text{FeS}_2$ ) und Fe(III)-NOM-Komplexen in den unteren anoxischen Torfschichten aufzeigten, war As primär an reduzierten organischen S gebunden. Dieser Befund deutet darauf hin, dass die Bindung von As an Sulfhydrylgruppen der NOM präferentiell stattfindet und andere Arsensorptionsmechanismen, wie die Substitution von S durch As in der Pyritstruktur, effektiv unterbunden werden. Auf Grund fehlender Belege für die Bildung ternärer As(III)-Fe(III)-NOM-Komplexe oder die Reaktion von Arsenit mit Hydroxyl-/Phenolgruppen der NOM im *Gola di Lago* Torf wurde die kovalente Bindung von dreiwertigem As durch reduzierten organischen S als Hauptmechanismus für As-NOM Interaktionen in S- und NOM-reichen anoxischen Systemen vorgeschlagen.

Da Veränderungen im Redoxpotential in Mooren, ausgelöst durch Schwankungen im Wasserspiegel, der mikrobiellen Aktivität sowie Landnutzungsänderungen, einen



grossen Einfluss auf die Dynamik von redoxsensitiven Elementen wie As haben können, wurde die Oxidationskinetik von an Sulfhydrylgruppen gebundenem As und Realgar in einem Langzeitoxidationsexperiment untersucht. Basierend auf diesen Ergebnissen konnte gezeigt werden, dass die Oxidation des organisch gebundenen As und Realgars mit einer jeweiligen Halbwertszeit von 312-379 und 215-312 Tagen relativ langsam verläuft und hauptsächlich durch abiotische Prozesse gesteuert wird. Das während der Oxidation freigesetzte As wurde zu einem Grossteil (>97%) an bereits vorhandene und neu gebildete Eisen(hydr)oxide gebunden. Dennoch war deren Arsenimmobilisierungsvermögen, vermutlich durch einen begrenzten Zugang der mineralischen Oberflächen für As, eingeschränkt, so dass die Lösungskonzentrationen von As über allgemein gültige Trinkwassergrenzwerte anstiegen. Zusätzlich wurde eine schnellere Oxidationskinetik für reduzierte Schwefelphasen (z.B. Merkaptane und Pyrit) im Vergleich zu NOM gebundenem As und Realgar festgestellt, was einen schnellen Verlust von potentiell arsenbindenden Schwefelspezies infolge eines Wasserspiegelabfalls nach sich ziehen würde. Generell zeigen die Befunde des Oxidationsexperimentes, dass oxidierende Bedingungen im *Gola di Lago* Moor zu einer Langzeitmobilisierung von As führen würden, weshalb die Erhaltung von reduzierten Bedingungen in diesem oder geochemisch ähnlichen As-belasteten Feuchtgebieten von zentraler Bedeutung ist.

Zusammenfassend hat diese Doktorarbeit unser Verständnis von Arsenfestlegungsprozessen in NOM-reichen Umweltsystemen deutlich verbessert. Speziell der Nachweis von NOM als quantitativ wichtiger Sorbent für As in S-reichen reduzierten Systemen macht die Berücksichtigung von NOM in der Bewertung der Spezierung, Mobilität und Toxizität von As in NOM-reichen Systemen zwingend erforderlich.



# 1. Introduction

## 1.1. Research motivation

The metalloid As is widely recognized as a toxic trace element threatening soils and drinking water resources in many parts of the world and often having profoundly negative effects on human health [Smedley and Kinniburgh, 2002]. Arsenic in soils and sediments is mainly of geological origin and thus dependent on the concentration of As in the parent rock. Average As concentrations in parent rocks can range from 1-10 mg As kg<sup>-1</sup> in igneous and metamorphic rocks to 0.3-500 mg As kg<sup>-1</sup> in sedimentary rocks with maxima found in shales, claystones, and coals [Adriano, 2001; Plant et al., 2004]. Human activities may cause additional local inputs of As into soils and sediments. Specifically the excessive use of arsenical fertilizers and pesticides, As-rich waste disposal, the manufacture of As chemicals, fossil fuel combustion, or mining and smelting activities lead to local and regional As contaminations in soils exceeding several thousand mg As kg<sup>-1</sup> [Smedley and Kinniburgh, 2002; Henke, 2009].

Although As levels in uncontaminated soils seldom exceeds values of 10 mg As kg<sup>-1</sup>, large scale-low concentration releases of As into the groundwater are a recognized problem in many regions of the world including Argentina, Bangladesh, China, Hungary, and Mexico [Smedley and Kinniburgh, 2002]. These large-scale natural As groundwater problem areas can be typically found in two types of environment: firstly, closed basins in arid or semi-arid areas, and secondly, strongly reducing aquifers [Smedley and Kinniburgh, 2002]. While in the first environment the release of As in the groundwater is triggered by high pH values (>8.5) as a result of mineral weathering and high water evaporation rates, the development of strongly reducing conditions at near-neutral pH-values in the second environment leads to the reductive dissolution of metal-(hydr)oxides, thereby causing the release of associated As [Smedley and Kinniburgh, 2002] with severe consequences for groundwater use. For example, the reduced high-As groundwaters in South and Southeast Asia (Bangladesh, West Bengal, Nepal, Cambodia,

and Vietnam) became the main drinking water source for tens of millions of people in the past 20-50 years, mostly because the groundwaters were less likely to contain microbial pathogens responsible for high infant mortality rates than surface waters used at this time [Berg et al., 2001; Shrestha et al., 2003; Swartz et al., 2004; Berg et al., 2007]. Later, it was discovered that more than half of the tube wells installed in these regions were not meeting the World Health Organization guideline of  $10 \mu\text{g As L}^{-1}$  for drinking water [WHO, 2008]. As a result, symptoms of As poisoning including liver, bladder or lung cancer, cardiovascular diseases, or mental underdevelopment of children were increasingly observed in local populations utilizing the As-rich groundwater as drinking water [Fendorf et al., 2010]. Numerous studies focusing on the soils and aquifer sediments in South and Southeast Asia [Nickson et al., 2000; Smedley and Kinniburgh, 2002; McArthur et al., 2004; Fendorf et al., 2010] revealed that the mobility and bioavailability of As was strongly controlled by natural organic matter (NOM), driving the reductive dissolution of metal-(hydr)oxides and thus the release of As.

Wetlands, which include swamps, marshes, and peatlands, are frequently or permanently flooded environments rich in NOM [National Wetlands Working Group, 1997; Reddy and DeLaune, 2008], and typically play a major role in the storage, transformation, and mobilization of trace elements such as As. Peatlands are of special relevance as they cover approximately 4% of the Earth's total land area [Shotyk, 1988], and have been shown to serve as important sinks for As [González A. et al., 2006; Bauer et al., 2008; Cloy et al., 2009; Rothwell et al., 2010]. They are most commonly classified as either ombrotrophic or minerotrophic. While ombrotrophic peatlands receive water and nutrient inputs from atmospheric deposition, minerotrophic peatlands are influenced by surface and/or groundwaters, and thus feature higher nutrient levels and pH values than ombrotrophic peatlands [National Wetlands Working Group, 1997]. Consequently, As concentrations found in minerotrophic peatlands are typically higher than in ombrotrophic peatlands and frequently exceed threshold values of environmental concern [Minkinen and Yliruokanen, 1978; Hvatum et al., 1983; Schell, 1986; Zoltai, 1988; Harty et al., 1991; Shotyk, 1996; Qureshi et al., 2003; Szramek et al., 2004; Ukonmaanaho et al., 2004; Frank, 2005; González A. et al., 2006; Bauer et al., 2008; Cloy et al., 2009; Rothwell et al., 2009; Rothwell et al., 2010; Silamikele et al., 2011].

For example, a degraded minerotrophic peatland soil in southern Germany contained up to 3,239 mg As kg<sup>-1</sup> [Bauer et al., 2008]. Dissolved As concentrations at this site were below 10 µg As L<sup>-1</sup> at the peat surface but increased to 467 µg As L<sup>-1</sup> with depth (100-250 cm) [Bauer et al., 2008]. The latter value exceeds the As solution concentrations measured in ombrotrophic peat soils in North West England by up to 64 times [Rothwell et al., 2009]. Likewise, minerotrophic peat of the *Gola di Lago* peatland in Switzerland contained up to 300 mg As kg<sup>-1</sup> in depths of 10-20 cm, and 450 mg As kg<sup>-1</sup> at 230-240 cm [González A. et al., 2006]. Studies on ombrotrophic peat soils in North West England and Scotland revealed solid-phase As concentrations of 1.9-31.3 mg As kg<sup>-1</sup>, reflecting the emissions from diverse anthropogenic sources such as mining and smelting activities [Cloy et al., 2009; Rothwell et al., 2009; Rothwell et al., 2010]. Similar comparatively low As concentrations have been reported for other ombrotrophic peat soils from around the globe (Canada: 1.0-19.6 mg As kg<sup>-1</sup>; Finland: 0-17.8 mg As kg<sup>-1</sup>; Jamaica: 2.2-25.7 mg As kg<sup>-1</sup>; Norway: 0.07-0.13 mg As kg<sup>-1</sup>; Switzerland: 0.16-3.6 mg As kg<sup>-1</sup>; USA: 2.6 mg As kg<sup>-1</sup>) [Hvatum et al., 1983; Schell, 1986; Zoltai, 1988; Harty et al., 1991; Shotyk, 1996; Ukonmaanaho et al., 2004; Frank, 2005].

Sulfide minerals and metal-(hydr)oxides have been identified as major controls of As cycling in wetland soils [La Force et al., 2000; Fox and Doner, 2003; Beauchemin and Kwong, 2006; Huang and Matzner, 2006; Blodau et al., 2008; Rothwell et al., 2009]. In contrast, the influence of NOM on the fate of As in wetlands and related environments has been mainly discussed in terms of reductive dissolution of As-bearing metal-(hydr)oxides [Nickson et al., 2000; Smedley and Kinniburgh, 2002; Blodau et al., 2008], competitive adsorption and redox reactions [Grafe et al., 2001; Grafe et al., 2002; Redman et al., 2002; Simeoni et al., 2003; Bauer and Blodau, 2006; Jiang et al., 2009], the stabilization of As-bearing mineral colloids [Ritter et al., 2006; Bauer and Blodau, 2009], and the precipitation of As-bearing minerals [Moore et al., 1988; Rittle et al., 1995]. However, several wetland systems and peaty sediments showed As enrichments not related to the presence of As-bearing mineral phases, suggesting an immobilization of As through complexation with NOM [Anawar et al., 2003; Yamazaki et al., 2003; González A. et al., 2006; Bauer et al., 2008; Blodau et al., 2008; Rothwell et al., 2009; Ahmed et al., 2010]. Despite the association of As with amorphous and crystalline Fe(III)-(hydr)oxides in

degraded minerotrophic peatland soils (8-3,239 mg As kg<sup>-1</sup>) in southern Germany, Bauer et al. [2008] observed a significant correlation between the As and NOM content ( $r = 0.78, p < 0.01$ ). Together with a substantial portion of As (10-30% of total As) mobilized by the dispersion of NOM, these findings suggested a direct association of As with NOM [Bauer et al., 2008]. Similar results were obtained by Rothwell et al. [2009] who found a close correlation of solid-phase As and Fe ( $r = 0.85, p < 0.05$ ) in oxic ombrotrophic peat soils ( $\leq 28.3$  mg As kg<sup>-1</sup>) in North West England, but no indication of the association of As with sulfide minerals under reducing conditions. Instead, the observed immobilization of As under waterlogged-conditions was suggested to be due to the association of As with NOM [Rothwell et al., 2009].

Although many laboratory studies have documented an association of As with NOM [Thanabalasingam and Pickering, 1986; Redman et al., 2002; Buschmann et al., 2006; Wang and Mulligan, 2009; Liu and Cai, 2010], conclusive spectroscopic evidence for a specific binding mechanism has not been presented so far. The major goal of this thesis was thus a mechanistic understanding of As-NOM interactions that allows for a more accurate assessment of the mobility and bioavailability of As in NOM-dominated soils and sediments.

In the following sections, an overview on the biogeochemistry of As will be given with special focus on its solution chemistry as well as on minerals and NOM as main factors controlling the fate of As in soil environments.

## 1.2. Biogeochemistry of As

### 1.2.1. Speciation of dissolved As

Arsenic is a redox-sensitive trace element that may exist as one or more dissolved species in natural waters, depending on pH, redox potential ( $E_h$ ), other ionic species, and biological activity. In most natural waters (pH < 9), As primarily occurs as arsenite (As(III),  $\text{H}_3\text{AsO}_3^0$ ) and arsenate (As(V),  $\text{H}_2\text{AsO}_4^-$  and  $\text{HAsO}_4^{2-}$ ) [Cullen and Reimer, 1989]. While As(III) is the thermodynamically stable As species under moderately anoxic

conditions (between +300 mV at pH 4 to -200 mV at pH 9), As(V) usually dominates in oxic waters [Inskeep et al., 2002; Nordstrom and Archer, 2003]. Predominant inorganic As species in the As-O-H system as a function of  $E_h$  and pH are illustrated in Figure 1.1.

Organoarsenicals such as methylarsonic acid (MA), dimethylarsinic acid (DMA), and trimethylarsine oxide (TMAO) are often absent or contribute less than inorganic As species to the total As solution concentration [Cullen and Reimer, 1989; Mandal and Suzuki, 2002]. An exception are aquatic environments with high primary productivity like surface waters or photic zones in sea waters [Francesconi and Kuehnelt, 2002]. The presence of MA and DMA in these environments is thought to be the result of redox transformation and methylation of As(V) within phytoplankton [Francesconi and Kuehnelt, 2002]. In NOM-rich soils and sediments, NOM can also drive the redox transformation and methylation of As by microorganisms [Oremland et al., 2004; Huang and Matzner, 2006; Lomax et al., 2012]. For example, organo-As species have been shown to contribute up to 70% ( $1.2 \mu\text{g As L}^{-1}$ ) of total As in the porewaters of an acid fen soil [Huang and Matzner, 2006].

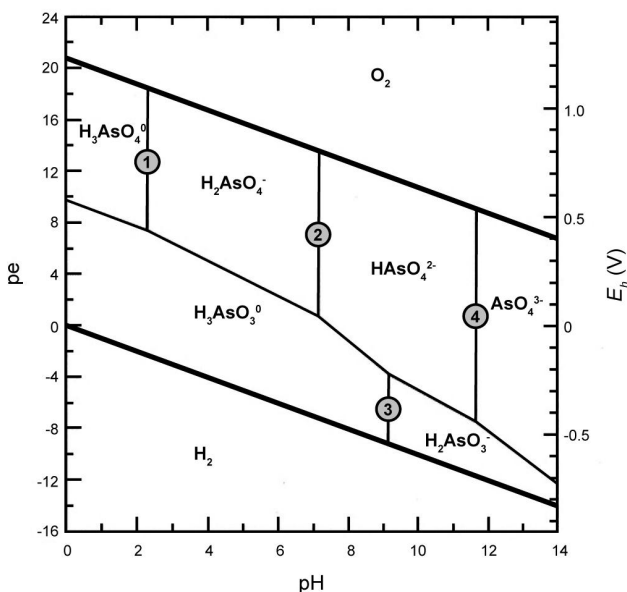


**Figure 1.1.** Pourbaix diagram (25 °C, 1 bar) for the predominant aqueous As species (activity:  $10^{-6}$ ) at equilibrium (modified after Nordstrom and Archer [2003]). The vertical boundary lines are identified by their numbers in Table 1.1.

**Table 1.1.** Acid-base reactions and proton dissociation constants ( $K_a$ ) according to Nordstrom and Archer [2003]. The vertical boundary lines (nos. 1-4) are illustrated in Figure 1.1.

Reaction	log $K_a$	boundary line (no.)
$\text{H}_3\text{AsO}_4^0 \leftrightarrow \text{H}_2\text{AsO}_4^- + \text{H}^+$	-2.30	pH = 2.30 (1)
$\text{H}_2\text{AsO}_4^- \leftrightarrow \text{HAsO}_4^{2-} + \text{H}^+$	-6.99	pH = 6.99 (2)
$\text{H}_3\text{AsO}_3^0 \leftrightarrow \text{H}_2\text{AsO}_3^- + \text{H}^+$	-9.17	pH = 9.17 (3)
$\text{HAsO}_4^{2-} \leftrightarrow \text{AsO}_4^{3-} + \text{H}^+$	-11.80	pH = 11.80 (4)

Depending on the water composition, As may also form dissolved species with  $\text{NH}_3$ ,  $\text{CN}^-$ ,  $\text{F}^-$  [Ballantyne and Moore, 1988; Williams, 2001], or in sulfidic systems with S [Wilkin et al., 2003; Planer-Friedrich et al., 2010]. Thioarsenic species like thioarsenites ( $\text{H}_x\text{AsO}_n\text{S}_{3-n}^{3-x}$  with  $n$  and  $x < 3$ ) may even dominate the As speciation at neutral pH and sulfide concentrations  $>10^{-4.3}$  M [Wilkin et al., 2003]. Another formation process of thioarsenic species can be the dissolution of As-bearing sulfide minerals like orpiment ( $\text{As}_2\text{S}_3$ ) and arsenopyrite ( $\text{FeAsS}$ ) under neutral to alkaline conditions [Suess and Planer-Friedrich, 2012].

Changes in the oxidation state of As in aqueous solutions can be driven by a variety of abiotic and biotic processes. While the oxidation of As(III) to As(V) proceeds very slowly when  $\text{O}_2$  is the only oxidant [Stollenwerk, 2003], the presence of redox-sensitive species like Mn-oxides [Oscarson et al., 1983; Scott and Morgan, 1995] or Fe(III)-(hydr)oxides [Greenleaf et al., 2003] can increase the rate of As(III) oxidation over a wide pH range. In contrast,  $\text{H}_2\text{S}$  is increasingly capable of reducing As(V) to As(III) with decreasing pH under abiotic conditions [Rochette et al., 2000]. Additionally, microorganisms can oxidize As(III) or reduce As(V) during dissimilatory respiration to gain energy [Inskeep et al., 2002]. Since the health effects by the uptake of inorganic As(III) and As(V) can be devastating for (micro)organisms, detoxification is another process leading to changes in the oxidation and speciation of As in aqueous solutions. Amongst others, As-resistance may be achieved by the extrusion of either As(III) or As(V) from cells, or by methylation [Rosen, 2002].

### 1.2.2. Mineral controls

Concentrations of dissolved As in soil solutions are largely determined both by the precipitation-dissolution of As-containing minerals and by the adsorption-desorption



behavior of As on mineral surfaces. The kinetics of these processes can be very sensitive to a variety of environmental parameters like pH,  $E_h$ , ionic solution composition, and microbial activity [Masscheleyn et al., 1991; Bissen and Frimmel, 2003].

Adsorption reactions between As and mineral surfaces are generally the most important control of dissolved As concentration in soil solutions under oxidizing and moderately reducing conditions [Stollenwerk, 2003]. Particularly, metal-(hydr)oxides and clay minerals commonly occurring in soils have been shown to be important adsorbents of As [Pierce and Moore, 1982; Fuller et al., 1993; Manning and Goldberg, 1997a, b; Goldberg, 2002]. The extent of As adsorption mainly depends on the different affinities of As(V) and As(III) for adsorbents present in soils and is limited by the adsorbent's surface site concentration as well as the concentrations of other competing solutes like  $\text{PO}_4^{3-}$ ,  $\text{Si}(\text{OH})_4$ , or  $\text{CO}_3^{2-}$  [Smith et al., 2002b; Dixit and Hering, 2003; Brechbühl et al., 2012; Christl et al., 2012]. Some solutes like  $\text{Ca}^{2+}$  and  $\text{Mg}^{2+}$  have been reported to even enhance the adsorption of As by increasing the positive surface charge of the mineral adsorbent [Stollenwerk, 2003]. Arsenic adsorption by metal-(hydr)oxides and clay minerals mainly proceeds by a ligand exchange reaction, resulting in the formation of an inner-sphere complex [Stollenwerk, 2003]. Thus, pH is one of the most important controls of As(III) and As(V) adsorption as it influences both the aqueous As speciation as well as the speciation of surface functional groups due to protonation and deprotonation reactions [Stollenwerk, 2003]. At pH values less than the point of zero charge (pzc) of the adsorbing mineral the net particle charge is positive, which facilitates the adsorption of anions. Conversely, at pH values greater than the pzc, the net particle charge is negative and thus favors the adsorption of cations. The extent of As adsorption onto Fe(III)- and Al(III)-(hydr)oxides (pzc = 6.3-9.5 and 8.5-8.9, respectively [Cornell and Schwertmann, 2003; Essington, 2004]) is comparable due to their structural similarities. While As(V) adsorption onto both mineral phases decreases with increasing pH, As(III) adsorption is less pH-dependent but often reaches a maximum at higher pH (6.99-9.17). Maximal adsorption of As(V) at low pH is attributed to the more favorable adsorption energies between the more positively charged mineral surface and the negatively charged  $\text{H}_2\text{AsO}_4^-$ , the predominant As(V) species between pH 2.30 and 6.99 (Figure 1.1). Under moderately reducing conditions, As(III) adsorption to metal-(hydr)-

oxides is maximal at high pH values because the neutral form of As(III),  $\text{H}_3\text{AsO}_3^0$ , is more readily able to donate a proton to the mineral surface OH group than the negatively charged As(V) species (Figure 1.1) [Stollenwerk, 2003]. Manganese oxides like birnessite ( $\delta\text{-MnO}_2$ , pzc 3.76 [Essington, 2004]) typically have a low pzc, resulting in a net negative surface charge at neutral pH and hence a negligible As(V) adsorption [Oscarson et al., 1983]. In contrast, the neutral charge of As(III) under most environmentally relevant pH conditions enables its adsorption onto Mn-oxides [Oscarson et al., 1983; Scott and Morgan, 1995]. The adsorption of As onto clay minerals is largely determined by the clay mineral structure. For instance, the aluminol groups present at edges of aluminosilicate clay minerals like kaolinite ( $\text{Al}_2\text{Si}_2\text{O}_5(\text{OH})_4$ ) show an As adsorption behavior similar to that of Al(III)-(hydr)oxides, whereas the silanol groups of the tetrahedral Si layers are not predicted to react with As due to their negative charge at  $\text{pH} > 3.5$  [Stollenwerk, 2003; Essington, 2004]. In addition to pH, the specific surface area of the mineral adsorbent may also affect the extent of As adsorption. Dixit and Hering [2003] showed that the decrease in specific surface area and hence the number of sorption sites that accompanied the transformation of amorphous Fe(III)-(hydr)oxides to more crystalline phases like goethite ( $\alpha\text{-FeOOH}$ ) led to a decrease in As(V) and As(III) adsorption.

Changes in redox potential also have a pronounced effect on the extent of As adsorption to mineral surfaces by changing the redox speciation of As and hence its affinity towards mineral surfaces and by favoring the reductive dissolution of redox-active adsorbents, particularly Fe(III)-(hydr)oxides, at low  $E_h$  [Hering and Kneebone, 2002]. Dissimilatory Fe(III)-reducing bacteria can additionally trigger the dissolution of Fe(III)-(hydr)oxide phases, resulting in a release of the associated As into the soil solution [Nickson et al., 2000]. In some cases, Fe(II) and mixed Fe(II)-Fe(III) phases such as siderite ( $\text{FeCO}_3$ ) and magnetite ( $\text{Fe}_3\text{O}_4$ ) may rapidly form and scavenge the released As to some extent [Dixit and Hering, 2003; Islam et al., 2005; Coker et al., 2006; Jönsson and Sherman, 2008; Tufano and Fendorf, 2008].

The precipitation of authigenic As(V) minerals under oxidizing conditions is limited by their high solubility at slightly acidic or neutral pH, and is thus mostly observed in highly As polluted oxic low-pH environments like mining and industrial sites or sites with natural As anomalies [Hering and Kneebone, 2002; Drahota and Filippi, 2009]. For

instance, scorodite ( $\text{FeAsO}_4 \times 2\text{H}_2\text{O}$ ), a common weathering product of arsenopyrite in mine settings, is unstable under circum-neutral pH and transforms into Fe(III)-(hydr)-oxides sequestering part of the As(V) released from scorodite dissolution [Harvey et al., 2006].

Under strongly reducing conditions and sufficient supply of S from bacterial sulfate reduction, the formation of As-bearing sulfide minerals, particularly orpiment, realgar ( $\text{As}_4\text{S}_4$ ), arsenian pyrite ( $\text{FeAs}_x\text{S}_{2-x}$ ,  $x < 2$ ), or arsenopyrite, may control As solution concentrations [Moore et al., 1988; Rittle et al., 1995; Bostick and Fendorf, 2003; O'Day et al., 2004]. In hydrothermal and geothermal environments, the bacterial respiration of As(V) can also result in the precipitation of realgar and orpiment [Newman et al., 1997; Huber et al., 2000]. These phases are unstable in the presence of oxygen, and microorganisms can catalyze their oxidative dissolution [Gleisner and Herbert, 2002; Chen et al., 2013].

Most wetlands frequently undergo strong changes in the redox potential due to fluctuations in the water table and shifts in biological activity [Reddy and DeLaune, 2008]. In most studies investigating the retention and release of As in wetland soils under field conditions as well as in controlled laboratory experiments, the fate of As was primarily linked to the redox cycling of mineral Fe and S phases [La Force et al., 2000; Fox and Doner, 2003; Beauchemin and Kwong, 2006; Huang and Matzner, 2006; Blodau et al., 2008; Rothwell et al., 2009]. Blodau et al. [2008] investigated the retention and release of As during experimental drought and rewetting cycles in low-As (5-25 mg As  $\text{kg}^{-1}$ ) peat monoliths from the minerotrophic *Schlöppnerbrunnen II* peatland (Germany). Whereas during the rewetting cycle As release was mainly driven by the dissimilatory reduction of Fe(III)-(hydr)oxide phases, the drying cycle in these experiments caused the penetration of oxygen into the peat and the subsequent co-precipitation of As with reactive Fe(III)-(hydr)oxide phases. The substitution of As for S in Fe sulfide minerals or the precipitation of As-bearing sulfide minerals under reducing conditions was found to be of minor importance [Blodau et al., 2008]. Similar results were obtained by Rothwell et al. [2009] who observed a close correlation of solid-phase As and Fe in ombrotrophic peat soils in North West England under oxic conditions, but no indication of sulfide mineral-associated As under reducing conditions.

### 1.2.3. NOM controls

Natural organic matter in soils principally consists of living biomass, undecayed or partially decayed plant and animal tissues, and humus [Stevenson, 1994]. The last pool typically dominates in most agricultural, forest and wetland soils, and consists of humic (humic and fulvic acid, humin) and nonhumic substances (e.g., carbohydrates, nitrogen compounds, lipids, and lignin) [Tipping, 2002]. Humic substances are formed during the process of humification involving microbe-mediated and abiotic reactions transforming plant and animal residues into sugars, quinones, and amino compounds, while nonhumic substances principally serve as metabolic energy source for microbes [Tipping, 2002; Essington, 2004]. The extent in humic substance accumulation strongly depends upon turnover times, climate, vegetation, parent material, topography, and land use [Stevenson, 1994]. Humification rates are typically slow in water saturated soils because the excess moisture retards the decomposition of NOM [Kirk, 2004]. Fossil C/N ratios measured in the *Slave Lake* peatland (Canada), for instance, revealed a peat decomposition rate of 50% after 1,700 years and 65% after 7,500 years for the deeper anoxic peat deposits, corresponding to a cumulative loss of  $19.4 \text{ g C m}^{-2} \text{ year}^{-1}$ , while the average accumulation rate has been  $28.0 \text{ g C m}^{-2} \text{ year}^{-1}$  over the last 1,174 years [Kuhry and Vitt, 1996]. Thus, peatlands almost entirely consist of NOM, of which 20% is typically present as humic substances [Tipping, 2002], and account for approximately half of the soil C pool on earth [Reddy and DeLaune, 2008].

The chemical reactivity of humus as the major pool of NOM in soils is directly related to the quantities and types of organic functional groups and structural components that are present [Essington, 2004]. The vast majority of functional groups in humus contain O or N atoms, including carboxylic (-COOH), phenolic (-OH), or amino groups (-NH<sub>2</sub>) [Stevenson, 1994; Essington, 2004]. Functional groups containing S such as sulfhydryl groups (-SH) are less common (e.g., Thurman [1985]) but are highly reactive in terms of binding soft Lewis acids such as Ag, Hg, or Cu(I) [Smith et al., 2002a].

Owing to its intrinsic heterogeneity, NOM can affect the mobility and bioavailability of As in water and soil environments through various processes including the competition with As for adsorption sites of mineral phases [Grafe et al., 2001; Grafe et al., 2002;

Redman et al., 2002; Simeoni et al., 2003; Bauer and Blodau, 2006], the catalysis of redox reactions with As [Redman et al., 2002; Jiang et al., 2009], the stabilization of As-bearing mineral colloids [Ritter et al., 2006; Bauer and Blodau, 2009], the precipitation of As-bearing minerals [Moore et al., 1988; Rittle et al., 1995], and the direct binding of As [Thanabalasingam and Pickering, 1986; Redman et al., 2002; Buschmann et al., 2006; Wang and Mulligan, 2009; Mikutta and Kretzschmar, 2011; Hoffmann et al., 2013].

Functional groups of NOM vary in their ability to develop charge following protonation or deprotonation reactions [Essington, 2004]. The majority of them, including carboxyl groups, however, are negatively charged at neutral pH. Negatively charged NOM species readily adsorb onto positively charged metal-(hydr)oxides and clay minerals [Stevenson, 1994] and are thus able to displace As from mineral surfaces or hinder its adsorption [Grafe et al., 2001; Simeoni et al., 2003].

The ability of NOM to reduce oxidized metal(oid)s such as As(V), Fe(III), Cr(VI), and U(VI), or to oxidize their reduced forms has been documented in a number of studies [Szilágyi, 1973; Chen et al., 2003; Gu and Chen, 2003; Jiang et al., 2009]. Particularly, quinones moieties were suggested to cause the reversible redox-reactivity of NOM [Scott et al., 1998; Cory and McKnight, 2005; Aeschbacher et al., 2010]. Jiang et al. [2009] reported the oxidation of dissolved As(III) to As(V) by reactive semiquinone radicals formed during microbial or chemical reduction of the humic substance model quinone AQDS (9,10-anthraquinone-2,6-disulfonic acid). This reaction was pH dependent with more As(III) being oxidized at pH 11 ( $\leq 67.3\%$ ) as compared to pH 7 ( $\leq 27.9\%$ ) and pH 3 ( $\leq 18.3\%$ ) [Jiang et al., 2009]. The additionally produced hydroquinones during quinone reduction were shown to reduce As(V) to As(III) at neutral and acidic pH ( $\leq 12\%$ ) but not at alkaline pH [Jiang et al., 2009]. Redman et al. [2002] observed that the redox speciation of As(III) (20-50%) and to a minor extent the one of As(V) was altered during incubation (90 h) of dissolved As(III) or As(V) with 6 different NOM samples ( $10 \text{ mg C L}^{-1}$ ), and suggested that redox-active moieties of NOM like quinones or others [Ratasuk and Nanny, 2007] mediated these As redox changes.

The mobility of As in wetlands is also affected by the ability of NOM molecules to disperse As-bearing minerals like Fe(III)-(hydr)oxides [Liang and Morgan, 1990], thus facilitating the colloidal transport of As in solution [Ritter et al., 2006; Bauer and Blodau,

2009]. This process might be particularly relevant in waters discharging from peatlands under oxic conditions [Bauer and Blodau, 2009].

Under anoxic conditions, NOM can additionally stimulate the microbial activity prompting the reductive dissolution of As-bearing Fe(III)-(hydr)oxides and the formation of As sulfide minerals under sulfate-reducing conditions [Henke, 2009]. Despite significant correlations observed between As and NOM contents in peat soils and peaty sediments [Anawar et al., 2003; Yamazaki et al., 2003; González A. et al., 2006; Bauer et al., 2008; Blodau et al., 2008; Rothwell et al., 2009; Ahmed et al., 2010] as well as in the solution phase [Rothwell et al., 2009; Guo et al., 2011], the direct binding of As to NOM as another potential As sequestration pathway has received little attention. The binding mechanisms proposed for the most prominent As species, As(V) and As(III), are diverse. The majority of studies suggest the formation of ternary As-NOM complexes in which polyvalent cations such as Fe serve as a bridge between As and an organic ligand to explain experimental results [Redman et al., 2002; Buschmann et al., 2006; Ritter et al., 2006; Sharma et al., 2010]. Figure 1.2a shows a schematic representation of a ternary As(V)-Fe(III)-NOM complex in which As(V) is linked to an  $\text{Fe}(\text{O},\text{OH})_6$  octahedron via a single  $\mu$ -oxo bridge (single corner-sharing polyhedrons). The formation of ternary

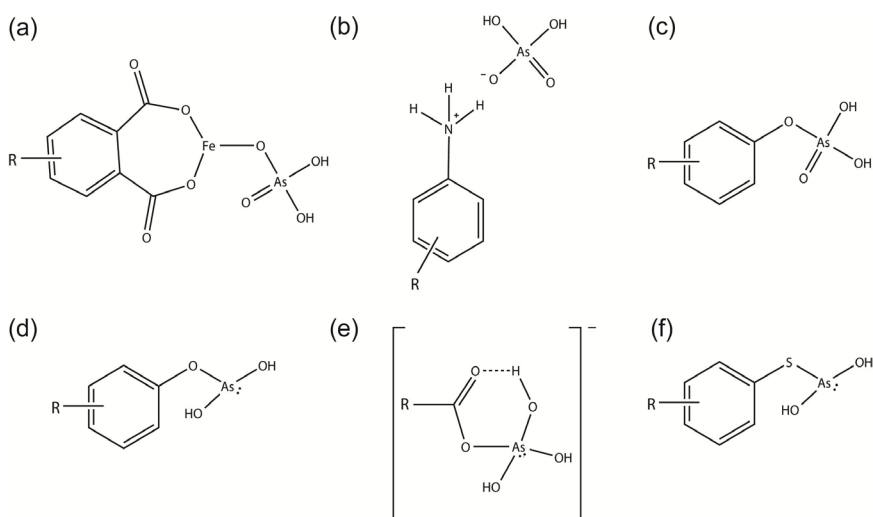


**Figure 1.2.** Schematic representation of complexes formed between As and NOM. (a) Ternary As(V) complex with Fe(III) bridging between As(V) and carboxyl groups of NOM, (b) As(V) bound by a protonated amino group, and (c) a phenolic group. (d) As(III) complexation by a phenolic group, (e) a carboxylic group, and (f) a sulfhydryl group of NOM. The 'R' in each panel represents an alkyl or aryl group.

complexes of As(V) was recently confirmed by Mikutta and Kretzschmar [2011] who spiked humic substances (humic and fulvic acid) with 1 wt.% Fe(III) and reacted the resulting Fe(III)-humate and -fulvate complexes with As(V) at pH 7 (molar Fe/As ~10). The local coordination environment of As and Fe were subsequently studied by means of X-ray absorption spectroscopy (XAS). Results revealed that 70-90% of As(V) was bound to the formed Fe(III)-NOM complex via inner-sphere complexation. The interatomic As-Fe distance in these complexes was found to be 3.30 Å, consistent with a monodentate binuclear ( $^2\text{C}$ ) and monodentate mononuclear ( $^1\text{V}$ ) complex stabilized by H-bonds [Mikutta and Kretzschmar, 2011]. The formation of ternary As(III)-Fe(III)-NOM complexes has been a matter of debate until very recently. For example, Liu et al. [2011] observed the association of As(III) with Fe(III)-loaded NOM based on the co-elution of As, Fe, and NOM during size exclusion chromatography coupled to UV/Vis absorption spectroscopy and inductively coupled plasma-mass spectrometry. However, a clear separation between colloidal Fe(III) and organic Fe(III) complexes was not possible, and a direct association of As(III) and NOM could not be excluded. Other studies faced similar problems [Liu and Cai, 2010; Sharma et al., 2011]. The first spectroscopic evidence for ternary As(III)-Fe(III)-NOM complex formation was provided by Hoffmann et al. [2013] who reacted peat (40-250  $\mu\text{m}$  size fraction, 1.0 g Fe  $\text{kg}^{-1}$ ) with 0-15 g Fe  $\text{kg}^{-1}$  at pH <2, and subsequently equilibrated the Fe(III) complexes formed with 900 mg As  $\text{kg}^{-1}$  peat at pH 7.0, 8.4, and 8.8 (molar Fe/As ratio ~8-46). The solid-phase speciation of Fe and As studied by means of XAS revealed that (i) the majority of Fe in the peat was present as mononuclear Fe(III) complexes ( $R_{\text{Fe-C}} = 2.82\text{-}2.88 \text{ \AA}$ ) accompanied by small Fe(III) clusters ( $R_{\text{Fe-Fe}} = 3.25\text{-}3.46 \text{ \AA}$ ) at high pH values and elevated Fe contents, and (ii) about 50 to 90% of As(III) formed bidentate mononuclear ( $R_{\text{As-Fe}} = 2.88\text{-}2.94 \text{ \AA}$ ) and monodentate binuclear ( $R_{\text{As-Fe}} = 3.35\text{-}3.41 \text{ \AA}$ ) complexes with these Fe (III) species. Other polyvalent cations like Al(III) were demonstrated not to serve as a cation bridge between As and NOM [Buschmann et al., 2006].

In the last decades, several functional groups of NOM were hypothesized to promote potential binding sites for As. Thanabalasingam and Pickering [1986] investigated the effect of either EDTA,  $\text{F}^-$ ,  $\text{PO}_4^{3-}$ ,  $\text{SO}_4^{2-}$ , or  $\text{CO}_3^{2-}$  on the adsorption of As(III) and As(V) (10  $\mu\text{mol L}^{-1}$ ) by two humic acids at pH 5.5. Since more than half of the complexed

As(III) and As(V) was released from the humic acids by each added anion, the authors suggested the outer-sphere binding of As(III) and As(V) to strongly basic amino groups (Figure 1.2b).

In contrast to outer-sphere complexation, several As-NOM inner-sphere binding mechanisms have been proposed by Buschmann et al. [2006]. Using an equilibrium dialysis method, the binding of As(III) and As(V) onto two humic acids was determined at four different pH values (4.6-8.4) and different As/NOM ratios. Buschmann et al. [2006] suggested a ligand exchange reaction of As(V) and As(III) with phenolate groups of NOM (Figure 1.2c and 1.2d), the formation of an adduct between As(III) and carboxylate groups stabilized by H-bonding (Figure 1.2e), as well as hydrophobic As(III)-NOM interactions. At all pH values, As(V) was more strongly bound than As(III), which was suggested to be caused by the higher formal charge of As(V), a stabilization through the phenolate entity, additional chelation by other functional groups, and/or H-bridges [Buschmann et al., 2006]. In addition, the results implied that under environmentally relevant conditions (pH 7, NOM = 5 mg L<sup>-1</sup>, As(V) = 67 nM) about 10% of As(V) would be bound to NOM, whereas the binding of As(III) to NOM (>10 %) would be only relevant at very low As(III)/NOM ratios [Buschmann et al., 2006].

The reaction of As(III) with sulfhydryl groups of NOM could be another plausible inner-sphere binding mechanism (Figure 1.2f). Particularly in the metabolism of higher plants, the complexation of As(III) by sulfhydryl groups of phytochelatins is a well-documented detoxification mechanism [Zhao et al., 2009]. The formation of a trigonal-pyramidal complex with sulfhydryl groups of NOM and As(III) was previously verified by XAS for a keratin-rich biomass [Teixeira and Ciminelli, 2005] as well as several plant species [Pickering et al., 2000; Seyfferth et al., 2011; Castillo-Michel et al., 2012]. Since reduced organic S can account for 14-87% of total S in peatlands depending on the prevailing redox conditions [Xia et al., 1998; Skyllberg et al., 2000; Zhao et al., 2006; Prietzel et al., 2007; Prietzel et al., 2009], the reaction between sulfhydryl groups and As(III) could be a potentially important binding mechanism for As in NOM-rich anoxic environments.



### 1.3. Research objective and approach

At the beginning of this project, the binding of As to NOM was poorly understood (Sections 1.1 and 1.2.3) and hence our understanding of the biogeochemical As cycle in NOM-rich environments essentially incomplete. The major goal of this project was thus to provide fundamental data on (i) the relevance of NOM for As binding at an As-enriched field site characterized by a high abundance of NOM and low mineral matter content, (ii) the general mechanism(s) of As binding to NOM, and (iii) the effect of changing redox conditions on the fate of As in NOM-rich environments.

Therefore, the speciation and distribution of As was investigated at the naturally As-enriched minerotrophic peatland *Gola di Lago* (canton Ticino, Switzerland). In a previous study focusing on the spatial distribution of As, Se, and U at this site, González A. et al. [2006] observed that (i) up to 73% of extractable As was associated with NOM in nondried peat, (ii) only a minor part of As was associated with the metal-(hydr)-oxide fraction, and that (iii) an intermittent stream entering the peatland contained up to 408  $\mu\text{g As L}^{-1}$  while the permanent stream leaving the peatland only contained  $<2 \mu\text{g As L}^{-1}$ . These findings suggested that the *Gola di Lago* peatland represents a sink for As and that NOM is an important sorbent for As. The peatland was therefore ideally suited to study the mechanism(s) and relevance of NOM for the retention of As in NOM-rich environments using synchrotron-based techniques such as bulk X-ray absorption spectroscopy (XAS), microfocused X-ray absorption spectroscopy ( $\mu$ -XAS), and microfocused X-ray fluorescence ( $\mu$ -XRF) spectrometry. These techniques allow for a nondestructive analysis of crystalline and noncrystalline forms of many different elements occurring in trace or abundant concentrations in soil and mineral samples with little or no sample pretreatment requirements [Kelly et al., 2008]. In particular, bulk XAS analyses can be used to determine the average coordination environment of a specific element within a sample, while  $\mu$ -XRF spectrometry and  $\mu$ -XAS reveal information on its spatial distribution, elemental correlations, and chemical speciation at the microscale. The XAS spectra collected can be subdivided into two regions: the X-ray absorption near-edge structure (XANES) region, which provides information on the oxidation-state of the X-ray absorbing atom as well as its coordination geometry, and the extended X-ray

absorption fine structure (EXAFS) region, which yields information on the element's local molecular structure (e.g., coordination numbers, interatomic distances, bond disorder) [Kelly et al., 2008]. The result of  $\mu$ -XRF spectrometry is a set of maps, one for each element or fluorescence line observed, that enables to locate a particular element within a sample and to correlate it with other trace and major elements by creating tricolor (RGB) maps and scatterplots [Manceau et al., 2002]. The combination of bulk XAS with  $\mu$ -XRF spectrometry and  $\mu$ -XAS analyses is thus ideally suited to reveal an element's (spatial) speciation and distribution in a complex sample.

In the first part of this thesis (Chapter 2), the solid-phase speciation of As and Fe was studied in selected near-surface (0-41 cm) and deep peat layer samples (150-250 cm) of four peat cores collected close to the As-rich intermittent stream of the *Gola di Lago* peatland. By analyzing bulk As *K*-edge XANES and EXAFS spectra, for example, by shell-fit and wavelet-transform analyses, the average oxidation state and local coordination environment of As was investigated. Major As and Fe species were then quantified by linear combination fitting (LCF) of bulk As and Fe *K*-edge EXAFS spectra following a combination of principal component analyses and target transformation testing (PCA-TT). Based on the spectroscopic results, the relevance of the identified As-NOM interaction mechanism was discussed for NOM-rich soils and sediments.

In the second part (Chapter 3), the microscale distribution and speciation of As was investigated in thin sections of selected *Gola di Lago* peat samples. According to the findings of the proceeding study (Chapter 2), the specific objectives of this study were to (i) assess the size and distribution of As sulfide minerals in the near-surface peat layers, (ii) investigate the distribution patterns of the NOM-associated As in the deep peat layers, and (iii) identify minor As species using  $\mu$ -XRF spectrometry and  $\mu$ -XAS. From these findings, potential formation processes of selected As species present in the *Gola di Lago* peatland were inferred.

The third part (Chapter 4) focuses on the oxidation kinetics of the NOM-associated As and realgar in *Gola di Lago* peat. The solid-phase speciation of As, Fe, and S was determined with bulk XAS to (i) investigate the oxidation-induced loss of the NOM-associated As and realgar, (ii) test if their oxidation is controlled by abiotic or biotic

processes, and (iii) compare observed with predicted oxidation rates. Additionally, selective extractions were used to track the release and speciation of dissolved As in the peat as a function of time. Based on these findings, implications for the fate of As under prolonged oxidizing conditions in the *Gola di Lago* peatland and other As-rich wetlands are discussed.

In the last part of this thesis (Chapter 5), all experimental results will be discussed with regard to the fate of As in NOM-dominated environmental systems, including recent findings of a companion Ph.D. project of the Soil Chemistry Group at ETH Zurich on As(III)-NOM interactions under reducing conditions [Hoffmann, 2013]. The thesis will be closed by an outlook on further research directions.

## References

- Adriano, D. C. (2001) *Trace elements in terrestrial environments. Biogeochemistry, bioavailability, and risks of metals*. Springer: New York.
- Aeschbacher, M., Sander, M., Schwarzenbach, R. P. (2010) Novel electrochemical approach to assess the redox properties of humic substances. *Environ. Sci. Technol.* 44, 87-93.
- Ahmed, F., Bibi, M. H., Ishiga, H., Fukushima, T., Maruoka, T. (2010) Geochemical study of arsenic and other trace elements in groundwater and sediments of the Old Brahmaputra river plain, Bangladesh. *Environ. Earth Sci.* 60, 1303-1316.
- Anawar, H. M., Akai, J., Komaki, K., Terao, H., Yoshioka, T., Ishizuka, T., Safiullah, S., Kato, K. (2003) Geochemical occurrence of arsenic in groundwater of Bangladesh: Sources and mobilization processes. *J. Geochem. Explor.* 77, 109-131.
- Ballantyne, J. M., Moore, J. N. (1988) Arsenic geochemistry in geothermal systems. *Geochim. Cosmochim. Acta* 52, 475-483.
- Bauer, M., Blodau, C. (2006) Mobilization of arsenic by dissolved organic matter from iron oxides, soils and sediments. *Sci. Total Environ.* 354, 179-190.
- Bauer, M., Blodau, C. (2009) Arsenic distribution in the dissolved, colloidal and particulate size fraction of experimental solutions rich in dissolved organic matter and ferric iron. *Geochim. Cosmochim. Acta* 73, 529-542.
- Bauer, M., Fulda, B., Blodau, C. (2008) Groundwater derived arsenic in high carbonate wetland soils: Sources, sinks, and mobility. *Sci. Total Environ.* 401, 109-120.
- Beauchemin, S., Kwong, Y. T. J. (2006) Impact of redox conditions on arsenic mobilization from tailings in a wetland with neutral drainage. *Environ. Sci. Technol.* 40, 6297-6303.
- Berg, M., Stengel, C., Trang, P. T. K., Viet, P. H., Sampson, M. L., Leng, M., Samreth, S., Fredericks, D. (2007) Magnitude of arsenic pollution in the Mekong and Red River Deltas - Cambodia and Vietnam. *Sci. Total Environ.* 372, 413-425.
- Berg, M., Tran, H. C., Nguyen, T. C., Pham, H. V., Schertenleib, R., Giger, W. (2001) Arsenic contamination of groundwater and drinking water in Vietnam: A human health threat. *Environ. Sci. Technol.* 35, 2621-2626.
- Bissen, M., Frimmel, F. H. (2003) Arsenic - a review. Part 1: Occurrence, toxicity, speciation, mobility. *Acta Hydrochim. Hydrobiol.* 31, 9-18.
- Blodau, C., Fulda, B., Bauer, M., Knorr, K.-H. (2008) Arsenic speciation and turnover in intact organic soil mesocosms during experimental drought and rewetting. *Geochim. Cosmochim. Acta* 72, 3991-4007.
- Bostick, B. C., Fendorf, S. (2003) Arsenite sorption on troilite (FeS) and pyrite (FeS<sub>2</sub>). *Geochim. Cosmochim. Acta* 67, 909-921.

- Brechbühl, Y., Christl, I., Elzinga, E. J., Kretzschmar, R. (2012) Competitive sorption of carbonate and arsenic to hematite: Combined ATR-FTIR and batch experiments. *J. Colloid Interface Sci.* 377, 313-321.
- Buschmann, J., Kappeler, A., Lindauer, U., Kistler, D., Berg, M., Sigg, L. (2006) Arsenite and arsenate binding to dissolved humic acids: Influence of pH, type of humic acid, and aluminum. *Environ. Sci. Technol.* 40, 6015-6020.
- Castillo-Michel, H., Hernandez-Viezcas, J. A., Servin, A., Peralta-Videa, J. R., Gardea-Torresdey, J. L. (2012) Arsenic localization and speciation in the root-soil interface of the desert plant *Prosopis juliflora-velutina*. *Appl. Spectrosc.* 66, 719-727.
- Chen, J., Gu, B. H., Royer, R. A., Burgos, W. D. (2003) The roles of natural organic matter in chemical and microbial reduction of ferric iron. *Sci. Total Environ.* 307, 167-178.
- Chen, P., Yan, L., Yue, X., Li, H. (2013) Optimal parameters for bioleaching of realgar using *Acidithiobacillus ferrooxidans* under different growth conditions and mathematical analysis. *Biocatal. Biotransform.* 31, 33-41.
- Christl, I., Brechbühl, Y., Graf, M., Kretzschmar, R. (2012) Polymerization of silicate on hematite surfaces and its influence on arsenic sorption. *Environ. Sci. Technol.* 46, 13235-13243.
- Cloy, J. M., Farmer, J. G., Graham, M. C., Mackenzie, A. B. (2009) Retention of As and Sb in ombrotrophic peat bogs: Records of As, Sb, and Pb deposition at four Scottish sites. *Environ. Sci. Technol.* 43, 1756-1762.
- Coker, V. S., Gault, A. G., Pearce, C. I., Van der Laan, G., Telling, N. D., Charnock, J. M., Polya, D. A., Lloyd, J. R. (2006) XAS and XMCD evidence for species-dependent partitioning of arsenic during microbial reduction of ferrihydrite to magnetite. *Environ. Sci. Technol.* 40, 7745-7750.
- Cornell, R. M., Schwertmann, U. (2003) *The iron oxides: Structures, properties, reactions, occurrences and uses*. Wiley-VCH: Weinheim.
- Cory, R. M., McKnight, D. M. (2005) Fluorescence spectroscopy reveals ubiquitous presence of oxidized and reduced quinones in dissolved organic matter. *Environ. Sci. Technol.* 39, 8142-8149.
- Cullen, W. R., Reimer, K. J. (1989) Arsenic speciation in the environment. *Chem. Rev.* 89, 713-764.
- Dixit, S., Hering, J. G. (2003) Comparison of arsenic(V) and arsenic(III) sorption onto iron oxide minerals: Implications for arsenic mobility. *Environ. Sci. Technol.* 37, 4182-4189.
- Drahota, P., Filippi, M. (2009) Secondary arsenic minerals in the environment: A review. *Environ. Int.* 35, 1243-1255.
- Essington, M. E. (2004) *Soil and water chemistry: An integrative approach*. CRC Press: Boca Raton.
- Fendorf, S., Michael, H. A., van Geen, A. (2010) Spatial and temporal variations of groundwater arsenic in South and Southeast Asia. *Science* 328, 1123-1127.

- Fox, P. M., Doner, H. E. (2003) Accumulation, release, and solubility of arsenic, molybdenum, and vanadium in wetland sediments. *J. Environ. Qual.* 32, 2428-2435.
- Francesconi, K. A., Kuehnelt, D. (2002) Arsenic compounds in the environment. In Frankenberger, W. T. (Ed.) *Environmental chemistry of arsenic*. Marcel Dekker: New York, pp. 51-94.
- Frank, J. (2005) Determination of arsenic and arsenic species in ombrotrophic peat bogs from Finland. Ph.D. thesis, Institut für Geowissenschaften, Ruprecht-Karls-Universität Heidelberg.
- Fuller, C. C., Davis, J. A., Waychunas, G. A. (1993) Surface chemistry of ferrihydrite. Part 2: Kinetics of arsenate adsorption and coprecipitation. *Geochim. Cosmochim. Acta* 57, 2271-2282.
- Gleisner, M., Herbert, R. B. (2002) Sulfide mineral oxidation in freshly processed tailings: Batch experiments. *J. Geochem. Explor.* 76, 139-153.
- Goldberg, S. (2002) Competitive adsorption of arsenate and arsenite on oxides and clay minerals. *Soil Sci. Soc. Am. J.* 66, 413-421.
- González A., Z. I., Krachler, M., Cheburkin, A. K., Shoty, W. (2006) Spatial distribution of natural enrichments of arsenic, selenium, and uranium in a minerotrophic peatland, Gola di Lago, canton Ticino, Switzerland. *Environ. Sci. Technol.* 40, 6568-6574.
- Grafe, M., Eick, M. J., Grossl, P. R. (2001) Adsorption of arsenate(V) and arsenite(III) on goethite in the presence and absence of dissolved organic carbon. *Soil Sci. Soc. Am. J.* 65, 1680-1687.
- Grafe, M., Eick, M. J., Grossl, P. R., Saunders, A. M. (2002) Adsorption of arsenate and arsenite on ferrihydrite in the presence and absence of dissolved organic carbon. *J. Environ. Qual.* 31, 1115-1123.
- Greenleaf, J. E., Cumbal, L., Staina, I., Sengupta, A. K. (2003) Abiotic As(III) oxidation by hydrated Fe(III) oxide (HFO) microparticles in a plug flow columnar configuration. *Process Saf. Environ. Prot.* 81, 87-98.
- Gu, B. H., Chen, J. (2003) Enhanced microbial reduction of Cr(VI) and U(VI) by different natural organic matter fractions. *Geochim. Cosmochim. Acta* 67, 3575-3582.
- Guo, H., Zhang, B., Zhang, Y. (2011) Control of organic and iron colloids on arsenic partition and transport in high arsenic groundwaters in the Hetao basin, Inner Mongolia. *Appl. Geochem.* 26, 360-370.
- Harty, E. M., Lator, G. C., Robotham, H. (1991) Elemental concentrations in Jamaican peat. *Environ. Geochem. Health* 13, 197-202.
- Harvey, M. C., Schreiber, M. E., Rimstidt, J. D., Griffith, M. M. (2006) Scorodite dissolution kinetics: Implications for arsenic release. *Environ. Sci. Technol.* 40, 6709-6714.
- Henke, K. R. (2009) *Arsenic: Environmental chemistry, health threats, and waste treatment*. John Wiley & Sons Ltd: Chichester.
- Hering, J. G., Kneebone, P. E. (2002) Biogeochemical controls on arsenic occurrence and mobility in water supplies. In Frankenberger, W. T. (Ed.) *Environmental chemistry of arsenic*. Marcel Dekker: New York, pp. 155-181.

- Hoffmann, M. (2013) Mechanisms of arsenite binding to natural organic matter. Ph.D. thesis, Department of Environmental Systems Science, ETH Zurich.
- Hoffmann, M., Mikutta, C., Kretzschmar, R. (2013) Arsenite binding to natural organic matter: Spectroscopic evidence for ligand exchange and ternary complex formation. *Environ. Sci. Technol.* *47*, 12165-12173.
- Huang, J.-H., Matzner, E. (2006) Dynamics of organic and inorganic arsenic in the solution phase of an acidic fen in Germany. *Geochim. Cosmochim. Acta* *70*, 2023-2033.
- Huber, R., Huber, H., Stetter, K. O. (2000) Towards the ecology of hyperthermophiles: Biotopes, new isolation strategies and novel metabolic properties. *FEMS Microbiol. Rev.* *24*, 615-623.
- Hvatum, O. O., Bolviken, B., Steinnes, E. (1983) Heavy-metals in Norwegian ombrotrophic bogs. *Ecol. Bull.*, 351-356.
- Inskeep, W. P., McDermott, T. R., Fendorf, S. (2002) Arsenic (V)/(III) cycling in soils and natural waters: Chemical and microbiological processes. In Frankenberger, W. T. (Ed.) *Environmental chemistry of arsenic*. Marcel Dekker: New York, pp. 183-215.
- Islam, F. S., Pederick, R. L., Gault, A. G., Adams, L. K., Polya, D. A., Charnock, J. M., Lloyd, J. R. (2005) Interactions between the Fe(III)-reducing bacterium *Geobacter sulfurreducens* and arsenate, and capture of the metalloid by biogenic Fe(II). *Appl. Environ. Microbiol.* *71*, 8642-8648.
- Jiang, J., Bauer, I., Paul, A., Kappler, A. (2009) Arsenic redox changes by microbially and chemically formed semiquinone radicals and hydroquinones in a humic substance model quinone. *Environ. Sci. Technol.* *43*, 3639-3645.
- Jönsson, J., Sherman, D. M. (2008) Sorption of As(III) and As(V) to siderite, green rust (fougerite) and magnetite: Implications for arsenic release in anoxic groundwaters. *Chem. Geol.* *255*, 173-181.
- Kelly, S. D., Hesterberg, D., Ravel, B. (2008) Analysis of soils and minerals using X-ray absorption spectroscopy. In Ulery, A. L., Drees, L. R. (Eds.) *Methods of soil analysis. Part 5: Mineralogical methods*. Soil Science Society of America: Madison, pp. 387-463.
- Kirk, G. (2004) *The biogeochemistry of submerged soils*. Wiley: Chichester.
- Kuhry, P., Vitt, D. H. (1996) Fossil carbon/nitrogen ratios as a measure of peat decomposition. *Ecology* *77*, 271-275.
- La Force, M. J., Hansel, C. M., Fendorf, S. (2000) Arsenic speciation, seasonal transformations, and co-distribution with iron in a mine waste-influenced palustrine emergent wetland. *Environ. Sci. Technol.* *34*, 3937-3943.
- Liang, L., Morgan, J. J. (1990) Chemical aspects of iron oxide coagulation in water: Laboratory studies and implications for natural systems. *Aquat. Sci.* *52*, 32-55.
- Liu, G., Cai, Y. (2010) Complexation of arsenite with dissolved organic matter: Conditional distribution coefficients and apparent stability constants. *Chemosphere* *81*, 890-896.

- Liu, G., Fernandez, A., Cai, Y. (2011) Complexation of arsenite with humic acid in the presence of ferric iron. *Environ. Sci. Technol.* 45, 3210-3216.
- Lomax, C., Liu, W.-J., Wu, L., Xue, K., Xiong, J., Zhou, J., McGrath, S. P., Meharg, A. A., Miller, A. J., Zhao, F.-J. (2012) Methylated arsenic species in plants originate from soil microorganisms. *New Phytol.* 193, 665-672.
- Manceau, A., Marcus, M. A., Tamura, N. (2002) Quantitative speciation of heavy metals in soils and sediments by synchrotron X-ray techniques. In Fenter, P. A., Rivers, M. L., Sturchio, N. C., Sutton, S. R. (Eds.) *Applications of synchrotron radiation in low-temperature geochemistry and environmental sciences*. Mineralogical Society of America: Washington, DC, pp. 341-428.
- Mandal, B. K., Suzuki, K. T. (2002) Arsenic round the world: A review. *Talanta* 58, 201-235.
- Manning, B. A., Goldberg, S. (1997a) Adsorption and stability of arsenic(III) at the clay mineral-water interface. *Environ. Sci. Technol.* 31, 2005-2011.
- Manning, B. A., Goldberg, S. (1997b) Arsenic(III) and arsenic(V) adsorption on three California soils. *Soil Sci.* 162, 886-895.
- Masscheleyn, P. H., Delaune, R. D., Patrick, W. H. (1991) Effect of redox potential and pH on arsenic speciation and solubility in a contaminated soil. *Environ. Sci. Technol.* 25, 1414-1419.
- McArthur, J. M., Banerjee, D. M., Hudson-Edwards, K. A., Mishra, R., Purohit, R., Ravenscroft, P., Cronin, A., Howarth, R. J., Chatterjee, A., Talukder, T., Lowry, D., Houghton, S., Chadha, D. K. (2004) Natural organic matter in sedimentary basins and its relation to arsenic in anoxic ground water: The example of West Bengal and its worldwide implications. *Appl. Geochem.* 19, 1255-1293.
- Mikutta, C., Kretzschmar, R. (2011) Spectroscopic evidence for ternary complex formation between arsenate and ferric iron complexes of humic substances. *Environ. Sci. Technol.* 45, 9550-9557.
- Minkinen, E., Yliruokanen, I. (1978) The arsenic distribution in Finnish peat bogs. *Kemia Kemi* 5, 331-335.
- Moore, J. N., Ficklin, W. H., Johns, C. (1988) Partitioning of arsenic and metals in reducing sulfidic sediments. *Environ. Sci. Technol.* 22, 432-437.
- National Wetlands Working Group (1997) *The Canadian wetland classification system*. Wetland Research Centre, University of Waterloo: Waterloo.
- Newman, D. K., Beveridge, T. J., Morel, F. M. M. (1997) Precipitation of arsenic trisulfide by *Desulfotomaculum auripigmentum*. *Appl. Environ. Microbiol.* 63, 2022-2028.
- Nickson, R. T., McArthur, J. M., Ravenscroft, P., Burgess, W. G., Ahmed, K. M. (2000) Mechanism of arsenic release to groundwater, Bangladesh and West Bengal. *Appl. Geochem.* 15, 403-413.



- Nordstrom, D. K., Archer, D. G. (2003) Arsenic thermodynamic data and environmental geochemistry. In Welch, A. H., Stollenwerk, K. G. (Eds.) *Arsenic in ground waters: Geochemistry and occurrence*. Kluwer Academic Publications: Boston, pp. 1-25.
- O'Day, P. A., Vlassopoulos, D., Root, R., Rivera, N. (2004) The influence of sulfur and iron on dissolved arsenic concentrations in the shallow subsurface under changing redox conditions. *Proc. Natl. Acad. Sci. USA* 101, 13703-13708.
- Oremland, R. S., Stolz, J. F., Hollibaugh, J. T. (2004) The microbial arsenic cycle in Mono Lake, California. *FEMS Microbiol. Ecol.* 48, 15-27.
- Oscarson, D. W., Huang, P. M., Liaw, W. K., Hammer, U. T. (1983) Kinetics of oxidation of arsenite by various manganese dioxides. *Soil Sci. Soc. Am. J.* 47, 644-648.
- Pickering, I. J., Prince, R. C., George, M. J., Smith, R. D., George, G. N., Salt, D. E. (2000) Reduction and coordination of arsenic in Indian mustard. *Plant Physiol.* 122, 1171-1177.
- Pierce, M. L., Moore, C. B. (1982) Adsorption of arsenite and arsenate on amorphous iron hydroxide. *Water Res.* 16, 1247-1253.
- Planer-Friedrich, B., Suess, E., Scheinost, A. C., Wallschläger, D. (2010) Arsenic speciation in sulfidic waters: Reconciling contradictory spectroscopic and chromatographic evidence. *Anal. Chem.* 82, 10228-10235.
- Plant, J. A., Kinniburgh, D. G., Smedley, P. L., Fordyce, F. M., Klinck, B. A. (2004) Arsenic and selenium. In Lollar, B. S. (Ed.) *Treatise on geochemistry: Environmental geochemistry*. Elsevier: Amsterdam, pp. 17-66.
- Prietzl, J., Thieme, J., Salomé, M., Knicker, H. (2007) Sulfur K-edge XANES spectroscopy reveals differences in sulfur speciation of bulk soils, humic acid, fulvic acid, and particle size separates. *Soil Biol. Biochem.* 39, 877-890.
- Prietzl, J., Tyufekchieva, N., Eusterhues, K., Koegel-Knabner, I., Thieme, J., Paterson, D., McNulty, I., de Jonge, M., Eichert, D., Salomé, M. (2009) Anoxic versus oxic sample pretreatment: Effects on the speciation of sulfur and iron in well-aerated and wetland soils as assessed by X-ray absorption near-edge spectroscopy (XANES). *Geoderma* 153, 318-330.
- Qureshi, S., Richards, B. K., McBride, M. B., Baveye, P., Steenhuis, T. S. (2003) Temperature and microbial activity effects on trace element leaching from metalliferous peats. *J. Environ. Qual.* 32, 2067-2075.
- Ratasuk, N., Nanny, M. A. (2007) Characterization and quantification of reversible redox sites in humic substances. *Environ. Sci. Technol.* 41, 7844-7850.
- Reddy, K. R., DeLaune, R. D. (2008) *Biogeochemistry of wetlands: Science and applications*. CRC Press: Boca Raton.
- Redman, A. D., Macalady, D. L., Ahmann, D. (2002) Natural organic matter affects arsenic speciation and sorption onto hematite. *Environ. Sci. Technol.* 36, 2889-2896.
- Ritter, K., Aiken, G. R., Ranville, J. F., Bauer, M., Macalady, D. L. (2006) Evidence for the aquatic binding of arsenate by natural organic matter-suspended Fe(III). *Environ. Sci. Technol.* 40, 5380-5387.

- Rittle, K. A., Drever, J. I., Colberg, P. J. S. (1995) Precipitation of arsenic during bacterial sulfate reduction. *Geomicrobiol. J.* 13, 1-11.
- Rochette, E. A., Bostick, B. C., Li, G. C., Fendorf, S. (2000) Kinetics of arsenate reduction by dissolved sulfide. *Environ. Sci. Technol.* 34, 4714-4720.
- Rosen, B. P. (2002) Biochemistry of arsenic detoxification. *FEBS Lett.* 529, 86-92.
- Rothwell, J. J., Taylor, K. G., Ander, E. L., Evans, M. G., Daniels, S. M., Allott, T. E. H. (2009) Arsenic retention and release in ombrotrophic peatlands. *Sci. Total Environ.* 407, 1405-1417.
- Rothwell, J. J., Taylor, K. G., Chenery, S. R. N., Cundy, A. B., Evans, M. G., Allott, T. E. H. (2010) Storage and behavior of As, Sb, Pb, and Cu in ombrotrophic peat bogs under contrasting water table conditions. *Environ. Sci. Technol.* 44, 8497-8502.
- Schell, W. R. (1986) Deposited atmospheric chemicals. *Environ. Sci. Technol.* 20, 847-853.
- Scott, D. T., McKnight, D. M., Blunt-Harris, E. L., Kolesar, S. E., Lovley, D. R. (1998) Quinone moieties act as electron acceptors in the reduction of humic substances by humics-reducing microorganisms. *Environ. Sci. Technol.* 32, 2984-2989.
- Scott, M. J., Morgan, J. J. (1995) Reactions at oxide surfaces. 1. Oxidation of As(III) by synthetic birnessite. *Environ. Sci. Technol.* 29, 1898-1905.
- Seyfferth, A. L., Webb, S. M., Andrews, J. C., Fendorf, S. (2011) Defining the distribution of arsenic species and plant nutrients in rice (*Oryza sativa* L.) from the root to the grain. *Geochim. Cosmochim. Acta* 75, 6655-6671.
- Sharma, P., Ofner, J., Kappler, A. (2010) Formation of binary and ternary colloids and dissolved complexes of organic matter, Fe and As. *Environ. Sci. Technol.* 44, 4479-4485.
- Sharma, P., Rolle, M., Kocar, B., Fendorf, S., Kappler, A. (2011) Influence of natural organic matter on As transport and retention. *Environ. Sci. Technol.* 45, 546-553.
- Shotyk, W. (1988) Review of the inorganic geochemistry of peats and peatland waters. *Earth Sci. Rev.* 25, 95-176.
- Shotyk, W. (1996) Natural and anthropogenic enrichments of As, Cu, Pb, Sb, and Zn in ombrotrophic versus minerotrophic peat bog profiles, Jura Mountains, Switzerland. *Water Air Soil Pollut.* 90, 375-405.
- Shrestha, R. R., Shrestha, M. P., Upadhyay, N. P., Pradhan, R., Khadka, R., Maskey, A., Maharjan, M., Tuladhar, S., Dahal, B. M., Shrestha, K. (2003) Groundwater arsenic contamination, its health impact and mitigation program in Nepal. *J. Environ. Sci. Heal.* A 38, 185-200.
- Silamikele, I., Klavins, M., Nikodemus, O. (2011) Major and trace element distribution in the peat from ombrotrophic bogs in Latvia. *J. Environ. Sci. Heal.* A 46, 805-812.
- Simeoni, M. A., Batts, B. D., McRae, C. (2003) Effect of groundwater fulvic acid on the adsorption of arsenate by ferrihydrite and gibbsite. *Appl. Geochem.* 18, 1507-1515.

- Skylberg, U., Xia, K., Bloom, P. R., Nater, E. A., Bleam, W. F. (2000) Binding of mercury(II) to reduced sulfur in soil organic matter along upland-peat soil transects. *J. Environ. Qual.* 29, 855-865.
- Smedley, P. L., Kinniburgh, D. G. (2002) A review of the source, behaviour and distribution of arsenic in natural waters. *Appl. Geochem.* 17, 517-568.
- Smith, D. S., Bell, R. A., Kramer, J. R. (2002a) Metal speciation in natural waters with emphasis on reduced sulfur groups as strong metal binding sites. *Comp. Biochem. Phys. C* 133, 65-74.
- Smith, E., Naidu, R., Alston, A. M. (2002b) Chemistry of inorganic arsenic in soils: II. Effect of phosphorus, sodium, and calcium on arsenic sorption. *J. Environ. Qual.* 31, 557-563.
- Stevenson, F. J. (1994) *Humus chemistry: Genesis, composition, reactions*. Wiley: New York.
- Stollenwerk, K. G. (2003) Geochemical processes controlling transport of arsenic in groundwater: A review of adsorption. In Welch, A. H., Stollenwerk, K. G. (Eds.) *Arsenic in ground waters: Geochemistry and occurrence*. Kluwer Academic Publications: Boston, pp. 67-100.
- Suess, E., Planer-Friedrich, B. (2012) Thioarsenate formation upon dissolution of orpiment and arsenopyrite. *Chemosphere* 89, 1390-1398.
- Swartz, C. H., Blute, N. K., Badruzzman, B., Ali, A., Brabander, D., Jay, J., Besancon, J., Islam, S., Hemond, H. F., Harvey, C. F. (2004) Mobility of arsenic in a Bangladesh aquifer: Inferences from geochemical profiles, leaching data, and mineralogical characterization. *Geochim. Cosmochim. Acta* 68, 4539-4557.
- Szilágyi, M. (1973) Redox properties and determination of normal potential of peat-water system. *Soil Sci.* 115, 434-437.
- Szramek, K., Walter, L. M., McCall, P. (2004) Arsenic mobility in groundwater/surface water systems in carbonate-rich Pleistocene glacial drift aquifers (Michigan). *Appl. Geochem.* 19, 1137-1155.
- Teixeira, M. C., Ciminelli, V. S. T. (2005) Development of a biosorbent for arsenite: Structural modeling based on X-ray spectroscopy. *Environ. Sci. Technol.* 39, 895-900.
- Thanabalasingam, P., Pickering, W. F. (1986) Arsenic sorption by humic acids. *Environ. Pollut.* 12, 233-246.
- Thurman, E. M. (1985) *Organic geochemistry of natural waters*. Kluwer Academic Press: Boston.
- Tipping, E. (2002) *Cation binding by humic substances*. Cambridge University Press: Cambridge.
- Tufano, K. J., Fendorf, S. (2008) Confounding impacts of iron reduction on arsenic retention. *Environ. Sci. Technol.* 42, 4777-4783.
- Ukonmaanaho, L., Nieminen, T. M., Rausch, N., Shotyk, W. (2004) Heavy metal and arsenic profiles in ombrogenous peat cores from four differently loaded areas in Finland. *Water Air Soil Pollut.* 158, 277-294.
- Wang, S., Mulligan, C. N. (2009) Enhanced mobilization of arsenic and heavy metals from mine tailings by humic acid. *Chemosphere* 74, 274-279.

- WHO (2008) *Guidelines for drinking-water quality: Incorporating 1st and 2nd addenda*. World Health Organisation: Geneva.
- Wilkin, R. T., Wallschläger, D., Ford, R. G. (2003) Speciation of arsenic in sulfidic waters. *Geochem. Trans.* 4, 1-7.
- Williams, M. (2001) Arsenic in mine waters: An international study. *Environ. Geol.* 40, 267-278.
- Xia, K., Weesner, F., Bleam, W. F., Bloom, P. R., Skyllberg, U. L., Helmke, P. A. (1998) XANES studies of oxidation states of sulfur in aquatic and soil humic substances. *Soil Sci. Soc. Am. J.* 62, 1240-1246.
- Yamazaki, C., Ishiga, H., Ahmed, F., Itoh, K., Suyama, K., Yamamoto, H. (2003) Vertical distribution of arsenic in Ganges delta sediments in Deuli Village, Bangladesh. *Soil Sci. Plant Nutr.* 49, 567-574.
- Zhao, F. J., Lehmann, J., Solomon, D., Fox, M. A., McGrath, S. P. (2006) Sulphur speciation and turnover in soils: Evidence from sulphur K-edge XANES spectroscopy and isotope dilution studies. *Soil Biol. Biochem.* 38, 1000-1007.
- Zhao, F. J., Ma, J. F., Meharg, A. A., McGrath, S. P. (2009) Arsenic uptake and metabolism in plants. *New Phytol.* 181, 777-794.
- Zoltai, S. C. (1988) Distribution of base metals in peat near a smelter at Flin Flon, Manitoba. *Water Air Soil Pollut.* 37, 217-228.





## 2. Arsenic sequestration by organic sulfur in peat

This chapter was published with minor modifications in *Nature Geoscience*: Langner P., Mikutta C., Kretzschmar R. (2012) Arsenic sequestration by organic sulphur in peat. *Nat Geosci.* 5, 66-73.

### Abstract

Wetlands cover more than 6% of the global ice-free land area, and have been recognized as important sinks for As. Wetland soils and sediments are subject to frequent changes in redox conditions, driven by fluctuations in the water table and shifts in biological activity. Under oxic conditions, natural organic matter (NOM) promotes As release from metal-(hydr)oxides, thereby enhancing As mobility. Under strongly reducing conditions, however, NOM triggers the formation of As-sequestering sulfides, leading to a reduction in As mobility. Furthermore, the sorption of As to NOM is increasingly thought to suppress As mobility, but the binding mechanisms have remained elusive. Here we use X-ray absorption spectroscopy to analyze the speciation of solid-phase As in peat samples collected from a naturally As-enriched peatland in Switzerland. We show that NOM can completely sequester As through the formation of covalent bonds between trivalent As and organic S groups, which have an average As–S bond distance of 2.26 Å. We suggest that by binding As in this way, NOM plays an active role in As immobilization in S-enriched, anoxic wetlands.

## 2.1. Introduction

Wetlands cover more than 6% of the global ice-free land area [Reddy and DeLaune, 2008]. They typically play a major role in the storage, transformation, and mobilization of trace elements such as As originating from natural and anthropogenic sources [La Force et al., 2000; Bauer et al., 2008; Du Laing et al., 2009; Rothwell et al., 2009; Rothwell et al., 2010]. On the basis of numerous studies, mostly focusing on soils and aquifer sediments in Southeast Asia [Nickson et al., 2000; Smedley and Kinniburgh, 2002; McArthur et al., 2004], it is generally thought that the mobility and bioavailability of As in peat layers is strongly controlled by natural organic matter (NOM), driving the reductive dissolution of metal-(hydr)oxides, and thereby causing the release and redox transformation of associated arsenate, As(V), to the more toxic, charge-neutral arsenite, As(III). In addition to the reductive dissolution of As-bearing metal-(hydr)oxide phases, interactions of As and NOM have been generally discussed in terms of competitive adsorption and redox reactions [Redman et al., 2002; Bauer and Blodau, 2006; Wang and Mulligan, 2006], the stabilization of As-bearing mineral colloids [Bauer and Blodau, 2009], and the precipitation of As-bearing minerals [Kirk et al., 2004]. However, numerous wetland systems and peaty sediments show enrichments of As not related to the presence of As-bearing minerals, suggesting an immobilization through complexation with NOM [Anawar et al., 2003; Yamazaki et al., 2003; González A. et al., 2006; Bauer et al., 2008; Rothwell et al., 2009]. Although many laboratory studies document the association of As with NOM as well [Redman et al., 2002; Buschmann et al., 2006; Wang and Mulligan, 2009], no conclusive spectroscopic evidence for a particular binding mechanism has been presented so far. The mechanisms postulated for the two prevalent inorganic As species, As(III) and As(V), are diverse. Thanabalasingam and Pickering [1986] suggested the binding of As(V) to protonated amino groups of NOM. Buschmann et al. [2006] proposed the reaction of As(III) with phenolic OH groups, the formation of an adduct between As(III) and carboxylate groups stabilized by H-bonding, or hydrophobic As(III)-NOM interactions. They also proposed a nucleophile substitution reaction between phenolic OH groups and As(V). Most studies, however, advocate ternary complex formation as a likely cause for As sorption



to NOM [Redman et al., 2002; Buschmann et al., 2006; Bauer and Blodau, 2009; Liu and Cai, 2010]. In these complexes, polyvalent cations such as Fe(III) are thought to form bridges between As oxyanions and the functional entities of NOM [Redman et al., 2002; Liu and Cai, 2010]. The reaction of As with reduced S groups of NOM is also conceivable. Especially in the metabolism of higher plants, the complexation of As by reduced S groups of phytochelatins as an important As detoxification mechanism is well documented [Schmoeger et al., 2000; Zhao et al., 2009]. Hence, As(III) may readily form a trigonal-pyramidal complex with sulfhydryl groups of NOM, as was previously shown for a keratin-rich biomass [Teixeira and Ciminelli, 2005]. Because reduced S in humic acids, for example, can comprise 15-72% of total S depending on the prevailing redox conditions [Vairavamurthy et al., 1997; Xia et al., 1998], a reaction of sulfhydryl groups with As(III) could be a potentially important sequestration mechanism for As in anaerobic NOM-rich environments.

This paper reports on the solid-phase speciation of As and Fe in a naturally As-enriched minerotrophic (groundwater-fed) peatland located in Ticino, southern Switzerland. Previous water analyses indicated higher As inputs than outputs [González A. et al., 2006], stimulating the hypothesis that particulate NOM serves as a geochemical trap for As. High As concentrations in combination with variable Fe and S contents [González A. et al., 2006] rendered this peatland a key locality to explore the role of NOM for As sequestration. Our main objectives were to (i) provide spectroscopic evidence for As binding to NOM, (ii) identify the dominating binding mechanism, and (iii) quantify the extent of As binding to NOM. Therefore, selected peat samples differing in elemental composition were analyzed by means of bulk As and Fe *K*-edge X-ray absorption spectroscopy (XAS).

## 2.2. Materials and methods

### 2.2.1. Field site and sampling

Peat samples were collected in spring 2009 during the snow-melt period at the minerotrophic peatland *Gola di Lago* (Ticino, Switzerland). A detailed description of this study site is given in González A. et al. [2006]. In total, eight peat profiles (B1-B8) were sampled at the positions shown in Figure A.1, Appendix A. Core holes were drilled up to a maximum depth of 350 cm, using a HUMAX drilling system (Lucerne, Switzerland). The retrieved core material was cut into slices of 8 cm ( $n = 169$ ) and each slice was split into two halves. One half was used for on-site measurements of pH, redox potential and electrical conductivity, and general sample characterization in the laboratory, such as water and ash content, elemental composition and mineralogy. The other half, intended for XAS measurements, was immediately shock-frozen in liquid N<sub>2</sub>, transported on dry ice to the laboratory, processed in an anoxic glovebox (O<sub>2</sub> <1 ppm), and kept anoxic until the final measurements at the synchrotron. In addition, the vegetation was mapped at three sampling positions (B1, B3, and B5) within a radius of 3 m according to the Braun-Blanquet [1932] cover-abundance scale. Results are given in Table A.1, Appendix A.

### 2.2.2. General sample characterization

Peat material used for the general sample characterization was oven-dried (60 °C), sieved (<2 mm), and milled (<50 μm) using an agate disk swing mill. Homogenized peat samples were analyzed for total element concentrations by energy-dispersive X-ray fluorescence (XRF) spectrometry (Spectro X-Lab 2000). The mineralogy was investigated by powder X-ray diffraction (XRD) analysis (Bruker AXS D4 Endeavor), and the total carbon content was determined in triplicate (mean relative standard deviation: 3%) using an elemental analyzer (Leco CHNS-932). For further information regarding XRD analysis and XRF method validation, see Appendix A. The water content of each field-moist peat sample (~10 g) was determined as weight loss after heating the sample for 24 h at 105 °C.

The amount of mineral matter was quantified using the loss on ignition method (5 h at 550 °C). For the analysis of selected peat samples (B5-2 and B1-23) by scanning electron microscopy – energy-dispersive X-ray spectroscopy (SEM-EDX), homogenized peat samples (<20 µm) were fixed on adhesive carbon tapes, coated with carbon, and analyzed with a FEIQuanta 200FEG instrument at acceleration voltages of 10 and 20 keV.

### 2.2.3. Synchrotron measurements

On the basis of XRD and XRF results, a subset of peat samples was selected and prepared for XAS analyses. The preparation included freeze-drying, homogenization and sieving to a particle size <500 µm, and subsequent filling into Plexiglas sample holders, which were sealed with Kapton tape.

Arsenic *K*-edge (11,867 eV) XAS spectra were collected at the bending magnet beamline BM29 of the European Synchrotron Radiation Facility (ESRF, Grenoble, France). Iron *K*-edge (7,112 eV) XAS spectra were collected at the bending magnet beamline C (CEMO) of the Hamburger Synchrotronstrahlungslabor (Hasylab, Hamburg, Germany). The Si(111) double-crystal monochromators were calibrated relative to the *L*3-edge energy of elemental Au (11,919 eV) or the *K*-edge energy of elemental Fe (7,112 eV). The metal foils were simultaneously measured with the samples to account for small energy offsets during the measurements. All spectra were collected in fluorescence mode using a Canberra solid-state 13-element germanium detector (As) or a 7-cell Si-drift-detector [Hansen et al., 2008] (Fe). The spectra of the As and Fe reference compounds were measured as pressed pellets in transmission mode. In addition, selected As reference spectra were collected at the wiggler beamline 4-1 of the Stanford Synchrotron Radiation Lightsource (SSRL, Menlo Park, USA). A list of all references analyzed is given in Table A.3 and A.4, Appendix A. All samples were measured at approximately 80 K using a N<sub>2</sub> Oxford cryostream or a cryostat. Normalized XAS spectra were extracted from the raw data using the software code Athena [Ravel and Newville, 2005]. The maximum of the first derivative was used to set  $E_0$ . For spectra normalization, the pre-edge region was fitted with a linear function and the post-edge

with a quadratic polynomial. The Fourier transforms were calculated over a  $k$ -range of 2-10  $\text{\AA}^{-1}$  using a Kaiser-Bessel window function with a window parameter of 3  $\text{\AA}^{-1}$ . Data analyses of extended X-ray absorption fine structure (EXAFS) spectra of peat were performed by means of linear combination fitting (LCF) using Athena after principal component analysis and target-transform testing (PCA-TT) in SIXPack [Webb, 2005]. The PCA-TT analysis was carried out on  $k^2$ -weighted As and Fe  $K$ -edge EXAFS spectra over a  $k$ -range of 2-10  $\text{\AA}^{-1}$  using the same  $E_0$  for all samples (11,868 eV for As and 7,132 eV for Fe). Least-squares fitting of selected Fourier-filtered As  $K$ -edge EXAFS spectra was performed using the software code Artemis [Ravel and Newville, 2005]. The Fourier transforms were calculated over a  $k$ -range of 2-12  $\text{\AA}^{-1}$  using a Kaiser-Bessel window function with a window parameter of 2.5  $\text{\AA}^{-1}$ . Shell fits were performed in  $q$ -space over an  $R + \Delta R$ -range of 1.2-2.3  $\text{\AA}$  ( $k$ -weight = 3). The amplitude reduction factor  $S_0^2$  was fixed to unity. Single scattering paths of As-S and As-O were extracted from the structure of di(phenylthio)arsenite. Theoretical phase-shift and amplitude functions were calculated with the plane-wave formalism using the FEFF 8.4 code [Ankudinov et al., 1998].

## 2.3. Results and discussion

### 2.3.1. The field system and its characteristics

To investigate the role of NOM for As sequestration, As-rich peat samples were collected from the minerotrophic peatland *Gola di Lago*. Detailed information about its location and prevalent vegetation can be found in Figure A.1 and Table A.1, Appendix A. The peatland (about 27,400 m<sup>2</sup>, 972 m above sea level) began to form approximately 13,000 years ago in a residual glacial lake environment [Zoller and Kleiber, 1971]. Located in the Strona-Ceneri zone, the bedrock is dominated by pre-Alpidic basement rocks including ortho- and paragneisses, amphibolites, and eclogites [Franz and Romer, 2007]. Weathering and erosion of associated As-bearing sulfide ore deposits during the past 1.5 million years has caused an enrichment of As in soils, moraines, and watersheds

in this area [Pfeifer et al., 2002].

In total we sampled eight peat profiles (B1-B8) down to the underlying bedrock at varying distances to the As-loaded intermittent stream (Figure A.1, Appendix A). Analyses of the field-moist samples ( $n = 169$ ) revealed a slightly acidic, anoxic to suboxic environment (pH  $5.8 \pm 0.4$ ;  $E_h$ : -160 to 460 mV; Figure 2.1). Total concentrations of As, Fe, S, and organic carbon on a dry matter basis of four representative peat cores (B1, B3, B5, and B6) are shown in Figure 2.1. The plots of the other four peat cores are given in Figure A.2, Appendix A. The mineral matter content varied between <1 and 99 wt%. The primary minerals identified in the peat comprised quartz, muscovite, albite, and chlorite. Pyrite ( $\text{FeS}_2$ ) as a secondary mineral [González A. et al., 2006] was only verified in samples originating from depths >150 cm. Arsenic concentrations ranged from 3 to 1,800 mg As  $\text{kg}^{-1}$  (Figure 2.1). We noticed two As enrichment patterns in the peat: Whereas in profiles B3 and B5 As was concentrated within the top 41 cm, As enrichments >100 mg As  $\text{kg}^{-1}$  were only observed at greater depths in profiles B1 and B6 (Figure 2.1). Surprisingly, the highest As concentrations (>1,000 mg As  $\text{kg}^{-1}$ ) were detected close to the peat surface (Figure 2.1). The molar Fe/As ratios in the As enrichment zones were comparable and varied from 14 to 523, whereas the molar S/Fe ratio differed significantly: 0-1 at depths <41 cm and 2-7 for 150-250 cm depth. We found no correlation between As and Fe, but observed a general tendency of increasing As concentrations with increasing S content (Figure 2.1). Arsenic concentrations measured for bedrock samples of less than 2 mg As  $\text{kg}^{-1}$  preclude the possibility of an authigenic As accumulation in the peat.

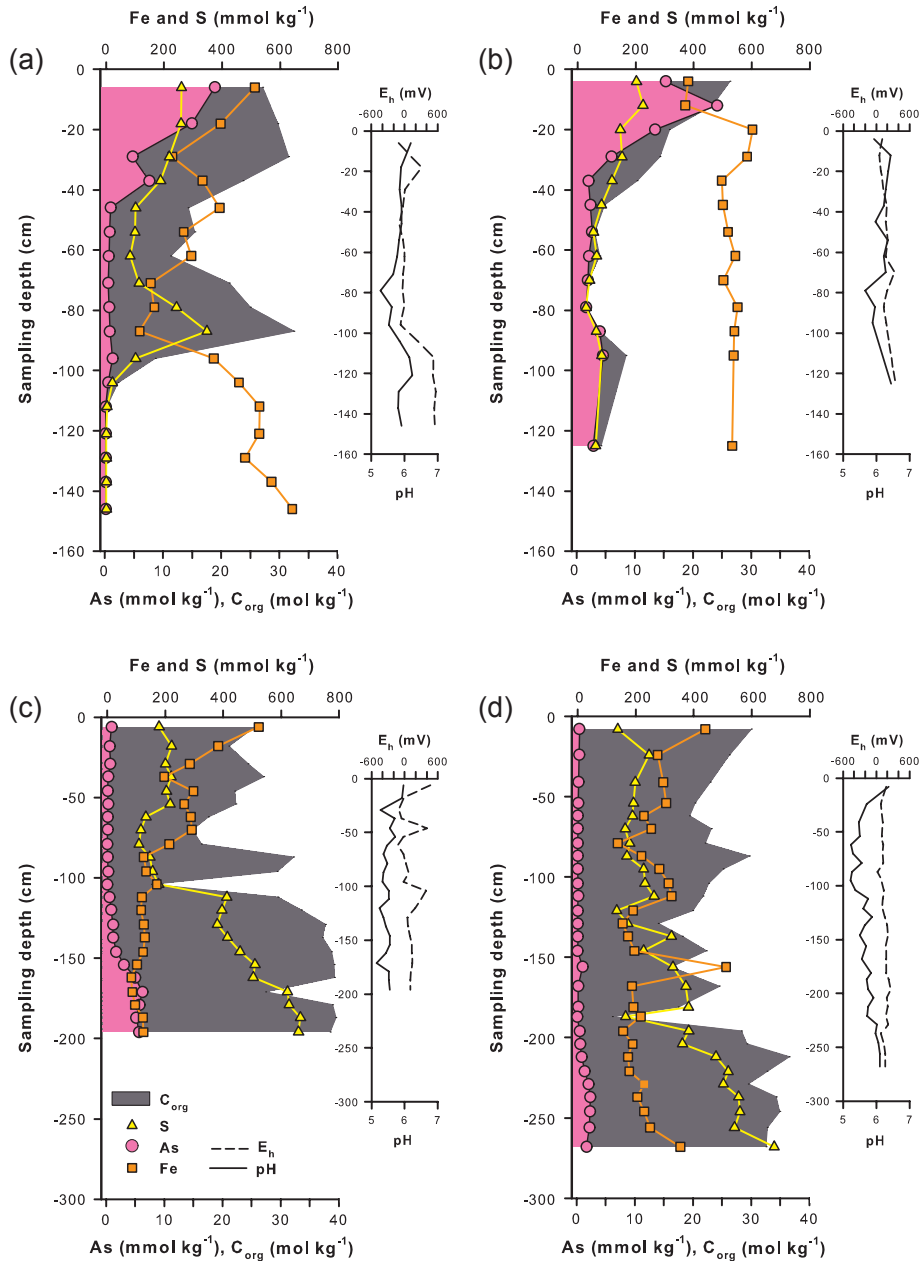


**Figure 2.1.** Element distribution and geochemical conditions in four selected peat profiles from *Gola di Lago*, Switzerland. (a-d) Illustrates the vertical distribution of C<sub>org</sub>, S, As, and Fe as well as the redox potential ( $E_h$ ) and pH at sites (a) B3, (b) B5, (c) B1, and (d) B6 (see Figure A.1, Appendix A). For better comparison, the data is calculated on a dry-weight basis and shown as molar concentrations. The legend in panel (c) is valid for all panels.

### 2.3.2. Solid-phase speciation of arsenic

On the basis of the elemental composition and mineralogy, we selected a subset of 14 peat samples for bulk As and Fe *K*-edge XAS analyses. To study the speciation and local coordination environment of both elements in ‘near-surface’ peat layers, we investigated peat samples from profiles B3 (0-41 cm) and B5 (0-16 cm). The As-enriched deep peat layers were covered by profiles B1 (150-200 cm) and B6 (233-250 cm).

Arsenic *K*-edge X-ray absorption near-edge structure (XANES) spectra,  $k^2$ -weighted EXAFS spectra, and their Fourier-transform magnitudes of representative peat samples and As reference compounds are illustrated in Figure 2.2. The white-line positions in the As *K*-edge XANES spectra (Figure 2.2) indicated that As in the deep peat layers was only present in its trivalent oxidation state. We analyzed the bulk As *K*-edge EXAFS spectra of the 14 peat samples by LCF to quantify major As species in the peat. Suitable reference compounds were identified on the basis of PCA-TT using As *K*-edge EXAFS reference spectra. A detailed description of our PCA-TT approach and a list of the reference spectra can be found in Appendix A.

The LCF results of all 14 peat samples are summarized in Table 2.1 and selected LCF fits are shown in Figure 2.2. We observed two principal speciation patterns of As as a function of sampling depth. In the near-surface peat samples of profiles B3 and B5, the major As species comprised realgar ( $\text{As}_4\text{S}_4$ , or its polymorphs pararealgar and alacranite) [O’Day et al., 2004] (41-88%), As(III)-NOM complexes (0-26%), as well as As(V) (0-33%) and As(III) sorbed to Fe(III)-(hydr)oxides (0-17%). Scanning electron microscopy – energy-dispersive X-ray spectroscopy analyses confirmed the presence of micrometer-sized (<2  $\mu\text{m}$ ) realgar in the near-surface peat samples (Figure A.5, Appendix A). In the deeper peat layers of profiles B1 and B6, As(III)-NOM complexes completely dominated the As speciation and no association of As with sulfide minerals such as arsenopyrite ( $\text{FeAsS}$ ) or orpiment ( $\text{As}_2\text{S}_3$ ) could be verified (Table 2.1).

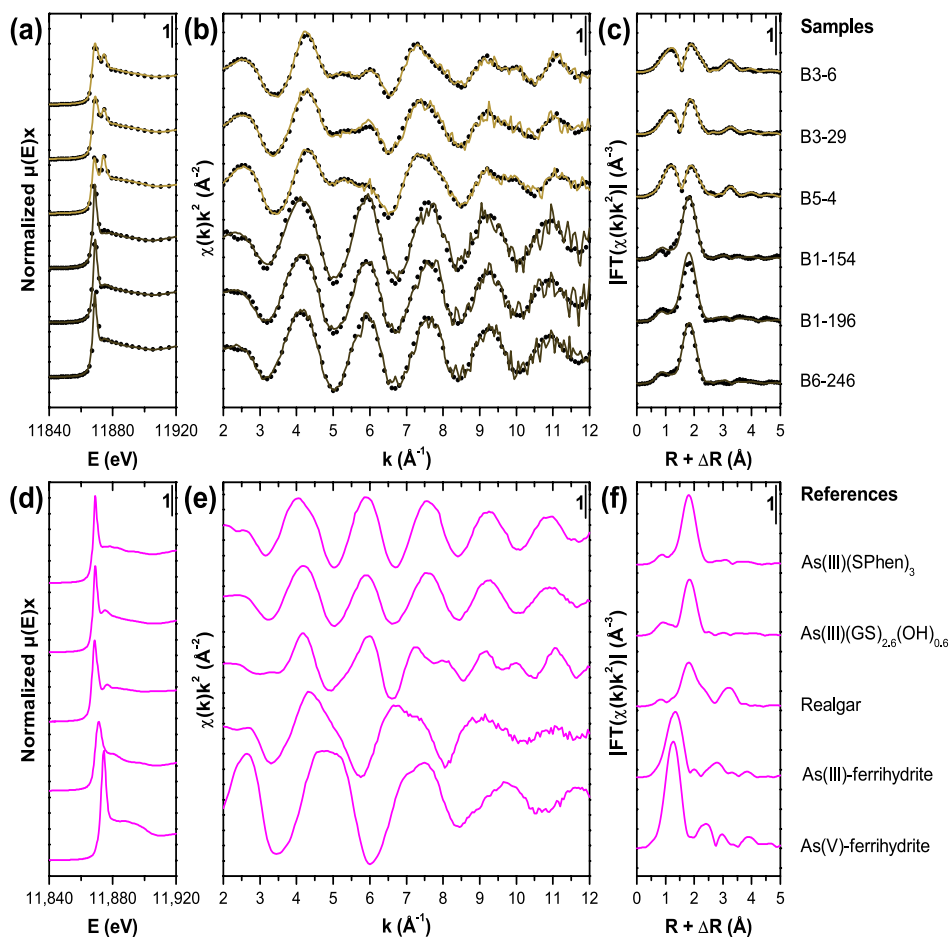


**Figure 2.2.** Arsenic  $K$ -edge XAS data of selected peat samples and reference compounds. The figure illustrates the As  $K$ -edge XANES spectra,  $k^2$ -weighted EXAFS spectra, and their Fourier-transform magnitudes: (a-c) show peat samples and (d-f) show reference compounds. Solid lines are experimental data and filled circles represent best model fits of LCF analyses. The sample notation indicates the profile number and the respective mean sampling depth in cm. Different colors in the upper part of the figure mark samples collected either from the peat surface (<33 cm, light brown) or from deep peat layers (>150 cm, dark brown). The bar in the top right hand corner of each plot designates the scale of the y-axis.



**Table 2.1.** Speciation of As in the peat samples based on linear combination fitting of  $k^2$ -weighted As  $K$ -edge EXAFS spectra. The samples ( $n = 14$ ) were selected from four profiles and covered two different depths (<41 cm and >150 cm). The depth of each peat section is given as a mean value and the sampling range is stated in parentheses. The component sums were normalized to 100% (fitted sum: 89-106%). The R-factor given in the last column represents the mean square misfit between the data and the fit.

Profile	Depth (cm)	As(III)-NOM <sup>a</sup>	Realgar	As(III)-Fh <sup>b</sup>		As(V)-Fh	R-factor <sup>c</sup> (-)
				(%)			
B3	6 (6)	-	63	17		20	0.030
	18 (6)	24 (0/24)	61	-		15	0.058
	29 (4)	25 (25/0)	41	13		21	0.050
	37 (4)	-	88	12		-	0.106
B5	4 (4)	18 (0/18)	49	-		33	0.023
	12 (4)	26 (0/26)	74	-		-	0.045
B1	154 (4)	100 (100/0)	-	-		-	0.051
	162 (4)	83 (83/0)	17	-		-	0.039
	171 (4)	100 (57/43)	-	-		-	0.054
	179 (4)	100 (100/0)	-	-		-	0.054
	187 (4)	100 (100/0)	-	-		-	0.074
	196 (4)	100 (41/59)	-	-		-	0.041
	237 (4)	100 (55/45)	-	-		-	0.068
B6	246 (4)	100 (51/49)	-	-		-	0.045

<sup>a</sup>Sum fraction of As(III)(SPhen)<sub>3</sub> and As(III)(GS)<sub>2,6</sub>(OH)<sub>0,6</sub>; values in parentheses indicated their respective fractions. <sup>b</sup>Fh = ferrihydrite. <sup>c</sup>R-factor =  $\sum_i (\text{data}_i - \text{fit}_i)^2 / \sum_i \text{data}_i^2$ .

### 2.3.3. Local coordination of arsenic in As(III)-NOM complexes

Two organic As model compounds were used as references for organically complexed As(III) in the LCF analysis of the peat As  $K$ -edge EXAFS spectra: tris(phenylthio)arsine and glutamylcysteinylglycinylothioarsenite (Figure 2.3). In these compounds As(III) is coordinated to S atoms. We performed a shell-fit analysis of the Fourier-filtered EXAFS signals ( $R + \Delta R$ -range: 1.2-2.3 Å) of these reference compounds and a peat sample in which speciation was entirely dominated by As(III)-NOM complexes (B1: 179 cm). The fit results are presented in Figure 2.3. The first coordination shell of As(III) in the tris(phenylthio)arsine, As(III)(SPhen)<sub>3</sub>, reference accords with a trigonal-pyramidal complex comprising  $3.0 \pm 0.4$  S atoms with an average As-S bond distance of  $2.26 \pm 0.01$  Å. Compared with the As(III)(SPhen)<sub>3</sub> reference, the glutamylcysteinylglycinylothioarsenite

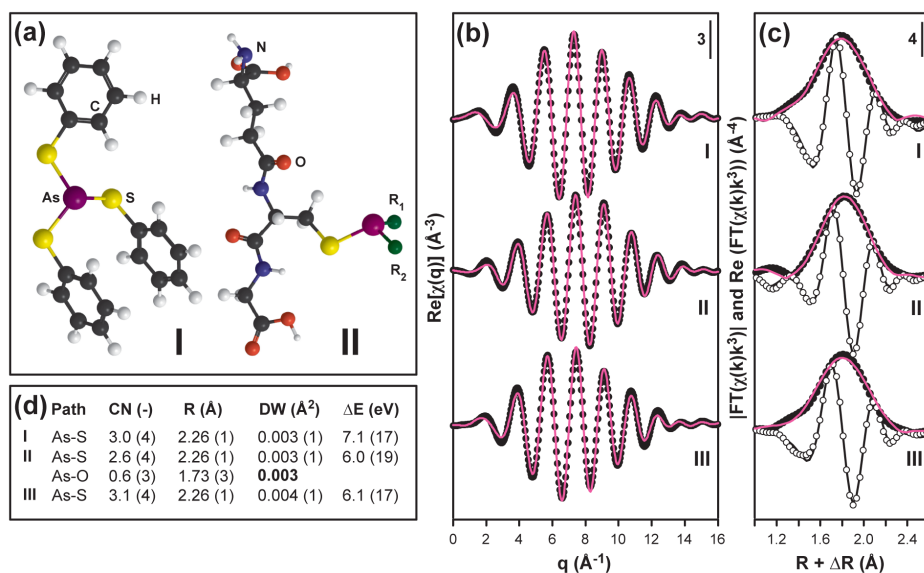


**Figure 2.3.** Shell-fit results for two organic As compounds (I, II) and a peat sample (III) from profile B1 (179 cm). (a) Structures of tris(phenylthio)arsine (I) and glutamylcysteinylglycinylothioarsenite (II). For the latter compound, residues  $R_1$  and  $R_2$  represent a glutathione side chain and/or an OH group. (b) Real parts of the back Fourier transforms over an  $R + \Delta R$ -range of 1.2-2.3 Å (lines) and their respective fits (symbols). (c) Magnitudes and real parts of the Fourier transforms (lines) and their respective fits (symbols). The bar in the top right corner of (b, c) designates the scale of the y-axis. (d) EXAFS parameters derived from the fits; CN refers to the coordination number,  $R$  is the bond distance, DW denotes the Debye-Waller parameter, and  $\Delta E$  is the energy-shift parameter. The value in bold was fixed in the fits. Fit uncertainties are given for the last significant figure. The mean square misfit between the data and the model defined as R-factor ( $= \sum_i (\text{data}_i - \text{fit}_i)^2 / \sum_i \text{data}_i^2 \times 100$ ) was 0.6% (I), 0.2% (II), and 0.3% (III).

reference had a slightly reduced Fourier-transform amplitude (Figure 2.2), suggesting a lower coordination number of S. The coordination number of S was initially fitted to  $2.4 \pm 0.5$ . To increase the overall fit quality, an As-O path had to be included in the fitting scheme and its Debye-Waller parameter ( $\sigma^2$ ) was fixed to that of the As-S path ( $0.003 \text{ \AA}^2$ ). Incorporation of an As-O path in our fit model decreased the mean square misfit (R-factor) from 1.4 to 0.2%. The final fit of this reference then included  $2.6 \pm 0.4$  S atoms with an As-S bond distance of  $2.26 \pm 0.01 \text{ \AA}$ . The coordination number of O and the As-O bond distance were fitted as  $0.6 \pm 0.3$  and  $1.73 \pm 0.03 \text{ \AA}$ , respectively (Figure 2.3). Hence, the final sum formula for this reference was determined as  $\text{As}(\text{GS})_{2.6}(\text{OH})_{0.6}$ , where GS represents a glutathione residue,  $\text{C}_{10}\text{H}_{16}\text{N}_3\text{O}_6\text{S}$ . The coordination numbers of S and O in this reference compound are consistent with a 1:1 mixture of 2- and 3-fold

S-coordinated As(III). The fact that, in some cases, both reference compounds were needed to properly fit the peat As *K*-edge EXAFS spectra (Table 2.1) indicates a variable S coordination of As(III) in the peat. Shell-fit results of a representative peat sample from profile B1 (179 cm) were in total agreement with those of the As(III)(SPhen)<sub>3</sub> reference (Figure 2.3). Both S coordination numbers and interatomic As-S distances obtained for the peat sample closely resemble those of As(III) bound to sulfhydryl groups of cysteine residues, where As is directly bound to S atoms with As-S bond distances of 2.25-2.26 Å [Shi et al., 1996; Teixeira and Ciminelli, 2005]. In wetland systems such as *Gola di Lago*, sulfate-reducing conditions may facilitate direct reactions of aqueous sulfide species with NOM [Aizenshtat et al., 1995] following As(III) complexation by freshly formed sulfhydryl groups. Another As-NOM complexation pathway could involve the sulfidization of aqueous As(III) and subsequent reaction of anionic thioarsenites [Helz and Tossell, 2008] with NOM. If the latter mechanism applies, polymeric thioarsenites can be ruled out because their As-S bond distances are notably shorter (2.21-2.23 Å) [Helz et al., 1995] than the one determined for the peat sample. It is worth noting that direct reactions of monomeric thioarsenites with NOM would result in a reaction product in which at least one sulfhydryl group is coordinated to trivalent As.

To exclude the presence of nanocrystalline As sulfides in the peat, we used wavelet-transform analysis and calculated Morlet wavelets [Funke et al., 2005] of  $k^1$ -weighted As *K*-edge EXAFS spectra of the peat and reference compounds. This analysis is detailed in Appendix A. A comparison of wavelets of the peat sample and the As(III)(SPhen)<sub>3</sub> reference with those of realgar, orpiment, and amorphous As<sub>2</sub>S<sub>3</sub> [Helz et al., 1995] revealed that all As sulfides exhibited As backscattering signals in the  $R + \Delta R$ -range of 2.5-3.5 Å. In contrast, the two organic samples lacked As backscattering signals, but instead showed the spectral features of low *Z*-elements (C/N/O backscatterers) at  $R + \Delta R \sim 3.0$  Å, implying the absence of nanocrystalline As sulfides in the peat and corroborating the predominance of trivalent As in monomeric As-sulfhydryl-NOM complexes.

### 2.3.4. Solid-phase speciation of iron

In most environmental systems the geochemical As cycle is strongly coupled to that of Fe. Several As sequestration mechanisms involve reactive Fe species such as Fe(III)-(hydr)oxides [Fuller et al., 1993; Manning and Goldberg, 1997], mixed-valence Fe-(hydr)oxides [Dixit and Hering, 2003; Jönsson and Sherman, 2008], Fe sulfide phases [Moore et al., 1988; O'Day et al. 2004], or Fe(III)-NOM complexes [Redman et al., 2002; Buschmann et al., 2006; Ritter et al., 2006]. The identification of major Fe species in the peatland is thus key to unraveling the relative importance of NOM for As binding.

Iron *K*-edge XANES spectra,  $k^2$ -weighted EXAFS spectra and their Fourier-transform magnitudes are shown in Figure 2.4 for six peat samples and the Fe reference compounds used for LCF analysis. These references were selected by PCA-TT using from a set of 23 EXAFS spectra of potentially relevant Fe compounds (see Appendix A). The best fit results of the LCF analysis of the peat samples are summarized in Table 2.2. Accordingly, Fe in the upper peat layers (<41 cm) was predominantly present as Fe(III)-(hydr)oxides (30-80%), chlorite (0-37%), and Fe(III)-NOM complexes (19-36%). Despite high contents of Fe(III)-(hydr)oxides and their high affinity for As, realgar was identified as the main As species (Table 2.1), suggesting the presence of S-rich high-As/low-Fe microenvironments. The coexistence of Fe(III)-(hydr)oxides and realgar in the upper peat layers implies nonequilibrium conditions induced by an oscillating water table and may be explained by the slow oxidation kinetics of realgar [Renock and Becker, 2010].

Iron(III)-NOM complexes (42-80%) and pyrite (16-58%) were the major Fe species identified in the deeper parts of the peat profiles (150-250 cm) (Table 2.2). The absence of Fe(III)-(hydr)oxides in the deep peat layers suggests stable anoxic conditions. Under these conditions, a large fraction of Fe is still stabilized in its ferric state because of complexation by organic ligands [Van Schaik et al., 2008]. Although Fe(III)-NOM complexes constituted a major Fe fraction in deep As-rich peat layers, As was completely coordinated to S groups of NOM (Table 2.1). This finding implies that ternary complexes involving As(III) and Fe(III)-NOM species as previously proposed [Buschmann et al., 2006; Liu and Cai, 2010] do not form in significant amounts at slightly acidic pH, where As(III) is present as a charge-neutral molecule ( $pK_{a1} = 9.2$ )

[Cherry et al., 1979]. Likewise, pyrite is known to effectively sequester As by means of adsorption or isomorphic substitution [Farquhar et al., 2002; Lowers et al., 2007]. This sequestration pathway was also of minor importance compared with the binding of As to sulfhydryl groups of NOM (Table 2.1). In agreement with our As speciation analysis, further SEM-EDX analyses did not confirm the incorporation of As into the structure of pyrite (Figure A.6, Appendix A).

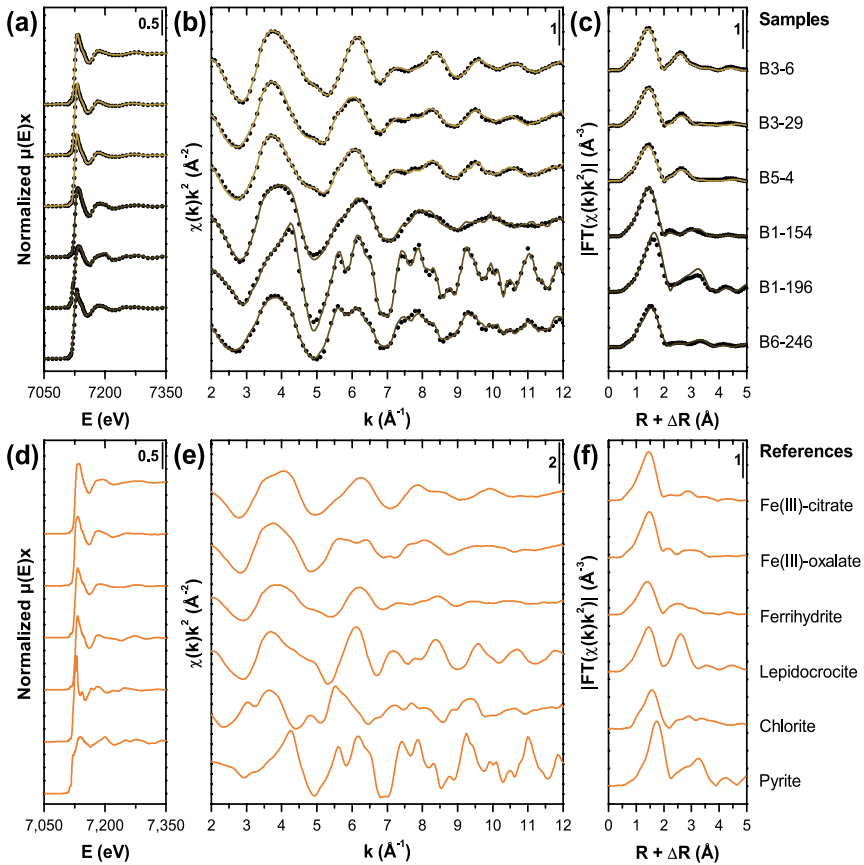


**Figure 2.4.** Iron  $K$ -edge XAS data of selected peat samples and reference compounds. The figure illustrates the Fe  $K$ -edge XANES spectra,  $k^2$ -weighted EXAFS spectra, and their Fourier-transform magnitudes: (a-c) show peat samples and (d-f) show reference compounds. Solid lines are experimental data and filled circles represent best model fits of LCF analyses. The sample notation indicates the profile number and the respective mean sampling depth in cm. Different colors in the upper part of the figure mark samples collected either from the peat surface ( $<33$  cm, light brown) or from deep peat layers ( $>150$  cm, dark brown). The bar in the top right hand corner of each plot designates the scale of the  $y$ -axis.

**Table 2.2.** Speciation of Fe in the peat samples based on linear combination fitting of  $k^2$ -weighted Fe  $K$ -edge EXAFS spectra. The samples ( $n = 14$ ) were selected from four profiles and covered two different depths (<41 cm and >150 cm). The depth of each peat section is given as a mean value and the sampling range is stated in parentheses. The component sums were normalized to 100% (fitted sum: 93-105%). The R-factor given in the last column represents the mean square misfit between the data and the fit.

Profile	Depth (cm)	Fe(III)-NOM <sup>a</sup>	Fe(III)-(hydr)oxides <sup>b</sup>	Chlorite	Pyrite	R-factor <sup>c</sup> (-)
		(%)				
B3	6 (6)	20 (0/20)	80 (52/28)	-	-	0.003
	18 (6)	20 (0/20)	60 (36/24)	20	-	0.004
	29 (4)	27 (0/27)	47 (27/20)	26	-	0.010
	37 (4)	36 (14/22)	30 (17/13)	34	-	0.012
B5	4 (4)	19 (0/19)	57 (38/19)	25	-	0.011
	12 (4)	21 (0/21)	42 (42/0)	37	-	0.020
B1	154 (4)	80 (51/29)	20 (20/0)	-	-	0.017
	162 (4)	79 (49/30)	21 (21/0)	-	-	0.013
	171 (4)	62 (31/31)	22 (22/0)	-	16	0.011
	179 (4)	53 (27/26)	13 (13/0)	-	34	0.014
	187 (4)	50 (27/23)	-	-	50	0.013
	196 (4)	42 (25/17)	-	-	58	0.016
B6	237 (4)	53 (33/20)	-	26	21	0.015
	246 (4)	46 (26/20)	-	34	20	0.016

<sup>a</sup>Sum fraction of Fe(III)-citrate and Fe(III)-oxalate; values in parentheses indicated their respective fractions.

<sup>b</sup>Sum fraction of ferrihydrite and lepidocrocite. <sup>c</sup>R-factor =  $\sum_i (\text{data}_i - \text{fit}_i)^2 / \sum_i \text{data}_i^2$ .

## 2.4. Environmental implications

Natural organic matter as a quantitatively important sorbent for As in reducing environments has not been reported so far [Smith et al., 1998; Smedley and Kinniburgh, 2002; Zhang and Selim, 2008]. Our results show that the majority of As was not associated with Fe(III)-(hydr)oxides, mixed-valence Fe-(hydr)oxides, or Fe sulfide phases, either as a minor substituent in pyrite or as the mineral arsenopyrite. Instead, we found that trivalent As bound to sulfhydryl groups of NOM was a major species in all peat samples and completely dominated the As speciation under stable anoxic conditions. Based on the lack of evidence for ternary As(III)-Fe(III)-NOM complex formation and As(III) reaction schemes involving phenolic OH or carboxyl groups of NOM [Buschmann et al., 2006; Liu and Cai, 2010] we postulate that covalent binding of trivalent As to NOM via organic S species is the primary mechanism of As-NOM interactions under sulfate-reducing conditions. The complexation of trivalent As with sulfhydryl groups of NOM

may also explain As-NOM associations observed in other European ombrotrophic [Cloy et al., 2009; Rothwell et al., 2009; Rothwell et al., 2010] and minerotrophic [Bauer et al., 2008] peatlands, as well as in some peats and peaty sediments of the Bengal Basin [Anawar et al., 2003; Yamazaki et al., 2003; Ahmed et al., 2010].

The mobility and bioavailability of As are generally thought to increase under reducing conditions owing to the reductive dissolution of metal-(hydr)oxides and the redox transformation of As(V) to the more toxic, charge-neutral As(III) [Smith et al., 1998; Smedley and Kinniburgh, 2002]. These processes are of undisputable relevance for mineral-rich systems but are not necessarily transferable to NOM- and S-rich environments. Here, NOM can effectively alleviate As mobility by formation of stable inner-sphere complexes. Wetlands enriched in S, Fe, and NOM can thus be considered as efficient geochemical traps for As both under reducing and oxidizing conditions: Whereas As is immobilized by NOM or As-bearing sulfide minerals under reducing conditions, re-oxidation may release As(V) that is subsequently sorbed to freshly precipitated metal-(hydr)oxides. These efficient retention mechanisms may control the dynamics of As in wetlands subject to interannual water-table fluctuations as seen for ombrotrophic peat bogs in England [Cloy et al., 2009; Rothwell et al., 2009; Rothwell et al., 2010]. The binding of trivalent As to NOM by means of reactive organic S species may not only be confined to particulate NOM but may also hold for As binding to dissolved OM. Arsenite-NOM interactions have been well documented in laboratory experiments with both dissolved NOM [Redman et al., 2002] or humic model substances [Thanabalasingam and Pickering, 1986; Buschmann et al., 2006; Liu and Cai, 2010]. The binding of As to sulfhydryl groups of NOM may also explain the recent findings of Guo et al. [2011], who reported a higher affinity of As towards organic rather than Fe colloids in anoxic high-As groundwaters of the Hetao basin, Inner Mongolia.

In conclusion, NOM can represent a major sorbent for As in S-rich anoxic environments. The covalent binding of trivalent As to sulfhydryl groups of NOM reduces the potential bioavailability of As and may impair other As sequestration pathways such as the formation of As-bearing pyrite or the precipitation of arsenopyrite. Although the binding of trivalent As to sulfhydryl groups of NOM may effectively trap As in the case of particulate NOM, it may otherwise enhance the mobility of As in environments with

high concentrations of dissolved NOM. Our results thus highlight the need to properly account for NOM when assessing the mobility and toxicity of As in NOM-rich soils and sediments.

### **Acknowledgements**

We thank K. Barmettler for his support in the soil chemistry laboratory, M. Hoffmann, F. Maurer, and K. Barmettler for field assistance, as well as S. Hassold and M. Maurer for mapping the vegetation at the field site (ETH Zurich). We acknowledge the ESRF for provision of synchrotron radiation facilities, and we would like to thank M. Chorro for assistance in using beamline BM29. Portions of this research were carried out at the light source DORIS III at DESY, a member of the Helmholtz Association (HGF). We are grateful to E. Welter for assistance in using beamline C (HASYLAB). Portions of this research were also carried out at the SSRL, a Directorate of SLAC National Accelerator Laboratory and an Office of Science User Facility operated for the U.S. Department of Energy Office of Science by Stanford University. We would like to thank J. Rogers for his support in using beamline 4-1. The authors furthermore acknowledge the support by the Electron Microscopy Center, ETH Zurich (EMEZ, Switzerland), in particular K. Kunze for performing the SEM-EDX analyses. Thanks to A. Massanek (TU Bergakademie Freiberg, Germany) and P. Brack (ETH Zurich) for their assistance in providing mineral reference compounds. We are also indebted to P. Poggiati and M. Sulmoni from the Department of Environment (Ticino, Switzerland) who granted the sampling permission for *Gola di Lago*. Financial support by the ETH Zurich (research grant 2708-2) is also gratefully acknowledged.





## References

- Ahmed, F., Bibi, M. H., Ishiga, H., Fukushima, T., Maruoka, T. (2010) Geochemical study of arsenic and other trace elements in groundwater and sediments of the Old Brahmaputra river plain, Bangladesh. *Environ. Earth Sci.* 60, 1303-1316.
- Aizenshtat, Z., Krein, E. B., Vairavamurthy, M. A., Goldstein, T. P. (1995) Role of sulfur in the transformations of sedimentary organic matter: A mechanistic overview. In Vairavamurthy, M. A., Schoonen, M. A. A. (Eds.) *Geochemical transformations of sedimentary sulfur*. American Chemical Society Washington, DC, pp. 16-37.
- Anawar, H. M., Akai, J., Komaki, K., Terao, H., Yoshioka, T., Ishizuka, T., Safiullah, S., Kato, K. (2003) Geochemical occurrence of arsenic in groundwater of Bangladesh: Sources and mobilization processes. *J. Geochem. Explor.* 77, 109-131.
- Ankudinov, A. L., Ravel, B., Rehr, J. J., Conradson, S. D. (1998) Real-space multiple-scattering calculation and interpretation of X-ray-absorption near-edge structure. *Phys. Rev. B: Condens. Matter* 58, 7565-7576.
- Bauer, M., Blodau, C. (2006) Mobilization of arsenic by dissolved organic matter from iron oxides, soils and sediments. *Sci. Total Environ.* 354, 179-190.
- Bauer, M., Blodau, C. (2009) Arsenic distribution in the dissolved, colloidal and particulate size fraction of experimental solutions rich in dissolved organic matter and ferric iron. *Geochim. Cosmochim. Acta* 73, 529-542.
- Bauer, M., Fulda, B., Blodau, C. (2008) Groundwater derived arsenic in high carbonate wetland soils: Sources, sinks, and mobility. *Sci. Total Environ.* 401, 109-120.
- Braun-Blanquet, J. (1932) *Plant sociology: The study of plant communities*. McGraw-Hill: New York.
- Buschmann, J., Kappeler, A., Lindauer, U., Kistler, D., Berg, M., Sigg, L. (2006) Arsenite and arsenate binding to dissolved humic acids: Influence of pH, type of humic acid, and aluminum. *Environ. Sci. Technol.* 40, 6015-6020.
- Cherry, J. A., Shaikh, A. U., Tallman, D. E., Nicholson, R. V. (1979) Arsenic species as an indicator of redox conditions in groundwater. *J. Hydrol.* 43, 373-392.
- Cloy, J. M., Farmer, J. G., Graham, M. C., Mackenzie, A. B. (2009) Retention of As and Sb in ombrotrophic peat bogs: Records of As, Sb, and Pb deposition at four Scottish sites. *Environ. Sci. Technol.* 43, 1756-1762.
- Dixit, S., Hering, J. G. (2003) Comparison of arsenic(V) and arsenic(III) sorption onto iron oxide minerals: Implications for arsenic mobility. *Environ. Sci. Technol.* 37, 4182-4189.
- Du Laing, G., Chapagain, S. K., Dewispelaere, M., Meers, E., Kazama, F., Tack, F. M. G., Rinklebe, J., Verloo, M. G. (2009) Presence and mobility of arsenic in estuarine wetland soils of the Scheldt estuary (Belgium). *J. Environ. Monit.* 11, 873-881.

- Farquhar, M. L., Charnock, J. M., Livens, F. R., Vaughan, D. J. (2002) Mechanisms of arsenic uptake from aqueous solution by interaction with goethite, lepidocrocite, mackinawite, and pyrite: An X-ray absorption spectroscopy study. *Environ. Sci. Technol.* 36, 1757-1762.
- Franz, L., Romer, R. L. (2007) Caledonian high-pressure metamorphism in the Strona-Ceneri zone (Southern Alps of Southern Switzerland and Northern Italy). *Swiss J. Geosci.* 100, 457-467.
- Fuller, C. C., Davis, J. A., Waychunas, G. A. (1993) Surface chemistry of ferrihydrite. Part 2: Kinetics of arsenate adsorption and coprecipitation. *Geochem. Cosmochim. Acta* 57, 2271-2282.
- Funke, H., Scheinost, A. C., Chukalina, M. (2005) Wavelet analysis of extended x-ray absorption fine structure data. *Phys. Rev. B: Condens. Matter* 71, 1-7.
- González A., Z. I., Krachler, M., Cheburkin, A. K., Shoty, W. (2006) Spatial distribution of natural enrichments of arsenic, selenium, and uranium in a minerotrophic peatland, Gola di Lago, canton Ticino, Switzerland. *Environ. Sci. Technol.* 40, 6568-6574.
- Guo, H., Zhang, B., Zhang, Y. (2011) Control of organic and iron colloids on arsenic partition and transport in high arsenic groundwaters in the Hetao basin, Inner Mongolia. *Appl. Geochem.* 26, 360-370.
- Hansen, K., Reckleben, C., Diehl, I., Klaer, H. (2008) A compact 7-cell Si-drift detector module for high-count rate X-ray spectroscopy. *Nucl. Instrum. Methods Phys. Res., Sect. A* 589, 250-258.
- Helz, G. R., Tossell, J. A. (2008) Thermodynamic model for arsenic speciation in sulfidic waters: A novel use of ab initio computations. *Geochim. Cosmochim. Acta* 72, 4457-4468.
- Helz, G. R., Tossell, J. A., Charnock, J. M., Patrick, R. A. D., Vaughan, D. J., Garner, C. D. (1995) Oligomerization in As(III) sulfide solutions: Theoretical constraints and spectroscopic evidence. *Geochim. Cosmochim. Acta* 59, 4591-4604.
- Jönsson, J., Sherman, D. M. (2008) Sorption of As(III) and As(V) to siderite, green rust (fougerite) and magnetite: Implications for arsenic release in anoxic groundwaters. *Chem. Geol.* 255, 173-181
- Kirk, M. F., Holm, T. R., Park, J., Jin, Q. S., Sanford, R. A., Fouke, B. W., Bethke, C. M. (2004) Bacterial sulfate reduction limits natural arsenic contamination in groundwater. *Geology* 32, 953-956.
- La Force, M. J., Hansel, C. M., Fendorf, S. (2000) Arsenic speciation, seasonal transformations, and co-distribution with iron in a mine waste-influenced palustrine emergent wetland. *Environ. Sci. Technol.* 34, 3937-3943.
- Liu, G., Cai, Y. (2010) Complexation of arsenite with dissolved organic matter: Conditional distribution coefficients and apparent stability constants. *Chemosphere* 81, 890-896.
- Lowers, H. A., Breit, G. N., Foster, A. L., Whitney, J., Yount, J., Uddin, N., Muneem, A. (2007) Arsenic incorporation into authigenic pyrite, Bengal Basin sediment, Bangladesh. *Geochim. Cosmochim. Acta* 71, 2699-2717.
- Manning, B. A., Goldberg, S. (1997) Arsenic(III) and arsenic(V) adsorption on three California soils. *Soil Sci.* 162, 886-895.

- McArthur, J. M., Banerjee, D. M., Hudson-Edwards, K. A., Mishra, R., Purohit, R., Ravenscroft, P., Cronin, A., Howarth, R. J., Chatterjee, A., Talukder, T., Lowry, D., Houghton, S., Chadha, D. K. (2004) Natural organic matter in sedimentary basins and its relation to arsenic in anoxic ground water: The example of West Bengal and its worldwide implications. *Appl. Geochem.* 19, 1255-1293.
- Moore, J. N., Ficklin, W. H., Johns, C. (1988) Partitioning of arsenic and metals in reducing sulfidic sediments. *Environ. Sci. Technol.* 22, 432-437.
- Nickson, R. T., McArthur, J. M., Ravenscroft, P., Burgess, W. G., Ahmed, K. M. (2000) Mechanism of arsenic release to groundwater, Bangladesh and West Bengal. *Appl. Geochem.* 15, 403-413.
- O'Day, P. A., Vlassopoulos, D., Root, R., Rivera, N. (2004) The influence of sulfur and iron on dissolved arsenic concentrations in the shallow subsurface under changing redox conditions. *Proc. Natl. Acad. Sci. USA* 101, 13703-13708.
- Pfeifer, H.-R., Beatrizotti, G., Berthoud, J., DeRossa, M., Girardet, A., Jaeggli, M., LaVanchy, J.-C., Reymond, D., Righetti, G., Schlegel, C., Schmit, V., Temgoua, E. (2002) Natural arsenic-contamination of surface and ground waters in Southern Switzerland (Ticino). *Bull. Appl. Geol.* 7, 81-103.
- Ravel, B., Newville, M. (2005) Athena, Artemis, Hephaestus: Data analysis for X-ray absorption spectroscopy using Ifeffit. *J. Synchrot. Radiat.* 12, 537-541.
- Reddy, K. R., DeLaune, R. D. (2008) *Biogeochemistry of wetlands: Science and applications*. CRC Press: Boca Raton.
- Redman, A. D., Macalady, D. L., Ahmann, D. (2002) Natural organic matter affects arsenic speciation and sorption onto hematite. *Environ. Sci. Technol.* 36, 2889-2896.
- Renock, D., Becker, U. (2010) A first principles study of the oxidation energetics and kinetics of realgar. *Geochim. Cosmochim. Acta* 74, 4266-4284.
- Ritter, K., Aiken, G. R., Ranville, J. F., Bauer, M., Macalady, D. L. (2006) Evidence for the aquatic binding of arsenate by natural organic matter-suspended Fe(III). *Environ. Sci. Technol.* 40, 5380-5387.
- Rothwell, J. J., Taylor, K. G., Ander, E. L., Evans, M. G., Daniels, S. M., Allott, T. E. H. (2009) Arsenic retention and release in ombrotrophic peatlands. *Sci. Total Environ.* 407, 1405-1417.
- Rothwell, J. J., Taylor, K. G., Chenery, S. R. N., Cundy, A. B., Evans, M. G., Allott, T. E. H. (2010) Storage and behavior of As, Sb, Pb, and Cu in ombrotrophic peat bogs under contrasting water table conditions. *Environ. Sci. Technol.* 44, 8497-8502.
- Schmoeger, M. E. V., Oven, M., Grill, E. (2000) Detoxification of arsenic by phytochelatins in plants. *Plant Physiol.* 122, 793-801.
- Shi, W., Dong, J., Scott, R. A., Ksenzenko, M. Y., Rosen, B. P. (1996) The role of arsenic-thiol interactions in metalloregulation of the ars operon. *J. Biol. Chem.* 271, 9291-9297.
- Smedley, P. L., Kinniburgh, D. G. (2002) A review of the source, behaviour and distribution of arsenic in natural waters. *Appl. Geochem.* 17, 517-568.

- Smith, E., Naidu, R., Alston, A. M. (1998) Arsenic in the soil environment: A review. *Adv. Agron.* 64, 149-195.
- Teixeira, M. C., Ciminelli, V. S. T. (2005) Development of a biosorbent for arsenite: Structural modeling based on X-ray spectroscopy. *Environ. Sci. Technol.* 39, 895-900.
- Thanabalasingam, P., Pickering, W. F. (1986) Arsenic sorption by humic acids. *Environ. Pollut.* 12, 233-246.
- Vairavamurthy, M. A., Maletic, D., Wang, S. K., Manowitz, B., Eglinton, T., Lyons, T. (1997) Characterization of sulfur-containing functional groups in sedimentary humic substances by X-ray absorption near-edge structure spectroscopy. *Energ. Fuel* 11, 546-553.
- Van Schaik, J. W. J., Persson, I., Kleja, D. B., Gustafsson, J. P. (2008) EXAFS study on the reactions between iron and fulvic acid in acid aqueous solutions. *Environ. Sci. Technol.* 42, 2367-2373.
- Wang, S., Mulligan, C. N. (2006) Effect of natural organic matter on arsenic release from soils and sediments into groundwater. *Environ. Geochem. Health* 28, 197-214.
- Wang, S., Mulligan, C. N. (2009) Enhanced mobilization of arsenic and heavy metals from mine tailings by humic acid. *Chemosphere* 74, 274-279.
- Webb, S. M. (2005) SIXPack: A graphical user interface for XAS analysis using Ifeffit. *Phys. Scr.* T115, 1011-1014.
- Xia, K., Weesner, F., Bleam, W. F., Bloom, P. R., Skyllberg, U. L., Helmke, P. A. (1998) XANES studies of oxidation states of sulfur in aquatic and soil humic substances. *Soil Sci. Soc. Am. J.* 62, 1240-1246.
- Yamazaki, C., Ishiga, H., Ahmed, F., Itoh, K., Suyama, K., Yamamoto, H. (2003) Vertical distribution of arsenic in Ganges delta sediments in Deuli Village, Bangladesh. *Soil Sci. Plant Nutr.* 49, 567-574.
- Zhang, H., Selim, H. M. (2008) Reaction and transport of arsenic in soils: Equilibrium and kinetic modeling. *Adv. Agron.* 98, 45-115.
- Zhao, F. J., Ma, J. F., Meharg, A. A., McGrath, S. P. (2009) Arsenic uptake and metabolism in plants. *New Phytol.* 181, 777-794.
- Zoller, H., Kleiber, H. (1971) Vegetationsgeschichtliche Untersuchungen in der montanen und subalpinen Stufe der Tessintäler. *Verh. Naturf. Ges. Basel* 81, 90-154.



### 3. Spatial distribution and speciation of arsenic in peat studied with micro-focused X-ray fluorescence spectrometry and X-ray absorption spectroscopy

This chapter was published with minor modifications in *Environmental Science and Technology*: Langner P., Mikutta C., Suess E., Marcus M.A., Kretzschmar R. (2013) Spatial distribution and speciation of arsenic in peat studied with microfocused X-ray fluorescence spectrometry and X-ray absorption spectroscopy. *Environ. Sci. Technol.* 47, 9706-9714.

#### Abstract

Arsenic binding by sulfhydryl groups of natural organic matter (NOM) was recently identified as an important As sequestration pathway in the naturally As-enriched minerotrophic peatland *Gola di Lago*, Switzerland. Here, we explore the microscale distribution, elemental correlations, and chemical speciation of As in the *Gola di Lago* peat. Thin sections of undisturbed peat samples from 0-37 cm and 200-249 cm depth were analyzed by synchrotron microfocused X-ray fluorescence ( $\mu$ -XRF) spectrometry and X-ray absorption spectroscopy ( $\mu$ -XAS). Additionally, peat samples were studied by bulk As, Fe, and S *K*-edge XAS. Micro-XRF analyses showed that As in the near-surface peat was mainly concentrated in 10-50  $\mu$ m sized hotspots, identified by  $\mu$ -XAS as realgar ( $\alpha$ -As<sub>4</sub>S<sub>4</sub>). In the deep peat layer samples, however, As was more diffusely distributed and mostly associated with particulate NOM of varying decomposition stages. The NOM-associated As was present as trivalent As bound by sulfhydryl groups. Arsenopyrite (FeAsS) and arsenian pyrite (FeAs<sub>x</sub>S<sub>2-x</sub>) of <25  $\mu$ m size, which have escaped detection by bulk As and Fe *K*-edge XAS, were found as minor As species in the peat. Bulk S *K*-edge XAS revealed that the deep peat layers were significantly enriched in reduced organic S spe-

cies. Our findings suggest an authigenic formation of realgar and arsenopyrite in strongly reducing microenvironments of the peat and indicate that As(III)-NOM complexes are formed by the passive sorption of As(III) to NOM. This reaction appears to be favored by a combination of abundant reduced organic S and comparatively low As solution concentrations preventing the formation of secondary As-bearing sulfides.

### 3.1. Introduction

Wetland soils are sensitive ecosystems that play an important role in the storage, transformation, and mobilization of nutrients and contaminants. Besides natural sources, anthropogenic emissions from mining and smelting, fossil fuel combustion and agriculture have led to the accumulation of toxic trace elements like As in a number of wetland soils and peaty sediments which may pose a continuing risk for surface and groundwater quality as well as ecosystem health [Lemly et al., 1993; La Force et al., 2000; Dittmar et al., 2010; Rothwell et al., 2010].

Arsenic is a redox-sensitive element whose toxicity and fate in the environment strongly depends on its oxidation state and speciation [Smedley and Kinniburgh, 2002]. Inorganic As commonly comprises arsenate, As(V), in oxic, and the more toxic arsenite, As(III), in anoxic environments low in S [Smedley and Kinniburgh, 2002]. In aerated soils and sediments, As(V) has a strong affinity toward mineral surfaces, rendering it comparatively immobile [Bowell, 1994; Manning and Goldberg, 1997; Smedley and Kinniburgh, 2002; Violante and Pigna, 2002]. In O<sub>2</sub> depleted soils and sediments, microbial decomposition of natural organic matter (NOM) drives the reductive dissolution of metal-(hydr)oxides and thus the release of associated As(V) and its redox transformation into As(III) [Masscheleyn et al., 1991; Anawar et al., 2003]. The released As(III) may subsequently be immobilized by Fe sulfides [Bostick and Fendorf, 2003; Lowers et al., 2007] or mixed valence metal-(hydr)oxides [Dixit and Hering, 2003; Root et al., 2007], or precipitate as As sulfide [Moore et al., 1988; Rittle et al., 1995; La Force et al., 2000]. In addition, several studies provided indirect evidence for an association of As with NOM under reducing conditions [Redman et al., 2002; Anawar et al., 2003; Buschmann et al.,



2006; González A. et al., 2006; Rothwell et al., 2010], but spectroscopic assessments of the governing binding mechanisms and their environmental relevance are still scarce. In a recent bulk X-ray absorption spectroscopy (XAS) study on the solid-phase speciation of As in a naturally As-enriched ( $\leq 1,800$  mg As kg<sup>-1</sup>), slightly acidic minerotrophic peatland (*Gola di Lago*, Switzerland), we observed that in deep peat layers (150-250 cm) As was predominantly sequestered by NOM in its trivalent oxidation state ('As(III)-NOM complexes'). Shell-fit analyses of As *K*-edge extended X-ray absorption fine structure (EXAFS) spectra of these samples revealed S coordination numbers of 2-3 and interatomic As-S distances of 2.26 Å, values typical of inner-sphere As(III) complexes with sulfhydryl groups [Langner et al., 2012]. In contrast to the deep peat layers, near-surface peat samples (0-41 cm) showed a variety of As species, including realgar ( $\alpha$ -As<sub>4</sub>S<sub>4</sub>), As(III/V) sorbed to Fe(III)-(hydr)oxides, and As(III)-NOM complexes. These two contrasting As speciation patterns suggest fundamental differences in the distribution of As within the peat. While bulk As *K*-edge XAS analyses yield information about the average coordination environment of As, they do not provide information on its spatial distribution, elemental correlations, and chemical speciation at the microscale. Bulk XAS analyses may also fail to detect minor As species having a potentially high geochemical activity. Here, we employed microfocused X-ray fluorescence ( $\mu$ -XRF) spectrometry in combination with microfocused XAS ( $\mu$ -XAS) to investigate the spatial distribution, elemental correlations, and speciation of As in the *Gola di Lago* peatland. These techniques have previously been used to investigate the distribution and to some extent the speciation of As in plant roots as well as As-rich soils and sediments [Strawn et al., 2002; Lowers et al., 2007; Castillo-Michel et al., 2011; Frommer et al., 2011; Zimmer et al., 2011; Landrot et al., 2012]. Hitherto, spatially resolved information on As distribution and speciation in NOM-dominated soils and sediments subject to permanent or periodic water-logging is currently not available but may provide new insights into geochemical conditions favoring particular As sequestration pathways.

The overall goal of this study was thus to provide the first information on the microscale distribution and speciation of As in a NOM-rich soil environment characterized by substantial differences in As speciation. More specifically, we used  $\mu$ -XRF spectrometry and  $\mu$ -XAS (i) to investigate the size and distribution of As sulfide minerals in the

uppermost peat layers of the *Gola di Lago* site, (ii) to assess the distribution pattern of As(III)-NOM complexes in the deep peat layers, and (iii) to identify minor As species.

## **3.2. Materials and methods**

### **3.2.1. Field site and sampling**

In a preceding study, we sampled peat cores at locations B1-B8 close to an As-rich intermittent stream of the minerotrophic peatland *Gola di Lago* (canton Ticino, Switzerland) and analyzed the solid-phase speciation of As and Fe by bulk XAS [Langner et al., 2012]. In September 2009, we collected two additional peat cores less than 25 cm away from each of the initial sampling locations B1, B3, and B5 [Langner et al., 2012]. These two peat cores are labeled ‘I’ and ‘II’ in the following. Undisturbed peat material was sampled in ~25 cm intervals using Kubiena boxes made of bladed Al (8 cm × 6 cm × 5 cm). The boxes and all samples used for bulk speciation measurements of S were instantly shock-frozen in liquid N<sub>2</sub>, transported on dry ice to the laboratory, and processed in an anoxic glovebox (O<sub>2</sub> <10 ppm). Additional material of each peat sample was used for general sample characterization as described in Langner et al. [2012]. Redox potential, pH, and electrical conductivity of the field-moist, mostly water-saturated peat samples were immediately measured on-site.

### **3.2.2. Sample preparation and synchrotron measurements**

On the basis of the elemental composition and previous results from bulk As and Fe XAS analyses [Langner et al., 2012], four samples were selected for the preparation of thin sections as well as for bulk XAS and synchrotron X-ray diffraction (SXRD) measurements from peat cores B1II (200-224 cm and 225-249 cm), B3II (25-37 cm), and B5II (0-24 cm) (Figure 3.1). For the sake of clarity, the sample notation will be confined

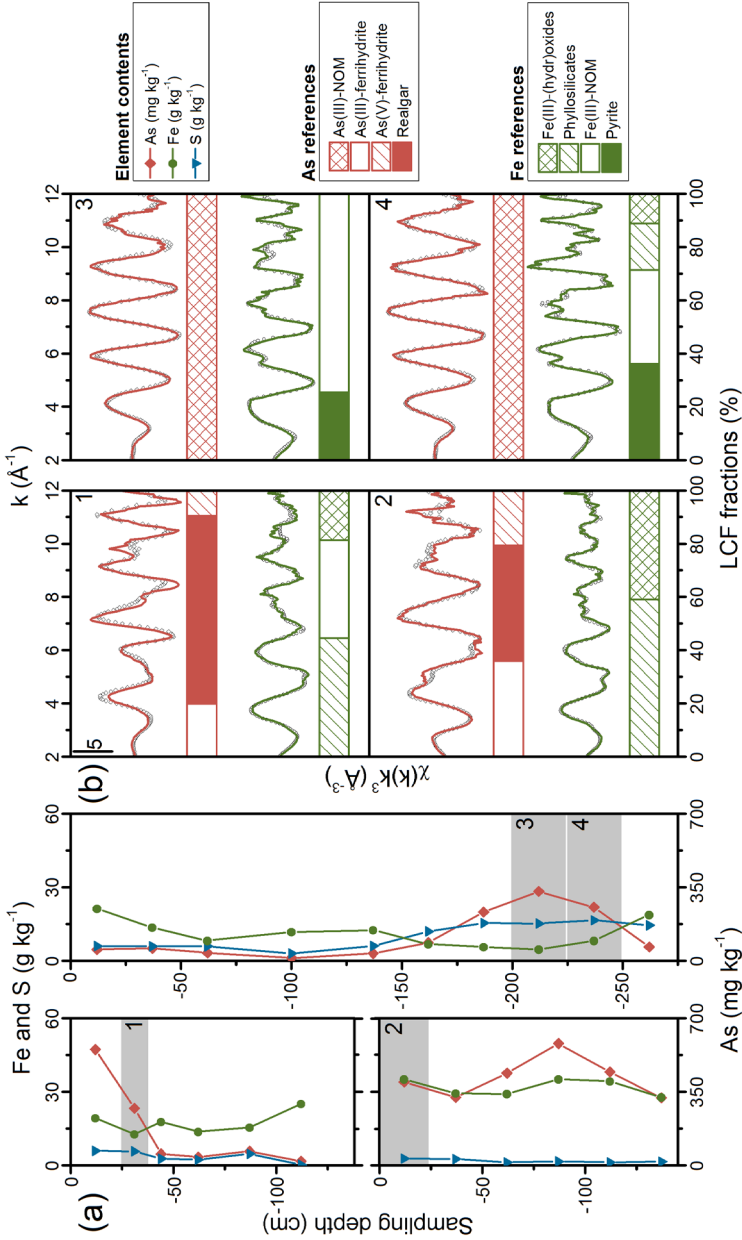


**Figure 3.1.** (a) Distribution of As, Fe, and S in peat cores B3II (top left), B5II (bottom left), and B III (right). Concentrations are given on a dry-weight basis. Gray-shaded boxes (1-4) indicate the depth intervals from which samples were taken for bulk and microspectroscopic analyses. (b) Bulk As and Fe K-edge EXAFS spectra (lines) and corresponding best model fits (symbols) are shown for each depth interval with the As K-edge EXAFS plotted on top of the respective Fe K-edge EXAFS. The numbers in the upper right corner of each box correspond with those in the gray-shaded boxes in (a). The horizontal bars display the percent fraction of each reference compound fitted in the LCF analysis. The concentrations of As, Fe, and S are summarized in Table B.1, Appendix B, and the bulk speciation results for As and Fe are reported in Tables B.2 and B.3, Appendix B.

to core label and mean sampling depth in centimeters, for example, B1II-212 or B3II-31. The four Kubiena boxes were freeze-dried and immediately transferred in Ar atmosphere into an anoxic glovebox, where they were impregnated with epoxy resin (Epotek 301-2FL, Epoxy Technology Inc., USA). Sections of 1 mm thickness were then cut using a diamond saw, mounted on As-free silica glass slides, and polished down to a thickness of 30  $\mu\text{m}$  under exclusion of  $\text{O}_2$  (Spectrum Petrographics Inc., USA). A sub-sample of each Kubiena box was prepared for bulk As and Fe XAS and SXR D analyses. The sample preparation for XAS analyses was identical to that described in Langner et al. [2012]. For SXR D measurements, homogenized peat material was filled into 1 mm o.d. borosilicate glass capillaries. Peat samples used for S *K*-edge XAS analysis were prepared in the same manner as those used for As and Fe XAS analyses, except that the samples were diluted to a concentration of 1,800 mg S  $\text{kg}^{-1}$  using BN in order to reduce overabsorption effects [Prietzel et al., 2011] and pressed into 1.3 cm pellets.

Bulk As *K*-edge (11,867 eV), Fe *K*-edge (7,112 eV), and S *K*-edge (2,472 eV) XAS spectra were collected in fluorescence mode at beamlines 11-2 (As), 4-1 (Fe), and 4-3 (S) of the Stanford Synchrotron Radiation Lightsource (SSRL, SLAC National Accelerator Laboratory, Menlo Park, USA). The thin sections were analyzed by  $\mu$ -XRF spectrometry and  $\mu$ -XAS at beamline 10.3.2 of the Advanced Light Source (ALS, Berkeley, USA) after identification of representative regions using plane- and cross-polarized light microscopy (Zeiss Axioskop 40 microscope). The mineralogy of the peat samples was investigated by SXR D. These measurements were conducted at the powder diffraction station of the Material Sciences (MS-Powder) beamline at the Swiss Light Source (SLS, Villigen, Switzerland). Details about all experimental setups, measurement conditions, and data evaluations can be found in Appendix B.

### 3.3. Results

#### 3.3.1. Peat characterization

For the investigation of the microscale distribution and speciation of As in the *Gola di Lago* peatland, three sampling locations characterized by two different As speciation patterns were selected. At locations B3 and B5, As was enriched in the top 41 cm and mainly present as realgar and As(III/V) sorbed to Fe(III)-(hydr)oxides. At location B1, however, As was concentrated at 150-200 cm depth and entirely sequestered as trivalent As by organic S [Langner et al., 2012]. The field-moist peat sampled in September 2009 and used for this study (cores B1I/II, B3I/II, and B5I/II) was slightly acidic (pH  $5.7 \pm 0.5$ ). The redox potential,  $E_h$ , ranged from -11 to 364 mV, and the mean ionic strength estimated from electrical conductivity values [Griffin and Jurinak, 1973] was  $9 \times 10^{-4}$  M ( $n = 54$ ). Arsenic, Fe, and S concentrations in the 'II' peat cores are displayed in Figure 3.1 and summarized together with those of other major elements in Table B.1, Appendix B. Except for core B5II, the As-enriched zones in peat cores B1II (175-249 cm) and B3II (0-37 cm) were located at approximately the same depths as those of the initial peat cores B1 and B3 collected in March 2009 [Langner et al., 2012]. The concentration maxima of As in the 'II' peat cores (331-580 mg As kg<sup>-1</sup>), however, were up to five times lower compared to the initial peat cores (469-1,800 mg As kg<sup>-1</sup>), emphasizing the high spatial variability of As at the decimeter scale.

Synchrotron XRD patterns of peat samples used for  $\mu$ -XRF and  $\mu$ -XAS analyses (Figure 3.1), which are displayed in Figure B.1, Appendix B, confirmed the presence of primary minerals in the near-surface peat samples B3II-31 and B5II-12, including quartz, phyllosilicates (biotite, muscovite, chlorite), and plagioclase (albite, oligoclase, anorthite). The deep peat layer samples of core B1II showed Bragg peaks belonging to quartz, muscovite, plagioclase (albite, oligoclase), and pyrite. Mineral-phase assemblages in the thin sections studied by  $\mu$ -XRF spectrometry and  $\mu$ -XAS were also investigated by light microscopy. These analyses revealed considerable amounts of mineral phases embedded in the organic matrix of the near-surface peat sample B3II-31, which included single particles ( $\sim 100$ -500  $\mu$ m) of plagioclase, quartz, mica-group minerals (bi-

otite, muscovite), some epidote, and chlorite, as well as altered rock fragments of mainly gneiss (~1-3 mm) (Figure B.2, Appendix B). In contrast, mineral phases were less abundant in the two thin sections of the deep peat layer samples B1II-212 and B1II-237, and only comprised quartz and mica particles (~10-50  $\mu\text{m}$ ) (Figures B.2 and B.3, Appendix B). Using cross-polarized light [Delvigne, 1998], however, we detected fine-grained, reddish-brown colored secondary Fe-(hydr)oxides in all thin sections, partially infilling pores or coating mineral surfaces (Figure B.3, Appendix B).

### 3.3.2. Bulk XAS analyses

Bulk As and Fe *K*-edge EXAFS spectra of all four peat samples used to prepare the thin sections are illustrated in Figure 3.1 along with the corresponding linear combination fits (LCF). The LCF results for As and Fe, shown as horizontal bars in Figure 3.1, are compiled in Tables B.2 and B.3, Appendix B. In the near-surface peat layer samples B3II-31 and B5II-12, the major As species comprised realgar (43-71%) and As(III) (20-36%) as well as As(V) (9-21%) sorbed to Fe(III)-(hydr)oxides. In contrast, As(III)-NOM complexes completely dominated the As speciation in the deep-peat layer samples B1II-212 and B1II-237, in agreement with our earlier findings [Langner et al., 2012]. The presence of pararealgar, a polymorph of realgar, in the near-surface peat samples can be excluded since its local As coordination (e.g.,  $R_{\text{As-As}} = 2.48\text{-}2.53$  vs.  $2.57$  Å) [Mullen and Nowacki, 1972; Bonazzi et al., 1995; Bonazzi and Bindi, 2008] and hence As *K*-edge EXAFS differs from that of realgar (not shown). Other modifications of realgar ( $\beta\text{-As}_4\text{S}_4$  and  $\text{As}_4\text{S}_4(\text{II})$ ) can also be dismissed since they do not form in low pressure/low temperature environments [Kutoglu, 1976; Bonazzi and Bindi, 2008; Tuktabiev et al., 2009]. Note also that orpiment ( $\text{As}_2\text{S}_3$ ) was not detected in any peat sample.

The LCF results of the bulk Fe *K*-edge EXAFS spectra revealed that the major Fe species in the near-surface peat layer samples included Fe(III)-(hydr)oxides (19-41%), phyllosilicates (44-59%), and Fe(III)-NOM complexes (0-37%). Iron in the deep peat layer samples was predominantly present as Fe(III)-NOM complexes (35-75%) and pyrite (25-36%), whereas Fe(III)-(hydr)oxides (0-11%) and phyllosilicates (0-18%) were much less abundant (Figure 3.1, Table B.3, Appendix B). These findings are in general

agreement with our SXRD, light microscopy, and As speciation results (Figures B.1-B.3, Table B.2, Appendix B).

The differences in As and Fe speciation observed for the near-surface and deep peat layer samples (Figure 3.1) suggest important differences in the bulk S speciation as a function of depth. For this reason, we also studied the speciation of S in peat material originating from peat cores B1I, B3I, and B5I. These samples were taken from similar depths as those of the ‘II’ peat cores and also had similar S contents (Table B.4, Appendix B). Figure 3.2 shows the S *K*-edge X-ray absorption near-edge structure (XANES) spec-

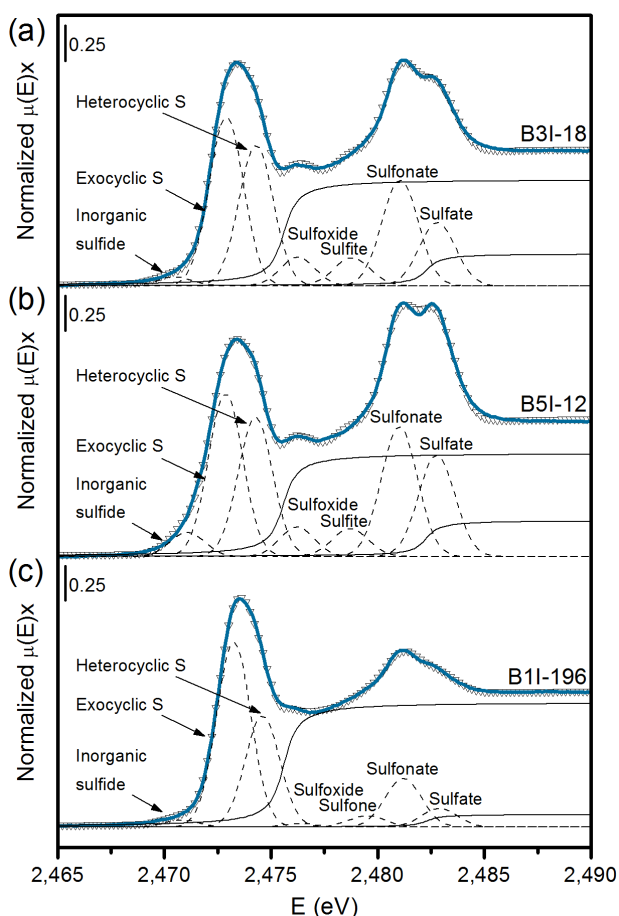


**Figure 3.2.** Deconvolution of normalized bulk S *K*-edge XANES spectra into several Gaussians and two arctangent curves of the near-surface peat samples (a) B3I-18 and (b) B5I-12, as well as the deep peat layer sample (c) B1I-196. Data is shown as solid blue lines, fit envelopes as symbols, fit components as dashed lines, and arctangent functions as solid black lines. Parameter values and fit results are summarized in Tables B.4 and B.5, Appendix B.

tra of peat samples B3I-18, B5I-12, and B1I-196, as well as their spectral deconvolution based on Gaussians representing resonance peaks of the main S functionalities [Vairavamurthy, 1998]. All peat samples showed two distinct resonance-peak ranges. The first peak range from 2,471 to 2,475 eV includes 'reduced S' species (inorganic sulfide and organic exocyclic/heterocyclic S), and the second peak ranging from 2,481 to 2,483 eV represents 'oxidized S' species (sulfonate and sulfate). 'Intermediate oxidized S' species (sulfoxide, sulfite, and sulfone) with resonance peaks located between 2,476 to 2,480 eV were generally of less quantitative importance (Tables B.4 and B.5, Appendix B).

Both 'oxidized' and 'intermediate oxidized' S species were more abundant in the near-surface peat samples B3I-18 and B5I-12 compared to the deep peat layer sample B1I-196 (Figure 3.2, Table B.4, Appendix B). However, the fitted fractions of sulfoxide, sulfite, and sulfone S as part of the 'intermediate oxidized S' are presumably overestimated in all samples, since the energy range 2,476-2,480 eV is significantly affected by post-edge absorption features of reduced organic S species as well as the first arctangent function [Manceau and Nagy, 2012]. Due to their low quantitative importance and in order to obtain a generally reasonable fit quality, these 'intermediate oxidized S' species were nonetheless included in our fitting procedure.

With 80-92% of total S, 'reduced S' was the dominant S form in all peat samples (Table B.4, Appendix B). Inorganic sulfide S only comprised 9-16% of the 'reduced S' pool. A significant attenuation of the inorganic sulfide signal due to the limited X-ray penetration depth at the S *K*-edge [Bolin, 2010] can be ruled out because the pyrites observed in the *Gola di Lago* peat were smaller than one absorption length calculated for pyrite at 2.5 keV [Langner et al., 2012]. Thus, according to the white-line positions [Vairavamurthy, 1998; Hoffmann et al., 2012; Manceau and Nagy, 2012], the majority of S can be attributed to reduced organic S species (64-83%), which falls at the high end of reduced organic S in peatlands (14-87%) [Xia et al., 1998; Skyllberg et al., 2000; Zhao et al., 2006; Prietzel et al., 2007; Prietzel et al., 2009; Manceau and Nagy, 2012]. Even though the relative amount of reduced organic S in the near-surface and deep peat layer samples was comparable, the deep peat layer sample contained 2-7 times more S. Thus, its reduced organic S pool significantly exceeded that of the shallow peat layer samples.



### 3.3.3. $\mu$ -XRF and $\mu$ -XAS analyses

Elemental mapping by  $\mu$ -XRF spectrometry was employed to investigate the distribution of As and its correlations with other elements, notably Fe and S. On the basis of the elemental associations of As,  $\mu$ -XAS analysis was used to identify major and minor As species at selected points of interest (POIs). Figure 3.3 shows coarse and fine elemental distribution maps of As, Fe, and S obtained from thin sections of the near-surface peat layer sample B3II-31 and the deep peat layer sample B1II-237. The distributions of As and Fe in the near-surface peat sample B5II-12 and the second deep peat layer sample B1II-212 are additionally depicted in Figure 3.4. The elemental distribution maps document that the distribution of As in the near-surface peat samples differed substantially from that in the deep peat layer samples. Whereas intense As hotspots of about 10-50  $\mu$ m size dominated the near-surface peat samples, As was for the most part more diffusely distributed in the deep peat layer samples and associated with plant fibers (Figure 3.3) and brownish NOM with a ‘cauliflower’-like morphology representing more humified NOM (Figure 3.4b, Figure B.3d-B.3f, Appendix B). At the As hotspots found mostly close to the peat surface, a clear correlation with S was recognized (Figure B.4a-B.4c, Appendix B). A second As-S correlation, characterized by lower As/S ratios, was additionally noticed in the near-surface peat sample B3II-31 and was linked to the diffuse As distribution in this particular sample (Figure B.4d-B.4f, Appendix B). For the deep peat layer thin sections, we also observed two pronounced correlations between As and S. Whereas the first correlation corresponds to the diffuse distribution of As, the second is restricted to rare but intense As hotspots (Figure B.4g-B.4l, Appendix B).

Correlations between As and Fe ranged from strong to nonexistent (Figure B.5, Appendix B). The most evident As-Fe correlation was found in a deep peat layer sample, where Fe-rich As hotspots were particularly enriched in S, pointing towards arsenopyrite and/or arsenian pyrite (Figure B.4g-B.4i vs. Figure B.5g-B.5i, Appendix B). In contrast, Fe correlated well with Mn in all samples, particularly in the near-surface peat samples (Figure B.6, Appendix B). Here, a significant portion of Fe and Mn was associated with Si-poor secondary Fe-(hydr)oxides identified by light microscopy (Figures B.3 and B.7, Appendix B).

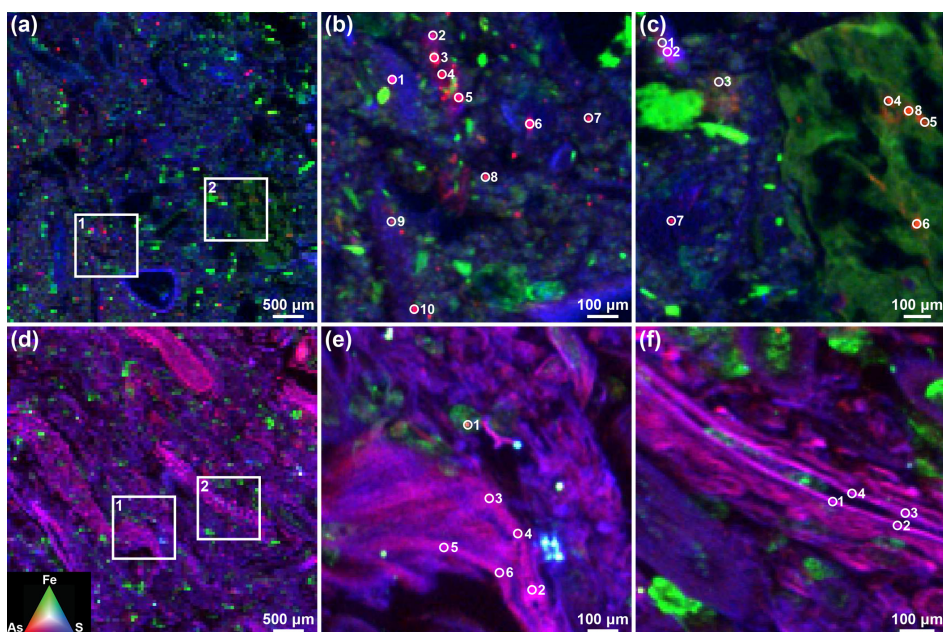


**Figure 3.3.** Tricolor (RGB)  $\mu$ -XRF maps of the distribution of As, Fe, and S in thin sections of (a-c) the near-surface peat layer sample B3II-31 and (d-f) the deep peat layer sample B1II-237. (a, d) Overview maps indicating the location of regions 1 and 2 in each thin section. (b, e) Fine maps of regions 1, and (c, f) fine maps of regions 2. The points of interest (POIs) selected for  $\mu$ -XAS analysis are shown in each fine map. The color code in (d) is valid for all panels.

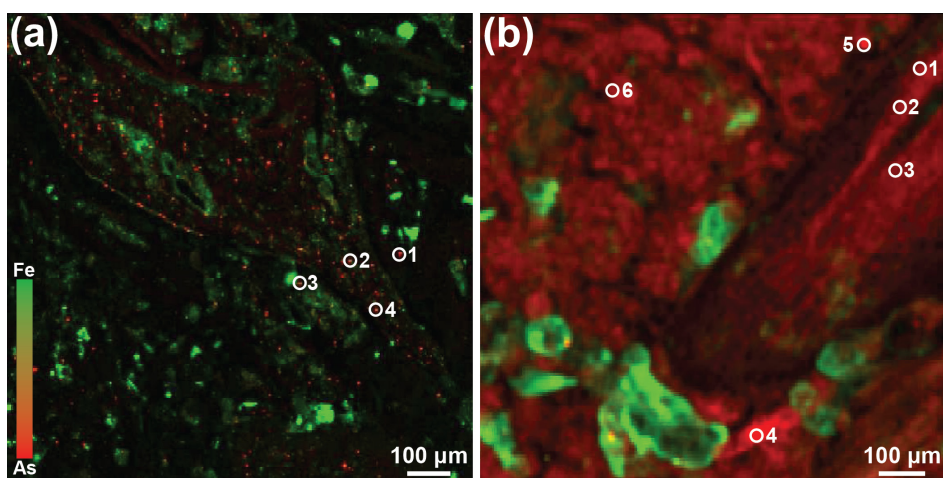


**Figure 3.4.** Bicolor (RG)  $\mu$ -XRF map of the As and Fe distribution in thin sections of (a) the near-surface peat layer sample B5II-12 and (b) the deep peat layer sample B1II-212. The points of interest (POIs) selected for  $\mu$ -XAS analysis are also shown in each map. The color code in (a) is valid for both panels.

The speciation of As was studied by As *K*-edge  $\mu$ -XAS at selected POIs indicated in each fine map shown in Figures 3.3 and 3.4. Similar POI spectra were averaged in order to increase the signal-to-noise ratio. The  $\mu$ -XANES spectra and their LCFs are illustrated in Figure 3.5 along with the  $k^2$ -weighted  $\mu$ -EXAFS spectra and their spectral reconstructions based on the LCF results, which are summarized in Table 3.1. All analyzed As hotspots in region 1 of the B3II-31 thin section (Figure 3.3b) entirely consisted of realgar. The POIs of region 2 of the B3II-31 sample (Figure 3.3c) were well fitted with variable mixtures of realgar (0-84%), As(III)-NOM complexes (0-44%), and As(III) (16-44%) as well as As(V) (0-71%) sorbed to Fe(III)-(hydr)oxides (Table 3.1). Interestingly, all POIs (4-6, 8) located on the highly altered gneiss fragment in the region 2 map (Figure 3.3c, Figure B.2, Appendix B) were dominated by As(III/V) sorbed to Fe(III)-(hydr)oxides, which are most likely weathering products of Fe-bearing silicates. Realgar was not the only As mineral detected in the near-surface peat samples. Figure 3.4 shows  $\sim 10 \mu\text{m}$  sized As hotspots partially strung along plant fibers in the B5I-12 sample. Micro-XAS analysis of these spots confirmed the presence of arsenopyrite (FeAsS) (Table 3.1).

Arsenic *K*-edge  $\mu$ -XAS analysis of the deep peat layer thin sections of core B1II revealed that trivalent As coordinated to sulfhydryl groups of NOM (Table 3.1) constitutes the diffusely distributed As found either on fibrous plant remains or on more humified NOM (Figure 3.3e-3.3f vs. Figure 3.4b, Figures B.2 and B.3, Appendix B). Besides As(III)-NOM complexes as dominating As species, several hotspots enriched in As, Fe, and S with an approximate size of less than  $25 \mu\text{m}$  were readily discernible in the deep peat layer samples (Figure 3.3e). While the whitish spots (rich in As, Fe, and S) indicate the presence of arsenopyrite, the As  $\mu$ -XAS spectrum collected at POI1 (Figure 3.3e) confirmed a mixture of 35% arsenopyrite and 65% arsenian pyrite (Table 3.1). Neither of these minerals was accepted as reference compound in LCF analyses of bulk As and Fe EXAFS spectra, implying that they were only present in trace amounts.

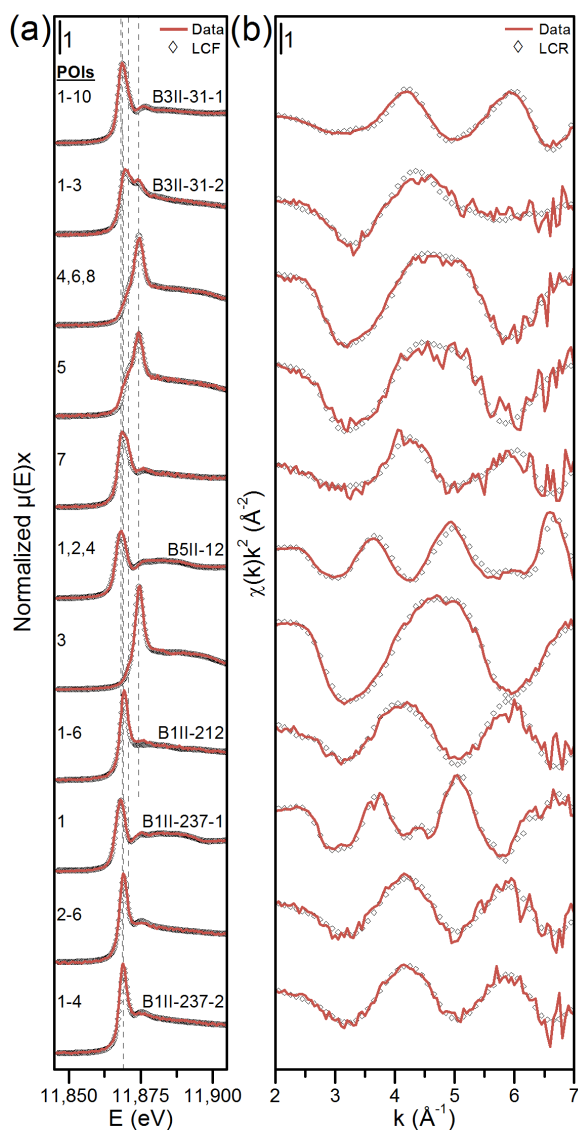


**Figure 3.5.** (a) Normalized As  $K$ -edge  $\mu$ -XANES and (b)  $k^2$ -weighted  $\mu$ -EXAFS spectra averaging selected POIs of thin sections from peat cores B1II, B3II, and B5II (Figures 3.3 and 3.4). The sample notation indicates core number, mean sampling depth of the thin section material in centimeters, and (where applicable) the number of the mapped region. Experimental data is shown as solid lines, and symbols represent linear combination fits (LCF) of the  $\mu$ -XANES spectra and linear combination reconstructions (LCR) of the  $\mu$ -EXAFS spectra based on the LCF results. LCF was performed from -15 to 20 eV ( $E-E_0$ ). The vertical lines in (a) indicate white-line positions of As(-I), As(II), As(III), and As(V) reference compounds (from left to right). The fit results are reported in Table 3.1.

**Table 3.1.** Arsenic speciation results based on linear combination fitting of  $\mu$ -XANES spectra collected at selected points of interest (POI) of the B1II, B3II, and B5II thin sections.

Sample ID <sup>a</sup>	POI	% of total As (normalized to a sum of 100%) <sup>b</sup>				Fitted sum (%) <sup>c</sup>	NSSR (%) <sup>d</sup>
		As(III)-NOM	Realgar	As-Fh	As-Py		
B3II-31-1	1-10	-	100	-	-	100	0.04
B3II-31-2	1-3	44 (0/44)	-	56 (44/12)	-	104	0.11
	4, 6, 8	-	-	100 (29/71)	-	102	0.08
	5	-	-	100 (44/56)	-	105	0.20
	7	-	84	16 (16/0)	-	104	0.20
B5II-12	1, 2, 4	-	-	-	100 (100/0)	100	0.11
	3	-	-	100 (0/100)	-	100	0.28
B1II-212	1-6	100 (100/0)	-	-	-	100	0.45
B1II-237-1	1	-	-	-	100 (35/65)	103	0.07
	2-6	100 (0/100)	-	-	-	100	0.23
B1II-237-2	1-4	100 (0/100)	-	-	-	100	0.52

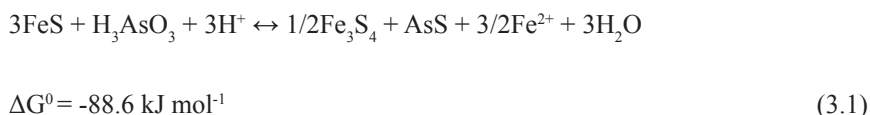
<sup>a</sup>The sample ID indicates core label, mean sampling depth of the thin section material in centimeters, and (where applicable) the number of the mapped regions shown in Figures 3.3 and 3.4. The POIs in the fine maps are also indicated in Figures 3.3 and 3.4.  $\mu$ -XANES spectra of all POIs are presented in Figure 3.5. <sup>b</sup>Values in parentheses indicate the fractions of the following reference compounds: As(III)-NOM = tris(phenylthio)arsine (As(III)(SPhen)<sub>3</sub>)/a mixture of a di- and triglutathione complex of As(III) (As(III)(GS)<sub>2,6</sub>(OH)<sub>0,6</sub>) [Langner et al., 2012], As-Fh = As(III)/As(V) sorbed to ferrihydrite, As-Py = arsenopyrite/arsenian pyrite. <sup>c</sup>Fitted sum of all references before normalization. <sup>d</sup>Normalized sum of squared residuals (NSSR (%)) =  $100 \times \sum_i (\text{data}_i - \text{fit}_i)^2 / \sum_i \text{data}_i^2$ .

### 3.4. Discussion

The bulk As speciation results (Figure 3.1) in conjunction with absent As-Fe correlations related to Fe(III)-(hydr)oxides (Figure B.5, Appendix B) show that these phases are of minor importance for the immobilization of As at the study site, despite that they typically play a crucial role in As sequestration [Bowell, 1994; Smedley and Kinniburgh, 2002]. Nonetheless, because they comprise up to 41% of total Fe, they can be expected to be effective scavengers of As released upon As sulfide oxidation following a seasonal drop in the water table.

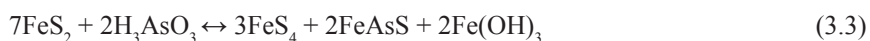
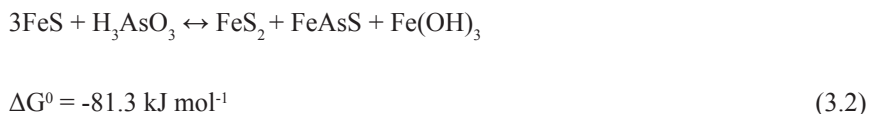
Our  $\mu$ -XRF and  $\mu$ -XAS analyses also document that the two distinct As enrichment patterns observed in the *Gola di Lago* peatland [Langner et al., 2012] are linked to two contrasting microscale As speciation and distribution patterns. Where As solution concentrations are high ( $\sim 5 \mu\text{M}$ ) as in the surface waters entering the peatland [González A. et al., 2006], they favor the precipitation of micrometer-sized (10-50  $\mu\text{m}$ ) As sulfides in shallow peat layers close to the stream inflow. The in-situ formation of realgar in

low-temperature/low pressure environments has so far only been observed in a shallow aquifer sediment [O'Day et al., 2004]. Reaction path modeling indicated that realgar precipitation is favored in anoxic circum-neutral pH environments, where the  $\text{H}_2\text{S}$  activity is buffered by the coexistence of Fe sulfides and Fe(II/III)-(hydr)oxides [O'Day et al., 2004]. Under such conditions, As(III) can be reduced by Fe monosulfides, leading to the formation of realgar and greigite ( $\text{Fe}_3\text{S}_4$ ) [Gallegos et al., 2007; Gallegos et al., 2008]:



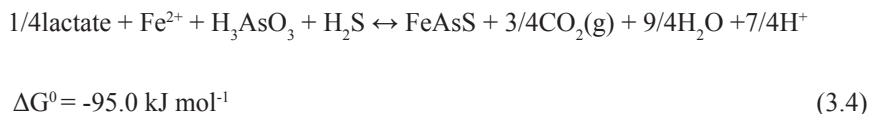
The Gibbs free energy change of reaction was calculated for mackinawite (FeS), and all thermodynamic data used for this and all subsequent reaction equations are tabulated in Table B.6, Appendix B. Despite that Equation 3.1 is thermodynamically favorable, we did not detect any Fe sulfide phase in the shallow peat layers by bulk Fe *K*-edge XAS and  $\mu$ -XRF analyses (Table B.3, Appendix B). A similar observation was reported by O'Day et al. [2004]. These results suggest the homogeneous precipitation of realgar or, alternatively, that nanometer-sized Fe sulfides [Wolthers et al., 2003] necessary for As(III) reduction (Equation 3.1) were below the analytical detection limits.

The discovery of arsenopyrite in the peat is another surprising finding because this mineral is unstable under the redox conditions encountered in the peat (Figure B.8, Appendix B) [Craw et al., 2003]. An intimate association of  $\sim 10 \mu\text{m}$  sized arsenopyrite particles with fibrous plant material (Figure 3.4) hints at an authigenic formation of arsenopyrite, which so far has only been reported for mining-affected sediments in a microcosm study [Rittle et al., 1995]. According to Bostick and Fendorf [2003], the formation of arsenopyrite can proceed by the reaction of As(III) with Fe sulfides:



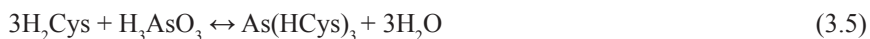
Here, FeS and  $\text{FeS}_2$  represent the troilite polymorph and pyrite, respectively. The reac-

tion products comprise poorly crystalline Fe(III)-(hydr)oxides as well as pyrite (Equation 3.2) and long chain polysulfides like Fe tetrasulfide (Equation 3.3). None of the proposed abiotic formation pathways of arsenopyrite involving Fe sulfides (Equations 3.2 and 3.3) are strictly supported by our data, which suggests direct biological controls on its formation. Equation 3.4, which couples the microbial respiration of organic matter to the reduction of As(III), may present an alternative arsenopyrite formation pathway not involving Fe sulfides but Fe(III)-(hydr)oxides and phyllosilicates like chlorite and biotite as potential Fe<sup>2+</sup> sources:



This reaction would be favored in reducing environments where the generated acidity is effectively buffered by the alkalinity produced during bacterial sulfate reduction. The occurrence of As sulfides in peat samples with ‘bulk’ redox potentials  $\geq -11$  mV generally highlights the presence of strongly reducing microenvironments with variable Fe and S solution concentrations (Figures B.8 and B.9, Appendix B).

In the deep peat layer samples, binding of As(III) by about three sulfhydryl groups was the major As sequestration mechanism (Figure 3.1, Table 3.1) despite that these samples contained high amounts of pyrite ( $\leq 36\%$  of  $\leq 8.3$  g Fe kg<sup>-1</sup>) known to be an effective host for As [Bostick and Fendorf, 2003; Lowers et al., 2007]. A maximum of 5 wt% in pyrite [Savage et al., 2000] would correspond to 24-78% of total As in the deep peat layer samples. This suggests that NOM is effectively inhibiting the sorption of As(III) to authigenic pyrite [González A. et al., 2006] and the substitution of As for S in its structure. The uptake of As by NOM rather than pyrite may be explained by a combination of fast pyrite precipitation, preventing As substitution reactions, and a high thermodynamic stability of the As(III)-NOM complexes. Indeed, the complexation of As(III) by sulfhydryl ligands in aqueous solution is highly favorable. For example, Rey et al. [2004] determined a log *K* of 29.84 ( $\Delta G^0 = -170.2$  kJ mol<sup>-1</sup>) for the reaction of cysteine (Cys = [C<sub>3</sub>H<sub>5</sub>NO<sub>2</sub>S]<sup>2-</sup>) with As(III):



Our As and S speciation results also indicate that the formation of As(III)-NOM complexes is favored by a high abundance of reduced organic S (Table B.4, Appendix B) and comparatively low As solution concentrations. Surface waters, increasingly depleted in As during infiltration from the near-surface peat layers downward, are likely more and more undersaturated in As with respect to As sulfides, and therefore, As(III) can be effectively sorbed by abundant sulfhydryl groups of NOM. The similar distribution of organic S-coordinated As in peat material featuring different degrees of decomposition (Figure 3.3e-3.3f vs. Figure 3.4b) supports a passive sorption mechanism [Hoffmann et al., 2012]. This reasoning is buttressed by findings showing that a direct uptake of As by plants would result in a localized As enrichment in individual plant tissue (e.g., xylem, cellular vacuoles, or vascular tissue) and does not always involve sulfhydryl groups [Pickering et al., 2006; Castillo-Michel et al., 2011; Seyfferth et al., 2011]. Moreover, As concentrations in various parts of plants collected at our sampling sites are too low to explain the formation of As(III)-NOM complexes by the uptake and intracellular detoxification of As by plants. The above-ground biomass only contained 0.13-11.9 mg As kg<sup>-1</sup> dry mass (mean: 2.5 mg As kg<sup>-1</sup>, *n* = 15), whereas root As concentrations, likely biased by high As contents of the peat at sites B3 and B5, ranged from 0.17 to 78.5 mg As kg<sup>-1</sup> dry mass (mean: 15.6 mg As kg<sup>-1</sup>, *n* = 8) (Table B.7, Appendix B). Our  $\mu$ -XAS/XRF study thus provides further evidence for sorptive As(III)-NOM interactions under conditions unfavorable for As sulfide precipitation and therefore emphasizes the need to account for NOM as a sorbent in geochemical equilibrium and transport models used to assess the fate of As in reduced NOM-rich environments.

### **Acknowledgements**

We gratefully acknowledge P. Poggiati and M. Sulmoni (Department of Environment, canton Ticino, Switzerland) for the sampling permit, and K. Barmettler, M. Hoffmann, P. Nievergelt, and D. Saile (ETH Zurich) for field and/or laboratory assistance. Micro-XRF/XAS analyses were carried out at the ALS, which is supported by the Director, Office of Science, Office of Basic Energy Sciences, of the U.S. Department of Energy under contract number DE-AC02-05CH11231. We are grateful to S. C. Fakra for her assistance



in using beamline 10.3.2. Bulk XAS spectra were measured at the SSRL, a Directorate of SLAC National Accelerator Laboratory and an Office of Science User Facility operated for the U.S. Department of Energy Office of Science by Stanford University. In this regard, we would like to thank M. J. Latimer and E. J. Nelson for their support in using beamline 4-3, and J. Bargar and M. J. Latimer for assistance in using beamline 11-2 and 4-1. Synchrotron XRD measurements were performed at the powder diffraction station of the MS-Powder beamline at the SLS, Paul Scherrer Institute, Villingen, Switzerland. The support of A. Cervellino (beamline scientist) and P. N. Mandaliev, K. Ehlert, and M. Hoffmann (ETH Zurich) is gratefully acknowledged. This research project was financially supported by the ETH Zurich under grant number 2708-2.

## References

- Anawar, H. M., Akai, J., Komaki, K., Terao, H., Yoshioka, T., Ishizuka, T., Safiullah, S., Kato, K. (2003) Geochemical occurrence of arsenic in groundwater of Bangladesh: Sources and mobilization processes. *J. Geochem. Explor.* 77, 109-131.
- Bolin, T. B. (2010) Direct determination of pyrite content in Argonne premium coals by the use of sulfur X-ray near edge absorption spectroscopy (S-XANES). *Energy Fuels* 24, 5479-5482.
- Bonazzi, P., Bindi, L. (2008) A crystallographic review of arsenic sulfides: Effects of chemical variations and changes induced by exposure to light. *Z. Kristallogr.* 223, 132-147.
- Bonazzi, P., Menchetti, S., Pratesi, G. (1995) The crystal structure of pararealgar, As<sub>4</sub>S<sub>4</sub>. *Am. Mineral.* 80, 400-403.
- Bostick, B. C., Fendorf, S. (2003) Arsenite sorption on troilite (FeS) and pyrite (FeS<sub>2</sub>). *Geochim. Cosmochim. Acta* 67, 909-921.
- Bowell, R. J. (1994) Sorption of arsenic by iron-oxides and oxyhydroxides in soils. *Appl. Geochem.* 9, 279-286.
- Buschmann, J., Kappeler, A., Lindauer, U., Kistler, D., Berg, M., Sigg, L. (2006) Arsenite and arsenate binding to dissolved humic acids: Influence of pH, type of humic acid, and aluminum. *Environ. Sci. Technol.* 40, 6015-6020.
- Castillo-Michel, H., Hernandez-Viezcas, J., Dokken, K. M., Marcus, M. A., Peralta-Videa, J. R., Gardea-Torresdey, J. L. (2011) Localization and speciation of arsenic in soil and desert plant *Parkinsonia florida* using  $\mu$ -XRF and  $\mu$ -XANES. *Environ. Sci. Technol.* 45, 7848-7854.
- Craw, D., Falconer, D., Youngson, J. H. (2003) Environmental arsenopyrite stability and dissolution: Theory, experiment, and field observations. *Chem. Geol.* 199, 71-82.
- Delvigne, J. E. (1998) *Atlas of micromorphology of mineral alteration and weathering*. Mineralogical Association of Canada: Ottawa.
- Dittmar, J., Voegelin, A., Roberts, L. C., Hug, S. J., Saha, G. C., Ali, M. A., Badruzzaman, A. B. M., Kretzschmar, R. (2010) Arsenic accumulation in a paddy field in Bangladesh: Seasonal dynamics and trends over a three-year monitoring period. *Environ. Sci. Technol.* 44, 2925-2931.
- Dixit, S., Hering, J. G. (2003) Comparison of arsenic(V) and arsenic(III) sorption onto iron oxide minerals: Implications for arsenic mobility. *Environ. Sci. Technol.* 37, 4182-4189.
- Frommer, J., Voegelin, A., Dittmar, J., Marcus, M. A., Kretzschmar, R. (2011) Biogeochemical processes and arsenic enrichment around rice roots in paddy soil: Results from micro-focused X-ray spectroscopy. *Eur. J. Soil Sci.* 62, 305-317.
- Gallegos, T. J., Han, Y.-S., Hayes, K. F. (2008) Model predictions of realgar precipitation by reaction of As(III) with synthetic mackinawite under anoxic conditions. *Environ. Sci. Technol.* 42, 9338-9343.

- Gallegos, T. J., Hyun, S. P., Hayes, K. F. (2007) Spectroscopic investigation of the uptake of arsenite from solution by synthetic mackinawite. *Environ. Sci. Technol.* 41, 7781-7786.
- González A., Z. I., Krachler, M., Cheburkin, A. K., Shoty, W. (2006) Spatial distribution of natural enrichments of arsenic, selenium, and uranium in a minerotrophic peatland, Gola di Lago, canton Ticino, Switzerland. *Environ. Sci. Technol.* 40, 6568-6574.
- Griffin, R. A., Jurinak, J. J. (1973) Estimation of activity coefficients from electrical conductivity of natural aquatic systems and soil extracts. *Soil Sci.* 116, 26-30.
- Hoffmann, M., Mikutta, C., Kretzschmar, R. (2012) Bisulfide reaction with natural organic matter enhances arsenite sorption: Insights from X-ray absorption spectroscopy. *Environ. Sci. Technol.* 46, 11788-11797.
- Kutoglu, A. (1976) Preparation and crystal-structure of a new isomeric form of  $As_4S_4$ . *Z. Anorg. Allg. Chem.* 419, 176-184.
- La Force, M. J., Hansel, C. M., Fendorf, S. (2000) Arsenic speciation, seasonal transformations, and co-distribution with iron in a mine waste-influenced palustrine emergent wetland. *Environ. Sci. Technol.* 34, 3937-3943.
- Landrot, G., Tappero, R., Webb, S. M., Sparks, D. L. (2012) Arsenic and chromium speciation in an urban contaminated soil. *Chemosphere* 88, 1196-1201.
- Langner, P., Mikutta, C., Kretzschmar, R. (2012) Arsenic sequestration by organic sulphur in peat. *Nat. Geosci.* 5, 66-73.
- Lemly, A. D., Finger, S. E., Nelson, M. K. (1993) Sources and impacts of irrigation drainwater contaminants in arid wetlands. *Environ. Toxicol. Chem.* 12, 2265-2279.
- Lowers, H. A., Breit, G. N., Foster, A. L., Whitney, J., Yount, J., Uddin, N., Muneem, A. (2007) Arsenic incorporation into authigenic pyrite, Bengal Basin sediment, Bangladesh. *Geochim. Cosmochim. Acta* 71, 2699-2717.
- Manceau, A., Nagy, K. L. (2012) Quantitative analysis of sulfur functional groups in natural organic matter by XANES spectroscopy. *Geochim. Cosmochim. Acta* 99, 206-223.
- Manning, B. A., Goldberg, S. (1997) Arsenic(III) and arsenic(V) adsorption on three California soils. *Soil Sci.* 162, 886-895.
- Masscheleyn, P. H., Delaune, R. D., Patrick, W. H. (1991) Effect of redox potential and pH on arsenic speciation and solubility in a contaminated soil. *Environ. Sci. Technol.* 25, 1414-1419.
- Moore, J. N., Ficklin, W. H., Johns, C. (1988) Partitioning of arsenic and metals in reducing sulfidic sediments. *Environ. Sci. Technol.* 22, 432-437.
- Mullen, D. J. E., Nowacki, W. (1972) Refinement of crystal structures of realgar,  $AsS$  and orpiment,  $As_2S_3$ . *Z. Kristallogr.* 136, 48-65.
- O'Day, P. A., Vlassopoulos, D., Root, R., Rivera, N. (2004) The influence of sulfur and iron on dissolved arsenic concentrations in the shallow subsurface under changing redox conditions. *Proc. Natl. Acad. Sci. USA* 101, 13703-13708.

- Pickering, I. J., Gumaelius, L., Harris, H. H., Prince, R. C., Hirsch, G., Banks, J. A., Salt, D. E., George, G. N. (2006) Localizing the biochemical transformations of arsenate in a hyperaccumulating fern. *Environ. Sci. Technol.* 40, 5010-5014.
- Prietzl, J., Botzaki, A., Tyufekchieva, N., Brettholle, M., Thieme, J., Klysubun, W. (2011) Sulfur speciation in soil by S K-edge XANES spectroscopy: Comparison of spectral deconvolution and linear combination fitting. *Environ. Sci. Technol.* 45, 2878-2886.
- Prietzl, J., Thieme, J., Salomé, M., Knicker, H. (2007) Sulfur K-edge XANES spectroscopy reveals differences in sulfur speciation of bulk soils, humic acid, fulvic acid, and particle size separates. *Soil Biol. Biochem.* 39, 877-890.
- Prietzl, J., Tyufekchieva, N., Eusterhues, K., Koegel-Knabner, I., Thieme, J., Paterson, D., McNulty, I., de Jonge, M., Eichert, D., Salomé, M. (2009) Anoxic versus oxic sample pretreatment: Effects on the speciation of sulfur and iron in well-aerated and wetland soils as assessed by X-ray absorption near-edge spectroscopy (XANES). *Geoderma* 153, 318-330.
- Redman, A. D., Macalady, D. L., Ahmann, D. (2002) Natural organic matter affects arsenic speciation and sorption onto hematite. *Environ. Sci. Technol.* 36, 2889-2896.
- Rey, N. A., Howarth, O. W., Pereira-Maia, E. C. (2004) Equilibrium characterization of the As(III)-cysteine and the As(III)-glutathione systems in aqueous solution. *J. Inorg. Biochem.* 98, 1151-1159.
- Rittle, K. A., Drever, J. I., Colberg, P. J. S. (1995) Precipitation of arsenic during bacterial sulfate reduction. *Geomicrobiol. J.* 13, 1-11.
- Root, R. A., Dixit, S., Campbell, K. M., Jew, A. D., Hering, J. G., O'Day, P. A. (2007) Arsenic sequestration by sorption processes in high-iron sediments. *Geochim. Cosmochim. Acta* 71, 5782-5803.
- Rothwell, J. J., Taylor, K. G., Chenery, S. R. N., Cundy, A. B., Evans, M. G., Allott, T. E. H. (2010) Storage and behavior of As, Sb, Pb, and Cu in ombrotrophic peat bogs under contrasting water table conditions. *Environ. Sci. Technol.* 44, 8497-8502.
- Savage, K. S., Tingle, T. N., O'Day, P. A., Waychunas, G. A., Bird, D. K. (2000) Arsenic speciation in pyrite and secondary weathering phases, Mother Lode Gold District, Tuolumne County, California. *Appl. Geochem.* 15, 1219-1244.
- Seyfferth, A. L., Webb, S. M., Andrews, J. C., Fendorf, S. (2011) Defining the distribution of arsenic species and plant nutrients in rice (*Oryza sativa* L.) from the root to the grain. *Geochim. Cosmochim. Acta* 75, 6655-6671.
- Skylberg, U., Xia, K., Bloom, P. R., Nater, E. A., Bleam, W. F. (2000) Binding of mercury(II) to reduced sulfur in soil organic matter along upland-peat soil transects. *J. Environ. Qual.* 29, 855-865.
- Smedley, P. L., Kinniburgh, D. G. (2002) A review of the source, behaviour and distribution of arsenic in natural waters. *Appl. Geochem.* 17, 517-568.
- Strawn, D., Doner, H., Zavarin, M., McHugo, S. (2002) Microscale investigation into the geochemistry of arsenic, selenium, and iron in soil developed in pyritic shale materials. *Geoderma* 108, 237-257.

- Tukhtabiev, M. A., Popova, S. V., Brazhkin, V. V., Lyapin, A. G., Katayama, Y. (2009) Compressibility and polymorphism of  $\alpha$ -As<sub>4</sub>S<sub>4</sub> realgar under high pressure. *J. Phys. Condens. Matter* 21, 1-7.
- Vairavamurthy, A. (1998) Using X-ray absorption to probe sulfur oxidation states in complex molecules. *Spectrochim. Acta, Part A* 54, 2009-2017.
- Violante, A., Pigna, M. (2002) Competitive sorption of arsenate and phosphate on different clay minerals and soils. *Soil Sci. Soc. Am. J.* 66, 1788-1796.
- Wolthers, M., Van der Gaast, S. J., Rickard, D. (2003) The structure of disordered mackinawite. *Am. Mineral.* 88, 2007-2015.
- Xia, K., Weesner, F., Bleam, W. F., Bloom, P. R., Skyllberg, U. L., Helmke, P. A. (1998) XANES studies of oxidation states of sulfur in aquatic and soil humic substances. *Soil Sci. Soc. Am. J.* 62, 1240-1246.
- Zhao, F. J., Lehmann, J., Solomon, D., Fox, M. A., McGrath, S. P. (2006) Sulphur speciation and turnover in soils: Evidence from sulphur K-edge XANES spectroscopy and isotope dilution studies. *Soil Biol. Biochem.* 38, 1000-1007.
- Zimmer, D., Kruse, J., Baum, C., Borca, C., Laue, M., Hause, G., Meissner, R., Leinweber, P. (2011) Spatial distribution of arsenic and heavy metals in willow roots from a contaminated floodplain soil measured by X-ray fluorescence spectroscopy. *Sci. Total Environ.* 409, 4094-4100.



## 4. Oxidation of organosulfur-coordinated arsenic and realgar in peat: Implications for the fate of arsenic

This chapter was published with minor modifications in *Environmental Science and Technology*: Langner P., Mikutta C., Kretzschmar R. (2014) Oxidation of organosulfur-coordinated arsenic and realgar in peat: Implications for the fate of arsenic. *Environ. Sci. Technol.* DOI 10.1021/es4049785.

### Abstract

Organosulfur-coordinated As(III) and realgar ( $\alpha$ -As<sub>4</sub>S<sub>4</sub>) have been identified as the dominant As species in the naturally As-enriched minerotrophic peatland *Gola di Lago*, Switzerland. In this study, we explored their oxidation kinetics in peat exposed to atmospheric O<sub>2</sub> for up to 180 days under sterile and nonsterile conditions (25 °C, ~100% relative humidity). Anoxic peat samples were collected from a near-surface (0-38 cm) and a deep peat layer (200-250 cm) and studied by bulk As, Fe, and S K-edge X-ray absorption spectroscopy as well as selective extractions as a function of time. Over 180 days, only up to 33% of organosulfur-coordinated As(III) and 44% of realgar were oxidized, corresponding to half-life times,  $t_{1/2}$ , of 312 and 215 days, respectively. The oxidation of both As species was mainly controlled by abiotic processes. Realgar was oxidized orders of magnitude slower than predicted from published mixed-flow reactor experiments, indicating that mass-transfer processes were rate-limiting. Most of the As released (>97%) was sequestered by Fe(III)-(hydr)oxides. However, water-extractable As reached concentrations of 0.7-19  $\mu\text{mol As L}^{-1}$ , exceeding the WHO drinking water limit by up to 145 times. Only a fraction (20-36%) of reduced S(-II to I) was sensitive to oxidation and was oxidized faster ( $t_{1/2}$  = 50-173 days) than organosulfur-coordinated As(III) and realgar, suggesting a rapid loss of reactive As-sequestering S species following

a drop in the water table. Our results imply that wetlands like *Gola di Lago* can serve as long-term sources for As under prolonged oxidizing conditions. The maintenance of reducing conditions is thus regarded the primary strategy in the management of this and other As-rich peatlands.

### 4.1. Introduction

Water-table fluctuations and shifts in biological activity frequently occur in wetlands [Reddy and DeLaune, 2008] and affect the dynamics of redox-sensitive, potentially hazardous metalloids like As. The effect of changing redox conditions on the mobility of As in wetland soils has been addressed in a number of field and laboratory studies, showing that the fate of As is primarily linked to the redox cycling of Fe and S [La Force et al., 2000; Fox and Doner, 2003; Beauchemin and Kwong, 2006; Blodau et al., 2008; Rothwell et al., 2009; Weber et al., 2010; Roberts et al., 2011]. While As is mainly associated with Fe(III)-(hydr)oxides under oxic conditions, their dissimilatory reductive dissolution under reducing conditions triggers the concomitant release of As and its sequestration by sulfide minerals under strongly reducing conditions [Smedley and Kinniburgh, 2002; Fendorf and Kocar, 2009]. However, several studies also reported As enrichments in strongly reduced wetland soils not related to the presence of Fe and S mineral phases, suggesting the direct binding of As by natural organic matter (NOM) [Blodau et al., 2008; Rothwell et al., 2009]. For this reason, we recently investigated the relevance of NOM as a sorbent for As in the naturally As-enriched ( $\leq 1,800$  mg As kg<sup>-1</sup>), slightly acidic minerotrophic peatland *Gola di Lago*, Switzerland [Langner et al., 2012]. Here, bulk X-ray absorption spectroscopy (XAS) revealed that As in anoxic deep peat layers (150-250 cm) was predominantly bound in its trivalent oxidation state to 2-3 sulfhydryl groups ('As(III)-NOM complexes') [Langner et al., 2012]. A similar microscale distribution of As in peat NOM featuring different decomposition stages implied that organo-sulfur-coordinated As(III) was mainly formed by the complexation of dissolved arsenite, As(III), by NOM under reducing conditions [Langner et al., 2013]. The validity of this 'passive sorption hypothesis' was confirmed in laboratory experiments for particulate



peat NOM and humic acid [Hoffmann et al., 2012].

To date, information about the stability of organosulfur-coordinated As(III) under oxidizing conditions in natural environments is completely lacking. Periodic or permanent soil drainage may cause a rapid oxidation of As(III)-NOM complexes, rendering wetlands with high abundances of organosulfur-coordinated As(III) undesirable sources for As. Indeed, laboratory studies indicate that complexes of As(III) and sulfhydryl ligands like glutathione or phytochelatins are extremely sensitive toward O<sub>2</sub> and disintegrate within hours to weeks [Raab et al., 2004; Kobayashi and Hirano, 2008; Bluemlein et al., 2009].

Besides the verification of As(III)-NOM complexes in deep peat layers of the *Gola di Lago* peatland, bulk and microfocused XAS analyses also revealed the presence of realgar ( $\alpha$ -As<sub>4</sub>S<sub>4</sub>) and As(III/V) sorbed to Fe(III)-(hydr)oxides in near-surface peat layers (<41 cm) [Langner et al., 2012; Langner et al., 2013]. The coexistence of these As species was explained by nonequilibrium conditions induced by a fluctuating water table [Langner et al., 2012], and the authigenic formation of realgar in strongly reducing microenvironments [Langner et al., 2013]. While the mechanisms and geochemical controls by which As is mobilized from Fe(III)-(hydr)oxides are well established [Masscheleyn et al., 1991; Smedley and Kinniburgh, 2002; Dixit and Hering, 2003], the release of As by the oxidative dissolution of realgar has not yet been investigated in field systems. Hitherto, the kinetics of realgar oxidation have been addressed in only a limited number of abiotic and biotic laboratory studies [Lengke and Tempel, 2003, 2005; Zhang et al., 2007; Chen et al., 2013]. Mixed-flow reactor experiments of Lengke and Tempel [2003, 2005] showed that the oxidation of As in natural realgar by dissolved O<sub>2</sub> ([DO] = 5.9-16.5 mg L<sup>-1</sup>) under steady-state conditions (pH 7.2-8.8, 25-40 °C) obeys an empirical rate law with fractional reaction orders for [DO] and [H<sup>+</sup>] of 0.51±0.08 and -0.28±0.05 at 25 °C, respectively. Quantum-mechanical calculations of Renock and Becker [2010] predicted a theoretical rate of realgar oxidation by molecular O<sub>2</sub> of  $\sim 1 \times 10^{-10}$  mol As<sub>realgar</sub> m<sup>-2</sup> s<sup>-1</sup> (pH 8, 25 °C), in agreement with the oxidation rate calculated by Lengke and Tempel [2003, 2005] for similar [DO] concentrations.

The role of microorganisms and aqueous Fe(II) in the oxidation of realgar remains largely elusive and was mainly studied for medical purposes at conditions irrelevant for most wetland systems [Zhang et al., 2007; Chen et al., 2013]. For example, Zhang et al.

[2007] showed that the oxidation of 'realgar' ( $\text{As}_4\text{S}_{5,6}$ ) at pH 1.8 and 30 °C was significantly enhanced in the presence of dissolved Fe(II) and mixed cultures of *Acidithiobacillus ferrooxidans* and *A. thiooxidans*, as compared to single culture experiments.

Even though these studies provide useful insights into the oxidation kinetics of realgar and their controls, the results cannot be transferred to field sites that significantly deviate from previous laboratory systems in terms of hydrologic conditions, realgar crystallinity, and solution chemistry, as well as microbial community composition and activity. The presence of both As(III)-NOM complexes and realgar in the *Gola di Lago* peat provided the unique possibility to study their oxidation kinetics and the resulting effects on As release.

Our main objective was to test whether prolonged oxidizing conditions in the As-rich *Gola di Lago* peat promote a net mobilization of As, or conversely, if (freshly precipitated) Fe(III)-(hydr)oxides lead to an As immobilization, as was shown for a low-As (5-25 mg As kg<sup>-1</sup>) peat soil [Blodau et al., 2008]. The specific goals of this study were to (i) investigate the oxidation kinetics of organosulfur-coordinated As(III) and realgar in the *Gola di Lago* peat, (ii) test whether their oxidation is controlled by abiotic or biotic processes, (iii) compare observed with predicted oxidation rates, and (iv) monitor the speciation and release of As in the peat. Therefore, anoxic peat samples collected from a near-surface (0-38 cm) and a deep peat layer (200-250 cm) of the *Gola di Lago* peatland were exposed to atmospheric O<sub>2</sub> in sterile (abiotic) and nonsterile (biotic) treatments for up to 180 days at 25 °C. Speciation changes of As, Fe, and S in the solid phase were followed with XAS and complemented by selective extractions.

## 4.2. Materials and methods

### 4.2.1. Experimental setup

Peat cores B3II and B1II were collected in the minerotrophic peatland *Gola di Lago* (canton Ticino, Switzerland) about 25 cm away from our initial sampling locations B3

and B1 [Langner et al., 2012]. The slightly acidic (pH  $5.3 \pm 0.1$ ), carbonate-free peat was retrieved from 0-38 cm (B3II) and 200-250 cm (B1II) depth and was immediately flash-frozen in liquid  $N_2$ , transported on dry ice to the laboratory, and defrosted in an anoxic glovebox ( $O_2 < 10$  ppm). A subsample of each peat batch was oven-dried ( $60^\circ C$ ), milled ( $< 50 \mu m$ ), and analyzed for total element concentrations by energy-dispersive X-ray fluorescence spectrometry (Spectro X-Lab 2000) and total C (equivalent to total organic C) using an elemental analyzer (Leco CHNS-932). The total As, C, Fe, and S contents of each peat batch are shown in Figure 4.1. Both peats differed fundamentally in their molar Fe/S ratio (B3II: 1.9, B1II: 0.2) and As speciation. Whereas realgar was the dominant As species in the near-surface B3II peat, the deep peat layer B1II batch was dominated by organosulfur-coordinated As(III) (see Chapter 4.3). The gravimetric water content of each field-moist peat batch was determined as weight loss after heating at  $105^\circ C$  for 24 h and constituted 77% for the B3II and 89% for the B1II batch. After general sample characterization, field-moist subsamples (2.8-5.1 g dry peat) from each homogenized batch were filled as  $< 5$  mm-thick layers into sterile cell culture flasks equipped with filter caps (Greiner Bio-One, CELLSTAR 650 mL) in a glovebox. Half of the 28 flasks prepared for monthly sampling over 180 days was subsequently sterilized using  $\gamma$ -radiation (34-37 kGy). All flasks were stored in an oven at  $25^\circ C$  and a relative humidity of 49-66% measured with a hygrometer. The partial pressure of  $O_2$  in the flasks, monitored with a fiber-optic oxygen meter system (Fibox 3-Trace, PreSens), was 21 kPa during the entire experiment. Water losses due to evaporation ( $< 6\%$ ) were compensated by monthly additions of sterile doubly deionized (DDI) water (Milli-Q, Millipore,  $\geq 18.2 M\Omega cm$ ). Every 30 days, a sterile and a nonsterile B3II and B1II flask were harvested for the measurements of pH, redox potential ( $E_h$ ), adenosine triphosphate (ATP) as an indicator for the viability of the microbial community, for selective extractions, as well as for the preparation of samples for bulk As, Fe, and S *K*-edge XAS analyses.

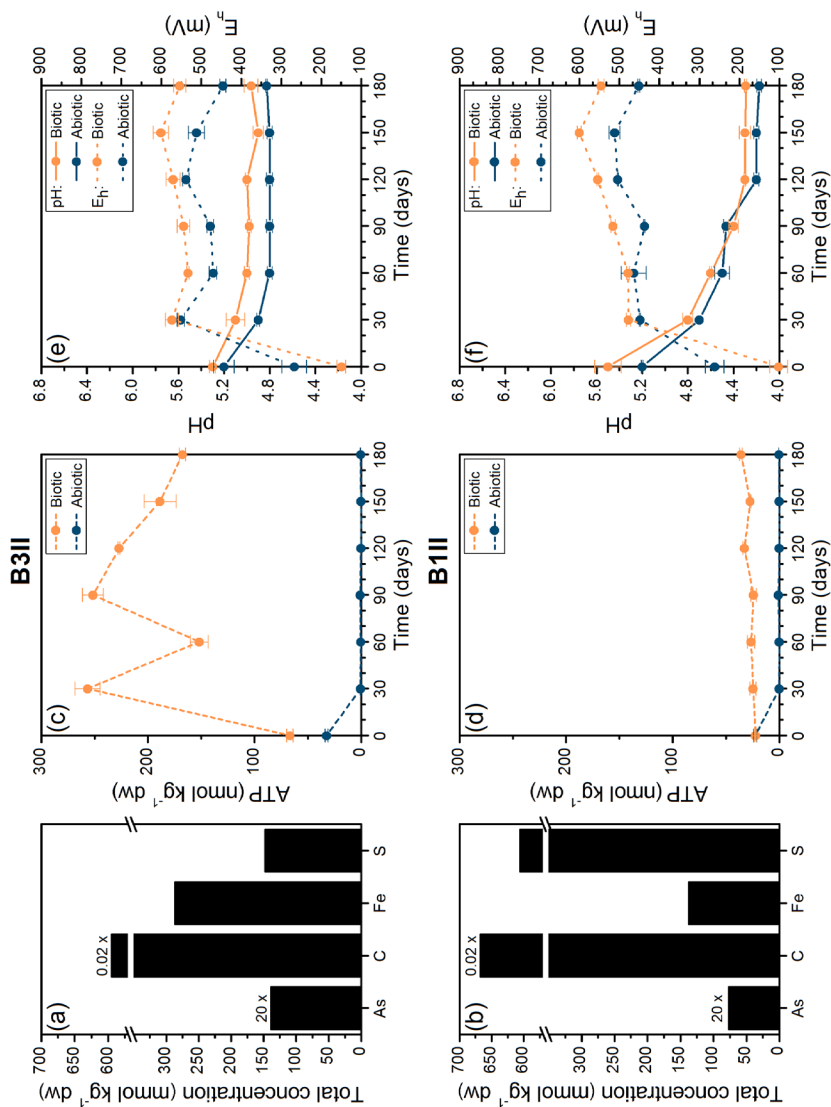


**Figure 4.1.** (a, b) Total concentrations of As, C, Fe, and S in the B3II and B1II peat batches, (c, d) adenosine triphosphate (ATP) concentrations, and (e, f) trends in pH and redox potential,  $E_{h,r}$ , in the abiotic and biotic experiments. Error bars denote standard deviations ( $n = 3$ ). In (a) and (b) the contents of As and C are scaled by factors of 20 and 0.02, respectively.

### 4.2.2. Adenosine triphosphate measurements

Two grams of moist peat were suspended in 50 mL sterile DDI water by sonication for 3 min. Three subsamples (2 mL) of the suspension were then diluted (1:10, v/v) with sterile, Mg-enriched (0.1 M MgCl<sub>2</sub>) Evian water and ATP was determined using the BacTiter-Glo Microbial Cell Viability Assay (G8231, Promega Corporation) and a GloMax 20/20 Luminometer (Turner BioSystems) following Hammes et al. [2010]. A pure ATP standard (100 nM, Promega Corporation) was used to calibrate luminescence intensity against ATP concentration. All measured ATP concentrations were normalized to the dry weight (dw) of the peat.

### 4.2.3. Selective extractions

Water and phosphate extractions were performed to assess oxidation-induced changes in the amount of 'labile' and 'strongly chemisorbed' As in the peat. The extraction scheme is based on Keon et al. [2001], but was slightly modified in terms of the solid-extractant ratios and centrifugation procedures. Triplicate field-moist peat samples containing ~0.8 g dry peat were weighed into 50-mL sealed Oak Ridge polycarbonate centrifuge tubes (Nalgene) and equilibrated with 30 mL anoxic DDI water or 1 M NaH<sub>2</sub>PO<sub>4</sub> solution (pH 5) on an overhead shaker for 24 h. The resulting solid-solution ratio ranged from 1:35.3 to 1:38.1. The phosphate extraction step was followed by an additional 30-min extraction step using anoxic DDI water [Keon et al., 2001] as described above in order to remove As remaining in the centrifugates. Both extracts were subsequently combined. After equilibration, the suspensions were centrifuged for 30 min at 5,615 g. The tubes were transferred into the glovebox, where the supernatants were decanted and filtered through 0.2- $\mu$ m cellulose nitrate membrane filters (Whatman). To estimate the amount of colloidal As in the phosphate extracts, an aliquot of each extract was additionally filtered through a 3-kDa membrane using centrifugal filter devices (Amicon Ultra-15, Millipore)

operated at 3,396 g for 50 min. All filtrates were stored in the glovebox until analysis. The concentrations of total As and As(III) were measured in nonacidified filtrates with a hydride generation atomic fluorescence spectrometer (AFS, Millennium Excalibur, PS Analytical Ltd.) according to Roberts et al. [2004]. The concentrations of Fe and S in the filtrates were determined with inductively coupled plasma-optical emission spectrometry (ICP-OES, Varian Vista-MPX) and dissolved organic C (DOC) was measured with a DIMATOC 2000 analyzer. For both analyses the filtrates were acidified with HCl. Standard deviations for the AFS, ICP-OES, and DOC measurements were calculated with an one-way ANOVA utilizing the statistics software R 2.15.2 [R-Core-Team, 2012].

### 4.2.4 Bulk X-ray absorption spectroscopy

Bulk As *K*-edge (11,867 eV), Fe *K*-edge (7,112 eV), and S *K*-edge (2,472 eV) XAS spectra were collected at beamlines 11-2 (As), 4-1 (Fe), and 4-3 (S) of the Stanford Synchrotron Radiation Lightsource (SSRL, SLAC National Accelerator Laboratory, Menlo Park, USA). Details about sample preparation, experimental setups, measurement conditions, and data evaluations can be found in Appendix C.

## 4.3. Results

### 4.3.1. Changes in geochemical parameters

Trends in ATP, pH, and  $E_h$  upon oxidation of the B3II and B1II peats under sterile and nonsterile conditions are shown in Figure 4.1. Owing to the short time elapsed between  $\gamma$ -irradiation and the first ATP measurements in the abiotic treatments, the ATP values measured at the start of the experiment were still comparatively high but remained close to zero ( $0.3 \pm 0.3$  nmol ATP kg<sup>-1</sup> dw) in the following 180 days. In the biotic treatments, the

concentration and variability of ATP in the near-surface B3II peat significantly exceeded those of the deep peat layer B1II batch ( $28 \pm 5$  vs.  $187 \pm 67$  nmol ATP kg<sup>-1</sup> dw), indicating a higher microbial activity in shallow peat layers of the *Gola di Lago* peatland.

The initial pH was comparable in both peat batches ( $5.3 \pm 0.1$ ) and decreased by only 0.3-0.4 units in the B3II peat, particularly during the first 60 days. In contrast, the pH decrease in the B1II peat was more pronounced (1.0-1.2 pH units) and lasted over the first 120 days. In both peat batches, the initial  $E_h$  values were lower in the biotic (101-149 mV) than in the abiotic treatments (261-267 mV). Within the first 30 days of oxidation,  $E_h$  values strongly increased by 187-424 mV in both peat batches and these changes were generally more distinct in the biotic treatments (Figure 4.1).

#### 4.3.2. Arsenic speciation changes

The solid-phase speciation of As in the sterile and nonsterile B3II and B1II peats was investigated after 0, 90, and 180 days of oxidation. The  $k^3$ -weighted extended X-ray absorption fine structure (EXAFS) spectra, their LCFs, and the corresponding fit results are illustrated in Figure 4.2 and summarized in Table C.2, Appendix C. In addition, As  $K$ -edge X-ray absorption near-edge structure (XANES) spectra are displayed in Figure C.1, Appendix C. The results show that at the start of the experiment, the near-surface B3II peat was dominated by realgar (91/100%). After 180 days of oxidation, 39 and 44% of As in realgar (As(II)) was transformed into As(V)-sorbed Fe(III)-(hydr)oxides. A similar speciation change was observed for the deep peat layer B1II batch. Here, As was initially present as As(III) coordinated to 2-3 sulfhydryl groups. Six months later, only 28 and 33% of the organosulfur-coordinated As(III) transformed into As(V) associated with Fe(III)-(hydr)oxides. The speciation data were fitted to a pseudo-first order kinetics (Figure 4.2), yielding half-life times for realgar and As(III)-NOM complexes in the biotic treatments of 215 and 312 days, respectively. Suppression of microbial activity caused a 45% increase in the half-life time of realgar and a 21% increase for As(III)-NOM complexes (Figure 4.2).

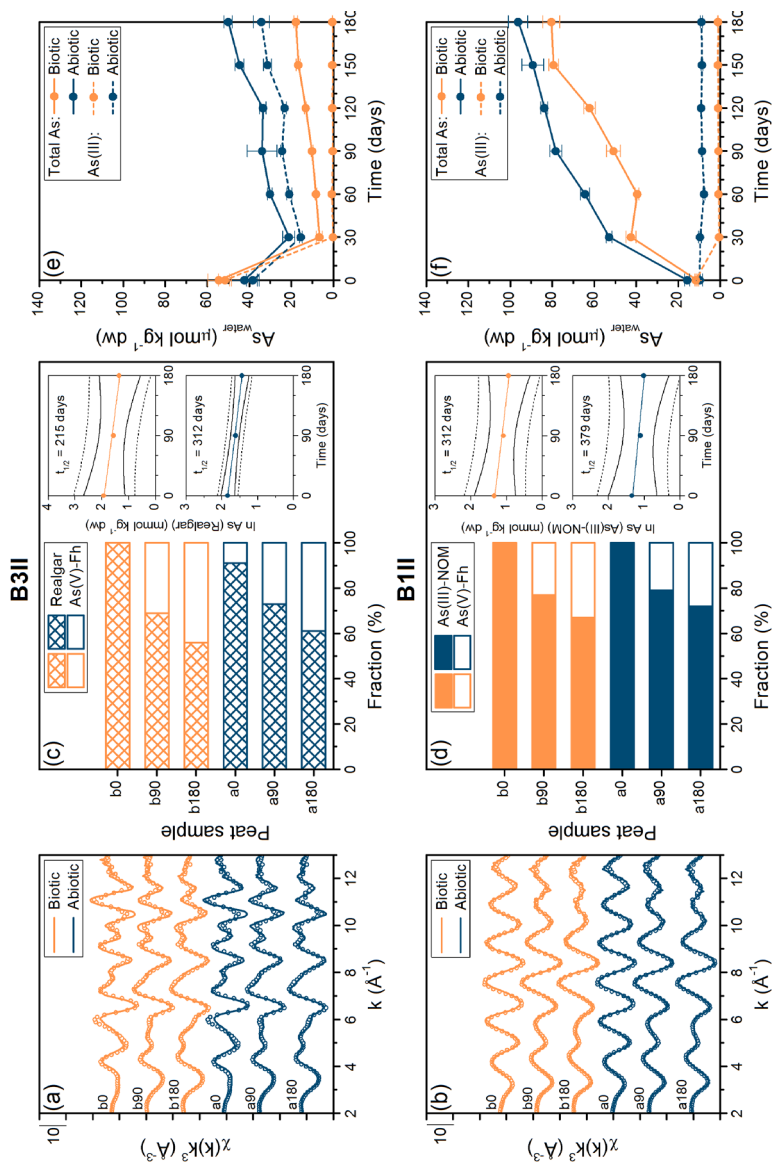


**Figure 4.2.** (a, b) Bulk As K-edge EXAFS spectra (lines) of the B3II and B1II peat batches and corresponding best model fits (symbols). Sample names indicate abiotic or biotic treatments (a/b) and day of sampling (0/90/180). (c, d) Fractions of each reference compound fitted in the LCF analyses (Table C.2, Appendix C). Insets display the linearized concentration data of (c) realgar and (d) organosulfur-coordinated As(III) and fits of a pseudo-first order kinetics. Here, solid and dashed lines mark, respectively, the 95% confidence and 95% prediction intervals. (e, f) Concentrations of total As (solid line) and As(III) (dashed line) in the 0.2-μm filtered water extracts. Error bars denote standard deviations ( $n = 3$ ).



The trends in water-extractable As of each peat batch, expressed as  $\mu\text{moles As per kilogram dry peat}$ , are also shown in Figure 4.2. The total amount of As released in the water extracts was always higher in the abiotic compared to the biotic treatments. In the B3II peat, the water-extractable As hardly exceeded the initial values of 42.3 and 54.5  $\mu\text{mol As kg}^{-1} \text{ dw}$  (Figure 4.2). On the basis of the As content of 6.9  $\text{mmol As kg}^{-1} \text{ dw}$  (Figure 4.1), only up to 0.8% of total As was water-extractable in the B3II peat, corresponding to a measured As solution concentration of  $\sim 6 \mu\text{mol As L}^{-1}$ . In contrast, a significant increase (6-7 times) in water-extractable As was observed for the deep peat layer B1II batch (Figure 4.2). In this case, the maximal amount of As released was 3% of total As (3.8  $\text{mmol As kg}^{-1} \text{ dw}$ , Figure 4.1), equivalent to a measured As solution concentration in the water extract of  $\sim 19 \mu\text{mol As L}^{-1}$ . The release kinetics of As also differed between the two peat batches. While the B3II peat exhibited an As concentration drop in all treatments after 30 days, there was a strong and steady increase in water-extractable As in the As(III)-NOM-dominated B1II peat (Figure 4.2). In addition, both peat batches showed marked dissimilarities in the aqueous-phase As speciation of the abiotic treatments. Initially, As(III) was always the dominant As species (90-100%) in the water extracts. Whereas As(III) remained the major species (68-73%) in the sterile B3II peat during the entire duration of the experiment, it only made up a minor and decreasing fraction (9-18%) of water-extractable As in the sterile B1II peat. In all biotic treatments, As(III) concentrations dropped to zero after 30 days of oxidation, rendering As(V) the dominant As solution species (Figure 4.2).

Phosphate-extractable As, which is considered to include strongly chemisorbed As, exceeded the water-extractable As by up to 57 times in the B3II and by only up to 3 times in the B1II peat. While the total amount of As released by phosphate was comparable in abiotic and biotic treatments, the amount of As(III) extracted was always lower in the biotic treatments and only comprised a negligible portion of total As (Figure C.2, Appendix C). We did not observe differences in As concentrations in the 0.2- $\mu\text{m}$  and 3-kDa filtered phosphate extracts, implying that all As was in the dissolved form (Figure C.2, Appendix C). Even though phosphate was added in excess (1 M) and 9-44% of As was associated with Fe(III)-(hydr)oxides (Table C.2, Appendix C) only 2-11% of total As was extracted, suggesting that this method is not entirely effective [Jackson and Miller,

2000] and/or that some sorption sites are specific to As(V) [Liu et al., 2001; Zeng et al., 2008; Zhang et al., 2008].

### 4.3.3. Iron speciation changes

The solid-phase speciation of Fe was investigated at the start and end of the experiment. Iron *K*-edge EXAFS spectra, their LCFs, and the corresponding fit results are illustrated in Figure 4.3 and summarized in Table C.3, Appendix C. The respective XANES spectra are displayed in Figure C.1, Appendix C. The LCF results show that the Fe speciation in the sterile/nonsterile near-surface peat B3II, which comprised Fe(III)-NOM complexes (28/30%), Fe(III)-(hydr)oxides (18/10%), and phyllosilicates (54/60%), did not change significantly. The sterile/nonsterile deep peat layer batch B1II initially comprised pyrite (26/26%), Fe(III)-NOM complexes (47/52%), and phyllosilicates (27/22%). After 180 days, pyrite was quantitatively transformed into Fe(III)-(hydr)oxides. We also noted nonsystematic variations in the fitted phyllosilicate fractions in each biotic treatment (Table C.3, Appendix C), which are presumably caused by sample heterogeneity and/or orientation effects [Manceau and Schlegel, 2001].

Water-extractable Fe, which likely constitutes dissolved Fe(II) and organic Fe complexes, dropped markedly after the start of the experiment, particularly in the B3II peat (Figure 4.3). The phosphate-extractable Fe exceeded the water-extractable Fe by up to 36 (B3II) and 53 times (B1II). While in the B3II sample, most of the phosphate-extractable Fe resided in the >3-kDa fraction (colloidal Fe), more than half of the phosphate-extractable Fe in the B1II sample comprised truly dissolved Fe (Figure C.2, Appendix C). On the basis of the total Fe content of 286 mmol Fe kg<sup>-1</sup> dw in the B3II and 137 mmol Fe kg<sup>-1</sup> dw in the B1II peat (Figure 4.1), the Fe released by phosphate only accounted for up to 0.3 and 0.2% of total Fe, respectively.

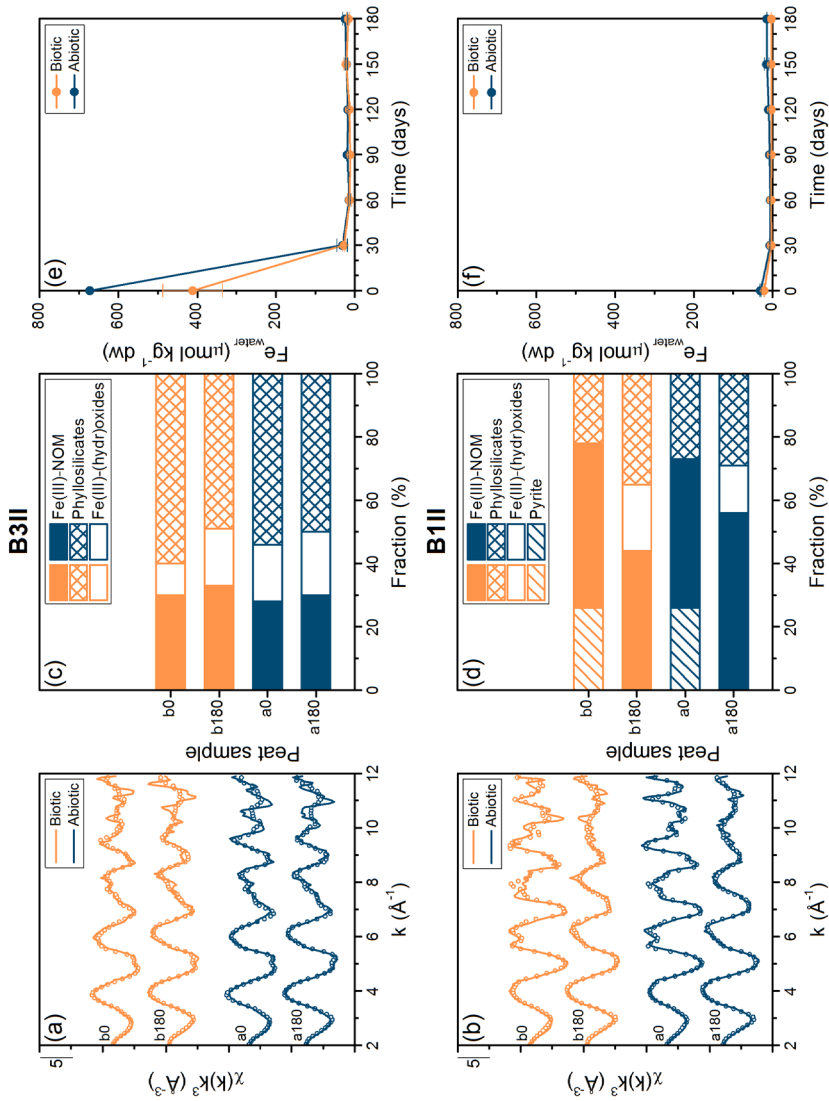


**Figure 4.3.** (a, b) Bulk Fe K-edge EXAFS spectra (lines) of the B3II and B1II peat batches and corresponding best model fits (symbols). Sample names indicate abiotic or biotic treatments (a/b) and day of sampling (0/180). (c, d) Fractions of each reference compound fitted in the LCF analyses (Table C.3, Appendix C). (e, f) Concentrations of Fe in the 0.2- $\mu\text{m}$  filtered water extracts. Error bars indicate standard deviations ( $n = 3$ ).

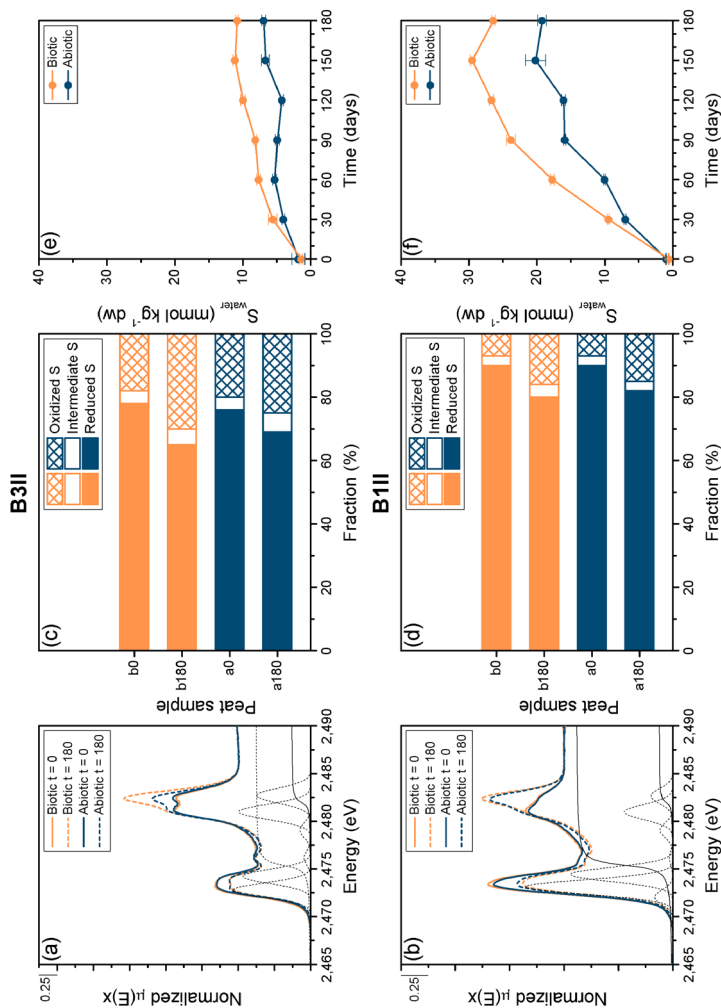
#### 4.3.4. Sulfur speciation changes

Figure 4.4 shows the evolution of S *K*-edge XANES spectra over time and the results of their Gaussian deconvolution based on the main S functionalities reduced S (inorganic sulfide S and exocyclic/heterocyclic organic S), intermediate oxidized S (sulfoxide, sulfite, and sulfone S), and oxidized S (sulfonate and sulfate S) (Table C.4, Appendix C). Initially, the sterile/nonsterile B3II peat contained 76/78% reduced S (71/71% reduced organic S), and 20/18% oxidized S, whereas the B1II peat comprised 90/90% reduced S (80/80% reduced organic S), and only 7/7% oxidized S (Figure 4.4, Table C.4, Appendix C). The fitted fractions of intermediate oxidized S species were of less quantitative importance (<6%, Figure 4.4, Table C.4, Appendix C), and are likely affected by post-edge absorption features of reduced organic S species as well as the first arctangent function [Manceau and Nagy, 2012]. In all samples, the amount of oxidized S increased by up to 12% (B3II) and 9% (B1II) at the expense of reduced S. The loss of reduced S was always slightly higher in the biotic compared to the abiotic treatments, and comprised up to 13% (thereof 8% reduced organic S) of the total S in the B3II peat and up to 10% (thereof 5% reduced organic S) in the B1II peat.

The oxidation kinetics of reduced S in both peat batches were fitted to a monoexponential model:

$$S_{\text{red}}(t) = S_{\text{red, const}} + S_{\text{red, ox}} \exp(-kt) \quad (4.1)$$

where  $S_{\text{red, const}}$  and  $S_{\text{red, ox}}$  are, respectively, the oxidation-resistant and oxidizable reduced S pool ( $\text{mmol kg}^{-1} \text{ dw}$ ),  $t$  is time (day), and  $k$  is the rate constant ( $\text{day}^{-1}$ ) ( $= \ln(2)/t_{1/2}$ ). The fits, illustrated in Figure C.4, Appendix C, imply that the majority of S in the  $S_{\text{red}}$  pool, dominated by reduced organic S (Tables C.4 and C.5, Appendix C), is not oxidized to higher oxidation states (II-VI), possibly due to the presence/formation of thioethers, organic di- or polysulfides, or due to  $\text{O}_2$  buffering by other functional groups of NOM [Hutchison et al., 2001]. The  $S_{\text{red, const}}$  pool comprised up to 64% of the total S in the B3II peat ( $147 \text{ mmol S kg}^{-1} \text{ dw}$ ) and 80% in the B1II peat ( $606 \text{ mmol S kg}^{-1} \text{ dw}$ ). The calculated half-lives of the  $S_{\text{red, ox}}$  pool, likely constituting mercaptans and inorganic sulfides, were short: 87 days in the nonsterile B3II and 50 days in the nonsterile B1II peat. In the abiotic treatments,  $t_{1/2}$  increased to 173 and 69 days, respectively (Table C.5, Appendix C).



**Figure 4.4.** (a, b) Normalized bulk S K-edge XANES spectra of the B3II and B1II peat batches collected at the start of the experiment (solid lines) and after 180 days of oxidation (dashed lines). The spectral deconvolutions into several Gaussians (black dotted lines) and two arctangent functions (black solid lines) are exemplarily shown for the biotic B3II and B1II samples ( $t = 0$  days). Parameter values are summarized in Table C.1, Appendix C. (c, d) Fractions of reduced (-II to I), intermediate oxidized (II to IV), and oxidized (V to VI) S forms obtained by Gaussian curve fitting. Sample names indicate abiotic or biotic treatments (a/b) and day of sampling (0/180). The spectra for all sampling days (0-180) and treatments are shown in Figure C.3 and the corresponding fit results are summarized in Table C.4, Appendix C. (e, f) Concentrations of S in the 0.2- $\mu\text{m}$  filtered water extracts. Error bars indicate standard deviations ( $n = 3$ ).

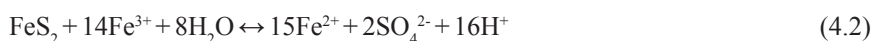
The oxidation of reduced S was accompanied by a continuous increase in water-extractable S. This increase was more pronounced in the biotic treatments and for the BIII batch (Figure 4.4), and accounted for up to 8% of total S in the B3II and 5% in the BIII peat.

## 4.4. Discussion

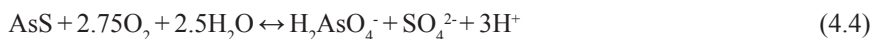
### 4.4.1. Changes in geochemical parameters

In the biotic treatments, ATP values ranged from 28 to 187 nmol ATP kg<sup>-1</sup> dw, which are low compared to values reported for horticultural peat (2.2-3.9 μmol ATP kg<sup>-1</sup> dw) [Sparling et al., 1981] or grass- and woodland samples (1.3-18 μmol ATP kg<sup>-1</sup> dw) [Contin et al., 2002]. This discrepancy may in part be related to the different ATP extraction methods employed (e.g., trichloroacetic-phosphate-paraquat reagent vs. water extraction). Nonetheless, the microbial activity was high enough to result in higher redox potentials in the biotic treatments (Figure 4.1), probably as a result of bacterial Fe, S, and/or N oxidation [Roden et al., 2004; Vymazal, 2007; Weiss et al., 2007; Wang et al., 2011].

The lower pH values in the deep peat layer BIII batch as compared to the B3II peat mainly resulted from the oxidation of pyrite (Figure 4.3). Under the prevailing pH conditions (pH 4.2-5.5) in the BIII peat, dissolved Fe(III) – presumably stabilized by Fe(III)-chelating ligands [Peiffer and Stubert, 1999] – can be considered the main oxidant for pyrite, whereas dissolved O<sub>2</sub> primarily sustains the pyrite oxidation by generating Fe(III) [Moses et al., 1987; Moses and Herman, 1991]. The Fe(III) mediated pyrite oxidation (Equation 4.2) holds for both the abiotic and biotic treatments [Moses et al., 1987; Moses and Herman, 1991]:



Moses et al. [1987] have shown that at elevated pH (>4.5) the pyrite oxidation depends more on the Fe(III) formation kinetics than on the reservoir of dissolved Fe(III), which is consistent with the low Fe concentrations measured in the water extracts (Figure 4.3). Iron-oxidizing bacteria might have additionally accelerated the pyrite oxidation by direct or indirect metabolic reactions [Evangelou and Zhang, 1995] in the biotic treatments. On the basis of the generalized Equation 4.3 for pyrite oxidation [Nordstrom, 1979] and a pyrite-S content of 71 mmol S kg<sup>-1</sup> dw in the B1II peat, approximately 142 mmol H<sup>+</sup> kg<sup>-1</sup> dw were produced. In contrast, the oxidation of a maximum of 44% realgar (equivalent to 3 mmol S kg<sup>-1</sup> dw) by dissolved O<sub>2</sub> (Equation 4.4) [Lengke et al., 2009] in the B3II peat would have only resulted in about 9 mmol H<sup>+</sup> kg<sup>-1</sup> dw.



#### 4.4.2. Oxidation of organosulfur-coordinated arsenic and realgar

The main initial As species realgar in the near-surface peat batch B3II and As(III)-NOM complexes in the deep peat layer batch B1II transformed into As(V) sorbed to Fe(III)-(hydr)oxides during 180 days of oxidation (Figure 4.2). The half-life times of realgar and As(III)-NOM complexes in the biotic treatments were 215 and 312 days, respectively, and increased only slightly under sterile conditions (Figure 4.2). These results imply that the oxidation of both As species was largely controlled by abiotic processes, and that As(III)-NOM complexes are more resistant toward oxidation than realgar whose oxidative dissolution (Equation 4.4) involves several intermediate surface oxidation steps [Lengke and Tempel, 2003]. The high stability of As(III)-NOM complexes is surprising because organosulfur-coordinated As(III) is typically extremely sensitive toward O<sub>2</sub> [Raab et al., 2004; Kobayashi and Hirano, 2008; Bluemlein et al., 2009]. For example, Raab et al. [2004] found an almost complete disintegration of As(III)-glutathione (As(III)-GS<sub>3</sub>) complexes in deionized water after 6 h at pH 6.5 and 25 °C. Likewise, As(III)-phytochelatin complexes in intact plant material stored at -20 °C

disintegrated after 4 weeks [Bluemlein et al., 2009]. Hence, we speculate that abundant reduced S species in the peat (65/90% of total S, Table C.4, Appendix C) effectively impaired the oxidation of As(III)-NOM complexes. This reasoning is supported by Kobayashi and Hirano [2008] showing that the presence of free glutathione stabilized As(III)-GS<sub>3</sub> complexes in rat bile.

The average oxidation rate of realgar in the B3II sample was estimated as  $3.9 \times 10^{-11}$  mol As<sub>realgar</sub> day<sup>-1</sup> under sterile and  $6.3 \times 10^{-11}$  mol As<sub>realgar</sub> day<sup>-1</sup> under nonsterile conditions, respectively. We also calculated the theoretical oxidation rate of As in realgar with the rate law established from mixed-flow reactor experiments by Lenke and Tempel [2003]:

$$R_{As} \text{ (mol m}^{-2} \text{ s}^{-1}\text{)} = 10^{-9.63} [\text{DO}]^{0.51} [\text{H}^+]^{-0.28} \quad (4.5)$$

where  $R_{As}$  indicates the oxidation rate of realgar-As, [DO] is the dissolved O<sub>2</sub> concentration (M), and [H<sup>+</sup>] is the proton concentration [M]. Here, we used a p[H] of 5, a DO concentration of  $2.65 \times 10^{-4}$  M ( $p\text{O}_2 = 21$  kPa,  $K_{\text{H}} = 1.26 \times 10^{-5}$  mol kg<sup>-1</sup> kPa<sup>-1</sup>, 25 °C), which resulted in a theoretical As oxidation rate of  $8.83 \times 10^{-11}$  mol As<sub>realgar</sub> m<sup>-2</sup> s<sup>-1</sup> ( $7.62 \times 10^{-6}$  mol As<sub>realgar</sub> m<sup>-2</sup> day<sup>-1</sup>). For rate comparisons, the initial surface area of realgar in the B3II peat needs to be assessed: The amount of realgar in the B3II peat calculated from the total As content and As speciation results was 3.4 and 3.8 mg (Figures 4.1 and 4.2, Table C.2, Appendix C), and the average size of realgar particles in the *Gola di Lago* peat, as judged from microfocused X-ray fluorescence spectrometry was about 30 μm [Langner et al., 2013]. Assuming a spherical particle size and a realgar density of 3.56 cm<sup>3</sup> g<sup>-1</sup> [Bonazzi et al., 1995], the surface area of realgar in the samples is calculated as  $1.9 \times 10^{-4}$  and  $2.1 \times 10^{-4}$  m<sup>2</sup>. These unrealistically low surface area estimates translate into theoretical realgar oxidation rates of  $1.45 \times 10^{-9}$  and  $1.62 \times 10^{-9}$  mol As<sub>realgar</sub> day<sup>-1</sup>, which are already about 30-fold higher than our experimental oxidation rates. Apparently, the oxidation kinetics of realgar in environmental systems characterized by stagnant pore waters are several order of magnitude slower compared to environments with advective flow. This suggests that the diffusion of O<sub>2</sub> to the realgar surface and/or product removal from the realgar surface controlled its oxidation kinetics in the peat. A negative effect of O<sub>2</sub> buffering by reduced organic S on the rate of realgar oxidation also cannot be



ruled out. The enhanced realgar oxidation in the biotic treatments may be caused by the production of Fe(III) oxidants upon bacterial Fe(II) oxidation [Zhang et al., 2007; Chen et al., 2013] and/or the dissolution of a protective  $S^0$  layer on realgar by S oxidizing bacteria [Zhang et al., 2007]. Like realgar, organosulfur-coordinated As(III) was also faster oxidized in the biotic treatments (Figure 4.2), probably as a result of bacterial As(III) detoxification and/or oxidation reactions [Weeger et al., 1999; Rosen, 2002; Oremland and Stolz, 2003]. This reasoning is supported by the absence of As(III) in the water extracts of the biotic treatments after 30 days of oxidation (Figure 4.2) and smaller amounts of phosphate-extractable As(III) in the biotic compared to the abiotic treatments (Figure C.2, Appendix C).

#### 4.4.3. Fate of arsenic released

In all treatments, most (>97%) of the As released during the oxidation of realgar and As(III)-NOM complexes was sequestered by pre-existing or newly formed Fe(III)-(hydr)oxides (Figure 4.2). However, water-extractable As still ranged between 7 and 96  $\mu\text{mol As kg}^{-1} \text{ dw}$ , corresponding to measured As solution concentrations of 0.7 and 19  $\mu\text{mol As L}^{-1}$ , respectively. These concentrations, probably underestimated by a factor of 4-11 due to the low solid-solution ratio employed, well exceed the WHO drinking water limit of 0.13  $\mu\text{mol As L}^{-1}$  (10  $\mu\text{g As L}^{-1}$ ) [WHO, 2008]. Our results thus show that freshly formed and/or initially present Fe(III)-(hydr)oxides (Figure 4.3) do not result in a long-term immobilization of As released upon oxidation (Figure 4.2). In the B3II peat, they only exerted a short negative net effect on water-extractable As (Figure 4.2).

Surprisingly, the amount of water-extractable As in the deep peat layer B1II batch exceeded that of the surface-near B3II peat by up to 5 times in the abiotic and 12 times in the biotic treatment, despite that the total amount of Fe(III)-(hydr)oxides was only up to 3 times higher in the B3II peat (Figures 4.1-4.3) and the sorption of As(V) to Fe(III)-(hydr)oxides typically decreases with pH [Dixit and Hering, 2003]. This finding cannot be explained with sorption competition between As and dissolved organic ligands

[Redman et al., 2002; Bauer and Blodau, 2006], since the DOC concentrations measured in the B1II peat were lower than in the B3II peat and did not increase during the 180-day oxidation period (Figure C.5, Appendix C). These results collectively suggest that the accessibility of mineral surfaces for As was physically limited in the B1II peat, possibly due to an entrapment of freshly formed Fe(III)-(hydr)oxides in the organic matrix. This notion is supported by the phosphate extraction results. Here, the amount of As extracted by phosphate only significantly exceeded the water extractable As in the B3II peat, whereas similar concentrations were measured in water and phosphate extracts in the B1II peat (Figures 4.2 and C.2, Appendix C). Likewise, the colloidal Fe comprised a substantially greater portion of Fe released by an excess of phosphate in the surface-near B3II compared to the deep peat layer B1II batch (Figure C.2, Appendix C).

### **4.5. Environmental implications**

Our results show that the oxidation kinetics of organosulfur-coordinated As(III) and realgar in peat are comparatively slow. The calculated half-life times imply that a nearly complete oxidation (99%) of both reduced As species, for example, as a result of peat drainage for agricultural purposes [Brinson and Malvárez, 2002] can be expected within 4-7 years. Arsenic released via oxidation of As(III)-NOM complexes and realgar is almost entirely sorbed to Fe(III)-(hydr)oxides (>97%). However, the efficiency of pre-existing and freshly formed Fe(III)-(hydr)oxides to sequester As can be limited, partly because of a reduced accessibility of Fe(III)-(hydr)oxide surfaces for As(V), which may cause As solution concentrations to locally rise above common drinking water limits. While previous investigations implied that wetlands like *Gola di Lago* can serve as effective sinks for As under reducing conditions due to the covalent binding of As(III) to NOM and/or the formation of As sulfides [Hoffmann et al., 2012; Langner et al., 2012; Langner et al., 2013], this study shows that prolonged oxidizing conditions render such wetlands long-term sources for As. Our results also suggest that the oxidation kinetics of reduced S species susceptible to oxidation (e.g., mercaptans and pyrite) are considerably faster than

the oxidation kinetics of As(III)-NOM complexes and realgar (Figure 4.2 vs. Figure C.4, Appendix C). The rapid oxidation-induced loss of potentially As-sequestering S species may thus contribute to the mobilization of As following fluctuations in the water table. Because our results document a high As mobilization potential in the As-contaminated *Gola di Lago* wetland under sustained oxidizing conditions, the maintenance of anoxic conditions must be considered an effective management strategy of this and other As-rich wetlands.

#### **Acknowledgments**

We gratefully acknowledge P. Poggiati and M. Sulmoni (Department of Environment, canton Ticino, Switzerland) for the sampling permit, and K. Barmettler, R. Brankatschk, A. Franchini, M. Hoffmann (ETH Zurich), and F. Hammes (Eawag) for field and/or laboratory assistance. Bulk XAS spectra were measured at the SSRL, a Directorate of SLAC National Accelerator Laboratory and an Office of Science User Facility operated for the U.S. Department of Energy Office of Science by Stanford University. In this regard, we would like to thank M.J. Latimer and E.J. Nelson for their support in using beamline 4-3, and J. Bargar, R.C. Davis, E.J. Nelson, and M.J. Latimer for assistance in using beamlines 11-2 and 4-1. This research project was financially supported by a research grant (no. 2708-2) from ETH Zurich.

## References

- Bauer, M., Blodau, C. (2006) Mobilization of arsenic by dissolved organic matter from iron oxides, soils and sediments. *Sci. Total Environ.* 354, 179-190.
- Beauchemin, S., Kwong, Y. T. J. (2006) Impact of redox conditions on arsenic mobilization from tailings in a wetland with neutral drainage. *Environ. Sci. Technol.* 40, 6297-6303.
- Blodau, C., Fulda, B., Bauer, M., Knorr, K.-H. (2008) Arsenic speciation and turnover in intact organic soil mesocosms during experimental drought and rewetting. *Geochim. Cosmochim. Acta* 72, 3991-4007.
- Bluemlein, K., Raab, A., Feldmann, J. (2009) Stability of arsenic peptides in plant extracts: Off-line versus on-line parallel elemental and molecular mass spectrometric detection for liquid chromatographic separation. *Anal. Bioanal. Chem.* 393, 357-366.
- Bonazzi, P., Menchetti, S., Pratesi, G. (1995) The crystal structure of pararealgar, As<sub>4</sub>S<sub>4</sub>. *Am. Mineral.* 80, 400-403.
- Brinson, M. M., Malvárez, A. I. (2002) Temperate freshwater wetlands: Types, status, and threats. *Environ. Conserv.* 29, 115-133.
- Chen, P., Yan, L., Yue, X., Li, H. (2013) Optimal parameters for bioleaching of realgar using *Acidithiobacillus ferrooxidans* under different growth conditions and mathematical analysis. *Biocatal. Biotransform.* 31, 33-41.
- Contin, M., Jenkinson, D. S., Brookes, P. C. (2002) Measurement of ATP in soil: Correcting for incomplete recovery. *Soil Biol. Biochem.* 34, 1381-1383.
- Dixit, S., Hering, J. G. (2003) Comparison of arsenic(V) and arsenic(III) sorption onto iron oxide minerals: Implications for arsenic mobility. *Environ. Sci. Technol.* 37, 4182-4189.
- Evangelou, V. P., Zhang, Y. L. (1995) A review: Pyrite oxidation mechanisms and acid-mine drainage prevention. *Crit. Rev. Environ. Sci. Technol.* 25, 141-199.
- Fendorf, S., Kocar, B. D. (2009) Biogeochemical processes controlling the fate and transport of arsenic: Implications for South and Southeast Asia In Sparks, D. L. (Ed.) *Advances in Agronomy*. Elsevier Academic Press Inc: San Diego, pp. 137-164.
- Fox, P. M., Doner, H. E. (2003) Accumulation, release, and solubility of arsenic, molybdenum, and vanadium in wetland sediments. *J. Environ. Qual.* 32, 2428-2435.
- Hammes, F., Goldschmidt, F., Vital, M., Wang, Y., Egli, T. (2010) Measurement and interpretation of microbial adenosine tri-phosphate (ATP) in aquatic environments. *Water Res.* 44, 3915-3923.

- Hoffmann, M., Mikutta, C., Kretzschmar, R. (2012) Bisulfide reaction with natural organic matter enhances arsenite sorption: Insights from X-ray absorption spectroscopy. *Environ. Sci. Technol.* 46, 11788–11797.
- Hutchison, K. J., Hesterberg, D., Chou, J. W. (2001) Stability of reduced organic sulfur in humic acid as affected by aeration and pH. *Soil Sci. Soc. Am. J.* 65, 704-709.
- Jackson, B. P., Miller, W. P. (2000) Effectiveness of phosphate and hydroxide for desorption of arsenic and selenium species from iron oxides. *Soil Sci. Soc. Am. J.* 64, 1616-1622.
- Keon, N. E., Swartz, C. H., Brabander, D. J., Harvey, C., Hemond, H. F. (2001) Validation of an arsenic sequential extraction method for evaluating mobility in sediments. *Environ. Sci. Technol.* 35, 2778-2784.
- Kobayashi, Y., Hirano, S. (2008) Effects of endogenous hydrogen peroxide and glutathione on the stability of arsenic metabolites in rat bile. *Toxicol. Appl. Pharm.* 232, 33-40.
- La Force, M. J., Hansel, C. M., Fendorf, S. (2000) Arsenic speciation, seasonal transformations, and co-distribution with iron in a mine waste-influenced palustrine emergent wetland. *Environ. Sci. Technol.* 34, 3937-3943.
- Langner, P., Mikutta, C., Kretzschmar, R. (2012) Arsenic sequestration by organic sulphur in peat. *Nat. Geosci.* 5, 66-73.
- Langner, P., Mikutta, C., Kretzschmar, R. (2013) Spatial distribution and speciation of arsenic in peat studied with microfocused X-ray fluorescence spectrometry and X-ray absorption spectroscopy. *Environ. Sci. Technol.* 47, 9706–9714.
- Lengke, M. F., Sanpawanitchakit, C., Tempel, R. N. (2009) The oxidation and dissolution of arsenic-bearing sulfides. *Can. Mineral.* 47, 593-613.
- Lengke, M. F., Tempel, R. N. (2003) Natural realgar and amorphous AsS oxidation kinetics. *Geochim. Cosmochim. Acta* 67, 859-871.
- Lengke, M. F., Tempel, R. N. (2005) Geochemical modeling of arsenic sulfide oxidation kinetics in a mining environment. *Geochim. Cosmochim. Acta* 69, 341-356.
- Liu, F., De Cristofaro, A., Violante, A. (2001) Effect of pH, phosphate and oxalate on the adsorption/desorption of arsenate on/from goethite. *Soil Sci.* 166, 197-208.
- Manceau, A., Nagy, K. L. (2012) Quantitative analysis of sulfur functional groups in natural organic matter by XANES spectroscopy. *Geochim. Cosmochim. Acta* 99, 206-223.
- Manceau, A., Schlegel, M. L. (2001) Texture effect on polarized EXAFS amplitude. *Phys. Chem. Miner.* 28, 52-56.

- Masscheleyn, P. H., Delaune, R. D., Patrick, W. H. (1991) Effect of redox potential and pH on arsenic speciation and solubility in a contaminated soil. *Environ. Sci. Technol.* 25, 1414-1419.
- Moses, C. O., Herman, J. S. (1991) Pyrite oxidation at circumneutral pH. *Geochim. Cosmochim. Acta* 55, 471-482.
- Moses, C. O., Nordstrom, D. K., Herman, J. S., Mills, A. L. (1987) Aqueous pyrite oxidation by dissolved oxygen and by ferric iron. *Geochim. Cosmochim. Acta* 51, 1561-1571.
- Nordstrom, D. K. (1979) Aqueous pyrite oxidation and the consequent formation of secondary iron minerals. In Kral, D. M. (Ed.) *Acid sulfate weathering*. SSSA Special Publication: Fort Collins, pp. 37-56.
- Oremland, R. S., Stolz, J. F. (2003) The ecology of arsenic. *Science* 300, 939-944.
- Peiffer, S., Stubert, I. (1999) The oxidation of pyrite at pH 7 in the presence of reducing and nonreducing Fe(III)-chelators. *Geochim. Cosmochim. Acta* 63, 3171-3182.
- R-Core-Team, 2012. R: A language and environment for statistical computing. R Foundation for Statistical Computing, Vienna, Austria.
- Raab, A., Meharg, A. A., Jaspars, M., Genney, D. R., Feldmann, J. (2004) Arsenic-glutathione complexes - their stability in solution and during separation by different HPLC modes. *J. Anal. At. Spectrom.* 19, 183-190.
- Reddy, K. R., DeLaune, R. D. (2008) *Biogeochemistry of wetlands: Science and applications*. CRC Press: Boca Raton.
- Redman, A. D., Macalady, D. L., Ahmann, D. (2002) Natural organic matter affects arsenic speciation and sorption onto hematite. *Environ. Sci. Technol.* 36, 2889-2896.
- Renock, D., Becker, U. (2010) A first principles study of the oxidation energetics and kinetics of realgar. *Geochim. Cosmochim. Acta* 74, 4266-4284.
- Roberts, L. C., Hug, S. J., Ruettimann, T., Billah, M., Khan, A. W., Rahman, M. T. (2004) Arsenic removal with iron(II) and iron(III) waters with high silicate and phosphate concentrations. *Environ. Sci. Technol.* 38, 307-315.
- Roberts, L. C., Hug, S. J., Voegelin, A., Dittmar, J., Kretzschmar, R., Wehrli, B., Saha, G. C., Badruzzaman, A. B. M., Ali, M. A. (2011) Arsenic dynamics in porewater of an intermittently irrigated paddy field in Bangladesh. *Environ. Sci. Technol.* 45, 971-976.
- Roden, E. E., Sobolev, D., Glazer, B., Luther, G. W. (2004) Potential for microscale bacterial Fe redox cycling at the aerobic-anaerobic interface. *Geomicrobiol. J.* 21, 379-391.

- Rosen, B. P. (2002) Biochemistry of arsenic detoxification. *FEBS Lett.* 529, 86-92.
- Rothwell, J. J., Taylor, K. G., Ander, E. L., Evans, M. G., Daniels, S. M., Allott, T. E. H. (2009) Arsenic retention and release in ombrotrophic peatlands. *Sci. Total Environ.* 407, 1405-1417.
- Smedley, P. L., Kinniburgh, D. G. (2002) A review of the source, behaviour and distribution of arsenic in natural waters. *Appl. Geochem.* 17, 517-568.
- Sparling, G. P., Ord, B. G., Vaughan, D. (1981) Microbial biomass and activity in soils amended with glucose. *Soil Biol. Biochem.* 13, 99-104.
- Vymazal, J. (2007) Removal of nutrients in various types of constructed wetlands. *Sci. Total Environ.* 380, 48-65.
- Wang, J., Vollrath, S., Behrends, T., Bodelier, P. L. E., Muyzer, G., Meima-Franke, M., Den Oudsten, F., Van Cappellen, P., Laanbroek, H. J. (2011) Distribution and diversity of *Gallionella*-like neutrophilic iron oxidizers in a tidal freshwater marsh. *Appl. Environ. Microbiol.* 77, 2337-2344.
- Weber, F.-A., Hofacker, A. F., Voegelin, A., Kretzschmar, R. (2010) Temperature dependence and coupling of iron and arsenic reduction and release during flooding of a contaminated soil. *Environ. Sci. Technol.* 44, 116-122.
- Weeger, W., Lievremont, D., Perret, M., Lagarde, F., Hubert, J. C., Leroy, M., Lett, M. C. (1999) Oxidation of arsenite to arsenate by a bacterium isolated from an aquatic environment. *Biometals* 12, 141-149.
- Weiss, J. V., Rentz, J. A., Plaia, T., Neubauer, S. C., Merrill-Floyd, M., Lilburn, T., Bradburne, C., Megonigal, J. P., Emerson, D. (2007) Characterization of neutrophilic Fe(II)-oxidizing bacteria isolated from the rhizosphere of wetland plants and description of *Ferritrophicum radicolica* gen. nov. sp. nov., and *Sideroxydans paludicola* sp. nov. *Geomicrobiol. J.* 24, 559-570.
- WHO (2008) *Guidelines for drinking-water quality: Incorporating 1st and 2nd addenda*. World Health Organisation: Geneva.
- Zeng, H., Fisher, B., Giammar, D. E. (2008) Individual and competitive adsorption of arsenate and phosphate to a high-surface-area iron oxide-based sorbent. *Environ. Sci. Technol.* 42, 147-152.
- Zhang, J., Zhang, X., Ni, Y., Yang, X., Li, H. (2007) Bioleaching of arsenic from medicinal realgar by pure and mixed cultures. *Process Biochem.* 42, 1265-1271.
- Zhang, J. S., Stanforth, R., Pehkonen, S. O. (2008) Irreversible adsorption of methyl arsenic, arsenate, and phosphate onto goethite in arsenic and phosphate binary systems. *J. Colloid Interface Sci.* 317, 35-43.





## 5. Conclusions and outlook

This thesis examined the bulk and microscale speciation and distribution of As in a naturally As-enriched peatland. Based on synchrotron XRF and XAS analyses as the main analytical tools, potential (trans)formation processes of As species identified in the peat were inferred. In the following, the key findings of this thesis will be summarized and complemented by a discussion on the relevance of the results for the retention and release of As in NOM-rich environments. Finally, suggestions for further research directions will close the thesis.

The investigations in the As-enriched *Gola di Lago* peatland revealed two distinct As enrichment patterns characterized by a different As speciation and microscale distribution (Chapters 2 and 3): The near-surface peat layers (<41 cm), which are subject to annual changes in redox conditions due to fluctuations of the water table, showed primarily micrometer-sized (10-50  $\mu\text{m}$ ) intense hotspots of As consisting of the As sulfide mineral realgar. To a minor extent, As was associated with Fe(III)-(hydr)oxides mainly located on highly altered gneiss fragments or present as  $\sim 10\text{-}\mu\text{m}$  sized arsenopyrite particles partially strung along plant fibers. In the permanently anoxic deep peat layers (150-250 cm), As was completely bound in its trivalent oxidation state to sulfhydryl groups of NOM and primarily contributed to the diffusely distributed As found either on fibrous plant remains or on more humified NOM. Shell-fit analyses of the peat samples revealed S coordination numbers of 2-3 and interatomic As-S distances of 2.26 Å for this As(III)-NOM complex, values closely resembling those of As(III) bound to sulfhydryl groups of cysteine residues of a keratin-rich biomass [Teixeira and Ciminelli, 2005]. These results showed that particulate NOM can be a quantitatively important sorbent for As under reducing conditions, which until then had not been reported in the literature [Smith et al., 1998; Smedley and Kinniburgh, 2002; Zhang and Selim, 2008].

Iron *K*-edge XAS analyses of the deep peat layer samples revealed that pyrite and Fe(III)-NOM complexes comprise a major Fe fraction with  $\leq 58\%$  and 35-80% of total Fe, respectively (Chapters 2 and 3). However, As was primarily associated with organic

S, suggesting that the complexation of As(III) by sulfhydryl groups was highly favorable under anoxic conditions and effectively inhibited other As sequestration pathways like the substitution of As for S in pyrite [Bostick and Fendorf, 2003; Lowers et al., 2007]. Because of the lack of evidence for ternary As(III)-Fe(III)-NOM complex formation in the *Gola di Lago* peat and As(III) reaction schemes involving hydroxylic/phenolic groups of NOM [Hoffmann et al., 2013], the covalent binding of trivalent As to organic S species was proposed as major As-NOM interaction mechanism for S- and NOM-rich anoxic environments. This supposition is supported by recent flow-through experiments in which freshwater lake sediments were treated with solutions containing 200  $\mu\text{M}$   $\text{Na}_2\text{SO}_4$  and 20  $\mu\text{M}$  As(V) or As(III), and after 21 days also 200  $\mu\text{M}$  Na-lactate [Couture et al., 2013]. Here, sulfhydryl groups verified by S *K*-edge XANES and sequential extraction were shown to form within days to weeks in the uppermost sediment layer (0-2 cm) containing high amounts of labile NOM, and sequestered the As from solution [Couture et al., 2013]. The complexation of As(III) by sulfhydryl groups of NOM may thus be a plausible explanation for As-NOM associations observed in other ombrotrophic [Cloy et al., 2009; Rothwell et al., 2009] and minerotrophic peatlands [Bauer et al., 2008; Blodau et al., 2008], as well as in some peat(y) sediments of the Bengal Basin [Anawar et al., 2003; Yamazaki et al., 2003; Ahmed et al., 2010].

The results of Chapter 3 suggested that the binding of As by sulfhydryl groups is favored by the high abundance of reduced organic S (83% of total S) and comparatively low As solution concentrations preventing the formation of As sulfide minerals. The similar microscale distribution of organosulfur-coordinated As(III) in peat material of different decomposition stages pointed towards a passive sorption mechanism [Hoffmann et al., 2012]. An active formation of the organosulfur-coordinated As(III) via the uptake and intracellular detoxification of As by plants [Zhao et al., 2009] was considered less likely owing to the low As concentrations detected in various parts of plants collected at the *Gola di Lago* field site. Therefore, as discussed in Chapter 2, the direct reaction of aqueous sulfide species with NOM [Aizenshtat et al., 1995; Hoffmann et al., 2012] and the subsequent sequestration of As(III) by newly formed sulfhydryl groups [Hoffmann et al., 2012; Couture et al., 2013] and/or the sulfidization of aqueous As(III) [Wilkin et al., 2003; Helz and Tossell, 2008; Planer-Friedrich et al., 2010] and the ensuing reaction

of thioarsenites with NOM are presently considered as viable formation pathways of organosulfur-coordinated As(III) in the *Gola di Lago* peatland.

In addition to organosulfur-coordinated As(III), realgar was verified as the second major As species in the *Gola di Lago* peat. The formation of realgar in the near-surface peat layers was of particular interest since its in-situ formation, indicated by its absence in the bedrock (Chapter 2), in low-temperature/low pressure environments has so far only been reported for a shallow aquifer sediment [O'Day et al., 2004]. As discussed in Chapter 3, the precipitation of realgar in the near-surface peat layers may have been favored by comparatively high As solution concentrations ( $\sim 5 \mu\text{M}$ ) in surface waters entering the peatland [González A. et al., 2006]. Under anoxic circum-neutral conditions, the reduction of As(III) by Fe monosulfides may lead to the formation of realgar [Gallegos et al., 2007; Gallegos et al., 2008]. However, no Fe sulfide phases were detected by bulk Fe *K*-edge XAS and  $\mu$ -XRF analyses, implying that the nanometer-sized Fe sulfide phases necessary for As(III) reduction were below the analytical detection limits or, alternatively, that realgar precipitated homogeneously in supersaturated pore waters (Chapter 3).

Besides the in-situ formation of realgar, the observation of arsenopyrite in the moderately anoxic peat ( $E_h = -11$  to  $364$  mV) was another unexpected finding (Chapter 3). Only observed by  $\mu$ -XRF spectrometry and  $\mu$ -XAS, the association of  $\sim 10$ - $\mu\text{m}$  sized arsenopyrite particles with fibrous plant material pointed to an authigenic arsenopyrite formation, which so far has only been reported for mining-affected sediments in a microcosm study [Rittle et al., 1995]. Proposed abiotic formation pathways of arsenopyrite involving the reaction of As(III) with Fe sulfide minerals and the subsequent formation of pyrite, Fe(III)-(hydr)oxides, and/or polysulfides as reaction products [Bostick and Fendorf, 2003] were not strictly supported by the data. Thus, the microbe-mediated formation of arsenopyrite in strongly reducing microenvironments involving Fe(III)-(hydr)oxides and/or phyllosilicates as potential  $\text{Fe}^{2+}$  sources instead of Fe sulfides was suggested as a possible alternative formation pathway (Chapter 3).

Because changes in redox potential due to water-table fluctuations, shifts in biological activity, or land-use changes frequently occur in peatlands and affect the dynamics of redox-sensitive elements like As, the oxidation kinetics of organosulfur-coordinated

As(III) and realgar were investigated under prolonged oxidizing conditions with special focus on the fate of As released (Chapter 4). Results showed that the oxidation kinetics of organosulfur-coordinated As(III) and realgar in the peat were comparatively slow with calculated half-life times of 312-379 and 215-312 days, respectively, and mainly controlled by abiotic processes. Thus, a 99% oxidation of both reduced As species as a result of peat drainage can be expected within 4-7 years. Arsenic released during the oxidation of the organosulfur-coordinated As(III) and realgar was almost entirely sequestered by pre-existing and newly formed Fe(III)-(hydr)oxides (>97%). However, their efficiency to sorb As was limited, presumably due to a reduced accessibility of mineral sorption sites for As, causing As solution concentration to rise beyond common drinking water limits [WHO, 2008]. The considerably faster oxidation kinetics observed for reduced S species (e.g., mercaptans and pyrite) in comparison to those of organosulfur-coordinated As(III) and realgar implied a fast oxidation-induced loss of potentially As-sequestering reduced S species. This could be of particular relevance under conditions of peat re-wetting caused by a rise in the water table, where As is released during the dissimilatory reduction of metal-(hydr)oxides.

While the findings presented in Chapters 2 and 3 imply that wetlands like *Gola di Lago* can serve as effective sinks for As under reducing conditions due to the covalent binding of As(III) to sulfhydryl groups of NOM and/or the formation of As sulfides, the results of Chapter 4 showed that prolonged oxidizing conditions render such wetlands long-term sources for As. Consequently, the maintenance of anoxic conditions was suggested as the prime strategy for the management of the *Gola di Lago* peatland and other As-rich wetlands.

In this thesis, it has been shown that the sequestration of As under reducing conditions is not solely linked to mineral phases. Instead, NOM was found to be a quantitatively important sorbent for As. To fully account for NOM when assessing the mobility and toxicity of As in NOM-rich systems similar to the investigated field site, there are still several research needs to be addressed in the future. Particularly, the available thermodynamic data on organosulfur-coordinated As(III) required for chemical speciation calculations needs to be reassessed. For example, stability constants of  $\log K = 33.28$  and  $6.45$  published by Rey et al. [2004] and Spuches et al. [2005] for the

formation of the 1:3 complex of As(III) and glutathione (GSH) in solution ( $3\text{H}_2\text{GSH}^- + \text{H}_3\text{AsO}_3 \leftrightarrow (\text{HGSH}^-)_3\text{As} + 3\text{H}_2\text{O}$ ) deviate by one order of magnitude, implying that this reaction would be either highly or only moderately favorable. Therefore, the accuracy of existing thermodynamic data needs to be assessed and field observations should be reconciled with this data. Furthermore, the mechanism(s) of the organosulfur-coordinated As(III) formation should be addressed in more detail. In principle, dissolved thioarsenic species formed as a result of As sulfide mineral dissolution [Suess and Planer-Friedrich, 2012] or the sulfidization of aqueous As(III) [Wilkin et al., 2003; Helz and Tossell, 2008; Planer-Friedrich et al., 2010] could be involved in the formation of organosulfur-coordinated As(III). However, thioarsenites are extremely unstable even under anoxic conditions, and rapidly convert to thioarsenates when exposed to atmospheric  $\text{O}_2$  [Planer-Friedrich et al., 2010]. Therefore, thioarsenates are more likely in sulfide-rich pore waters [Planer-Friedrich et al., 2010] and could potentially be reduced and sequestered by reactive functional groups of NOM (Chapter 1.2.3). The microbial transformation of thioarsenates to As(III) [Härtig and Planer-Friedrich, 2012] and its subsequent complexation by NOM [Hoffmann et al., 2012; Couture et al., 2013] may represent an alternative formation pathway of organosulfur-coordinated As(III). Both passive formation pathways are conceivable but have not been verified so far. Likewise, the net effect of redox oscillations (oxidation-reduction cycles) on the speciation and mobility of As in wetlands like *Gola di Lago* still remains elusive. Particularly the effect of the fast oxidation-induced loss of potentially As-sequestering reduced S species (Chapter 4) on the capability of wetlands to serve as net As sinks requires clarification. Finally, the detection, quantification, and molecular-scale characterization of NOM-associated As in environments such as peats or peaty sediments [Anawar et al., 2003; Yamazaki et al., 2003; Bauer et al., 2008; Blodau et al., 2008; Rothwell et al., 2009; Ahmed et al., 2010] is a future key task necessary to judge on the environmental relevance of the information gathered in this thesis. This objective calls for spectroscopic information on the solid-phase speciation of As and Fe, which is currently missing for environments similar to *Gola di Lago*.

## References

- Ahmed, F., Bibi, M. H., Ishiga, H., Fukushima, T., Maruoka, T. (2010) Geochemical study of arsenic and other trace elements in groundwater and sediments of the Old Brahmaputra river plain, Bangladesh. *Environ. Earth Sci.* 60, 1303-1316.
- Aizenshtat, Z., Krein, E. B., Vairavamurthy, M. A., Goldstein, T. P. (1995) Role of sulfur in the transformations of sedimentary organic matter: A mechanistic overview. In Vairavamurthy, M. A., Schoonen, M. A. A. (Eds.) *Geochemical transformations of sedimentary sulfur*. American Chemical Society Washington, DC, pp. 16-37.
- Anawar, H. M., Akai, J., Komaki, K., Terao, H., Yoshioka, T., Ishizuka, T., Safiullah, S., Kato, K. (2003) Geochemical occurrence of arsenic in groundwater of Bangladesh: Sources and mobilization processes. *J. Geochem. Explor.* 77, 109-131.
- Bauer, M., Fulda, B., Blodau, C. (2008) Groundwater derived arsenic in high carbonate wetland soils: Sources, sinks, and mobility. *Sci. Total Environ.* 401, 109-120.
- Blodau, C., Fulda, B., Bauer, M., Knorr, K.-H. (2008) Arsenic speciation and turnover in intact organic soil mesocosms during experimental drought and rewetting. *Geochim. Cosmochim. Acta* 72, 3991-4007.
- Bostick, B. C., Fendorf, S. (2003) Arsenite sorption on troilite (FeS) and pyrite (FeS<sub>2</sub>). *Geochim. Cosmochim. Acta* 67, 909-921.
- Cloy, J. M., Farmer, J. G., Graham, M. C., Mackenzie, A. B. (2009) Retention of As and Sb in ombrotrophic peat bogs: Records of As, Sb, and Pb deposition at four Scottish sites. *Environ. Sci. Technol.* 43, 1756-1762.
- Couture, R.-M., Wallschläger, D., Rose, J., Van Cappellen, P. (2013) Arsenic binding to organic and inorganic sulfur species during microbial sulfate reduction: A sediment flow-through reactor experiment. *Environ. Chem.* 10, 285-294.
- Gallegos, T. J., Han, Y.-S., Hayes, K. F. (2008) Model predictions of realgar precipitation by reaction of As(III) with synthetic mackinawite under anoxic conditions. *Environ. Sci. Technol.* 42, 9338-9343.
- Gallegos, T. J., Hyun, S. P., Hayes, K. F. (2007) Spectroscopic investigation of the uptake of arsenite from solution by synthetic mackinawite. *Environ. Sci. Technol.* 41, 7781-7786.
- González A., Z. I., Krachler, M., Cheburkin, A. K., Shotykh, W. (2006) Spatial distribution of natural enrichments of arsenic, selenium, and uranium in a minerotrophic peatland, Gola di Lago, canton Ticino, Switzerland. *Environ. Sci. Technol.* 40, 6568-6574.
- Härtig, C., Planer-Friedrich, B. (2012) Thioarsenate transformation by filamentous microbial mats thriving in an alkaline, sulfidic hot spring. *Environ. Sci. Technol.* 46, 4348-4356.
- Helz, G. R., Tossell, J. A. (2008) Thermodynamic model for arsenic speciation in sulfidic waters: A novel use of ab initio computations. *Geochim. Cosmochim. Acta* 72, 4457-4468.

- Hoffmann, M., Mikutta, C., Kretzschmar, R. (2012) Bisulfide reaction with natural organic matter enhances arsenite sorption: Insights from X-ray absorption spectroscopy. *Environ. Sci. Technol.* *46*, 11788–11797.
- Hoffmann, M., Mikutta, C., Kretzschmar, R. (2013) Arsenite binding to natural organic matter: Spectroscopic evidence for ligand exchange and ternary complex formation. *Environ. Sci. Technol.*, *47*, 12165-12173.
- Lowers, H. A., Breit, G. N., Foster, A. L., Whitney, J., Yount, J., Uddin, N., Muneem, A. (2007) Arsenic incorporation into authigenic pyrite, Bengal Basin sediment, Bangladesh. *Geochim. Cosmochim. Acta* *71*, 2699-2717.
- O'Day, P. A., Vlassopoulos, D., Root, R., Rivera, N. (2004) The influence of sulfur and iron on dissolved arsenic concentrations in the shallow subsurface under changing redox conditions. *Proc. Natl. Acad. Sci. USA* *101*, 13703-13708.
- Planer-Friedrich, B., Suess, E., Scheinost, A. C., Wallschläger, D. (2010) Arsenic speciation in sulfidic waters: Reconciling contradictory spectroscopic and chromatographic evidence. *Anal. Chem.* *82*, 10228-10235.
- Rey, N. A., Howarth, O. W., Pereira-Maia, E. C. (2004) Equilibrium characterization of the As(III)-cysteine and the As(III)-glutathione systems in aqueous solution. *J. Inorg. Biochem.* *98*, 1151-1159.
- Rittle, K. A., Drever, J. I., Colberg, P. J. S. (1995) Precipitation of arsenic during bacterial sulfate reduction. *Geomicrobiol. J.* *13*, 1-11.
- Rothwell, J. J., Taylor, K. G., Ander, E. L., Evans, M. G., Daniels, S. M., Allott, T. E. H. (2009) Arsenic retention and release in ombrotrophic peatlands. *Sci. Total Environ.* *407*, 1405-1417.
- Smedley, P. L., Kinniburgh, D. G. (2002) A review of the source, behaviour and distribution of arsenic in natural waters. *Appl. Geochem.* *17*, 517-568.
- Smith, E., Naidu, R., Alston, A. M. (1998) Arsenic in the soil environment: A review. *Adv. Agron.* *64*, 149-195.
- Spuches, A. M., Kruszyna, H. G., Rich, A. M., Wilcox, D. E. (2005) Thermodynamics of the As(III)-thiol interaction: Arsenite and monomethylarsenite complexes with glutathione, dihydrolipoic acid, and other thiol ligands. *Inorg. Chem.* *44*, 2964-2972.
- Suess, E., Planer-Friedrich, B. (2012) Thioarsenate formation upon dissolution of orpiment and arsenopyrite. *Chemosphere* *89*, 1390-1398.
- Teixeira, M. C., Ciminelli, V. S. T. (2005) Development of a biosorbent for arsenite: Structural modeling based on X-ray spectroscopy. *Environ. Sci. Technol.* *39*, 895-900.
- WHO (2008) *Guidelines for drinking-water quality: Incorporating 1st and 2nd addenda*. World Health Organisation: Geneva.
- Wilkin, R. T., Wallschläger, D., Ford, R. G. (2003) Speciation of arsenic in sulfidic waters. *Geochem. Trans.* *4*, 1-7.

- Yamazaki, C., Ishiga, H., Ahmed, F., Itoh, K., Suyama, K., Yamamoto, H. (2003) Vertical distribution of arsenic in Ganges delta sediments in Deuli Village, Bangladesh. *Soil Sci. Plant Nutr.* 49, 567-574.
- Zhang, H., Selim, H. M. (2008) Reaction and transport of arsenic in soils: Equilibrium and kinetic modeling. *Adv. Agron.* 98, 45-115.
- Zhao, F. J., Ma, J. F., Meharg, A. A., McGrath, S. P. (2009) Arsenic uptake and metabolism in plants. *New Phytol.* 181, 777-794.







## **A. Supporting Information to Chapter 2**

**'Arsenic sequestration by organic sulfur in peat'**

### A.1. Location of the field site

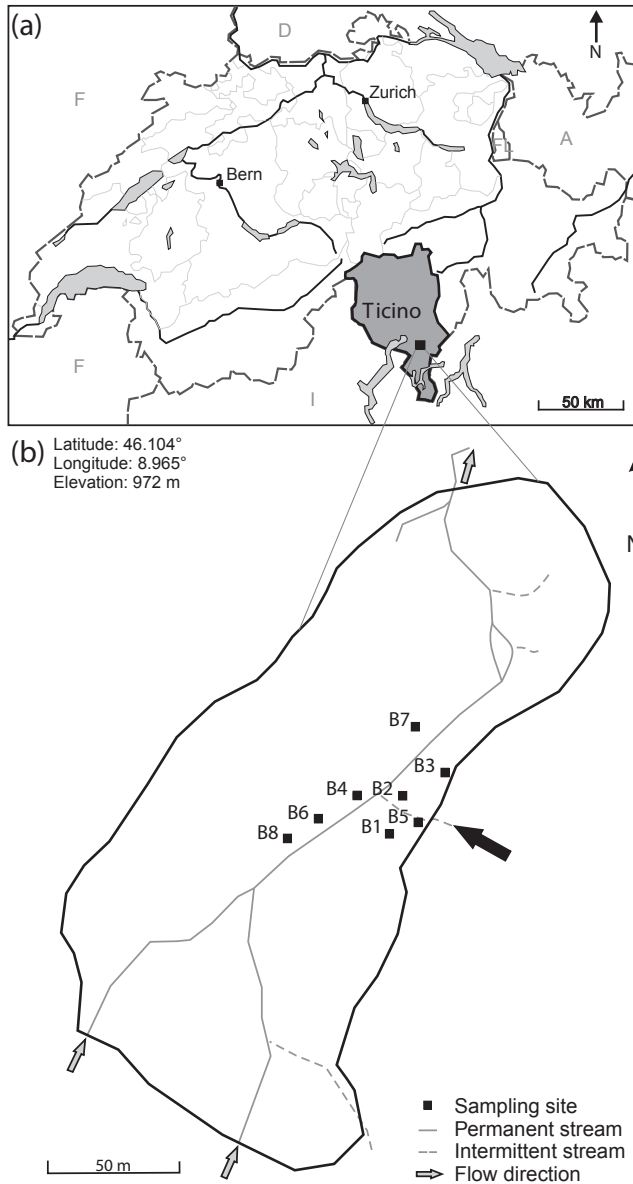


**Figure A.1. Map of the field site.** (a) Location of *Gola di Lago* peatland in Ticino, Switzerland. (b) Overview of the sampling sites (B1-B8) as well as the hydrographic situation of the peatland (adapted from González A. et al. [2006]). The location of the As-loaded intermittent stream is indicated by the black arrow.

## **A.2. Vegetation at the sampling sites**

In Table A.1 the results of the vegetation mapping within a radius of 3 m around selected sampling sites (B1, B3, and B5) are shown. The range of plant cover was classified according to the Braun-Blanquet [1932] cover-abundance scale: + = <1%, 1 = 1-5%, 2 = 5-25%, 3 = 25-50%, 4 = 50-75%, and 5 = 75-100%.

**Table A.1.** Vegetation at three sampling sites.

<b>Common name</b>	<b>Species</b>	<b>Family</b>	<b>Dominance</b>
<b>B1</b>			
Purple moorgrass	<i>Molinia caerulea</i>	Poaceae	5
Tufted bulrush	<i>Trichophorum cespitosum</i>	Cyperaceae	3
Jointleaf rush	<i>Juncus articulatus</i>	Juncaceae	2
Smooth black sedge	<i>Carex nigra</i>	Cyperaceae	2
Buckbean	<i>Menyanthes trifoliata</i>	Menyanthaceae	1
Roundleaf sundew	<i>Drosera rotundifolia</i>	Droseraceae	1
Sphagnum	<i>Sphagnum</i> sp.	Sphagnaceae	1
Marsh horsetail	<i>Equisetum palustre</i>	Equisetaceae	+
<b>B3</b>			
Smooth black sedge	<i>Carex nigra</i>	Cyperaceae	5
Purple moorgrass	<i>Molinia caerulea</i>	Poaceae	3
Sphagnum	<i>Sphagnum</i> sp.	Sphagnaceae	2
Buckbean	<i>Menyanthes trifoliata</i>	Menyanthaceae	2
Jointleaf rush	<i>Juncus articulatus</i>	Juncaceae	1
Erect cinquefoil	<i>Potentilla erecta</i>	Rosaceae	1
Common rush	<i>Juncus effusus</i>	Juncaceae	+
Marsh horsetail	<i>Equisetum palustre</i>	Equisetaceae	+
Red raspberry	<i>Rubus idaeus</i>	Rosaceae	+
Shrubby blackberry	<i>Rubus fruticosus</i>	Rosaceae	+
<b>B5</b>			
Purple moorgrass	<i>Molinia caerulea</i>	Poaceae	5
Smooth black sedge	<i>Carex nigra</i>	Cyperaceae	4
Water whorlgrass	<i>Catabrosa aquatica</i>	Poaceae	4
Jointleaf rush	<i>Juncus articulatus</i>	Juncaceae	3
Buckbean	<i>Menyanthes trifoliata</i>	Menyanthaceae	1
Marsh horsetail	<i>Equisetum palustre</i>	Equisetaceae	1
Prickly sedge	<i>Carex spicata</i>	Cyperaceae	1
Common rush	<i>Juncus effusus</i>	Juncaceae	1
Shrubby blackberry	<i>Rubus fruticosus</i>	Rosaceae	1
Erect cinquefoil	<i>Potentilla erecta</i>	Rosaceae	+

### A.3. Element distribution and geochemical conditions

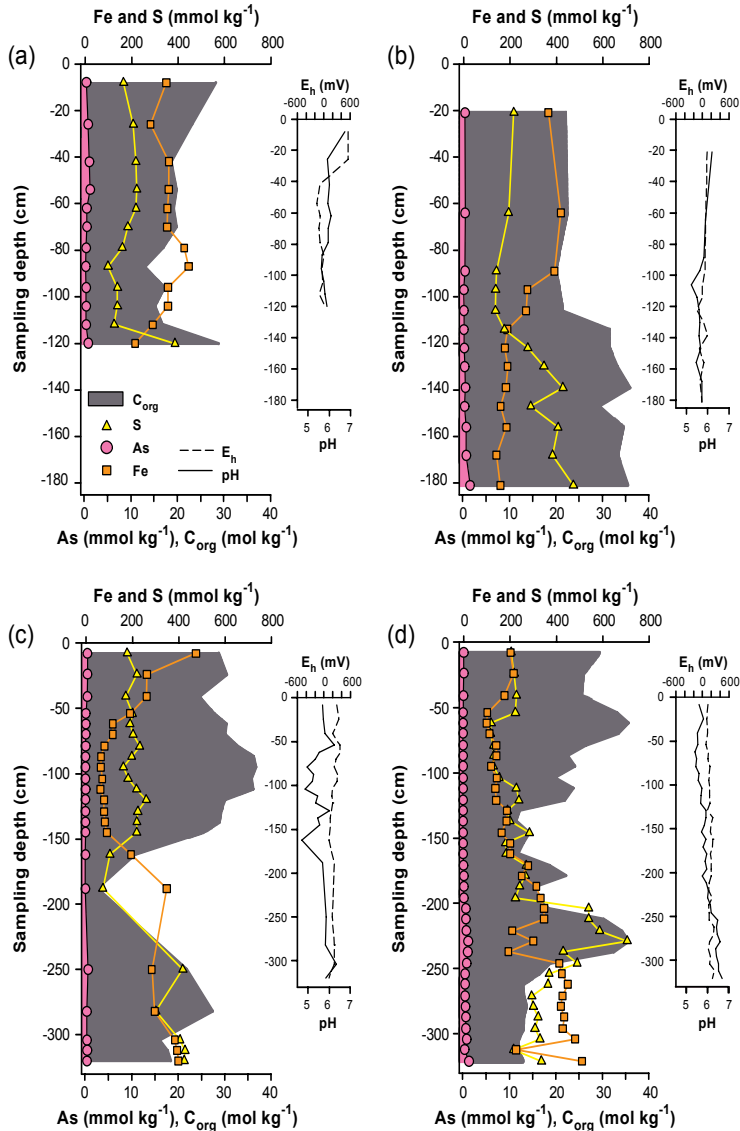


**Figure A.2.** Element distribution and geochemical conditions in the four remaining peat profiles from Gola di Lago, Switzerland. (a-d) Illustrates the vertical distribution of  $C_{\text{org}}$ , S, As, and Fe, as well as the redox potential ( $E_h$ ) and pH at sites (a) B2, (b) B8, (c) B4, and (d) B7 (see Figure A.1). For better comparison, the data is calculated on a dry-weight basis and shown as molar concentrations. The legend in panel (a) is valid for all panels.

## A.4. Analytical methods

### A.4.1. X-ray fluorescence spectrometry - method validation

The elemental composition of peat samples was determined by energy-dispersive X-ray fluorescence (XRF) spectrometry (Spectro X-Lab 2000). Sample preparation included the mixing of 4 g of milled, homogenized peat (<50  $\mu\text{m}$ ) with 0.9 g of Licowax C Micropowder PM and the subsequent pressing into a 32-mm pellet. In order to validate the XRF method for the analysis of As in the peat samples, five certified loamy clay XRF standards with As concentrations in the range of 100 to 2,000 mg As  $\text{kg}^{-1}$  (Table A.2) were repeatedly analyzed. The results show that the measured As values for three out of the five standards were within the certified limits. The maximum calculated difference between certified and measured mean values was 11%. Because the mean difference between certified and measured mean values accounted for only 3%, no correction was applied to the measured As concentrations of the peat samples.

**Table A.2.** Analyses of As standard material.

Standard material (supplier)	Certified values for As		Measured values for As		$n^b$
	Mean	Expanded uncertainty <sup>a</sup>	Mean	Expanded uncertainty	
	(mg $\text{kg}^{-1}$ )				(-)
Loamy clay (RTC)	100	$\pm 3$	99	$\pm 3$	17
	200	$\pm 6$	207	$\pm 5$	17
	590	$\pm 6$	626	$\pm 12$	14
	1,090	$\pm 32$	1,206	$\pm 15$	14
	2,000	$\pm 58$	1,939	$\pm 72$	17

<sup>a</sup>Confidence interval = 95%, expanded uncertainty = standard uncertainty  $\times$  coverage factor ( $k = 2$ ). <sup>b</sup>Number of analyses.

### A.4.2. X-ray diffraction

Qualitative mineral phase analyses of all peat samples were performed by powder X-ray diffraction (XRD). X-ray diffractograms of milled (<50  $\mu\text{m}$ ) peat samples were collected on a Bruker AXS D4 Endeavor  $2\theta$ - $\theta$  diffractometer in Bragg-Brentano geometry using Cu  $K\alpha$  radiation ( $\lambda = 1.5406 \text{ \AA}$ , 40 kV and 40 mA) and an energy-dispersive X-ray Si(Li)-



detector (Sol-X). An automatic divergence slit was used for constant area irradiation. Diffractograms were recorded from 2 to 80°2θ with a step size of 0.02°2θ and 10 s acquisition time per step. The qualitative mineral phase analyses were carried out with the EVA 10.0 evaluation software (Bruker AXS).

## A.5. X-ray absorption spectroscopy references

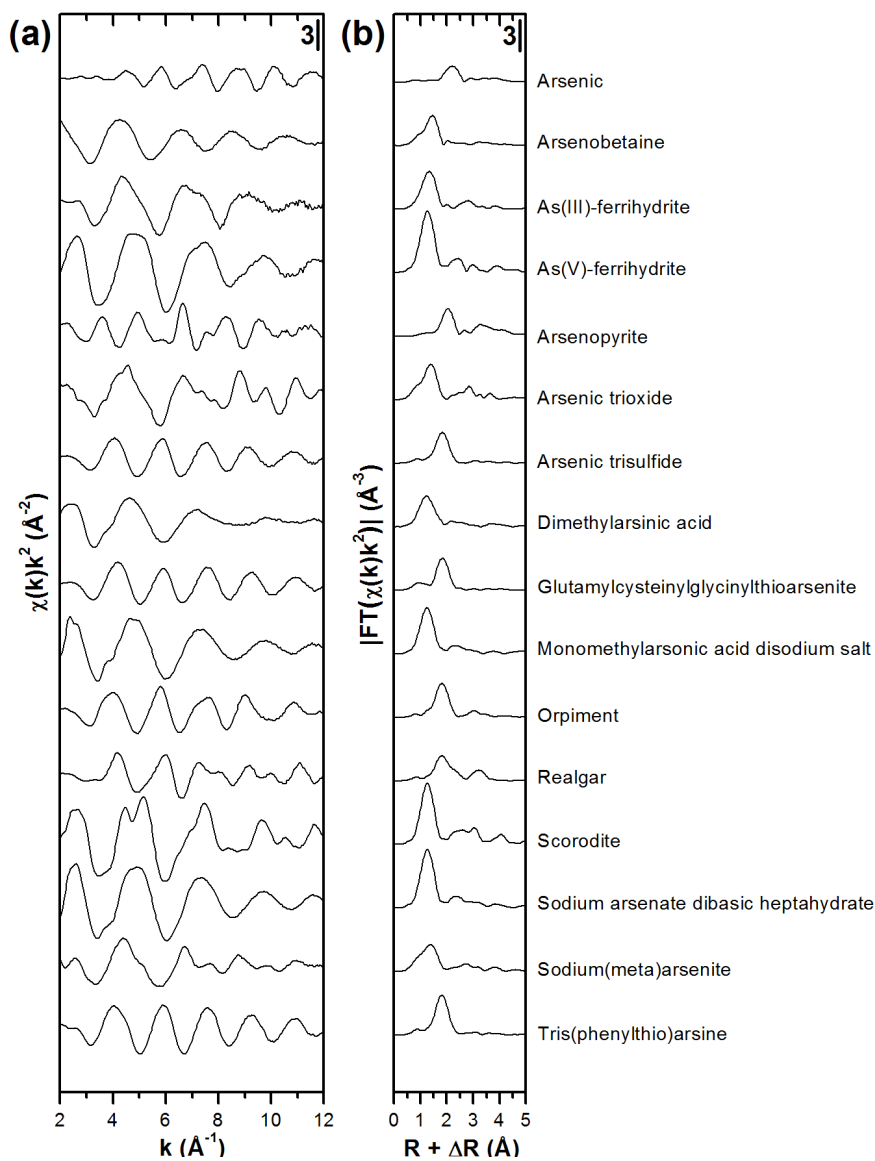
### A.5.1. Arsenic reference compounds

Table A.3 provides an alphabetic list of As reference compounds that were analyzed by X-ray absorption spectroscopy (XAS) and used in the linear combination fit (LCF) analysis of the peat samples (see Section A.5.4). Figure A.3 shows the  $k^2$ -weighted As  $K$ -edge extended X-ray absorption fine structure (EXAFS) spectra and corresponding magnitude of the Fourier transforms of the As reference compounds.

**Table A.3.** Arsenic reference compounds analyzed by XAS.

Compound	Chemical formula	Source/synthesis reference
Arsenic	As	natural <sup>a</sup>
Arsenobetaine	C <sub>3</sub> H <sub>11</sub> AsO <sub>2</sub>	commercial (Sigma-Aldrich)
As(III)-ferrihydrite	As <sub>0.05</sub> (Fe(OH) <sub>3</sub> ) <sub>0.95</sub> <sup>b</sup>	synthetic [Mikutta et al., 2010]
As(V)-ferrihydrite	As <sub>0.05</sub> (Fe(OH) <sub>3</sub> ) <sub>0.95</sub> <sup>b</sup>	synthetic [Mikutta et al., 2010]
Arsenopyrite	FeAsS	natural <sup>a</sup>
Arsenic trioxide	As <sub>2</sub> O <sub>3</sub>	commercial (Fluka)
Arsenic trisulfide	As <sub>2</sub> S <sub>3</sub>	commercial (Alfa Aesar)
Dimethylarsinic acid	(CH <sub>3</sub> ) <sub>2</sub> As(O)OH	commercial (Sigma)
Glutamylcysteinylglycylthioarsenite	As(C <sub>10</sub> H <sub>17</sub> N <sub>3</sub> O <sub>6</sub> S) <sub>2.6</sub> (OH) <sub>0.6</sub>	synthetic [Raab et al., 2004]
Monomethylarsonic acid disodium salt	CH <sub>3</sub> AsO <sub>3</sub> Na	commercial (Argus Chemicals)
Orpiment	As <sub>2</sub> S <sub>3</sub>	natural <sup>a</sup>
Realgar	As <sub>4</sub> S <sub>4</sub>	natural <sup>a</sup>
Scorodite	FeAsO <sub>4</sub> × 2H <sub>2</sub> O	natural <sup>a</sup>
Sodium arsenate dibasic heptahydrate	Na <sub>2</sub> HAsO <sub>4</sub> × 7H <sub>2</sub> O	commercial (Fluka)
Sodium(meta)arsenite	NaAsO <sub>2</sub>	commercial (Sigma-Aldrich)
Tris(phenylthio)arsine	C <sub>18</sub> H <sub>5</sub> AsS <sub>3</sub>	commercial (Aldrich)

<sup>a</sup>Provided by the TU Bergakademie Freiberg (Germany). <sup>b</sup>Estimated.



**Figure A.3.** Arsenic *K*-edge XAS reference spectra. (a) Arsenic *K*-edge EXAFS spectra, and (b) corresponding magnitude of the Fourier transforms of reference compounds included in the principal component analysis and target-transform testing.

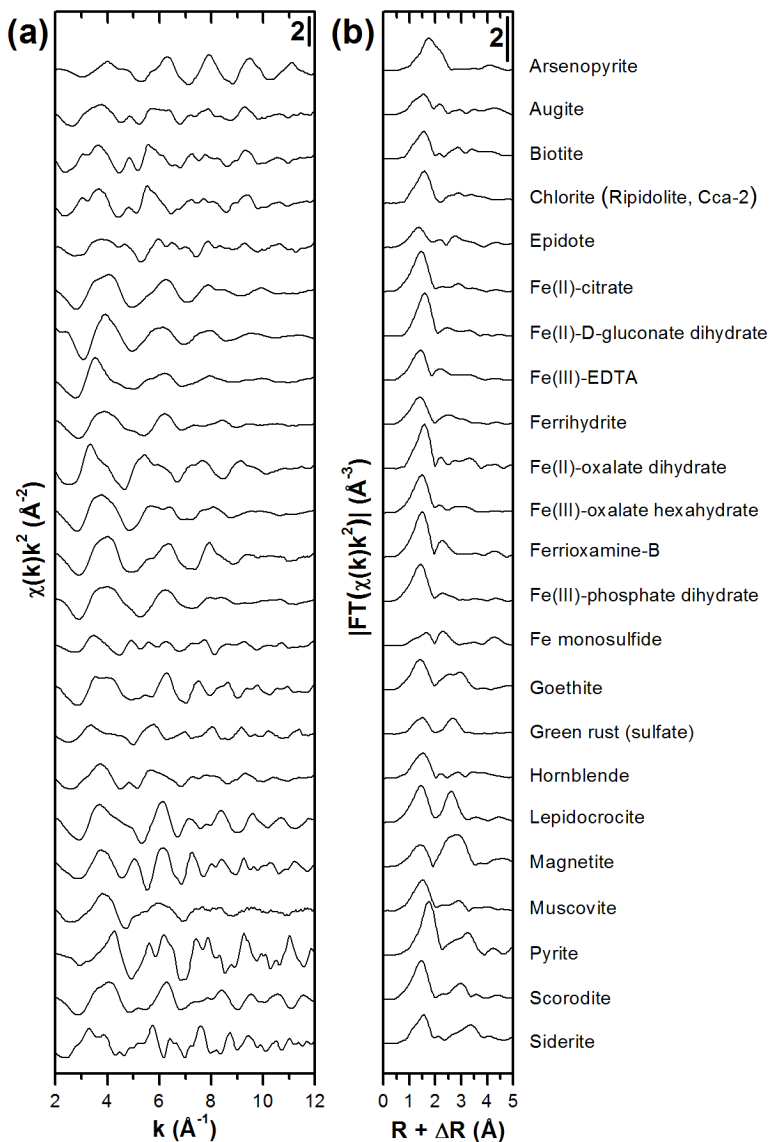
## A.5.2. Iron reference compounds

Table A.4 provides an alphabetic list of Fe reference compounds that were analyzed by XAS and used in the LCF analysis of the peat samples (see Section A.5.4). Figure A.4 shows the  $k^2$ -weighted Fe  $K$ -edge EXAFS spectra and corresponding magnitude of the Fourier transforms of the Fe reference compounds.

**Table A.4.** Iron reference compounds analyzed by XAS.

Compound	Chemical formula	Source/synthesis reference
Arsenopyrite	FeAsS	natural <sup>a</sup>
Augite	NaCa(Mg,Fe(II),Fe(III),Al,Ti)[(Si,Al) <sub>2</sub> O <sub>6</sub> ]	natural <sup>b</sup>
Biotite	K(Mg,Fe) <sub>3</sub> [(OH,F,Cl) <sub>2</sub> AlSi <sub>3</sub> O <sub>10</sub> ]	natural <sup>b</sup>
Chlorite (Ripidolite, Cca-2)	(Ca <sub>0.55</sub> )(Mg <sub>4.44</sub> Fe(III) <sub>3.47</sub> Fe(II) <sub>3.02</sub> Al <sub>0.60</sub> Mn <sub>0.01</sub> Ti <sub>0.06</sub> )(Si <sub>4.51</sub> Al <sub>13.49</sub> )O <sub>20</sub> (OH) <sub>16</sub>	natural <sup>c</sup>
Epidote	Ca <sub>2</sub> Fe(III)Al <sub>2</sub> (SiO <sub>4</sub> ) <sub>3</sub> (OH)	natural <sup>b</sup>
Fe(III)-citrate	C <sub>6</sub> H <sub>5</sub> FeO <sub>7</sub>	commercial (Fluka)
Fe(II)-D-gluconate dihydrate	C <sub>12</sub> H <sub>22</sub> FeO <sub>14</sub> × 2H <sub>2</sub> O	commercial (Aldrich)
Fe(III)-EDTA	C <sub>10</sub> H <sub>12</sub> FeN <sub>2</sub> NaO <sub>8</sub> × nH <sub>2</sub> O	commercial (Aldrich)
Ferrihydrite	Fe(OH) <sub>3</sub>	synthetic [Mikutta et al., 2010]
Fe(II)-oxalate dihydrate	Fe(C <sub>2</sub> O <sub>4</sub> ) × 2H <sub>2</sub> O	commercial (Alfa Aesar)
Fe(III)-oxalate hexahydrate	Fe <sub>2</sub> (C <sub>2</sub> O <sub>4</sub> ) <sub>3</sub> × 6H <sub>2</sub> O	commercial (Alfa Aesar)
Ferrioxamine-B	C <sub>25</sub> H <sub>43</sub> FeN <sub>6</sub> O <sub>8</sub>	synthetic [Mikutta et al., 2010]
Fe(III)-phosphate dihydrate	FePO <sub>4</sub> × 2H <sub>2</sub> O	commercial (Aldrich)
Fe monosulfide	FeS	commercial (Fluka)
Goethite	α-FeOOH	synthetic [Mikutta et al., 2009]
Green rust (sulfate)	(Fe(II) <sub>4</sub> ,Fe(III) <sub>2</sub> )(OH) <sub>12</sub> SO <sub>4</sub> × nH <sub>2</sub> O	courtesy of T. Borch
Hornblende	Ca <sub>2</sub> (Mg,Al,Fe) <sub>5</sub> (Al,Si) <sub>8</sub> O <sub>22</sub> (OH) <sub>2</sub>	natural <sup>b</sup>
Lepidocrocite	β-FeOOH	synthetic [Borer et al., 2009]
Magnetite	Fe <sub>3</sub> O <sub>4</sub>	natural <sup>b</sup>
Muscovite	KAl <sub>2</sub> (Al Si <sub>3</sub> O <sub>10</sub> ) (OH,F) <sub>2</sub>	natural <sup>b</sup>
Pyrite	FeS <sub>2</sub>	natural <sup>b</sup>
Scorodite	FeAsO <sub>4</sub> × 2H <sub>2</sub> O	natural <sup>a</sup>
Siderite	FeCO <sub>3</sub>	natural <sup>b</sup>

<sup>a</sup>Provided by the TU Bergakademie Freiberg (Germany). <sup>b</sup>Provided by the ETH Zurich (Switzerland). <sup>c</sup>Source Clays Repository (Origin: Flagstaff Hill, El Dorado County, California, USA).



**Figure A.4.** Iron K-edge XAS reference spectra. (a) Iron K-edge EXAFS spectra, and (b) corresponding magnitude of the Fourier transforms of reference compounds included in the principal component analysis and target-transform testing.

### A.5.3. Principal component analysis

The results of the principal component analysis (PCA) including the eigenvalues, the indicator values (IND), the cumulative variances, as well as the total normalized sum of squared residuals (NSSR) are given for the first six components of the As and Fe data sets in Tables A.5 and A.6. The empirical IND function is supposed to be minimum when the correct number of factors is employed in order to determine the true factor space [Malinowski, 1977]. The PCA of As *K*-edge EXAFS spectra of the peat samples yielded two statistically significant spectral components based on the IND function (Table A.5), explaining 64% of the variance in the peat EXAFS spectra. For the Fe data set, IND reached a minimum for four components, which explained 94% of the variance in the peat Fe *K*-edge EXAFS spectra (Table A.6). The quality of the spectral reconstructions was evaluated by the total NSSR value, which describes the residuals between the  $k^2$ -weighted fit and the experimental data as shown in Equation A.1:

$$\text{Total NSSR} = \frac{\sum_{\text{spectra}} \sum_i (k^2 \chi_{\text{exp}} - \sum_{\text{components}} k^2 \chi_{\text{reconst}})^2}{\sum_{\text{spectra}} \sum_i (k^2 \chi_{\text{exp}})^2} \times 100 \quad (\text{A.1})$$

Here,  $\chi$  represents the sum of contributions from all scattering paths of the photoelectron and  $k$  derives from the wavenumber [Kelly et al., 2008]. The evaluation of the total NSSR as well as the visual inspection of the As *K*-edge EXAFS data set showed that for a satisfactorily reconstruction of all 14 peat EXAFS spectra, three components were required (cumulative variance: 70%, Table A.5).

**Table A.5.** PCA output parameters for As.

Component	Eigenvalue	IND	Cum. variance	Total NSSR (%)
1	23.5	$1.49 \times 10^{-2}$	0.49	12.99
2	7.3	$1.09 \times 10^{-2}$	0.64	4.62
3	3.0	$1.13 \times 10^{-2}$	0.70	3.21
4	2.0	$1.28 \times 10^{-2}$	0.74	2.55
5	1.8	$1.49 \times 10^{-2}$	0.78	2.06
6	1.6	$1.81 \times 10^{-2}$	0.81	1.68

**Table A.6.** PCA output parameters for Fe.

Component	Eigenvalue	IND	Cum. variance	Total NSSR (%)
1	23.4	$1.34 \times 10^{-2}$	0.61	10.77
2	6.9	$0.88 \times 10^{-2}$	0.79	3.12
3	3.7	$0.57 \times 10^{-2}$	0.88	0.85
4	2.1	$0.27 \times 10^{-2}$	0.94	0.12
5	0.5	$0.29 \times 10^{-2}$	0.95	0.08
6	0.4	$0.32 \times 10^{-2}$	0.96	0.05

#### A.5.4. Target-transform testing and linear combination fitting

The suitability of reference spectra for LCF analysis was determined by target-transform testing (TT) using the first three or four components calculated by PCA for As and Fe, respectively. The quality of the transformation was evaluated by the empirical SPOIL value categorized by Malinowski [1978]: 0-1.5 excellent, 1.5-3 good, 3-4.5 fair, 4.5-6 acceptable, and >6 for an unacceptable reference spectrum. Among all tested As references (Table A.3), the following As species were assigned with the lowest SPOIL values (<4.5): monomethylarsonic and dimethylarsinic acid, tris(phenylthio)arsine, glutamylcysteinylglycinyllthioarsenite, As(III)- and As(V)-sorbed ferrihydrite, realgar, and scorodite. Poor spectral reconstructions with high SPOIL values (>4.5) were found for all other As species. Among all tested Fe references listed in Table A.4, Fe(III)-citrate, Fe(III)-oxalate, ferrihydrite, lepidocrocite, Fe(III)-phosphate, pyrite, hornblende, biotite, and chlorite were assigned with the lowest SPOIL values (<6). Unacceptable reconstructions with high SPOIL values (>6) were found for all other Fe species, indicating that the local Fe coordination typical of either of these species is absent or negligible in the peat. However, the obtained number of As and Fe reference spectra suitable for LCF analysis based on TT was larger than the number of principal components determined by PCA. This may be due to (i) similar local As and Fe coordination environments in reference compounds identified by TT or (ii) the occurrence of several species in constant proportions in all analyzed spectra [Manceau et al., 2002]. Since we could not exclude the latter effect, LCF analyses were performed using all eight As references with SPOIL values <4.5 and all nine Fe references with SPOIL values <6. Each experimental spectrum was least-squares simulated in Athena [Ravel and Newville, 2005] by calculating all single-

to six-component fits. The number of components included in the fit was successively increased and each additional component was retained in the fit when the NSSR value decreased by at least 10% [Kelly et al., 2008]. All LCF results were recalculated to a component sum of 100%. Initial deviations from a component sum of 100% were  $\leq 11\%$  for As and  $\leq 7\%$  for Fe LCFs. The best fit LCF results for the 14 peat As *K*-edge EXAFS spectra included five out of eight As *K*-edge EXAFS reference spectra used in the LCF analysis. In the case of Fe, six out of nine reference species were retained to best explain the spectral variations in the Fe *K*-edge EXAFS spectra of the peat samples.

### **A.6. Scanning electron microscopy – energy-dispersive X-ray spectroscopy analyses of realgar (As<sub>4</sub>S<sub>4</sub>) and pyrite (FeS<sub>2</sub>)**

Scanning electron microscopy – energy-dispersive X-ray spectroscopy (SEM-EDX) analysis was mainly applied to verify the results obtained by XAS, particularly the presence of realgar and pure pyrite in the peat. Realgar was detected in the surface samples of profiles B3 and B5 (<41 cm) by XAS; however, verification via XRD was impossible due to its low abundance. Figure A.5 shows the secondary and backscattered electron images as well as the semi-quantitative EDX analyses of a realgar particle in a peat sample from profile B5 (12 cm) and a realgar reference by courtesy of TU Bergakademie Freiberg, Germany. The SEM-EDX analyses of both samples revealed an identical molar As/S ratio, thus supporting the presence of realgar in the peat. Figure A.6 depicts the secondary and backscattered electron images as well as the semi-quantitative EDX analysis of pyrite in a peat sample from profile B1 (196 cm). The EDX spectrum of this pyrite was identical to that of pure pyrite [Reed, 1996]. Although (i) pyrite can contain up to 100 g As kg<sup>-1</sup> [Wilkin and Ford, 2006] and (ii) the detection limit of EDX spectroscopy is approximately 5 mg As kg<sup>-1</sup>, no As was detected in the analyzed pyrite samples ( $n = 5$ ). This result testifies that As sequestration by pyrite is of secondary importance at the *Gola di Lago* site.

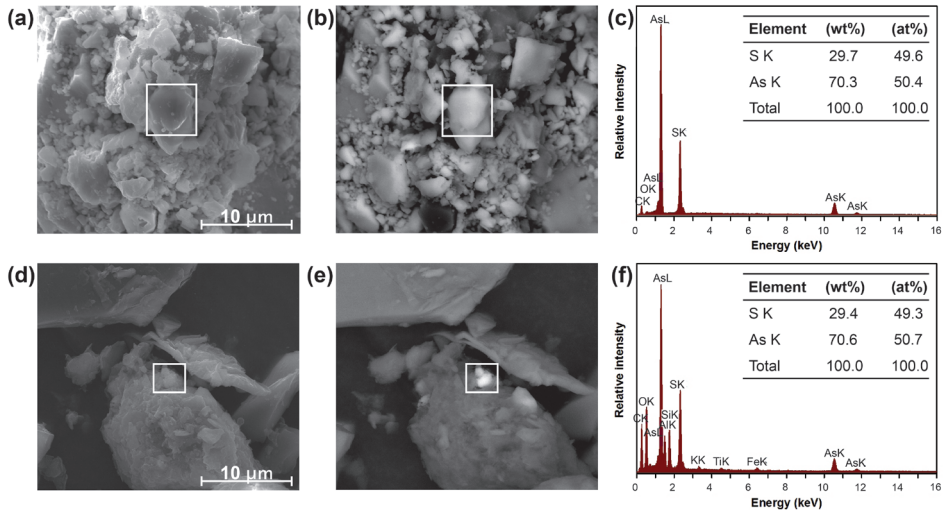


**Figure A.5.** SEM-EDX analyses of a realgar reference and a realgar particle of a *Gola di Lago* peat sample (profile B5, 12 cm). (a) Secondary electron image, (b) backscattered electron image, and (c) semi-quantitative EDX analysis of the realgar reference. (d) Secondary electron image, (e) backscattered electron image, and (f) semi-quantitative EDX analysis of the peat realgar particle, which was associated with an aluminosilicate phase embedded in organic matter.

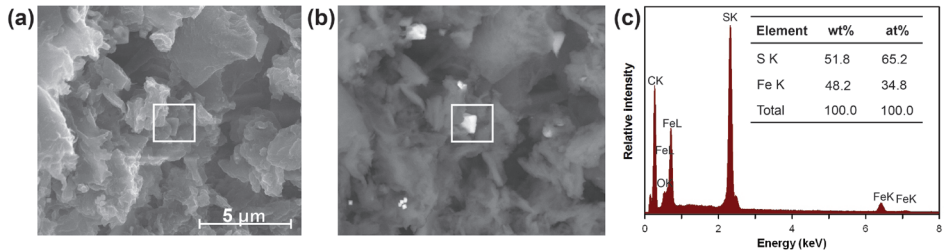


**Figure A.6.** SEM-EDX analysis of a pyrite particle of a *Gola di Lago* peat sample (profile B1, 196 cm). (a) Secondary electron image, (b) backscattered electron image, and (c) semi-quantitative EDX analysis of pyrite. The spectrum was identical to that of pure pyrite [Reed, 1996]. The surrounding matrix is organic material.



## A.7. Wavelet-transform analysis

Realgar (or its polymorphs) as well as orpiment ( $\text{As}_2\text{S}_3$ ) yield strong As backscattering signals in the Fourier transforms of their As  $K$ -edge EXAFS spectra between 2.5 and 3.5 Å (uncorrected for phase shift; Figure A.3). Here we tested the presence of As backscattering signals in the As  $K$ -edge EXAFS spectrum of a peat sample from profile B1 (179 cm) using wavelet-transform analysis. Linear combination fitting suggested that trivalent As in this particular sample was entirely coordinated to sulfhydryl groups of the peat natural organic matter (NOM) (Table 2.1 and Figure 2.3).

We utilized the Fortran-based HAMA code to calculate Morlet wavelets [Funke et al., 2005] of  $k^1$ -weighted As  $K$ -edge EXAFS spectra of realgar and orpiment over an  $R + \Delta R$ -range of 2.5-3.5 Å. For appropriate resolution in  $R$ - and  $k$ -space, we employed a wavelet parameter combination of  $\kappa = 7$  and  $\sigma = 2$ . The wavelet transforms of both As sulfide minerals were then compared with those obtained for the tris(phenylthio)arsine reference and the peat sample from profile B1. The result of this analysis is illustrated in Figure A.7. While both As sulfides showed a strong backscattering signal of As at  $k \sim 6\text{-}12 \text{ \AA}^{-1}$ , there was no evidence for heavy backscattering atoms in both organic samples. A decreased short-range order in poorly crystalline As sulfides, however, likely causes the destructive interference of As-As scattering waves. Consequently, these phases exhibit a strongly reduced Fourier-transform amplitude in the  $R + \Delta R$ -range of 2.5-3.5 Å when compared to their crystalline counterparts [Helz et al., 1995]. For this reason, the use of crystalline As sulfide references in the wavelet-transform analysis may be considered inappropriate.

In order to compare our peat sample with a nanocrystalline  $\text{As}_2\text{S}_3$  solid, we digitized a published As  $K$ -edge EXAFS spectrum of the latter phase ('amorphous  $\text{As}_2\text{S}_3$ ' in Figure 2c by Helz et al. [1995]) and calculated the wavelet of its  $k^1$ -weighted As  $K$ -edge EXAFS spectrum. In order to increase the resolution in  $R$ -space, we employed a Morlet parameter combination of  $\kappa = 7$  and  $\sigma = 5$ . Figure A.8 displays the resulting wavelets of crystalline  $\text{As}_2\text{S}_3$  (orpiment), amorphous  $\text{As}_2\text{S}_3$ , tris(phenylthio)arsine, and the peat sample. Orpiment yields a strong signal at  $\sim 3 \text{ \AA}$ , which extends to higher  $R + \Delta R$ -values (Figure A.8). This signal is due to backscattering from As and S atoms located between

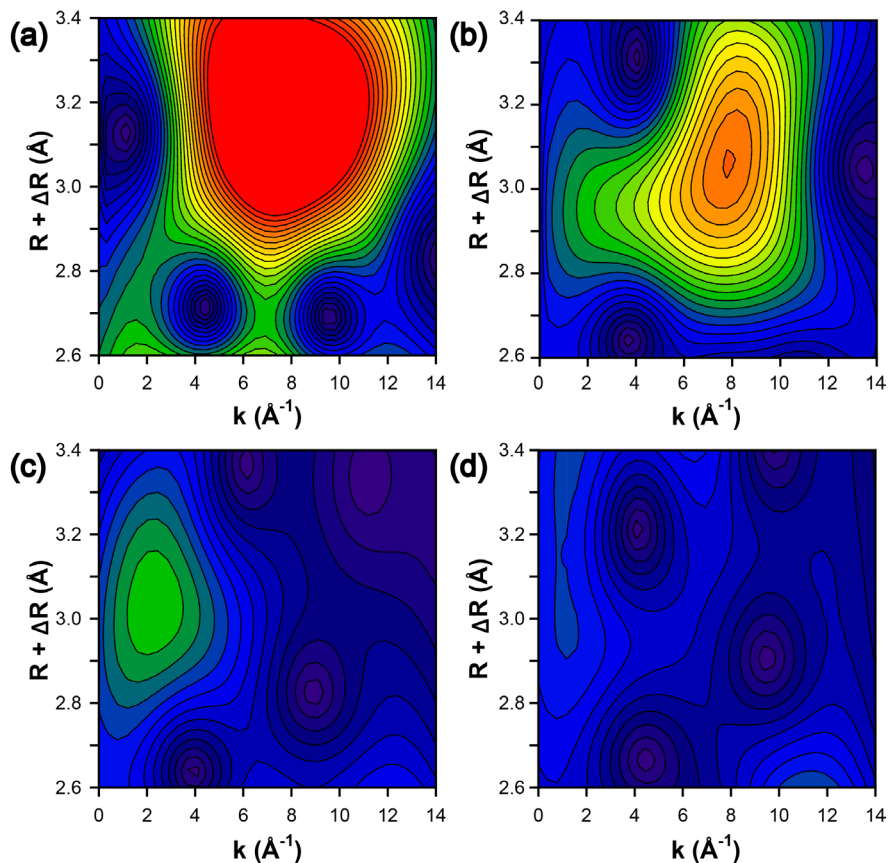


**Figure A.7.** Morlet wavelets of  $k^1$ -weighted As  $K$ -edge EXAFS spectra of As reference compounds and a peat sample ( $\kappa = 7$ ,  $\sigma = 2$ ). Contour plots showing the wavelet transforms of (a) realgar, (b) orpiment, (c) tris(phenylthio)arsine, and (d) a peat sample from profile B1 (179 cm). For direct comparison, the scale of the  $z$ -axis (color code) was identical for all samples (range: 0-0.1).

3.19 and 3.64 Å about the central As absorber [Mullen and Nowacki, 1972; Helz et al., 1995]. In amorphous  $\text{As}_2\text{S}_3$  the signal occurring at  $R + \Delta R \sim 3.2$  Å accords with the fitted As-As distance of 3.55 Å [Helz et al., 1995]. This signal is clearly absent in the tris(phenylthio)arsine reference and the peat sample. Both samples only show a signal at  $\sim 3.0$  Å, which originates from backscattering by low- $Z$  elements (C/N/O) and/or multiple scattering. In the case of the peat sample this finding points towards a direct association between trivalent As and NOM. The wavelet-transform analysis thus supports the absence of significant amounts of nanocrystalline As sulfide minerals in the peat sample. This conclusion is also corroborated by a direct comparison of the Fourier transforms of As  $K$ -edge EXAFS spectra of the amorphous  $\text{As}_2\text{S}_3$  and the peat

sample (Figure A.9). The peat sample lacked the distinct Fourier-transform amplitude at  $R + \Delta R \sim 3.2$  Å. In addition, the Fourier-transform maximum of the first coordination shell in amorphous  $\text{As}_2\text{S}_3$  is shifted towards higher  $R + \Delta R$ -values, signifying a longer As-S bond in the mineral compared to the peat sample. Indeed, the As-S bond distance fitted for the amorphous  $\text{As}_2\text{S}_3$  was 2.28 Å [Helz et al., 1995], which is longer than the 2.26 Å determined for the peat sample (Figure 2.3). In summary, our wavelet-transformation results are in agreement with the interpretation that monomeric As-NOM complexes dominate the speciation of As in the peat.

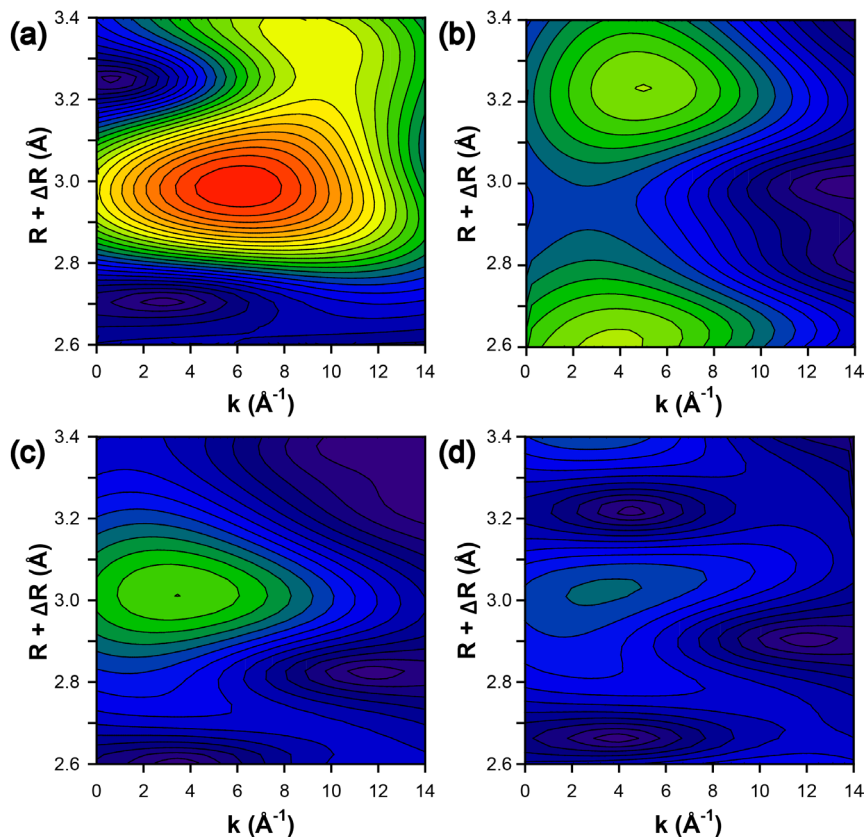


**Figure A.8.** Morlet wavelets of  $k^1$ -weighted As  $K$ -edge EXAFS spectra of As reference compounds and a peat sample ( $\kappa = 7$ ,  $\sigma = 5$ ). Contour plots showing the wavelet transforms of (a) orpiment, (b) amorphous  $\text{As}_2\text{S}_3$ , (c) tris(phenylthio)arsine, and (d) a peat sample from profile B1 (179 cm). For direct comparison, the scale of the  $z$ -axis (color code) was identical for all samples (range: 0-0.05).

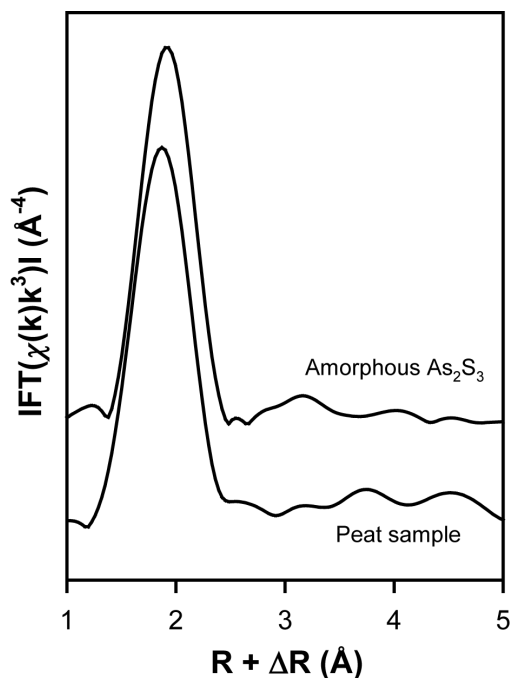


**Figure A.9.** Fourier transforms of  $k^3$ -weighted As  $K$ -edge EXAFS spectra of amorphous  $\text{As}_2\text{S}_3$  taken from Helz et al. [1995] and a peat sample from profile B1 (179 cm). The Fourier transforms were calculated over a  $k$ -range of  $4$ – $11 \text{\AA}^{-1}$  using a Kaiser-Bessel window function with a window sill  $dk$  of  $3 \text{\AA}^{-1}$ . The Fourier transforms of both samples were scaled to the same magnitude of the first-shell peak in order to facilitate a direct comparison.



## References

- Borer, P., Sulzberger, B., Hug, S. J., Kraemer, S. M., Kretzschmar, R. (2009) Photoreductive dissolution of iron(III) (hydr)oxides in the absence and presence of organic ligands: Experimental studies and kinetic modeling. *Environ. Sci. Technol.* *43*, 1864-1870.
- Braun-Blanquet, J. (1932) *Plant sociology: The study of plant communities*. McGraw-Hill: New York.
- Funke, H., Scheinost, A. C., Chukalina, M. (2005) Wavelet analysis of extended x-ray absorption fine structure data. *Phys. Rev. B: Condens. Matter* *71*, 1-7.
- González A., Z. I., Krachler, M., Cheburkin, A. K., Shoty, W. (2006) Spatial distribution of natural enrichments of arsenic, selenium, and uranium in a minerotrophic peatland, Gola di Lago, canton Ticino, Switzerland. *Environ. Sci. Technol.* *40*, 6568-6574.
- Helz, G. R., Tossell, J. A., Charnock, J. M., Patrick, R. A. D., Vaughan, D. J., Garner, C. D. (1995) Oligomerization in As(III) sulfide solutions: Theoretical constraints and spectroscopic evidence. *Geochim. Cosmochim. Acta* *59*, 4591-4604.
- Kelly, S. D., Hesterberg, D., Ravel, B. (2008) Analysis of soils and minerals using X-ray absorption spectroscopy. In Ulery, A. L., Drees, L. R. (Eds.) *Methods of soil analysis. Part 5: Mineralogical methods*. Soil Science Society of America: Madison, pp. 387-463.
- Malinowski, E. R. (1977) Determination of the number of factors and the experimental error in a data matrix. *Anal. Chem.* *49*, 612-617.
- Malinowski, E. R. (1978) Theory of error for target factor analysis with applications to mass spectrometry and nuclear magnetic resonance spectrometry. *Anal. Chim. Acta* *103*, 339-354.
- Manceau, A., Marcus, M. A., Tamura, N. (2002) Quantitative speciation of heavy metals in soils and sediments by synchrotron X-ray techniques. In Fenter, P. A., Rivers, M. L., Sturchio, N. C., Sutton, S. R. (Eds.) *Applications of synchrotron radiation in low-temperature geochemistry and environmental sciences*. Mineralogical Society of America: Washington, DC, pp. 341-428.
- Mikutta, C., Frommer, J., Voegelin, A., Kaegi, R., Kretzschmar, R. (2010) Effect of citrate on the local Fe coordination in ferrihydrite, arsenate binding, and ternary arsenate complex formation. *Geochim. Cosmochim. Acta* *74*, 5574-5592.
- Mikutta, C., Wiederhold, J. G., Cirpka, O. A., Hofstetter, T. B., Bourdon, B., Von Gunten, U. (2009) Iron isotope fractionation and atom exchange during sorption of ferrous iron to mineral surfaces. *Geochim. Cosmochim. Acta* *73*, 1795-1812.
- Mullen, D. J. E., Nowacki, W. (1972) Refinement of crystal structures of realgar, AsS and orpiment, As<sub>2</sub>S<sub>3</sub>. *Z. Kristallogr.* *136*, 48-65.

- Raab, A., Meharg, A. A., Jaspars, M., Genney, D. R., Feldmann, J. (2004) Arsenic-glutathione complexes - their stability in solution and during separation by different HPLC modes. *J. Anal. At. Spectrom.* 19, 183-190.
- Ravel, B., Newville, M. (2005) Athena, Artemis, Hephaestus: Data analysis for X-ray absorption spectroscopy using Ifeffit. *J. Synchrot. Radiat.* 12, 537-541.
- Reed, S. J. B. (1996) *Electron microbe analysis and scanning electron microscopy in geology*. Cambridge University Press: Cambridge.
- Wilkin, R. T., Ford, R. G. (2006) Arsenic solid-phase partitioning in reducing sediments of a contaminated wetland. *Chem. Geol.* 228, 156-174.





## **B. Supporting Information to Chapter 3**

**'Spatial distribution and speciation of arsenic in peat  
studied with microfocused X-ray fluorescence  
spectrometry and X-ray absorption spectroscopy'**

## B.1. Synchrotron measurements and data analyses

### B.1.1. Bulk X-ray absorption spectroscopy – arsenic and iron

Arsenic *K*-edge (11,867 eV) and Fe *K*-edge (7,112 eV) X-ray absorption near-edge structure (XANES) and extended X-ray absorption fine structure (EXAFS) spectra were collected over an energy range of 11,667-12,520 eV (As) and 6,880-7,794 eV (Fe). Higher harmonics in the beam were rejected by detuning the Si(220) double-crystal monochromators to 70% of their maximal intensity. The nominal energy resolution  $\Delta E/E$  was about  $\sim 10^{-4}$ . The monochromators were calibrated relative to the  $L_3$ -edge energy of elemental Au (11,919 eV) or the *K*-edge energy of elemental Fe (7,112 eV). All samples were measured in fluorescence mode using solid-state Ge detectors with samples placed in a He cryostat ( $\sim 10$  K) at  $45^\circ$  relative to the incident beam. Four to eight scans per sample were collected and averaged. X-ray absorption spectroscopy (XAS) data analyses were performed using Athena [Ravel and Newville, 2005 a,b]. For spectra normalization, the Autobk algorithm was applied by fitting a linear function in the pre-edge region ( $E_0 - E = 30$ -140 eV for As and 30-130 eV for Fe) and a quadratic polynomial in the post-edge region ( $E - E_0 = 150$ -600 eV for As and 50-650 eV for Fe).  $E_0$  values were determined from the maximum of the first derivative of the measured XAS spectra. Linear combination fitting (LCF) of  $k^3$ -weighted bulk As and Fe *K*-edge EXAFS spectra was performed over a *k*-range of 3-12  $\text{\AA}^{-1}$  utilizing a large set of As and Fe reference spectra [Langner et al., 2012].

### B.1.2. Bulk X-ray absorption spectroscopy – sulfur

Sulfur *K*-edge (2,472 eV) XANES spectra were collected using a Si(111) double-crystal monochromator ( $\Delta E/E \sim 10^{-4}$ ) and a Ni-coated harmonic rejection mirror. The sample stage was placed in a He atmosphere in which the  $O_2$  content (typically  $< 0.1\%$ ) was continuously monitored. Data collection was performed in fluorescence mode using a Lytle detector and with samples placed at  $45^\circ$  relative to the incident beam. All samples were measured at  $\sim 25$  K using a liquid He cryostream. The monochromator was calibrated

relative to the white-line energy of a  $\text{Na}_2\text{S}_2\text{O}_3$  standard (2,472.02 eV), which was repeatedly measured in between sample runs. Up to five scans were recorded in the energy range 2,400-2,650 eV for each peat sample. For spectra normalization in Athena, the Autobk algorithm was applied by fitting a linear function in the pre-edge region ( $E_0 - E = 15-70$  eV) and a quadratic polynomial in the post-edge region ( $E - E_0 = 15-20$  eV).  $E_0$  values were determined from the maximum of the first derivative of the measured XAS spectra. To identify oxidation states of S and quantify S species in the peat samples, data processing of the normalized S *K*-edge XANES spectra was carried out using WinXAS 3.2 [Ressler, 1998] following the fitting approach recommended by Manceau and Nagy [2012]. Deconvolution of the peat spectra into pseudo-components was performed in the energy range 2,465-2,490 eV using a series of Gaussians for the S  $s \rightarrow p$  transition peaks and two arctangent functions. The positions of the Gaussians were chosen based on the white-line energy positions of S reference compounds [Vairavamurthy, 1998; Hoffmann et al., 2012; Manceau and Nagy, 2012]. The first and second arctangent functions represent the edge step of reduced (2,475.6 eV) and oxidized S species (2,482.3 eV), respectively [Xia et al., 1998; Manceau and Nagy, 2012]. The positions and widths of all Gaussians and arctangent functions were fixed, whereas the peak heights were allowed to vary in the fits. The areas of the Gaussians were calculated and subsequently corrected for the oxidation state-dependent change in the absorption cross-section based on the generic curve published in Manceau and Nagy [2012]. To calculate the relative contribution of every S species to the total S in the sample, the corrected peak area for each S species was normalized to the sum of all peak areas.

### **B.1.3. Microfocused X-ray fluorescence spectrometry and X-ray absorption spectroscopy**

Elemental distribution maps of As, Fe, S, and other elements were collected with beam spot sizes between  $6 \times 6$  and  $15 \times 6 \mu\text{m}^2$  (H  $\times$  V) and step sizes between 6 and 50  $\mu\text{m}$ , depending on the size of the map. The thin sections were placed in a  $45^\circ$  angle to the incident beam, and the fluorescence signal was recorded at a  $90^\circ$  angle using a solid-state Ge detector. Each defined region was mapped at three incident photon energies:

(1) 2,802 eV (S, Si), (2) 7,000 eV (Mn), and (3) 13,001 eV (Fe, As). In each map, several points of interest (POI) were selected for extended As *K*-edge  $\mu$ -XANES analysis in the energy range 11,751-12,192 eV. The spectra were dead-time corrected and averaged using software tools developed at ALS beamline 10.3.2. Linear combination fit analyses of the  $\mu$ -XANES spectra were performed in Athena. The reference spectrum of arsenian pyrite used in the data evaluation was taken from Bostick and Fendorf [2003]. The fit results were validated by the reconstruction of experimental  $k^2$ -weighted  $\mu$ -EXAFS spectra ( $k = 2-7 \text{ \AA}^{-1}$ ) based on the fitted fractions of As reference compounds.

#### **B.1.4. Synchrotron X-ray diffractometry**

Diffraction patterns were collected at room temperature up to  $120^\circ 2\theta$  with an incident photon energy of  $\sim 20 \text{ keV}$  ( $\lambda = 0.6199 \text{ \AA}$ ) utilizing a solid-state Si microstrip detector (MYTHEN II). The experimental setup was calibrated using a Si powder standard (NIST 640c). Experimental powder patterns were evaluated with Match! 1.10d (Crystal Impact, Germany).

## B.2. Concentrations of major elements in peat cores B3II, B5II, B1II

**Table B.1.** Concentrations of major elements in peat cores B3II, B5II, and B1II. Values are given in g kg<sup>-1</sup> dry weight except for As (mg kg<sup>-1</sup>).

Core	Depth (cm) <sup>a</sup>	Al	As	C <sup>b</sup>	Ca	Fe	K	Mg	Mn	N	P	S	Si
B3II	12 (12)	6.45	551.1	377.5	7.01	19.3	2.41	0.93	0.19	19.7	0.61	5.91	35.8
	31 (6)	17.2	271.5	336.4	6.35	12.7	4.64	2.31	0.12	17.5	0.84	5.73	52.3
	44 (6)	55.9	54.5	134.8	5.37	17.8	13.0	5.30	0.23	9.62	1.48	2.72	148.3
	62 (12)	65.4	39.3	148.2	6.11	13.7	13.7	4.36	0.21	8.42	1.63	2.34	158.9
	87 (12)	61.5	67.3	173.1	9.54	15.5	11.1	3.98	0.17	5.20	1.58	4.69	114.9
	112 (12)	58.0	19.3	9.00	9.36	25.1	15.4	9.03	0.42	0.03	0.60	0.23	165.7
B5II	12 (12)	51.0	397.1	122.2	7.19	35.1	13.7	7.49	0.36	8.12	1.18	2.83	134.3
	37 (12)	52.8	323.4	108.4	6.92	29.4	13.4	7.60	0.33	8.23	1.24	2.61	165.5
	62 (12)	59.6	438.9	22.3	6.80	29.2	15.6	9.06	0.37	1.65	1.09	1.28	182.9
	87 (12)	69.9	580.1	58.7	7.25	35.1	16.5	10.4	0.38	4.96	1.97	1.59	178.8
	112 (12)	73.0	444.6	56.1	7.54	34.3	17.3	10.1	0.40	3.88	1.93	1.25	173.6
B5II	137 (12)	74.0	321.2	59.8	7.87	27.8	17.4	9.08	0.36	3.22	2.08	1.50	166.5
B1II	12 (12)	32.3	55.2	247.3	6.97	21.3	7.69	4.08	0.22	17.0	1.12	6.07	115.1
	37 (12)	22.8	60.1	299.4	6.01	13.7	5.19	2.77	0.15	17.8	0.77	5.97	79.0
	62 (12)	9.65	38.2	356.3	4.69	8.26	2.31	1.08	0.08	25.0	0.50	5.95	48.7
	100 (25)	43.9	14.3	183.3	6.50	11.8	11.7	3.15	0.17	11.9	1.04	3.08	132.0
	137 (12)	18.5	35.5	291.2	7.25	12.6	5.44	1.07	0.13	15.9	0.74	6.14	57.4
	162 (12)	4.57	87.2	439.4	13.4	6.85	1.15	0.32	0.03	19.5	0.37	12.1	9.00
	187 (12)	2.20	233.3	452.8	14.0	5.70	0.42	0.26	0.02	20.2	0.26	15.5	2.41
	212 (12)	2.21	331.0	452.8	14.1	4.69	0.53	0.41	0.03	21.3	0.28	15.3	3.06
	237 (12)	11.8	255.7	348.4	11.7	8.28	4.12	1.39	0.08	12.7	0.39	16.6	34.5
B1II	262 (12)	37.1	66.0	158.7	12.7	18.8	12.5	4.92	0.22	6.46	0.55	14.5	119.8

<sup>a</sup>The sampling depths are given as mean values with the sampling ranges (+/- mean value) in parentheses. Freeze-dried, homogenized, and ground (<50 µm) peat samples were analyzed by energy-dispersive X-ray fluorescence spectrometry (Spectro X-Lab 2000). Total C and N contents were determined in triplicate (mean relative standard deviation: 9.0%) with an elemental analyzer (Leco CHNS-932). <sup>b</sup>Represents organic C only because carbonates are absent as tested with 10% HCl.

### B.3. Bulk arsenic, iron, and sulfur speciation results

**Table B.2.** Speciation of As in the peat samples based on linear combination fitting of  $k^3$ -weighted bulk As  $K$ -edge EXAFS spectra.

Core	Depth (cm) <sup>a</sup>	% of total As (normalized to a sum of 100%) <sup>b</sup>			Fitted sum (%) <sup>c</sup>	NSSR (%) <sup>d</sup>
		As(III)-NOM	Realgar	As-Fh		
B3II	31 (6)	-	71	29 (20/9)	114	14.3
B5II	12 (12)	-	43	57 (36/21)	111	7.4
B1II	212 (12)	100 (63/37)	-	-	87	2.8
B1II	237 (12)	100 (46/54)	-	-	97	2.3

<sup>a</sup>The sampling depths are given as mean values with the sampling ranges (+/- mean value) in parentheses. <sup>b</sup>Values in parentheses indicate the fractions of the following reference compounds: As(III)-NOM = tris(phenylthio)arsine (As(III)(SPhen)<sub>3</sub>)/a mixture of a di- and triglutathione complex of As(III) (As(III)(GS)<sub>2,6</sub>(OH)<sub>0,6</sub>) [Langner et al., 2012], As-Fh = As(III)/As(V) sorbed to ferrihydrite. <sup>c</sup>Fitted sum of all references before normalization. <sup>d</sup>Normalized sum of squared residuals (NSSR (%) =  $100 \times \sum_i (\text{data}_i - \text{fit}_i)^2 / \sum_i \text{data}_i^2$ ).

**Table B.3.** Speciation of Fe in the peat samples based on linear combination fitting of  $k^3$ -weighted Fe  $K$ -edge EXAFS spectra.

Core	Depth (cm) <sup>a</sup>	% of total Fe (normalized to a sum of 100%) <sup>b</sup>				Fitted sum (%) <sup>c</sup>	NSSR (%) <sup>d</sup>
		Fe(III)-NOM	Fe(III)-(hydr)oxides	Phyllosilicates	Pyrite		
B3II	31 (6)	37 (0/37)	19 (0/19)	44 (0/20/24)	-	95	5.2
B5II	12 (12)	-	41 (30/11)	59 (0/23/36)	-	98	3.7
B1II	212 (12)	75 (21/54)	-	-	25	86	4.2
B1II	237 (12)	35 (0/35)	11 (0/11)	18 (18/0/0)	36	99	3

<sup>a</sup>The sampling depths are given as mean values with the sampling ranges (+/- mean value) in parentheses.

<sup>b</sup>Values in parentheses indicate the fractions of the following reference compounds: Fe(III)-NOM = Fe(III)-citrate/Fe(III)-oxalate, Fe(III)-(hydr)oxides = ferrihydrite/lepidocrocite, phyllosilicates = biotite/muscovite/chlorite. <sup>c</sup>Fitted sum of all references before normalization. <sup>d</sup>Normalized sum of squared residuals (NSSR (%) =  $100 \times \sum_i (\text{data}_i - \text{fit}_i)^2 / \sum_i \text{data}_i^2$ ).

**Table B.4.** Speciation of S in the peat samples.

Core	Depth (cm) <sup>a</sup>	S (g kg <sup>-1</sup> )	Reduced S (%) <sup>b</sup>		Intermediate oxidized S (%) <sup>c</sup>		Oxidized S (%) <sup>d</sup>	
			Inorganic sulfide	Exocyclic/Heterocyclic S	Sulfoxide	Sulfite/Sulfone	Sulfonate	Sulfate
B3I	18 (6)	8.3	14	69	3	2	8	4
B5I	12 (4)	2.4	16	64	3	2	9	6
B1I	196 (4)	16.8	9	83	1	1	5	1

<sup>a</sup>The sampling depths are given as mean values with the sampling ranges (+/- mean value) in parentheses.

<sup>b</sup>Energy range  $\leq 2,475$  eV and S oxidation states -II to +I. <sup>c</sup>Energy range 2,476-2,480 eV and S oxidation states +II to +IV. <sup>d</sup>Energy range  $\geq 2,481$  eV and S oxidation states +V to +VI.

**Table B.5.** Peak parameters of deconvoluted S *K*-edge XANES spectra shown in Figure 3.2 and atomic fractions of S functionalities after correction for the oxidation-state dependent cross section of S.

Core	Depth (cm) <sup>a</sup>	White-line energy (eV)	Assigned S functionality	Peak height	Fwhm (eV) <sup>b</sup>	Peak correction factor <sup>c</sup>	Uncorrected peak area	Corrected peak area	Corrected fraction (%)	NSSR (%) <sup>d</sup>
B31	18 (6)	2,470.50	inorganic sulfide	0.07	1.90	0.19	0.14	0.73	13.60	1.08
		2,472.90	exocyclic S	1.25	1.90	1.07	2.52	2.35	44.00	
		2,474.30	heterocyclic S	1.04	1.90	1.59	2.11	1.33	24.80	
		2,476.25	sulfoxide	0.21	1.90	2.31	0.43	0.19	3.50	
		2,478.80	sulfite	0.21	2.00	3.24	0.44	0.14	2.60	
		2,481.05	sulfonate	0.78	2.00	4.07	1.67	0.41	7.70	
		2,482.80	sulfate	0.47	2.00	4.72	1.00	0.21	4.00	
		2,471.10	inorganic sulfide	0.18	1.90	0.41	0.36	0.89	15.80	1.37
B51	12 (4)	2,472.90	exocyclic S	1.21	1.90	1.07	2.44	2.28	40.30	
		2,474.30	heterocyclic S	1.03	1.90	1.59	2.08	1.31	23.20	
		2,476.25	sulfoxide	0.22	1.90	2.31	0.45	0.19	3.40	
		2,478.75	sulfite	0.21	2.00	3.23	0.44	0.14	2.40	
		2,481.05	sulfonate	0.96	2.00	4.07	2.05	0.50	8.90	
		2,482.80	sulfate	0.75	2.00	4.72	1.60	0.34	6.00	
		2,470.80	inorganic sulfide	0.05	1.90	0.30	0.11	0.36	9.20	0.65
		2,473.25	exocyclic S	1.37	1.90	1.20	2.77	2.31	58.00	
B11	196 (4)	2,474.60	heterocyclic S	0.83	1.90	1.70	1.67	0.98	24.70	
		2,476.40	sulfoxide	0.03	1.90	2.36	0.05	0.02	0.60	
		2,479.50	sulfone	0.09	2.00	3.50	0.18	0.05	1.30	
		2,481.20	sulfonate	0.36	2.00	4.13	0.77	0.19	4.70	
		2,482.90	sulfate	0.14	2.00	4.76	0.29	0.06	1.60	

<sup>a</sup>The sampling depths are given as mean values with the sampling ranges (+/- mean value) in parentheses. <sup>b</sup>Full width at half maximum. <sup>c</sup>Based on the 'generic' equation of Manceau and Nagy [2012]. <sup>d</sup>Normalized sum of squared residuals  $SSR (\%) = 100 \times \sum_i (data_i - fit_i)^2 / \sum_i data_i^2$ .

### B.4. Synchrotron XRD analysis

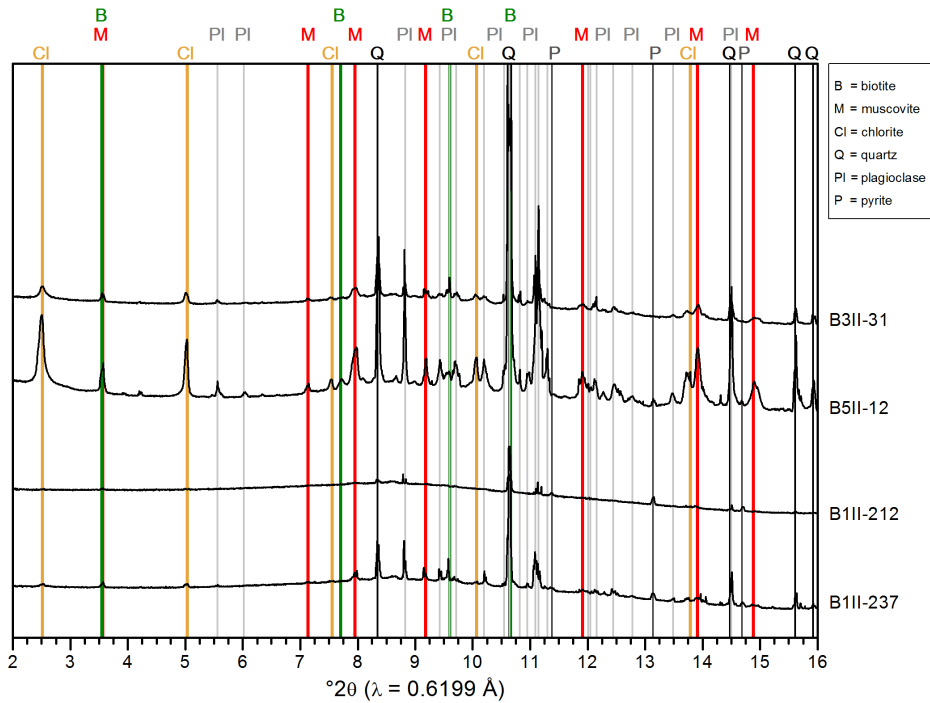


**Figure B.1.** Synchrotron XRD patterns of the near-surface (B3II-31 and B5II-12) and deep peat layer samples (B1II-212 and B1II-237) analyzed by  $\mu$ -XRF spectrometry and  $\mu$ -XAS.



## B.5. Light microscopy analysis

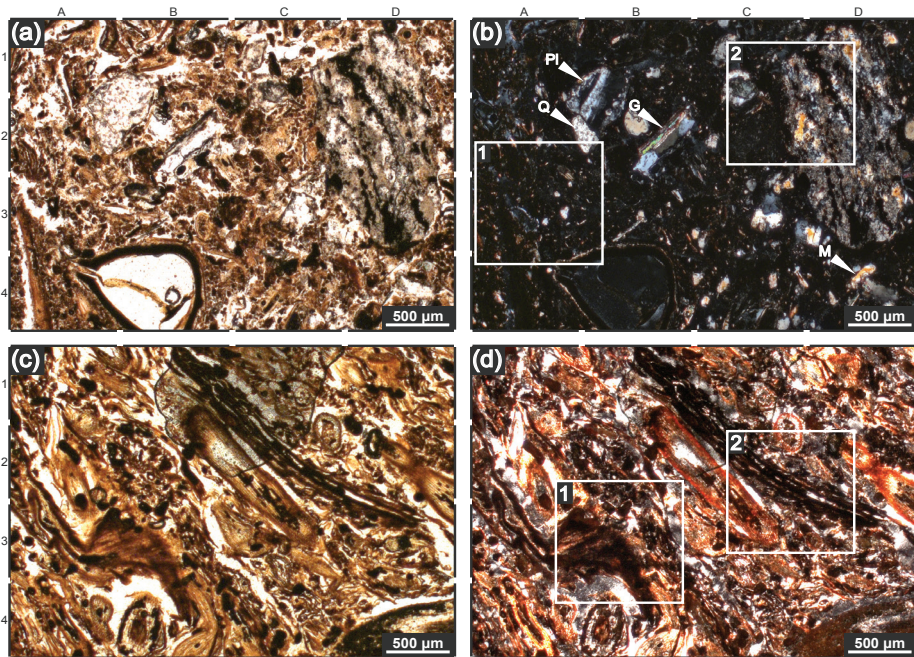


**Figure B.2.** (a, b) Photomicrographs of thin section B3II-31 in (a) plane-polarized light (PPL) and (b) cross-polarized light (CPL): Single plagioclase (A-B 1-2), quartz (A-B 2, A 3, C 1) and highly altered mica (D 4) particles ( $\sim 100\text{-}500\ \mu\text{m}$ ), as well as small  $\sim 1\text{-}3\text{-mm}$  sized rock fragments (e.g., gneiss: B 2, D 1-3) are embedded in the organic matrix. One example for each mineral and rock fragment is indicated in panel (b): Q = quartz, Pl = plagioclase, M = mica, and G = gneiss. (c, d) Photomicrographs of thin section B1II-237 in (c) PPL and (d) CPL: Organic matrix with small embedded quartz and mica particles of  $10\text{-}50\ \mu\text{m}$  size (not visible here). White boxes show the regions mapped by  $\mu\text{-XRF}$  spectrometry (Figure 3.3).

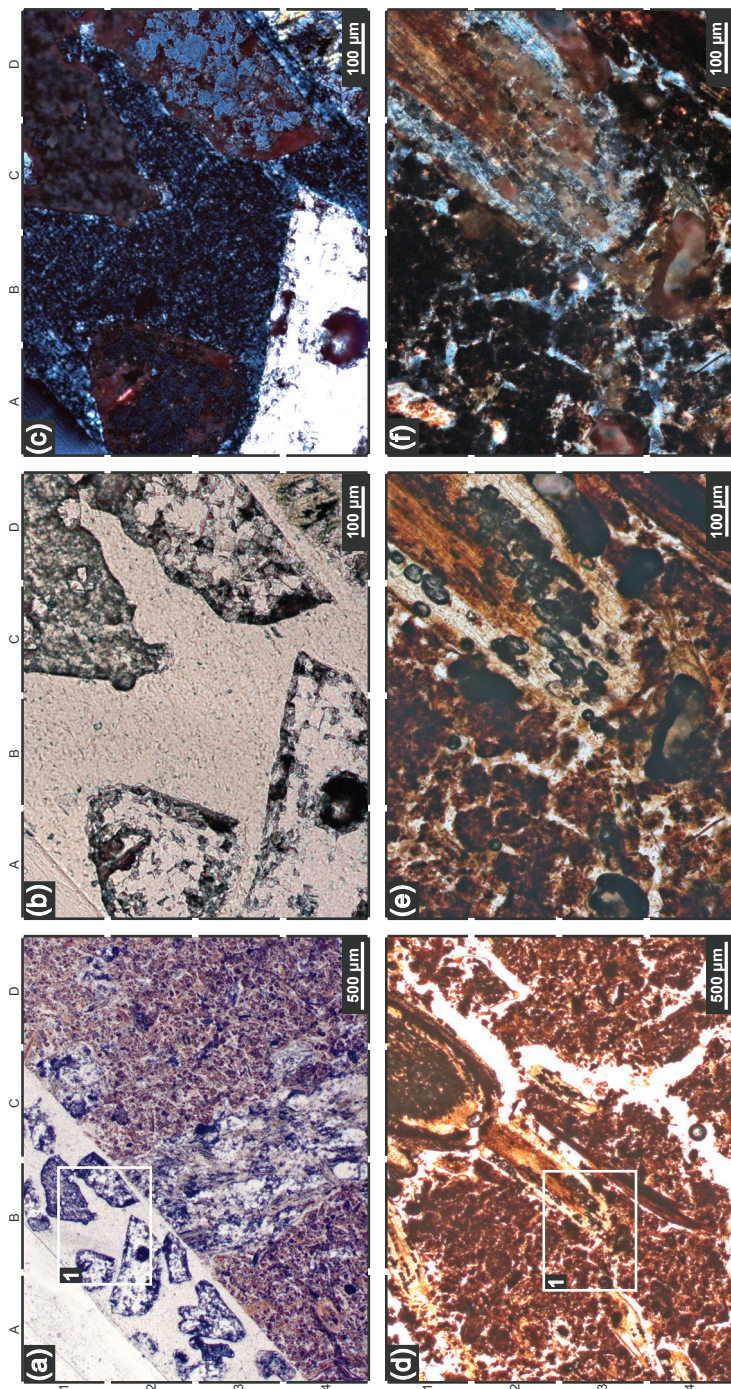


**Figure B.3.** (a-c) Photomicrographs of thin section B3II-31 in (a, b) plane-polarized light (PPL) and (c) cross-polarized light (CPL). The white box in (a) indicates the location magnified in (b) and (c). In (c) reddish-brown secondary Fe-(hydr)oxides are present on mineral surfaces (A 1-2, A 4, C-D 1-3). (d-f) Photomicrographs of thin section BIII-212 in (d, e) PPL and (f) CPL. The white box in (d) indicates region 1 mapped by  $\mu$ -XRF spectrometry (Figure 3.4) and is magnified in (e) and (f). The CPL image also shows secondary Fe-(hydr)oxides with a reddish-brown color (A 3, B 4, D 2-3).

## B.6. Elemental correlation plots

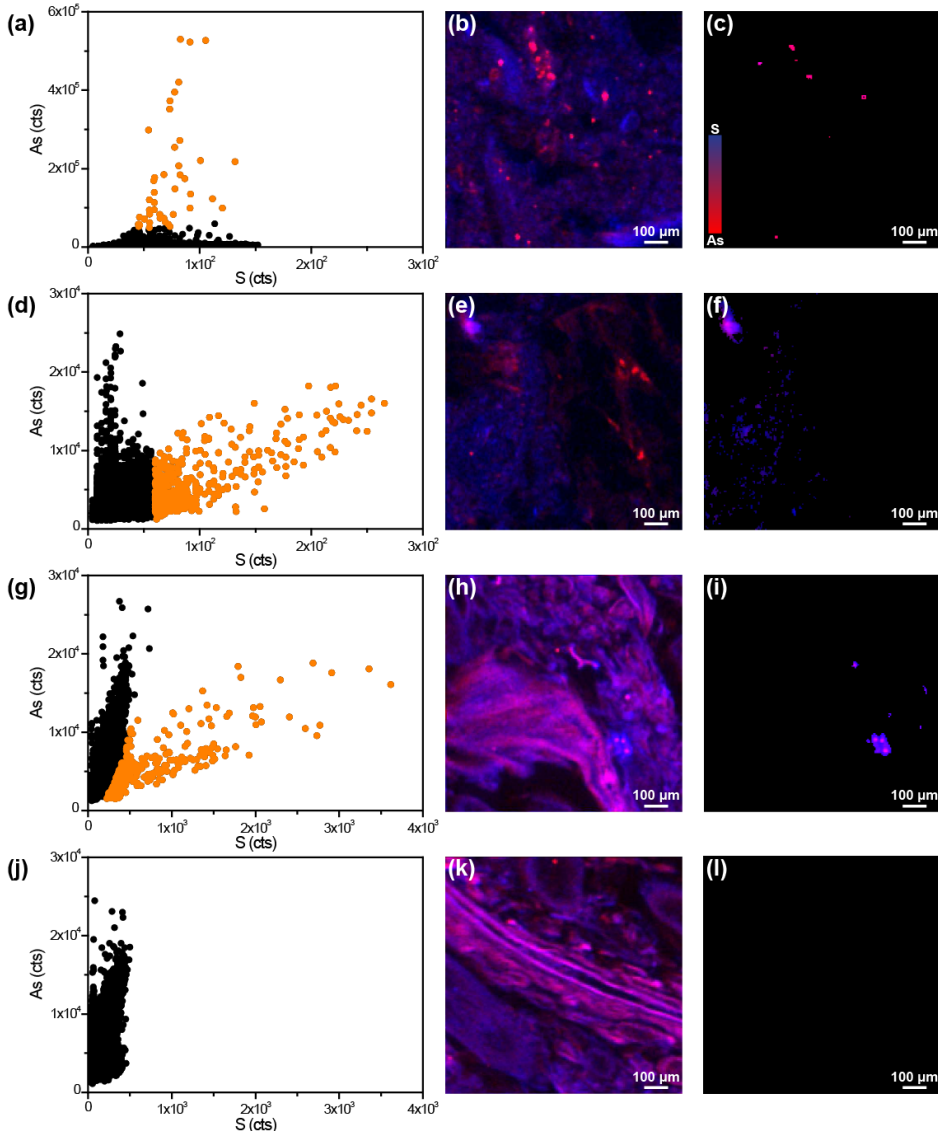


**Figure B.4.** Correlation plots of As and S fluorescence intensities and bicolor (RB)  $\mu$ -XRF elemental maps illustrating the distributions of As and S in (a-c) region 1 and (d-f) region 2 of thin section B3II-31, as well as (g-i) region 1 and (j-l) region 2 of thin section B1II-237 (Figure 3.3). The right-hand column displays  $\mu$ -XRF maps generated from the orange points in the correlation plots. The color code in (c) is valid for all panels. Note that the scales of the x- and y-axis vary in the correlation plots.

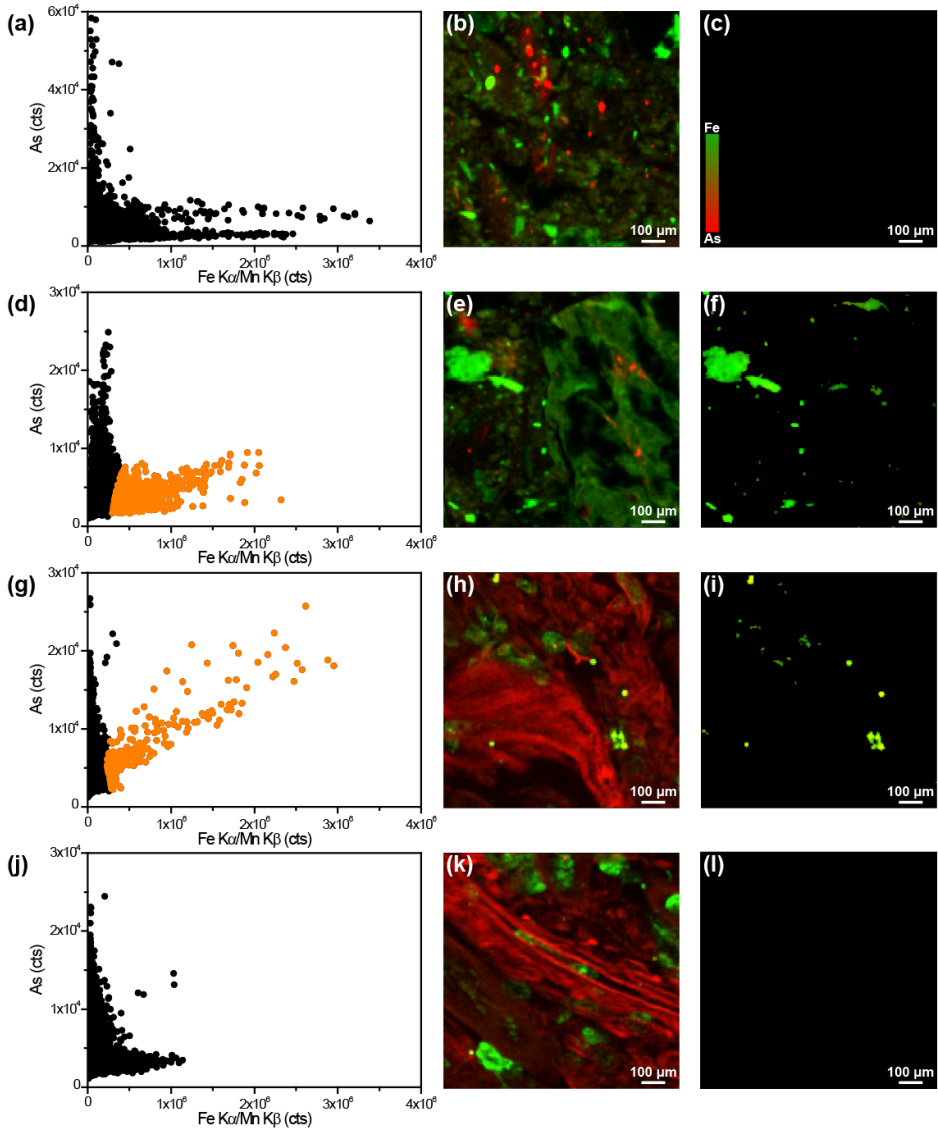


**Figure B.5.** Correlation plots of relative As and Fe fluorescence intensities and bicolor (RG)  $\mu$ -XRF elemental maps illustrating the distribution of As and Fe in (a-c) region 1 and (d-f) region 2 of thin section B3II-31, as well as (g-i) region 1 and (j-l) region 2 of thin section B1II-237 (Figure 3.3). The right-hand column displays  $\mu$ -XRF maps generated from the orange points in the correlation plots. The color code in (c) is valid for all panels. Note that the scale of the y-axis varies in the correlation plots.

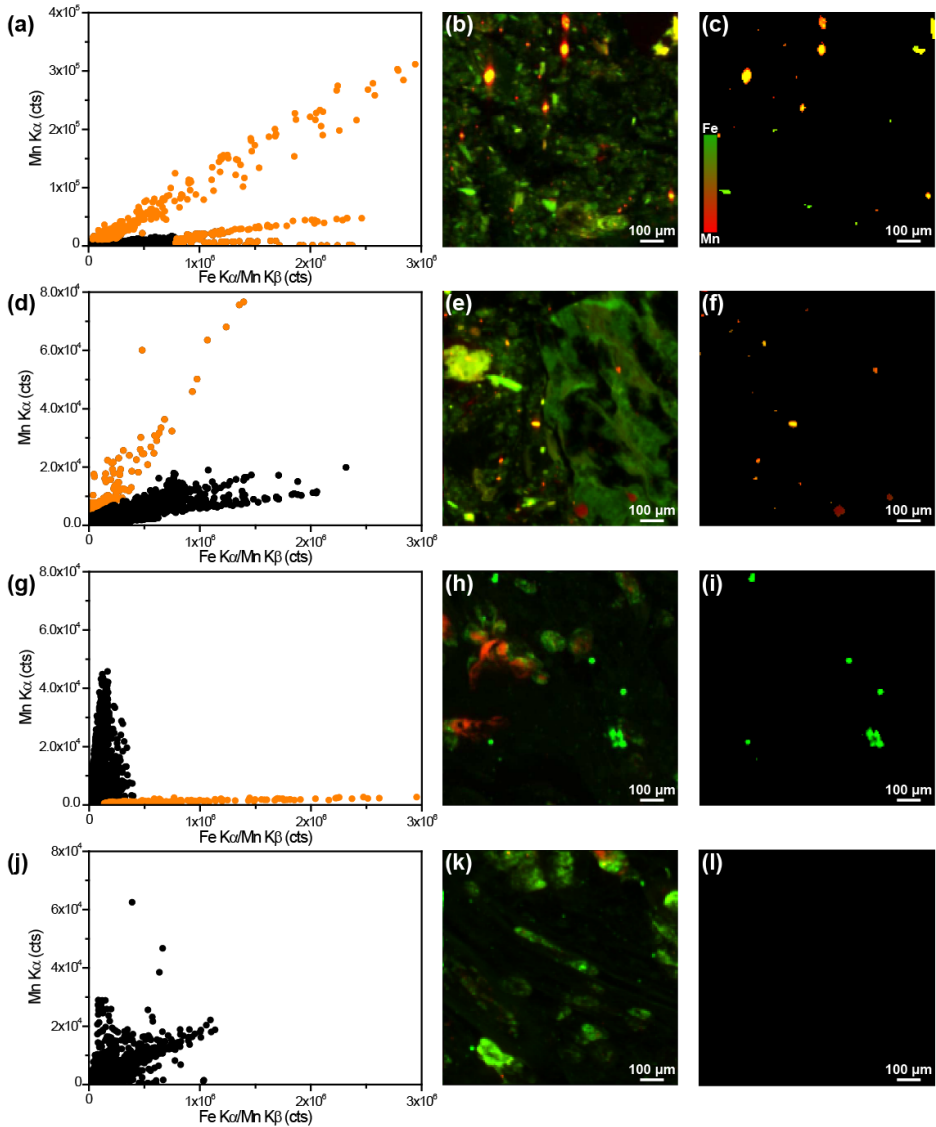


**Figure B.6.** Correlation plots of relative Mn and Fe fluorescence intensities and bicolor (RG)  $\mu$ -XRF elemental maps illustrating the distribution of Mn and Fe in (a-c) region 1 and (d-f) region 2 of thin section B3II-31, as well as (g-i) region 1 and (j-l) region 2 of thin section B1II-237 (Figure 3.3). The right-hand column displays  $\mu$ -XRF maps generated from the orange points in the correlation plots. The color code in (c) is valid for all panels. Note that the scales of the x- and y-axis vary in the correlation plots.

## B.7. Tricolor elemental maps

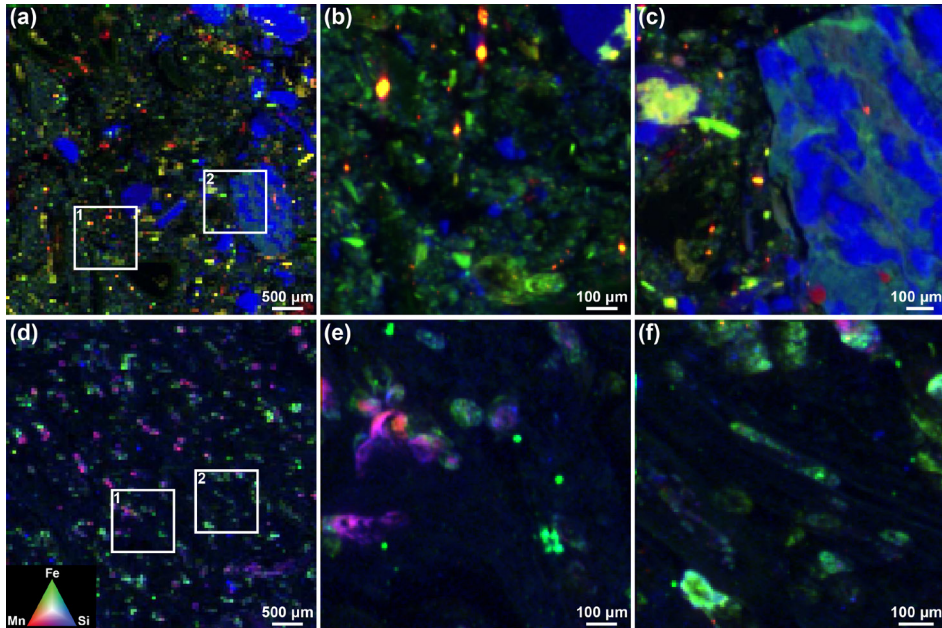


**Figure B.7.** Tricolor (RGB)  $\mu$ -XRF elemental maps of Mn, Fe, and Si in (a-c) thin section B3II-31 and (d-f) thin section B1II-237. (a, d) Overview maps indicating the locations of regions 1 and 2 mapped in each thin section. Fine maps of regions 1 are shown in (b, e) and those of regions 2 in (c, f). The color code in (d) is valid for all panels.

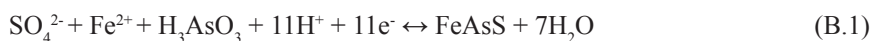
## B.8. Thermodynamic data

**Table B.6.** Thermodynamic data used to calculate the change in Gibbs free energy of reaction ( $\Delta G^0$ ).

Species/Reaction	Mineral name	$\Delta G_{298}^0$ (kJ mol <sup>-1</sup> )	log <i>K</i>	Source
H <sub>2</sub> O		-237.18		[Stumm and Morgan, 1996]
H <sup>+</sup>		0		[Stumm and Morgan, 1996]
H <sub>2</sub> S		-27.87		[Stumm and Morgan, 1996]
SO <sub>4</sub> <sup>2-</sup>		-744.5		[Shock and Helgeson, 1988]
H <sub>3</sub> AsO <sub>3</sub>		-639.7		[Vink, 1996]
Fe <sup>2+</sup>		-78.87		[Stumm and Morgan, 1996]
amorphous Fe(OH) <sub>3</sub>	ferrihydrite	-713.0		[Lindsay, 1979]
FeS	mackinawite	-93.30		[Berner, 1967]
FeS	troilite	-97.91		[Lindsay, 1979]
FeS <sub>2</sub>	pyrite	-160.2		[Robie et al., 1978]
Fe <sub>3</sub> S <sub>4</sub>	greigite	-290.4		[Berner, 1967]
AsS	realgar	-33.18		[Pokrovski et al., 1996]
FeAsS	arsenopyrite	-141.6		[Pokrovski et al., 2002]
1/4CO <sub>2</sub> (g) + 11/12H <sup>+</sup> + e <sup>-</sup> = 1/12lactate + 1/4H <sub>2</sub> O			0.68	[Morel and Hering, 1993]

## B.9. $E_h$ -pH diagrams

Pourbaix ( $E_h$ -pH) diagrams were calculated to illustrate the relative stabilities of realgar, orpiment, and arsenopyrite as a function of pH, redox potential, and varying abundances of Fe and S. The diagrams were calculated with the Act2 program of the Geochemist's Workbench package v.8.0 (Aqueous Solutions LLC, USA). Arsenopyrite formation was implemented in the thermo\_wateq4f database using Gibbs free energies of formation tabulated in Table B.6 and a  $\Delta G^0$  value of  $-141.6 \text{ kJ mol}^{-1}$  for arsenopyrite [Pokrovski et al., 2002]:



$$\Delta G_0 = -338.76 \text{ kJ mol}^{-1}$$

Except for the  $\text{AsS(OH)(HS)}^-$  and  $\text{As}_3\text{S}_4(\text{HS})_2^-$  species already present in the data base, additional thioarsenic species were disregarded in these calculations. Figure B.8 shows  $E_h$ -pH diagrams calculated for a fixed log activity of -6 for As and different log activity ratios of Fe and S. The calculations indicate that under the 'bulk' redox conditions encountered in the peat ( $E_h = -11$  to  $364 \text{ mV}$ ) the solutions would be undersaturated with respect to all three As sulfide minerals. Arsenopyrite is predicted to be the most stable As sulfide at the slightly acidic pH of the peat ( $\text{pH } 5.7 \pm 0.5$ ). Based on the  $E_h$ -pH diagrams, an authigenic arsenopyrite formation would be favored in microenvironments with redox potentials of approximately less than  $-100 \text{ mV}$ . It must be stressed that if a  $\Delta G^0$  value of  $-50.0 \text{ kJ mol}^{-1}$  is used for arsenopyrite [Gallegos et al., 2008], this phase is predicted to be unstable under any conditions used to calculate the speciation diagrams. Thus, the new  $\Delta G^0$  value of  $-141.6 \text{ kJ mol}^{-1}$  for arsenopyrite [Pokrovski et al., 2002] is in better agreement with our field observations. A similar conclusion was reached by Craw et al. [2003] based on field observations focusing on natural and mined arsenopyrite occurrences in Otago Schist, New Zealand.

In addition, our calculations show that realgar formation is generally more favorable under strongly reducing conditions preventing the formation of arsenopyrite (low Fe) and dissolved thioarsenic species (low Fe and S) (Figure B.9).



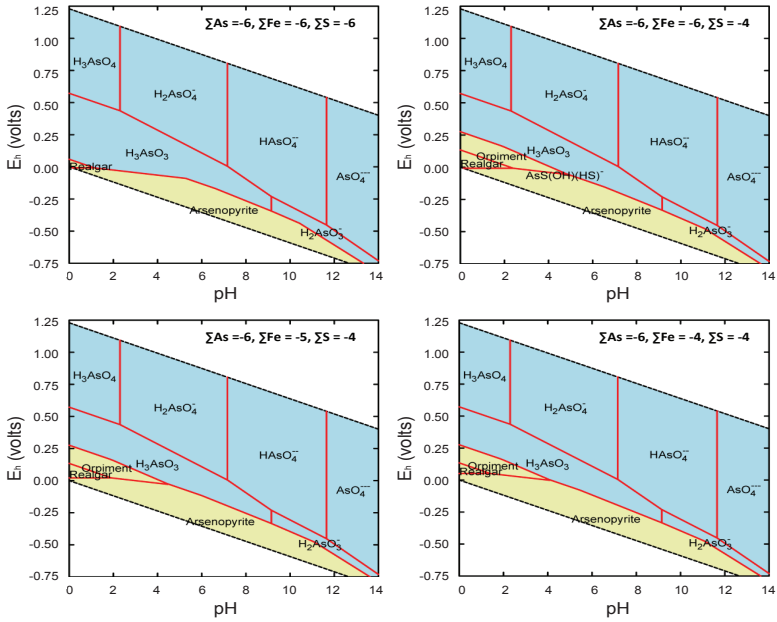


**Figure B.8.** Pourbaix diagrams (25 °C, 1 bar) calculated for a fixed log activity of -6 for As and different log activity ratios of Fe and S in the As-Fe-O-H-S system.

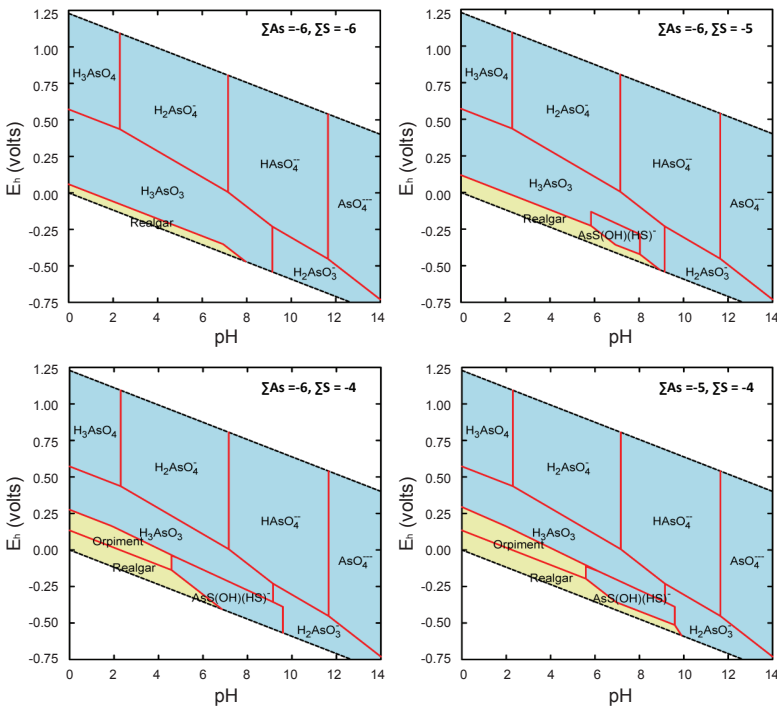


**Figure B.9.** Pourbaix diagrams (25 °C, 1 bar) calculated for different log activities of As (-6, -5) and S (-6 to -4) in the As-O-H-S system.

## B.10. Arsenic concentrations in plants

Major plants species of the *Gola di Lago* peatland were collected in September 2009 within a radius of 3 m around the sampling points B1, B3, and B5. Approximately 10 plants of each species were harvested, immediately shock frozen in liquid N<sub>2</sub>, transported on dry-ice in the laboratory, and stored at -22 °C before further processing. An overview of all collected plant species and their abundance according to the Braun-Blanquet scale [1932] is given in Langner et al. [2012].

The frozen samples were washed several times with tap water, rinsed with deionized water, and freeze-dried for 72 h. The individual plants of each species were then combined into one sample and separated into root, stem/leaf, and blossom, which were subsequently homogenized in a ZrO<sub>2</sub> ball mill (Retsch, MM 200) for 4 min at 24 s<sup>-1</sup>. Aliquots of the ground plant material (0.2 g) were then added to 1.5 mL ultrapure water (Milli-Q, Millipore, ≥18.2 MΩ cm), 2.5 mL HNO<sub>3</sub> (67% w/w), and 1.5 mL H<sub>2</sub>O<sub>2</sub> (30% w/w) and digested in triplicate using a MLS microwave (turboWave, MLS GmbH). The samples were pre-reacted for 1 h and digested for 25 min at a maximal pressure and temperature of 120 bar and 250 °C, respectively. The efficiency of the digestion procedure was validated with various reference materials (olive leaves (BCR-062), apple leaves (SRM NIST 1515) as well as bush branches and leaves (NIM-GBW07603, NCS DC73349). The digests were diluted to 10 mL with ultrapure water and analyzed for As by inductively coupled plasma – mass spectrometry (Agilent, 7500 Series) in addition to other elements needed for quality control. The average and blank corrected As concentrations, calculated on a dry weight basis, are reported in Table B.7.

**Table B.7.** Arsenic concentrations in plants collected at sampling sites B1, B3, and B5.

Common name	Species	Family	Part of the plant	As (mg kg <sup>-1</sup> )
<b>B3</b>				
Purple moorgrass	<i>Molinia caerulea</i>	Poaceae	blossom	2.82
			leaf/stem	0.41
			root	1.88
Smooth black sedge	<i>Carex nigra</i>	Cyperaceae	leaf/stem	10.1
			root	78.5
Sphagnum	<i>Sphagnum</i> sp.	Sphagnaceae	leaf/stem	1.67
Jointleaf rush	<i>Juncus articulatus</i>	Juncaceae	blossom	11.9
			leaf/stem	5.93
			root	not determined
<b>B5</b>				
Purple moorgrass	<i>Molinia caerulea</i>	Poaceae	blossom	0.38
			leaf/stem	0.14
			root	26.7
Smooth black sedge	<i>Carex nigra</i>	Cyperaceae	leaf/stem	2.12
			root	0.17
Water whorlgrass	<i>Catabrosa aquatica</i>	Poaceae	leaf/stem	0.19
			root	0.86
Jointleaf rush	<i>Juncus articulatus</i>	Juncaceae	blossom	0.37
			leaf/stem	0.13
			root	1.62
<b>B1</b>				
Purple moorgrass	<i>Molinia caerulea</i>	Poaceae	blossom	0.55
			leaf/stem	0.19
			root	7.34
Tufted bulrush	<i>Trichophorum cespitosum</i>	Cyperaceae	leaf	0.32
			root	7.85
<b>Mean</b>				<b>7.05</b>
<b>Standard deviation</b>				<b>16.7</b>

## References

- Berner, R. A. (1967) Thermodynamic stability of sedimentary iron sulfides. *Am. J. Sci.* 265, 773-785.
- Bostick, B. C., Fendorf, S. (2003) Arsenite sorption on troilite (FeS) and pyrite (FeS<sub>2</sub>). *Geochim. Cosmochim. Acta* 67, 909-921.
- Braun-Blanquet, J. (1932) *Plant sociology: The study of plant communities*. McGraw-Hill: New York.
- Craw, D., Falconer, D., Youngson, J. H. (2003) Environmental arsenopyrite stability and dissolution: Theory, experiment, and field observations. *Chem. Geol.* 199, 71-82.
- Gallegos, T. J., Han, Y.-S., Hayes, K. F. (2008) Model predictions of realgar precipitation by reaction of As(III) with synthetic mackinawite under anoxic conditions. *Environ. Sci. Technol.* 42, 9338-9343.
- Hoffmann, M., Mikutta, C., Kretzschmar, R. (2012) Bisulfide reaction with natural organic matter enhances arsenite sorption: Insights from X-ray absorption spectroscopy. *Environ. Sci. Technol.* 46, 11788-11797.
- Langner, P., Mikutta, C., Kretzschmar, R. (2012) Arsenic sequestration by organic sulphur in peat. *Nat. Geosci.* 5, 66-73.
- Lindsay, W. L. (1979) *Chemical equilibria in soils*. John Wiley & Sons, Inc.: New York.
- Manceau, A., Nagy, K. L. (2012) Quantitative analysis of sulfur functional groups in natural organic matter by XANES spectroscopy. *Geochim. Cosmochim. Acta* 99, 206-223.
- Morel, F. M. M., Hering, J. G. (1993) *Principles and applications of aquatic chemistry*. John Wiley & Sons, Inc.: New York.
- Pokrovski, G., Gout, R., Schott, J., Zotov, A., Harrichoury, J. C. (1996) Thermodynamic properties and stoichiometry of As(III) hydroxide complexes at hydrothermal conditions. *Geochim. Cosmochim. Acta* 60, 737-749.
- Pokrovski, G. S., Kara, S., Roux, J. (2002) Stability and solubility of arsenopyrite, FeAsS, in crustal fluids. *Geochim. Cosmochim. Acta* 66, 2361-2378.
- Ravel, B., Newville, M. (2005a) Athena and Artemis: Interactive graphical data analysis using Ifeffit. *Phys. Scr. T115*, 1007-1010.
- Ravel, B., Newville, M. (2005b) Athena, Artemis, Hephaestus: Data analysis for X-ray absorption spectroscopy using Ifeffit. *J. Synchrot. Radiat.* 12, 537-541.
- Ressler, T. (1998) WinXAS: A program for X-ray absorption spectroscopy data analysis under MS-Windows. *J. Synchrot. Radiat.* 5, 118-122.

- 
- Robie, R. A., Hemingway, B. S., Fisher, J. R. (1978) *Thermodynamic properties of minerals and related substances at 298.15 K and 1 bar (105 Pascal) pressure and at higher temperatures*. U.S. Geological Survey Bulletin 1452: Washington.
- Shock, E. L., Helgeson, H. C. (1988) Calculation of the thermodynamic and transport properties of aqueous species at high pressures and temperatures: Correlation algorithms for ionic species and equation of state predictions to 5 kb and 1000°C. *Geochim. Cosmochim. Acta* 52, 2009-2036.
- Stumm, W., Morgan, J. J. (1996) *Aquatic chemistry. Chemical equilibria and rates in natural waters*. 3rd ed. John Wiley & Sons, Inc.: New York.
- Vairavamurthy, A. (1998) Using X-ray absorption to probe sulfur oxidation states in complex molecules. *Spectrochim. Acta, Part A* 54, 2009-2017.
- Vink, B. W. (1996) Stability relations of antimony and arsenic compounds in the light of revised and extended Eh-pH diagrams. *Chem. Geol.* 130, 21-30.
- Xia, K., Weesner, F., Bleam, W. F., Bloom, P. R., Skyllberg, U. L., Helmke, P. A. (1998) XANES studies of oxidation states of sulfur in aquatic and soil humic substances. *Soil Sci. Soc. Am. J.* 62, 1240-1246.



## **C. Supporting Information to Chapter 4**

**'Oxidation of organosulfur-coordinated arsenic and  
realgar in peat: Implications for the fate of arsenic'**

## C.1. Synchrotron measurements and data analysis

### C.1.1. Sample preparation

Every 30 days, a peat sample from each sterile and nonsterile B3II and B1II flask was prepared for bulk As, Fe, and S *K*-edge XAS analyses. The preparation included freeze-drying, homogenization, and sieving to a particle size <500  $\mu\text{m}$  in a glovebox. For bulk As and Fe *K*-edge XAS analyses, the sieved material was subsequently filled into Plexiglas sample holders, which were sealed with Kapton tape. Peat samples used for S *K*-edge XAS analyses were diluted to a S concentration of 1,800 mg S  $\text{kg}^{-1}$  using BN in order to reduce overabsorption effects [Prietz et al., 2011] and pressed into 1.3 cm pellets.

### C.1.2. Bulk X-ray absorption spectroscopy – arsenic and iron

Arsenic *K*-edge (11,867 eV) and Fe *K*-edge (7,112 eV) X-ray absorption near-edge structure (XANES) and extended X-ray absorption fine structure (EXAFS) spectra were collected over an energy range of 11,667-12,610 eV (As) and 6,880-7,723 eV (Fe). The Si(220) double-crystal monochromators ( $\phi = 90^\circ$ ) were detuned to 60-70% of their maximal intensity and calibrated relative to the  $L_3$ -edge energy of elemental Au (11,919 eV) for the As measurements or to the *K*-edge energy of elemental Fe (7,112 eV) for the Fe measurements. All samples were placed in a He cryostat ( $\sim 7\text{-}8\text{ K}$ ) and measured in fluorescence mode using solid-state Ge detectors. Four to eleven scans were averaged per sample. Data analyses were performed in Athena [Ravel and Newville, 2005a, b]. Normalized spectra were obtained by fitting a linear function to the pre-edge region ( $E_0 - E = 30\text{-}140\text{ eV}$ ) and a quadratic polynomial to the post-edge region ( $E - E_0 = 150\text{-}650\text{ eV}$  for As and  $150\text{-}550\text{ eV}$  for Fe). The maximum of the first derivative was used to set the edge energy,  $E_0$ . Linear combination fitting (LCF) was carried out on  $k^3$ -weighted EXAFS spectra over a  $k$ -range of  $3\text{-}13\text{ \AA}^{-1}$  (As) and  $3\text{-}10.5\text{ \AA}^{-1}$  (Fe) utilizing the same  $E_0$  for all samples (11,868 eV for As and 7,132 eV for Fe). Arsenic and Fe reference spectra used in the EXAFS data analyses were selected based on principal component analyses and target-transform testing (PCA-TT) [Langner et al., 2012]. A list



of all references used in the LCF analysis can be found in the Supporting Information of Langner et al. [2012] together with Figures displaying their  $k^2$ -weighted As and Fe  $K$ -edge EXAFS spectra.

### **C.1.3. Bulk X-ray absorption spectroscopy – sulfur**

Bulk S  $K$ -edge (2,472 eV) XANES spectra were recorded at SSRL beamline 4-3 using a Si(111) double-crystal monochromator calibrated relative to the white-line energy of a  $\text{Na}_2\text{S}_2\text{O}_3$  standard (2,472.02 eV). Data collection was performed in fluorescence mode at ~25 K using a liquid He cryostream and a Lytle detector. Six to fifteen scans were averaged per sample. Normalization of the spectra was performed in Athena by fitting a linear function to the pre-edge region ( $E_0 - E = 15\text{-}70$  eV) and setting the unit edge set ( $\Delta\mu x = 1.0$ ) to 2,490 eV. Gaussian curve fitting was carried out on the normalized spectra in the energy range 2,465-2,490 eV using WinXAS 3.2 [Ressler, 1998] following the approach of Manceau and Nagy [2012]. The positions of the Gaussians were chosen based on the white-line energy positions of S reference compounds [Vairavamurthy, 1998; Hoffmann et al., 2012; Manceau and Nagy, 2012]. In the fits, the positions and widths of all Gaussians and two arctangent functions (2,475.4 and 2,482 eV) were fixed (Table C.1), whereas the peak heights were allowed to vary. The areas of the Gaussians were corrected for the specific oxidation state-dependent absorption cross-section based on the generic curve published in Manceau and Nagy [2012]. The contribution of each S species to the total S pool was calculated by dividing its peak area by the summed areas of all Gaussians.

## C.2. Bulk arsenic *K*-edge and iron *K*-edge XANES spectra

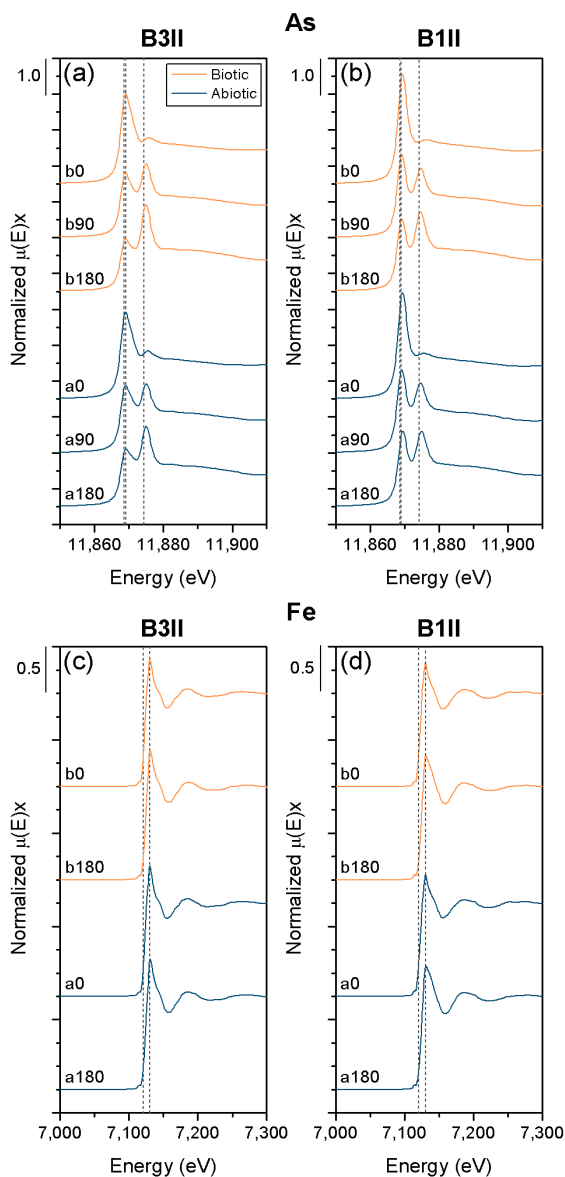


**Figure C.1.** Normalized (a, b) As and (c, d) Fe *K*-edge XANES spectra of the B3II and B1II peat batches. The legend in panel (a) is valid for all panels. Vertical lines in (a) and (b) indicate white-line positions of As(II), As(III), and As(V) reference compounds (from left to right). In (c) and (d) the vertical lines correspond to white-line positions of Fe(II) and Fe(III) reference compounds (from left to right).

## C.3. Phosphate extraction results

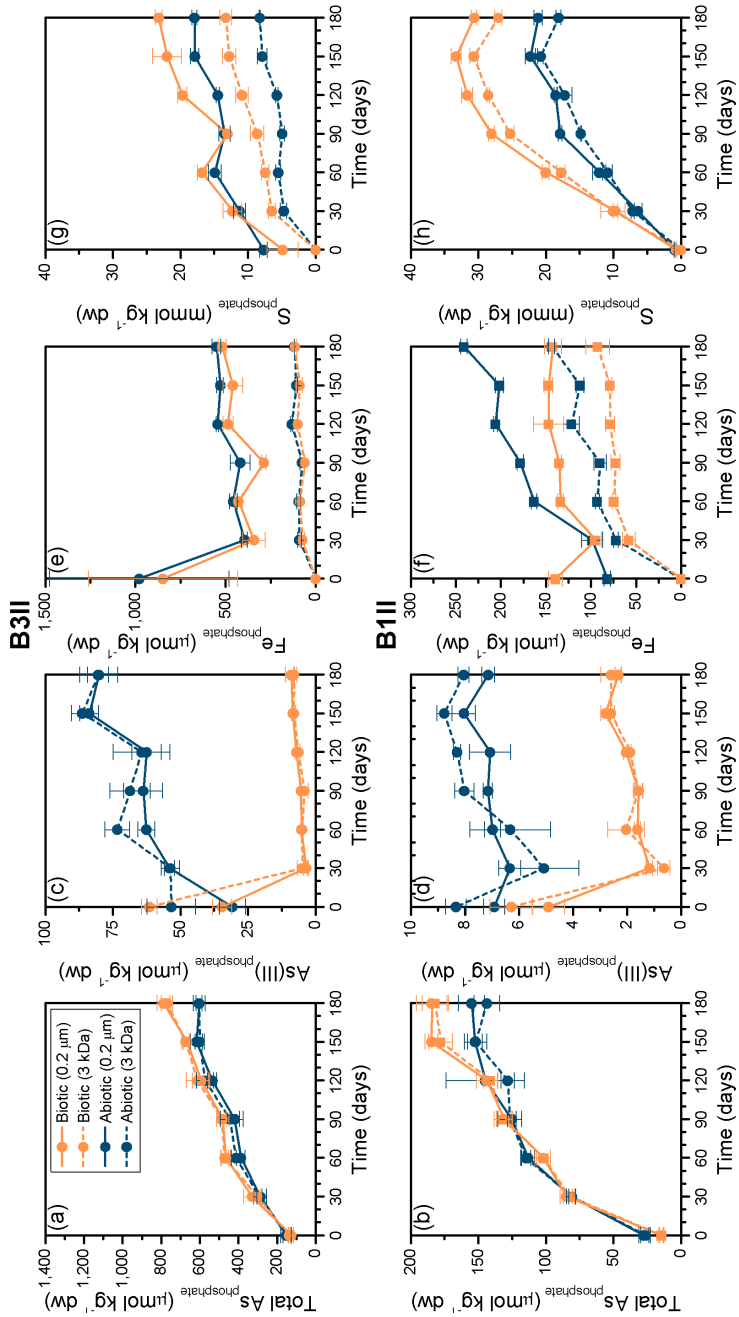


**Figure C.2.** Concentrations of (a, b) total As, (c, d) As(III), (e, f) Fe, and (g, h) S in the 0.2- $\mu\text{m}$  (solid line) and 3-kDa (dashed line) filtered phosphate extracts (1 M  $\text{NaH}_2\text{PO}_4$ , pH 5) of the B3II and B1II peat batches. Error bars denote standard deviations ( $n = 3$ ). The legend in (a) is valid for all panels.

### C.4. Bulk sulfur *K*-edge XANES spectra and Gaussian curve fitting parameters

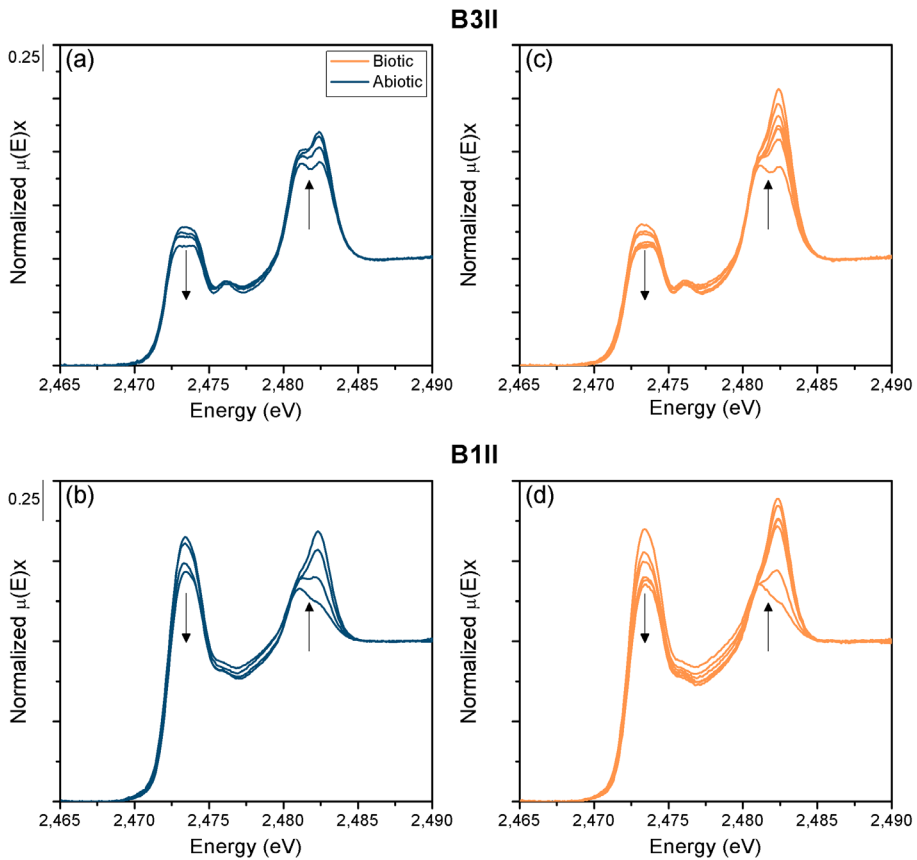


**Figure C.3.** Normalized S *K*-edge XANES spectra of the B3II and B1II peat batches. The arrows emphasize the decrease in reduced S and the concomitant increase in oxidized S during 180 days of oxidation. The legend in panel (a) is valid for all panels.

**Table C.1.** Peak parameters of deconvoluted S K-edge XANES spectra shown in Figure 4.4 and atomic fractions of S functionalities after correction for the oxidation-state dependent cross section of S.

Sample ID <sup>a</sup>	Depth (cm)	White-line energy (eV)	Assigned S functionality	Peak height	Fwhm (eV) <sup>b</sup>	Peak correction factor <sup>c</sup>	Uncorrected peak area	Corrected peak area	Corrected fraction (%)	NSSR (%) <sup>d</sup>
B3IIb0	0-38	2,471.10	inorganic sulfide	0.07	1.75	0.41	0.12	0.30	7.0	1.09
		2,472.79	exocyclic S	1.07	1.75	1.03	2.00	1.94	44.8	
		2,474.23	heterocyclic S	0.94	1.75	1.56	1.75	1.12	25.9	
		2,476.15	sulfoxide	0.09	1.75	2.27	0.17	0.08	1.8	
		2,479.06	sulfone	0.15	1.85	3.34	0.29	0.09	2.0	
		2,481.00	sulfonate	1.00	1.85	4.06	1.96	0.48	11.2	
		2,482.70	sulfate	0.75	1.85	4.68	1.47	0.31	7.3	
		2,472.05	inorganic sulfide	0.17	1.75	0.76	0.31	0.41	10.1	0.65
		2,473.13	exocyclic S	1.36	1.75	1.16	2.53	2.19	53.8	
		2,474.44	heterocyclic S	0.94	1.75	1.76	1.76	1.07	26.4	
B3IIIb0	200-250	2,476.15	sulfoxide	0.03	1.75	2.27	0.06	0.03	0.6	
		2,479.06	sulfone	0.12	1.85	3.34	0.23	0.07	1.7	
		2,480.98	sulfonate	0.45	1.85	4.05	0.88	0.22	5.4	
		2,482.65	sulfate	0.20	1.85	4.66	0.40	0.08	2.1	

<sup>a</sup>The sample ID indicates core label (B3II/B3III), treatment (b = biotic), and sampling time (days). <sup>b</sup>Full width at half maximum. <sup>c</sup>Based on the 'generic' equation of Manceau and Nagy [2012]. <sup>d</sup>Normalized sum of squared residuals (NSSR (%)) =  $100 \times \sum_i (\text{data} - \text{fit})^2 / \sum_i \text{data}^2$ .

## C.5. Bulk arsenic, iron, and sulfur speciation results

**Table C.2.** Temporal As speciation changes in the peat samples based on linear combination fitting of  $k^3$ -weighted As  $K$ -edge EXAFS spectra.

Sample ID <sup>a</sup>	% of total As (normalized to a sum of 100%) <sup>b</sup>			Fitted sum	NSSR
	As-NOM	Realgar	As(V)-Fh	(%) <sup>c</sup>	(%) <sup>d</sup>
B3IIa0	-	91	9	110	12.2
B3IIa90	-	73	27	124	11.2
B3IIa180	-	61	39	121	7.5
B3IIb0	-	100	-	120	11.5
B3IIb90	-	69	31	128	10.1
B3IIb180	-	56	44	122	5.3
B1IIa0	100	-	-	110	2.2
B1IIa90	79	-	21	107	3.1
B1IIa180	72	-	28	106	2.2
B1IIb0	100	-	-	113	2.4
B1IIb90	77	-	23	108	2.2
B1IIb180	67	-	33	106	2.2

<sup>a</sup>The sample ID indicates core label (B3II/B1II), treatment (a = abiotic, b = biotic), and sampling time (days).

<sup>b</sup>The main As species were fitted with the following references: As(III)-NOM = tris(phenylthio)arsine and a mixture of a di- and triglutathione complex (As(III)(GS)<sub>2,6</sub>(OH)<sub>0,6</sub>) [Langner et al., 2012]. <sup>c</sup>Fitted sum of all references before normalization. <sup>d</sup>Normalized sum of squared residuals (NSSR (%)) =  $100 \times \sum_i (\text{data}_i - \text{fit}_i)^2 / \sum_i \text{data}_i^2$ .

**Table C.3.** Temporal Fe speciation changes in the peat samples based on linear combination fitting of  $k^3$ -weighted Fe  $K$ -edge EXAFS spectra.

Sample ID <sup>a</sup>	% of total Fe (normalized to a sum of 100%) <sup>b</sup>				Fitted sum	NSSR (%) <sup>d</sup>
	Pyrite	Fe(III)-NOM	Fe(III)-(hydr)oxides	Phyllosilicates	(%) <sup>c</sup>	
B3IIa0	-	28	18	54	95	4.9
B3IIa180	-	30	20	50	99	3.6
B3IIb0	-	30	10	60	87	5.7
B3IIb180	-	33	18	49	87	4.8
B1IIa0	26	47	-	27	95	2.4
B1IIa180	-	56	15	29	102	2.5
B1IIb0	26	52	-	22	93	8.6
B1IIb180	-	44	21	35	98	5.3

<sup>a</sup>The sample ID indicates core label (B3II/B1II), treatment (a = abiotic, b = biotic), and sampling time (days). <sup>b</sup>The main Fe species were fitted with the following references: Fe(III)-NOM = Fe(III)-citrate and Fe(III)-oxalate, Fe(III)-(hydr)oxides = ferrihydrite and lepidocrocite, phyllosilicates = muscovite, chlorite, and vermiculite. <sup>c</sup>Fitted sum of all references before normalization. <sup>d</sup>Normalized sum of squared residuals (NSSR (%)) =  $100 \times \sum_i (\text{data}_i - \text{fit}_i)^2 / \sum_i \text{data}_i^2$ .

**Table C.4.** Temporal S speciation changes in the peat samples obtained by Gaussian curve fitting.

Sample ID <sup>a</sup>	Reduced S (%) <sup>b</sup>		Intermediate oxidized S (%) <sup>c</sup>		Oxidized S (%) <sup>d</sup>		NSSR (%) <sup>e</sup>
	Inorganic Sulfide	Exocyclic/ Heterocyclic S	Sulfoxide	Sulfite/Sulfone	Sulfonate	Sulfate	
B3IIa0	5	71	2	2	12	8	1.20
B3IIa30	3	71	3	2	12	9	1.24
B3IIa90	3	69	3	2	13	10	1.34
B3IIa180	1	68	3	3	14	11	1.38
B3IIb0	7	71	2	2	11	7	1.09
B3IIb30	3	70	3	2	12	10	1.24
B3IIb60	3	69	3	2	12	11	1.29
B3IIb90	3	66	3	2	12	14	1.44
B3IIb120	3	65	3	2	12	15	1.48
B3IIb150	2	64	3	2	13	16	1.62
B3IIb180	2	63	3	2	13	17	1.60
B1IIa0	10	80	1	2	5	2	0.87
B1IIa30	9	79	1	2	5	4	1.02
B1IIa90	8	76	1	2	6	7	1.07
B1IIa180	6	76	1	2	6	9	1.12
B1IIb0	10	80	1	2	5	2	0.94
B1IIb30	9	79	1	2	5	4	0.97
B1IIb60	7	76	1	2	5	9	1.18
B1IIb90	6	75	1	2	6	10	1.08
B1IIb120	5	74	1	2	6	12	1.09
B1IIb150	5	74	1	2	6	12	1.20
B1IIb180	5	75	2	2	6	10	1.02

<sup>a</sup>The sample ID indicates core label (B3II/B1II), treatment (a = abiotic, b = biotic), and sampling time (days).

<sup>b</sup>Energy range  $\leq 2,475$  eV and S oxidation states -II to I. <sup>c</sup>Energy range 2,476-2,480 eV and S oxidation states II to IV. <sup>d</sup>Energy range  $\geq 2,481$  eV and S oxidation states V to VI. <sup>e</sup>Normalized sum of squared residuals (NSSR (%) =  $100 \times \sum_i (\text{data}_i - \text{fit}_i)^2 / \sum_i \text{data}_i^2$ ).

## C.6. Oxidation kinetics of reduced sulfur

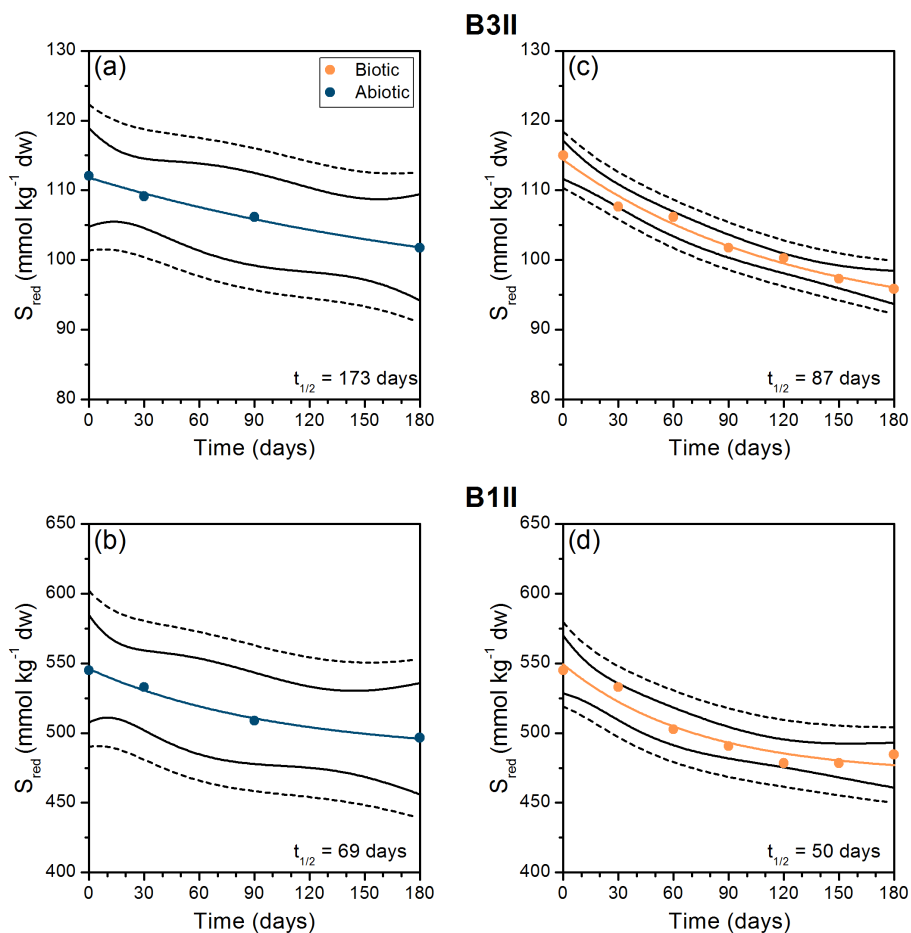


**Figure C.4.** Fits of the monoexponential model (Equation 4.1) to concentration data of reduced S of the B3II and B1II peat batches. Solid and dashed lines mark, respectively, the 95% confidence and 95% prediction intervals. Results of the fits are listed in Table C.5. The legend in panel (a) is valid for all panels.



**Table C.5.** Results of the fits shown in Figure C.4. Values in parentheses indicated standard errors.

Sample ID <sup>a</sup>	$S_{\text{red}}(t) = S_{\text{red, const}} + S_{\text{red, ox}} \exp(-kt)^b$			$t_{1/2}^c$ (day)	$R^2$	SE <sup>d</sup>
	$S_{\text{red, const}}$	$S_{\text{red, ox}}$	$k$			
	(mmol kg <sup>-1</sup> dw)	(mmol kg <sup>-1</sup> dw)	(day <sup>-1</sup> )			
B3IIb	90.6 (4.2)	23.8 (3.9)	0.008 (0.003)	87	0.98	1.07
B3IIa	93.4 (9.4)	18.5 (9.2)	0.004 (0.003)	173	0.99	0.61
B1IIb	470.6 (12.3)	78.8 (12.3)	0.014 (0.006)	50	0.94	7.86
B1IIa	485.6 (10.7)	60.5 (10.0)	0.010 (0.004)	69	0.99	3.21

<sup>a</sup>The sample ID indicates core label (B3II/B1II) and treatment (a = abiotic, b = biotic). <sup>b</sup> $S_{\text{red, const}}$  = oxidation-resistant reduced S,  $S_{\text{red, ox}}$  = oxidizable reduced S,  $t$  = time, and  $k$  = rate constant. <sup>c</sup> $t_{1/2} = \ln(2)/k$ . <sup>d</sup>Standard error of estimate.

## C.7. Dissolved organic carbon in water and phosphate extracts

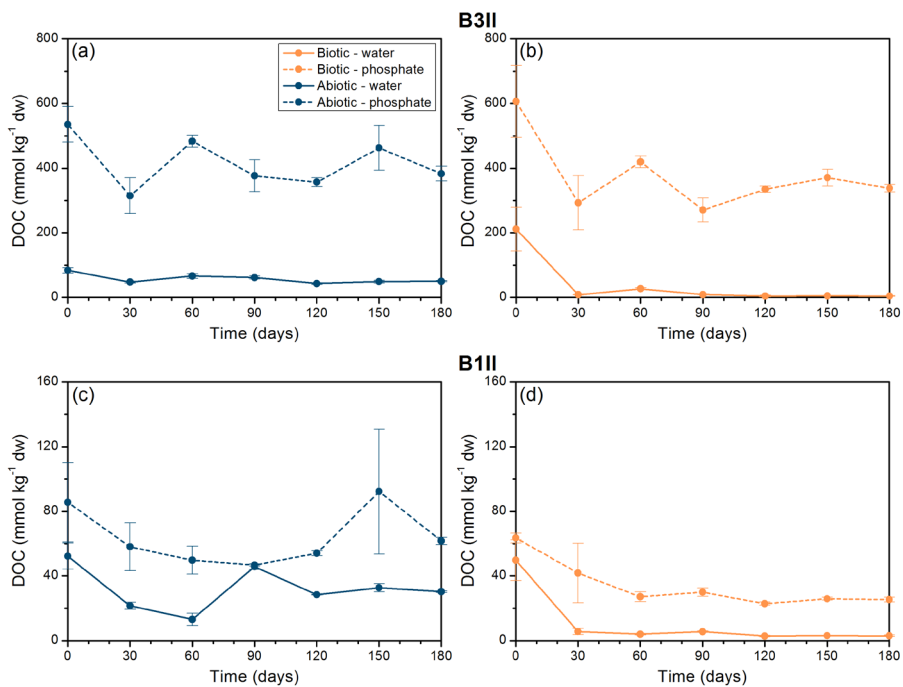


**Figure C.5.** DOC concentrations in the 0.2- $\mu$ m filtered water (solid lines) and phosphate (1 M NaH<sub>2</sub>PO<sub>4</sub>, pH 5) (dashed lines) extracts of the B3II and B1II peat batches. Error bars denote standard deviations ( $n = 3$ ). The legend in panel (a) is valid for all panels.

## References

- Hoffmann, M., Mikutta, C., Kretzschmar, R. (2012) Bisulfide reaction with natural organic matter enhances arsenite sorption: Insights from X-ray absorption spectroscopy. *Environ. Sci. Technol.* 46, 11788–11797.
- Langner, P., Mikutta, C., Kretzschmar, R. (2012) Arsenic sequestration by organic sulphur in peat. *Nat. Geosci.* 5, 66-73.
- Manceau, A., Nagy, K. L. (2012) Quantitative analysis of sulfur functional groups in natural organic matter by XANES spectroscopy. *Geochim. Cosmochim. Acta* 99, 206-223.
- Prietzl, J., Botzaki, A., Tyufekchieva, N., Brettholle, M., Thieme, J., Klysubun, W. (2011) Sulfur speciation in soil by S K-edge XANES spectroscopy: Comparison of spectral deconvolution and linear combination fitting. *Environ. Sci. Technol.* 45, 2878-2886.
- Ravel, B., Newville, M. (2005a) Athena and Artemis: Interactive graphical data analysis using Ifeffit. *Phys. Scr. T115*, 1007-1010.
- Ravel, B., Newville, M. (2005b) Athena, Artemis, Hephaestus: Data analysis for X-ray absorption spectroscopy using Ifeffit. *J. Synchrot. Radiat.* 12, 537-541.
- Ressler, T. (1998) WinXAS: A program for X-ray absorption spectroscopy data analysis under MS-Windows. *J. Synchrot. Radiat.* 5, 118-122.
- Vairavamurthy, A. (1998) Using X-ray absorption to probe sulfur oxidation states in complex molecules. *Spectrochim. Acta, Part A* 54, 2009-2017.





## ACKNOWLEDGEMENTS

My warmest gratitude is reserved for all the people that joined and supported me during my PhD time.

I am particularly indebted to Ruben Kretschmar for giving me the opportunity to do this PhD in his research group, for his constructive advice and supervision as well as his generosity and understanding that allowed me to coordinate and balance work and family.

I want to thank Christian Mikutta for being a great supervisor. I am grateful for his continuous support through all the years of my PhD, for his ideas and helpful feedback, and all the nice chats enabling me to see things sometimes differently.

Special thanks to James J. Rothwell for agreeing to be the external co-examiner on my PhD committee.

No data, no thesis! In this course, I greatly appreciated the time and effort of John R. Bargar, Matthieu Chorro, Ryan C. Davis, Sirine Fakra, Matthew J. Latimer, Matthew A. Marcus, Erik J. Nelson, and Edmund Welter in preparing and optimizing the respective beamlines at SSRL, ALS, ESRF and Hasylab for data collection, in trouble shooting and for some slight detours away from the user's perspective into the synchrotron world. In this course, I also want to thank 'The Rascals' for writing the song 'It's a beautiful morning'. I heard this wake-up song approximately 130 times at the synchrotron and no matter what time it was in the night it always put me a smile on my face.

For giving me an insight in the dark world of microorganisms, and lots of good practical advice for my experimental setup, I want to thank Robert Brankatschk, Fabio Ugolini, Frederik Hammes, Alessandro Franchini and Marco Meola.

Charlotte Wüstholtz and Kurt Barmettler are acknowledged for their help regarding administrative and laboratory issues. Besides cakes and chats, as well as snow and fun, I thank all former and present soil chemistry group members for creating a constructive working atmosphere. I am particularly indebted to Katrin Ehlert, Elke Suess, Laurel Thomas-Arrigo and Jessica Dittmar for being a bit more than just colleagues as well as to Martin Hoffmann for running the chemical helpdesk.

I am grateful for the financial support of ETH Zurich (research grant 2708-2) and the city council of Dietikon. The latter for enabling me to work on my PhD project while Yannek could stay at the day nursery having a wonderful time there. I thank my family and friends for their support, patience and encouragement through all the years as well as for all the cheerful moments. The last words are particularly dedicated to Richard, Yannek, and Maja my loves; I am thankful for you every single day.



## CURRICULUM VITAE

### PERSONAL DETAILS

Name Peggy Hofmann, born Langner  
Date of birth September 4, 1984  
Nationality German

### EDUCATION

2009-2013 PhD thesis, ETH Zurich, Switzerland, supervised by Prof. R. Kretzschmar and Dr. C. Mikutta

2003-2009 Study of Geology/Paleontology, TU Bergakademie Freiberg, Germany  
Thesis: *'Investigations of factors controlling mercury release from marine influenced sediments (Grizzly Bay and Liberty Island, CA, USA)'*  
Mapping: *'GIS-Atlas Mercury in Northern California'*  
Supervised by Prof. B. J. Merkel, Dr. G. R. Aiken and Dr. E. Suess

2003 Abitur, Gotthold-Ephraim-Lessing-Gymnasium Döbeln, Germany

### PROFESSIONAL EXPERIENCE

2006 Internship, Helmholtz Centre for Environmental Research (UFZ), Leipzig, Germany

2006 Internship, Saxon State Ministry of the Environment and Agriculture, Freiberg, Germany

2005-2007 Student research assistant, TU Bergakademie Freiberg, Germany

### AWARD

2009 Scholarship for research abroad, German Academic Exchange Service (DAAD)







This thesis is available on-  
line from the E-Collection  
of ETH Zurich

[http://e-collection.eth-  
bib.ethz.ch](http://e-collection.eth-bib.ethz.ch)

